Overcoming limitations in bioengineering Rubisco in higher plant chloroplasts

Yi-Leen Lim

A thesis submitted for the degree of

Doctor of Philosophy of The Australian National University

Plant Sciences

Research School of Biological Sciences

The Australian National University

June 2015

STATEMENT OF AUTHORSHIP

The results presented in this thesis are, except where otherwise acknowledged, my own original work.

Yi-Leen Lim

ACKNOWLEDGEMENTS

This piece of literature and the research opportunities that may further stem from this thesis could not have been accomplished without the insight of Associate Professor Spencer Whitney, whose influence and expertise in the field of Plant Sciences have given me countless academic exposure and network opportunities over the past few years. To Spencer – thank you for being an excellent leader, role model, friend and confidante.

I am fortunate to have had wonderful colleagues at the Whitney laboratory, and would like to especially thank Dr. Robert Sharwood for his vast knowledge and patience in sharing his academic experiences and technical skills. To Douglas Orr, Laura Gunn, Robbie Wilson and Sara Milward – I believe I finally made it. Thank you also to Elena Martin and Maxim Kapralov for your comments on the drafts as well as guidance on writing this thesis. To Rosemary Birch, Carly & Brendon Conlan and other members of the laboratory – thank you so much for your words of encouragement and support!

I would also like to address my gratitude to Eliza Middleton, Kevin Tee, Nadia Radzman and Piyankarie Jayatilaka for being my sparks of love and random joy during the hardest of times. To Janice Lee, Joyce Khoo, Klein Fernandez, Tam Tran and Timothy Wan – thank you for all the delicious home-cooked meals, and most importantly – for making Canberra feel like home.

Lastly, I would like to thank my parents for making it possible for me to embark on this five-year journey. There is undoubtedly no gift better than the challenging experience of living independently in a foreign country at a time I have now come to realise as my transition into adulthood. Mum & Dad – this thesis is yours as much as it is mine.

ABSTRACT

Better structure-function studies of higher plant Rubisco are imperative in improving catalytic potential of the enzyme Rubisco. In this thesis, a novel system to study Rubisco using an RNAi tobacco genotype is designed to provide a homogenous environment of large and small Rubisco subunits for a more genuine assessment of recombinant Rubisco catalysis, regulation and assembly as well as its photosynthetic capacity in tobacco. The application of technology and strategies discussed in this thesis will demonstrate a great leap forward in Rubisco bioengineering and recombinant protein expression in plant chloroplasts.

The *RbcS* RNAi of the $^{cm}trL^{RNAi\text{-}S}$ genotype is stable up to three generations, having selectable resistance against the Basta herbicide while boasting no accumulation of transcript mRNA from the tobacco *RbcS* multigene family. Access and ability to manipulate the Rubisco S-subunit in higher plants have been the final crux in bioengineering Rubisco and is now possible using the $^{cm}trL^{RNAi\text{-}S}$ master line. Additionally, application of the intron-containing hairpin loop construct in RNAi silencing and its effectiveness as shown in this thesis strongly validates the use of this technology to study other genomic and proteomic components of photosynthesis in higher plants.

The unperturbed growth of $^{cm}trL^{RNAi\text{-}S}$ to maturity in soil (albeit requiring elevated CO_2 environment) and therefore the development of fertile pollen enhances the prowess of the $^{cm}trL^{RNAi\text{-}S}$ line to include stable transfer of the RNAi-*RbcS* system into tobacco genotypes using cross-pollination. New genotypes generated using pollen from $^{cm}trL^{RNAi\text{-}S}$ to fertilise genotypes producing S-subunits in the chloroplast mirror similar *RbcS* silencing found in $^{cm}trL^{RNAi\text{-}S}$ thus resulting in populations of homogenous, chloroplast-made S-subunits in the absence of endogenous (cytosolic) S-subunits. In summary, a more accurate system for determining the innumerable factors and limitations in recombinant Rubisco expression and biogenesis in higher plants can be achieved using $^{cm}trL^{RNAi\text{-}S}$.

The recent advent of $^{cm}trL^{RNAi-S}$ to intrinsically manipulate the S-subunit encourages further possibilities for comprehensive studies to overcome limitations in bioengineering higher plant Rubisco. The curious nature of the S-subunit multigene family and its indispensable role in higher plant photosynthesis once perplexing now serve as tools to bring fresh perspectives on the S-subunit's import into the chloroplast, processing events and interaction with its counterpart subunit. The capacity to experiment on a single *RbcS* species in the chloroplast by its expression in an *rbcL-rbcS* dicistronic operon presents opportunities for differentiating members of the *RbcS* multigene family as well as to study the importance of structure-function differences between intra- and interspecies variants of *RbcS*. This thesis details preliminary knowledge gleaned from the first examples of homogenous hybrid Rubisco populations expressing foreign S-subunit genes from red Rubisco (*G. monilis*), C_3 (*N. tabacum* and *H. annuus*) and C_4 (*F. bidentis* and *S. bicolor*) plants as well as various approaches in regulatory elements and sequences for optimising synthesis of recombinant Rubisco in host surrogate tobacco.

The mention of $^{cm}trL^{RNAi-S}$ in preceding theses from the Whitney laboratory and its use in the Whitney laboratory for various other projects in parallel to work done in the thesis is proof of a pioneering method for stable bioengineering of S-subunit and subsequently L_8S_8 Rubisco in higher plants. Ultimately, this thesis showcases new strategies for improving the transition of transcript mRNA coding for foreign and recombinant Rubisco as well as other potential proteins of interest to comparable levels of translated product in higher plant chloroplasts.

TABLE OF CONTENTS

LIST OF FIGURES

LIST OF TABLES

LIST OF ABBREVIATIONS

General terms and processes

ANU	Australian National University
BRF	Biomolecular Resource Facility, ANU
BS	bundle sheath
BSC	bundle sheath cells
CBB	Calvin-Benson-Bassham cycle
CCM	carbon-concentrating mechanism
CER	controlled environment rooms
C-terminal	carboxyl (COOH)-terminal
EST	expressed sequence tags
ETC	electron transport chain
Fd/TRX	ferrodoxin/thioredoxin
gDNA	genomic DNA
GLB	gel-loading buffer
GOS	global ocean sampling
H_6	hexa-histidine
H_7	hepta-histidine
ihpRNAi	intron containing hairpin RNAi construct
IMAC	immobilised metal affinity chromatography
iPCR	inverse PCR
LB	Luria-Bertani medium
LRE	light responsive elements
MC	mesophyll cells
MS	mineral salts
nd	non-denaturing
Nt	*Nicotiana tabacum*
N-terminal	amino (NH)-terminal
NUE	nitrogen-use efficiency
OAA	oxaloacetate
OEC	oxygen evolving complex
PAGE	polyacrylamide gel electrophoresis
PCR	polymerase chain reaction
pDNA	plasmid DNA
PSI	Photosystem I
PSII	Photosystem II
PTGS	post transcriptional gene silencing
PTM	post-translational modification
RBCS	Rubisco S-subunit multigene family
RMOP	Murashige and Skoog medium
RNAi	RNA interference
RT-PCR	reverse transcriptase polymerase chain reaction
RUE	radiation-use efficiency
TCR	translational control region
TPU	trioise phosphate utilisation
UV	ultraviolet
WGS	whole shotgun contiguous sequences
WT	wild-type tobacco

WUE	water-use efficiency
YM	yeast mold medium

Units, formulas and measurements

°C	degree Celsius
A	absorbance
A	CO_2 assimilation rate
bar	metric unit for pressure
bp	base pair
C	CO_2 concentration in assay
C_a	CO_2 concentration in Li-COR leaf chamber
C_i	intracellular CO_2 concentration
cpm	counts per minute
C_t	total organic carbon
d	day(s)
F	farad
g	gram
g	Earth gravitational acceleration
g_m	stomatal conductance
h	hour(s)
Kb	kilobase-pair(s)
K_C	Michaelis constant for CO_2
k_{cat}	CO_2-saturated carboxylase activity
k_C^{cat}	carboxylation turnover rate
K_m	Michaelis-Menten constant
K_o	Michaelis constant for O_2
k_O^{cat}	oxygenation turnover rate
L	litre
M	molar
m^2	area in metre
min	minute(s)
nt	nucleotide
opm	orbits per minute
pH	negative log of the activity of the hydrogen ion in an aqueous solution
pK	logarithmic measure of the acid disassociation constant
psi	pound/square inch
q	solubility of CO_2 in water at 1 atm at 25°C (0.03292 Mol L^{-1} atm^{-1})
R	universal gas constant
Rs	Rubisco content per sample
R_d	Mitochondria respiration not associated with photorespiration
R_l	Rubisco content per lane
rpm	revolutions per minute
s	second(s)
$S_{c/o}$, τ, Ω	Rubisco relative specificity for CO_2 as opposed to O_2
V	volt(s)
v/v	volume per volume
v_b	volume of gel loading buffer

v_s	volume of sample
v_f	final volume of sample
V_c	Rubisco carboxylation rate
$V_{c\ max}$	maximal Rubisco carboxylation rate
V_o	Rubisco oxygenation rate
$V_{o\ max}$	maximal Rubisco oxygenation rate
w/v	weight per volume
Γ^*	CO_2 concentration where oxygenation: carboxylation is 2:1; CO_2 compensation point

Chemical compounds

$(NH_4)NO_3$	ammonium nitrate
CABP	2-carboxy-D-arabinitol 1,5-bisphosphate
$CaCl_2$	calcium chloride
$CaCl_2 \cdot 6H_2O$	calcium chloride hexahydrate
Cl	chloride
$CoCl_2 \cdot 6H_2O$	cobalt chloride hexahydrate
CPBP	carboxypentitiol-1,5-bisphosphate
CRBP	carboxyribitol-1,5-bisphosphate
CsCl	cesium chloride
CTAB	cetyl trimethylammonium bromide
$CuSO_4 \cdot 5H_2O$	copper sulfate pentahydrate
DMSO	dimethyl sulfoxide
DTT	dithiothreitol
EDTA	ethylenediamine tetra-acetic disodium salt
$FeCl_3 \cdot 6H_2O$	iron chloride hexahydrate
H_2O	water
H_3BO_4	boric acid
HCl	hydrochloric acid
HCO_3^-	bicarbonate
IPTG	isopropyl-C-D-thiogalactoside
$K_2HPO_4 \cdot 3H_2O$	dipotassium hydrogen phosphate trihydrate
Kan	kanamycin
KCN	potassium cyanide
KH_2PO_4	monopotassium phosphate
KI	potassium iodide
KNO_3	potassium nitrate
$MgCl_2$	magnesium chloride
$MgSO_4$	magnesium sulphate
$MgSO_4 \cdot 7H_2O$	magnesium sulfate heptahydrate
$MnSO_4 \cdot 2H_2O$	manganese(II) sulphate dihydrate
MOPS	3-(N-morpholino)propansulfonic acid
N_2	nitrogen (aqueous)
Na	sodium
Na_2HPO_4	disodium hydrogen phosphate
NAA	α – napthaleneacetic acid, auxin
NaCl	sodium chloride
$NaHPO_4$	sodium phosphate
$NaMoO_4 \cdot 2H_2O$	sodium molybdate dihydrate
NaOH	sodium hydroxide

NH_3	ammonia
Ni-NTA	nickel-nitrilotriacetic acid
PMSF	phenyl methyl sulfonyl fluoride
PVP-40	polyvinylpyrrolidone
PVPP	polyvinylpolypyrrolidone
SDS	sodium dodecyl sulphate
Spec	spectinomycin
SSC	sodium chloride sodium citrate
TAE	Tris, acetic acid and EDTA
TBS	Tris, boric acid and sodium chloride
TE	Tris-EDTA
Tris	tris(hydroxymethyl)aminomethane
X-gal	5-bromo-4-chloro-3-indoyl-β- D-galactopyranoside
$Zn_2SO_4 \cdot 7H2O$	zinc sulphate heptahydrate

Biochemical molecules and metabolites

1,3-PGA	1,3-bisphosphoglycerate
2-PG	2-phosphoglycolate
3-PGA	3-phosphoglycerate
ADP	adenosine diphosphate
ATP	adenosine triphosphate
BSA	bovine serum albumin
BSD2	BUNDLE SHEATH DEFECTIVE2; DnaJ-like protein
CA1P	2-carboxy-arabinitol 1-phosphate
cDNA	complementary DNA
ClpC	caseinlytic peptidase
CO_2	carbon dioxide
dATP	deoxyadenosine triphosphate
dCTP	deoxycytidine triphosphate
dGTP	deoxyguanosine triphosphate
DHAP	dihydroxyacetone phosphate
DNA	deoxyribonucleic acid
dNTP	deoxynucleoside triphosphate
dsRNA	double-stranded RNA
dTTP	deoxythymidine triphosphate
E4P	erythrose-4-phosphate
F1,6P	fructose-1,6-bisphosphate
F6P	fructose-6-phosphate
G3P	glyceraldehyde-3-phosphate
gDNA	genomic DNA
GTP	guanosine-5'-triphosphate
H^+	proton, cationic form of hydrogen
H_2O	water
HSP70	heat shock protein 70
KABP	3-ketoarabinitol-1, 5- bisphosphate
miRNA	microRNA
mRNA	messenger RNA
NAD+	nicotinamide adenine dinucleotide
NADH	nicotinamide adenine dinucleotide, reduced form
NADP+	nicotinamide adenine dinucleotide phosphate
NADPH	nicotinamide adenine dinucleotide phosphate, reduced

	form
Nt	nucleotide
O_2	oxygen
PDBP	pentadiulose 1,5-bisphosphate
P_i	inorganic phosphate
PKABP	2'-peroxy-3-ketoarabinitol 1,5-bisphosphate
R5P	ribulose-5-phosphate
RAF	Rubisco accumulation factor; Pterin-4a-carbinolamine dehydratase-like protein
RbcX	Rubisco assembly chaperone
RLP	Rubisco-like protein
RNA	ribonucleic acid
RuBP	D-ribulose-1,5-bisphosphate
RuP	ribulose-5-phosphate
S1, 7P	sedoheptulose-1,7-bisphosphate
S7P	sedoheptulose-7-phosphate
SAM	S-adenosyl-methionine
siRNA	small interfering RNA
SPP	stromal processing peptidase
sRNA	small RNA
T-DNA	transfer-DNA
TGS	transcriptional gene silencing
Tic	Translocon of the inner membrane of the chloroplast
Toc	Translocon of the outer membrane of the chloroplast
X5P	xylulose-5-phosphate
XuBP	D-xylulose-1,5-bisphosphate

Genes and coding regions

3'UTR	3' untranslated region
5'UTR	5' untranslated region
aadA	aminoglycoside-3-adenyltransferase (spectinomycin) resistance
accD	acetyl-CoA carboxylase beta subunit
atpB	ATP synthase CF1 beta chain
bar	Basta (glufosinate ammonium) resistance
CaMV 35S	cauliflower mosaic virus 35S promoter
CDS	coding sequence
CHI	chalcone synthase intron
^{cm}*rbcM*	codon-modified *R. rubrum* L-subunit gene
IEE	intergenic expression element
IS	intergenic sequence
LB	left border
loxP	*lox* sequence derived from bacteriophage P1
OCS	octopine synthase
Prrn	plastid rRNA operon promoter
psbA	photosystem II Protein D1 gene
RB	right border
rbcL	Rubisco large subunit
rbcM	*R. rubrum* L-subunit gene
RbcS	Rubisco small subunit

rca	Rubisco activase
rps16	ribosomal protein S16 gene
rrn	ribosomal RNA
SD	Shine-Dalgarno sequence
T7g10	major capsid protein of phage T7 gene
TATA	Goldberg-Hogness box; cis-regulatory DNA sequence found in the promoter region of genes in archaea and eukaryotes
tp	transit peptide

Proteins and enzymes

AAA+	ATPase-Associated Activity proteins
AGO1	Argonaute-1
CbbY	XuBP sugar phosphatase
Cre	tyrosine recombinase enzyme from P1 Bacteriophage
Cyt_{bf}	Cytochrome bf complex
DCL	DICER-LIKE1 protein
FBA	fructose-1,6-bisphosphate aldolase
FBPase	fructose-1,6-bisphosphatase
FNR	ferrodoxin $NADP^+$ oxidoreductase
GADPH	glyceraldehyde-3-phosphate dehydrogenase
GDC	glycine decarboxylase
GOGAT	glutamine oxoglutarate aminotransferase
GS	glutamine synthase
HEN1	HUA ENHANCER1
HSP70	heat shock protein 70
HYL1	HYPONASTIC LEAVES1
LSu	large subunit of Rubisco
NAD-ME	NAD malic enzyme
NADP-ME	NADP malic enzyme
NAT	*N*-acetyltransferase
P680	pigment 680; Photosystem II chlorophyll, primary electron donor
P700	pigment 700; Photosystem I chlorophyll, primary electron donor
PC	plastocyanins
PEP	phosphoenolpyruvate
PEPC	phosphoenolpyruvate carboxylase
PEPCK	phosphoenolpyruvate carboxykinase
PGK	phosphoglycerate kinase
PGK	phosphoglycerate kinase
PGPase	phosphoglycolate phosphatase
PQ	plastoquinones
PRK	phosphoribulokinase
Rca	Rubisco activase
RISC	RNA induced silencing complex
RISC	RNA-induced silencing complex
RNAse	ribonuclease
RPE	ribulose-5-phosphate 3-epimerase
RPI	ribose-5-phosphate isomerase

Rubisco	ribulose-1,5-bisphosphate carboxylase / oxygenase
SBPase	sedoheptulose-1,7-bisphosphatase
SE	SERRATE
SOD	superoxide dismutase
SPP	stromal protein peptidase
SSu	small subunit of Rubisco
TK	transketolase
TPI	triose phosphate isomerase

CHAPTER 1 – GENERAL INTRODUCTION

1.1 Photosynthesis – Carbohydrate synthesis and the sustenance of life

Most autotrophic organisms synthesize complex carbohydrates via photosynthesis using light energy. Ribulose-1,5-bisphosphate [RuBP] carboxylase/deoxygenase; EC 4.1.1.39 (Rubisco) is a fundamentally important enzyme in the carbon-assimilation steps of photosynthesis wherein it initiates the fixation of inorganic carbon dioxide (CO_2) from the atmosphere into carbohydrates that serve as the source of energy and biomass for all living species. Within the biosphere, the CO_2 and photosynthetic process of fixing CO_2 and light energy to produce O_2 and organic carbon derivatives is the essence that sustains life on earth (Blankenship, 2002).

1.1.1 The carbon fixation and light reactions of photosynthesis

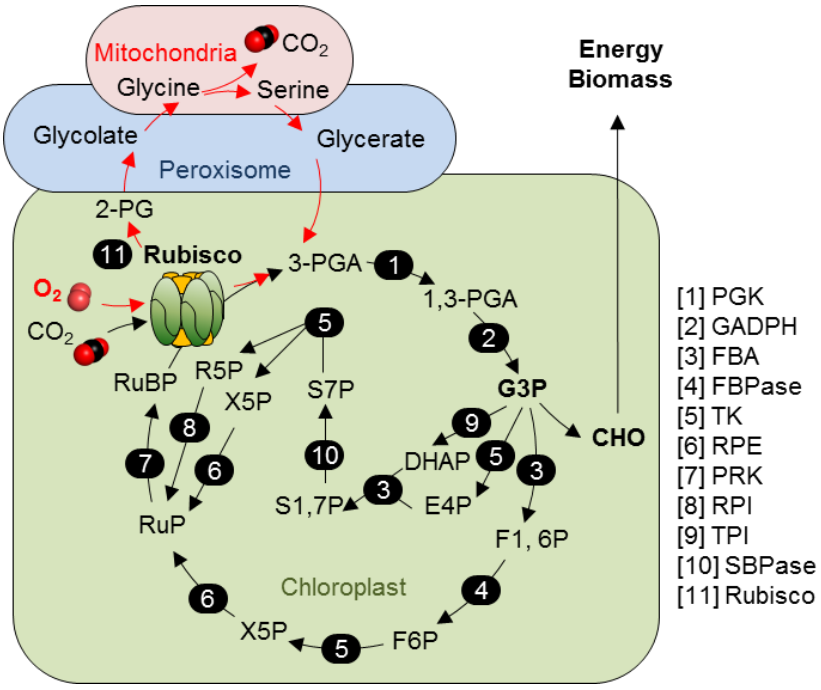

Figure 1.1 Enzymes and metabolites in the CBB and photorespiratory cycles.

Within the chloroplast stroma RuBP (ribulose-1,5-bisphosphate) and carbon dioxide (CO_2) are fixed by Rubisco (Ribulose 1,5-bisphosphate carboxylase/oxygenase) to produce two 3-phosphoglycerate (3-PGA) molecules that undergoes a series of reducing reactions (enzymes 1 & 2) to produce glyceraldehyde-3-phosphate (G3P, in bold). The G3P is either used for carbohydrate (CHO) synthesis or used to regenerate RuBP within the CBB cycle (enzymes 3 – 10). Fixation of O_2 to RuBP by Rubisco produces a 3-PGA and a 2-PG (2-phosphoglycolate) product that is recycled to 3-PGA via the photorespiratory cycle (red arrows) that spans the peroxisome and mitochondria. This pathway leads to loss of previously fixed CO_2 within the mitochondria. PGK, phosphoglycerate kinase; GAPDH, glyceraldehyde-3-phosphate dehydrogenase; FBA, fructose-1,6-bisphosphate aldolase; FBPase, fructose-1,6-bisphosphatase; TK, transketolase; RPE, ribulose-5-phosphate 3-epimerase; PRK, phosphoribulokinase; RPI, ribose-5-phosphate isomerase; TPI, triose phosphate isomerase; SBPase, sedoheptulose-1,7-bisphosphatase. Metabolites in the cycle include 1,3-PGA, 1,3-bisphosphoglycerate; DHAP, dihydroxyacetone phosphate; E4P, erythrose-4-phosphate; S1,7P, sedoheptulose-1,7-bisphosphate; S7P, sedoheptulose-7-phosphate; R5P, ribulose-5-phosphate; X5P, xylulose-5-phosphate; F1,6P, fructose-1,6-bisphosphate; F6P, fructose-6-phosphate; RuP, ribulose-5-phosphate. Figure modified from Michelet et al. (2013).

Of all the known pathways for CO_2-fixation, the Calvin-Benson-Bassham (CBB) cycle is most prevalent in autotrophs (Herrmann et al., 2015). In the cycle Rubisco fixes CO_2 onto the substrate RuBP and evenly cleaves the 6-carbon product into 3-phosphoglycerate (3-PGA) products that form the precursor molecules for carbohydrate synthesis (Figure 1.1).

The CBB cycle requires the co-ordinated functioning of 11 different enzymes to catalyse 13 different biochemical reactions. As many of these reactions require ATP and NADPH, flux through the CBB cycle is regulated by the supply of these energy equivalents from the photosynthetic light reactions (Michelet et al., 2013). As summarised in Figure 1.2, the light reactions of photosynthesis involve a series of integral thylakoid membrane protein complexes (PSII, PSI, cyt_{bf} and ATP synthase) and mobile electron carriers in chloroplasts that transmit the light energy captured by accessory pigments (e.g. chlorophylls and carotenoids) by the movement of protons and electrons to drive ATP and NADPH synthesis and enable the oxidation of H_2O to produce O_2.

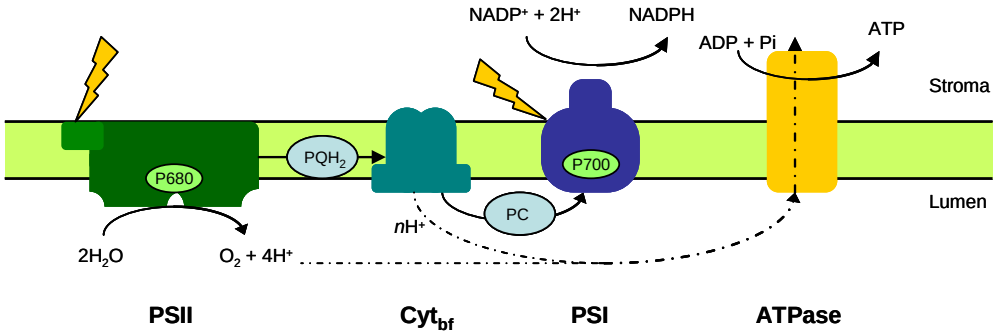

Figure 1.2 The light reactions of photosynthesis.

The photosystem I (PSI), photosystem II (PSII), cytochrome b_f complex (cyt_{bf}) and ATP synthase (ATPase) within the thylakoid membrane function synergistically to mediate a series of oxido-reduction reactions. Light energy absorbed by chlorophyll and carotenoids arranged in antennae complexes around the PSI and PSII complexes is funnelled to a special pair of chlorophyll molecules - called the P680 (in PSII) and P700 (in PSI) reaction centres. Electron transfer from P680/P700 oxidizes the reaction centres resulting in charge separation - the transfer of an electron to a neighbouring acceptor molecule initiates a suite of redox chemical reactions facilitated by electron transfer through a range of components known as the electron transport chain (ETC). Movement of electrons through various carriers such as plastoquinones (PQ) and plastocynanins (PC) ultimately culminates in the reduction of $NADP^+$ to NADPH. The initial source of the electrons in the ETC is H_2O. Within the oxygen evolving complex of PSII (OEC) electrons are removed from water to reduce oxidised P680 molecules. Oxidation of two H_2O molecules in the OEC liberates O_2 and four protons (H^+) into the thylakoid lumen. Similarly, H^+ is translocated into thylakoid lumen during linear electron transport from PSII to PSI via the cyt b_6f complex, resulting in a trans-thylakoid proton gradient that drives ATP synthesis via the ATP synthase complex (Eberhard et al., 2008).

1.1.2 Photosynthesis – a target for improvement to increase global crop yields

The significance of addressing the growing concerns on food security is hard to over-state. Food production needs to rise by >50% within the next 40 years to sustain the growing global population (Long et al., 2015). The genetic gains in plant productivity over the last ~50 years have come through plant breeding strategies to improve resistance to stress – drought, cold, high salinity, pests and diseases – and through more efficient water and fertilizer use. Adding to the challenge of increasing the global productivity of natural and cropping ecosystems are the human-induced rises in air temperature and deficiencies in the availability of additional arable lands. The grim reality is that further gains at current rates of increase will be insufficient to ensure future food security (Ainsworth and Ort, 2010). This has led to an increased urgency to develop new strategies to "supercharge" photosynthesis in C_3 crops to improve yield potential. There are a number of technological remedies being studied for supercharging photosynthesis. Many of these are targeted at enhancing photosynthetic efficiency by improving the catalytic properties of the CO_2-fixing enzyme Rubisco or by introducing CO_2-concentrating mechanisms that elevate CO_2 levels around the enzyme to increase its activity (von Caemmerer and Evans, 2010; Raines, 2011; Evans, 2013).

1.1.3 Rubisco - an enzyme in need of improvement

As the enzyme linking the inorganic and organic phases of the CBB cycle, the Rubisco carboxylation reaction is often identified as the initiating step in photosynthetic carbon assimilation. As highlighted below, Rubisco catalysis is relatively slow and unspecific compared with other plant enzymes often leading to its catalytic activity limiting flux through the CBB cycle (Evans, 2013; Parry et al., 2013). This has direct consequence on the level of glyceraldehyde 3-phosphate (G3P) and other triose phosphates made for hexose sugar production. These sugars are needed for plant metabolism and growth as well as supply of other CBB products that are substrates for other pathways essential for plant development (Raines, 2003; Vriet et al., 2014).

The evolution of oxygenic photosynthesis has seen the predominantly anaerobic, CO_2-rich atmosphere of earth some 3 billion years ago (Kaufman, 2014) increase to the life preserving levels (~20,600 ppm O_2) of today. The increasing abundance of O_2 however proved detrimental to the carboxylation chemistry of Rubisco that evolved in the absence of O_2 (Whitney et al., 2011a). As shown in Figure 1.1, O_2 is a competitive inhibitor of CO_2 during Rubisco catalysis. The oxygenation of RuBP by Rubisco produces one molecule of 3-PGA and 2-phosphoglycolate (2-PG) (Bowes et al., 1971;

Andrews et al., 1971). Although often considered a waste product, recent studies suggest 2-PG may play a role in regulating carbon-concentrating mechanism activity in cyanobacteria (Haimovich-Dayan et al., 2014), be important to the nitrogen flux in plants (Mallmann et al., 2014) and possibly serve as an electron sink for quenching excessive free radicals during photosynthesis (Silva et al., 2015). Nevertheless many photosynthetic organisms (e.g. algae, cyanobacteria, CAM and C_4 plants) have evolved carbon concentrating mechanisms (CCMs) to concentrate CO_2 around Rubisco (often at high expense in metabolic energy) to avoid RuBP oxygenation and evade the resource costs of recycling 2-PG via photorespiration (Figure 1.1). This process of recycling two molecules of 2-PG into a 3-PGA molecule by photorespiration spans three different organelles (chloroplasts, peroxisomes, and mitochondria) (Kisaki and Tolbert, 1969) in a process that requires energy (ATP and NADH) and through the action of glycine decarboxylase in the mitochondria can result in up to 50% of the photosynthetic fixed carbon being released as CO_2 (Figure 1.1). This bifunctional activity of Rubisco has made it a popular target for improving photosynthetic efficiency (Parry et al., 2013). Such bioengineering efforts in plant leaves are aimed at either directly improving the capacity of Rubisco itself to better discern CO_2 from O_2, or indirectly limiting its oxygenase activity by introducing CCM or photorespiratory bypass systems into leaf chloroplasts (Maurino and Peterhansel, 2010; Evans, 2013).

1.1.4 The complexity of Rubisco catalysis – an impediment to speed and specificity

It is paradoxical that as such a prominent biological catalyst Rubisco has not evolved greater catalytic efficiency. Having reportedly originated more than 3 billion years ago from an ancestral enzyme in an Archaean (Tabita et al., 2008) there has been ample opportunity for greater catalytic advancement than is currently seen in nature (Whitney et al., 2011a). While there is significant natural catalytic diversity to demonstrate that Rubisco catalysis has managed to adapt to the CO_2 and O_2 pressures around its cellular location (Tcherkez et al., 2006), Rubisco is still acknowledged as a sluggish, unspecific enzyme in need of catalytic improvement (Parry et al., 2013). Its slowness to adapt and improve appears largely attributable to the enzyme's difficult, multi-step catalytic chemistry (Figure 1.3) (Pearce, 2006; Kannappan and Gready, 2008) and structural complementation requirements with varied molecular partners for its biogenesis in cyanobacteria and chloroplasts (Mueller-Cajar and Whitney, 2008; Durão et al., 2015; Whitney et al., 2015).

In additional to its oxygenase activity, Rubisco catalysis is also impaired by a slow turnover rate (k_{cat}) and a tendency to bind sugar-phosphate molecules that resemble its catalytic transition state intermediates that inhibit function (Servaites, 1990; Carmo-Silva et al., 2014) (see Table 1.1 and Figure 1.3). Compared with superoxide dismutase (SOD) that catalyses at rates of up to 10^9 cycles per second (Gleason et al., 2014), Rubisco is capable of only undergoing 1 to 4 cycles per second in leaf chloroplasts (Whitney et al., 2011a). In plants like wheat, rice and tobacco this turnover typically incorporates one oxygenase reaction per three carboxylation reactions.

Table 1.1 Misfire products and biological molecules that inhibit Rubisco.

Inhibitor	Abbreviation
D-xylulose-1,5-bisphosphate	XuBP
3-ketoarabinitol-1, 5- bisphosphate	KABP
2-carboxy-D-arabinitol-1-phosphate	CA1P
Pentadiulose 1,5-bisphosphate	PDBP
Ribulose 1,5-bisphosphate	RuBP

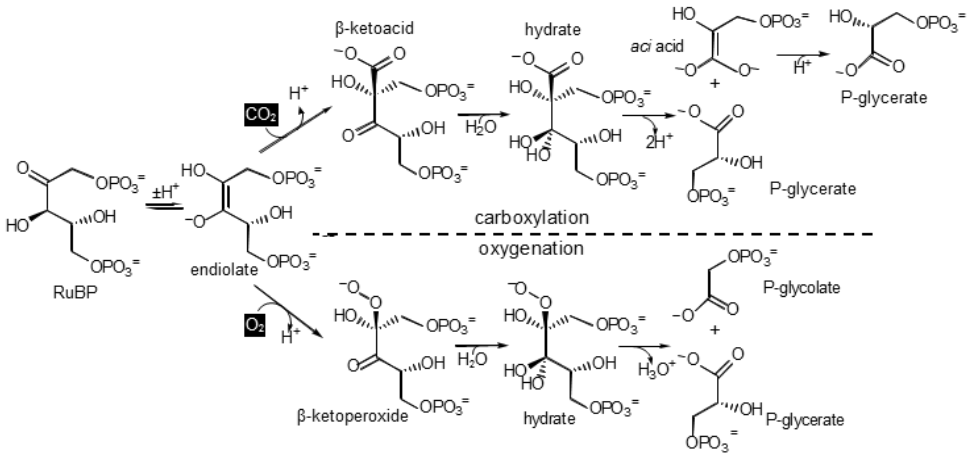

Figure 1.3 The multi-step reactions of Rubisco carboxylation and oxygenation.

Upon binding to a Rubisco active site the RuBP forms an enediol product that provides a nucleophilic site at the C2 carbon atom accessible for binding substrate CO_2 or O_2. CO_2 binding produces the 6 carbon intermediate product 2'-carboxy-3-ketoarabinitol 1,5-bisphosphate (CKABP) that is subsequently hydrated at the C3 carbon atom producing a gem diol (enediol) product that is deprotonated prior to carbon-carbon cleavage between the C2 and C3 carbon atoms to produces two 3PGA molecules. Alternatively O_2 binding to the enolised RuBP produces 2'-peroxy-3-ketoarabinitol 1,5-bisphosphate (PKABP) that also undergoes a series of hydration, protonation and cleavage partial reactions to form one 3PGA and one 2-PG. Rubisco can also undergo a number of side reactions to produce catalytic misfire products that constitute inhibitors of catalysis (see Table 1.1) (Orr, 2013)

As Rubisco does not directly bind CO_2 or O_2, the quaternary structure of Rubisco essentially serves to position conserved active site residues in an orientation that optimally orientates the bound RuBP-enediol for preferential reaction with atmospheric CO_2 rather than the more abundant O_2 (Andersson, 2008; Parry et al., 2013). Molecular

dynamic simulation *in silico* of the Rubisco catalytic chemistry (Kannappan and Gready, 2008) and understanding the energetic constraints of its highly conserved mechanism (Walter, 2006; Tcherkez, 2013) have proven of fundamental importance to better understand Rubisco function at the molecular level. Such studies provide rationales for the general observations that improvements in the catalytic speed of Rubisco are often attained at the expense of specificity for CO_2 over O_2, and *vice versa* (Tcherkez et al., 2006) – although greater exploration of Rubisco catalytic diversity and strategic mutagenic testing is needed to test the accuracy of these hypotheses (Parry et al., 2013; Galmés et al., 2014; Sharwood and Whitney, 2014).

As a consequence of its poor kinetics most plants invest considerable amounts of their resources into producing sufficient Rubisco to support adequate levels of carbon assimilation for plant growth and development. For example Rubisco typically constitutes 25 to 50% of the leaf protein in C_3 plants (such as wheat, cotton, rice, *Arabidopsis* and tobacco) (Whitney et al., 2011a; Sharwood and Whitney, 2014) which accounts for up to 25% of the total leaf nitrogen (Evans, 2013). This high level of investment bestows Rubisco with the dubious honour of being the most abundant enzyme on Earth (Ellis, 1979; Raven, 2013).

1.1.5 Structural and functional diversity among the varying isoforms of Rubisco

In nature, Rubisco takes on a variety of quaternary structures (Figure 1.4). All structures comprise oligomers of large (L-) subunits (e.g. Form II Rubisco, Form III Rubisco and Rubisco like proteins, RLP) or a hexadecameric structure of eight L-subunits and eight small (S-) subunits (*i.e.* Form I L_8S_8 Rubisco) whereby the dimer of two L-subunits (L_2) that are arranged in an anti-parallel fashion (*i.e.* "head-to-toe") and contain two active sites (Andersson and Backlund, 2008; van Lun et al., 2011; Stec, 2012) is the basal functional unit and is shared by all Rubisco isoforms. While the quaternary structure and generic conformation of L_8S_8 Rubisco has remained unperturbed somewhat in photosynthetic eukaryotes (e.g. plants and algae), there is significant variation in their catalytic properties (Whitney et al., 2011a) (further detailed in Chapter 4). This variation often correlates with the level of CO_2 in solution around Rubisco (Sharwood and Whitney, 2014; Galmes et al., 2014). For example Rubisco associated with a CCM generally has a faster k_{cat} but a lower affinity for CO_2 (*i.e.* a higher K_m for CO_2) and a reduced specificity for CO_2 over O_2 (termed the Rubisco CO_2/O_2 specificity factor; $S_{C/O}$) (Badger et al., 1998; Parry et al., 2013). There is also increasing evidence that catalytic properties of plant Rubisco have adapted to growth conditions of elevated temperature

by producing Rubisco isoforms with higher $S_{C/O}$ to evade the increased propensity for oxygenase activity at higher temperatures (Galmés et al., 2005; Galmés et al., 2014).

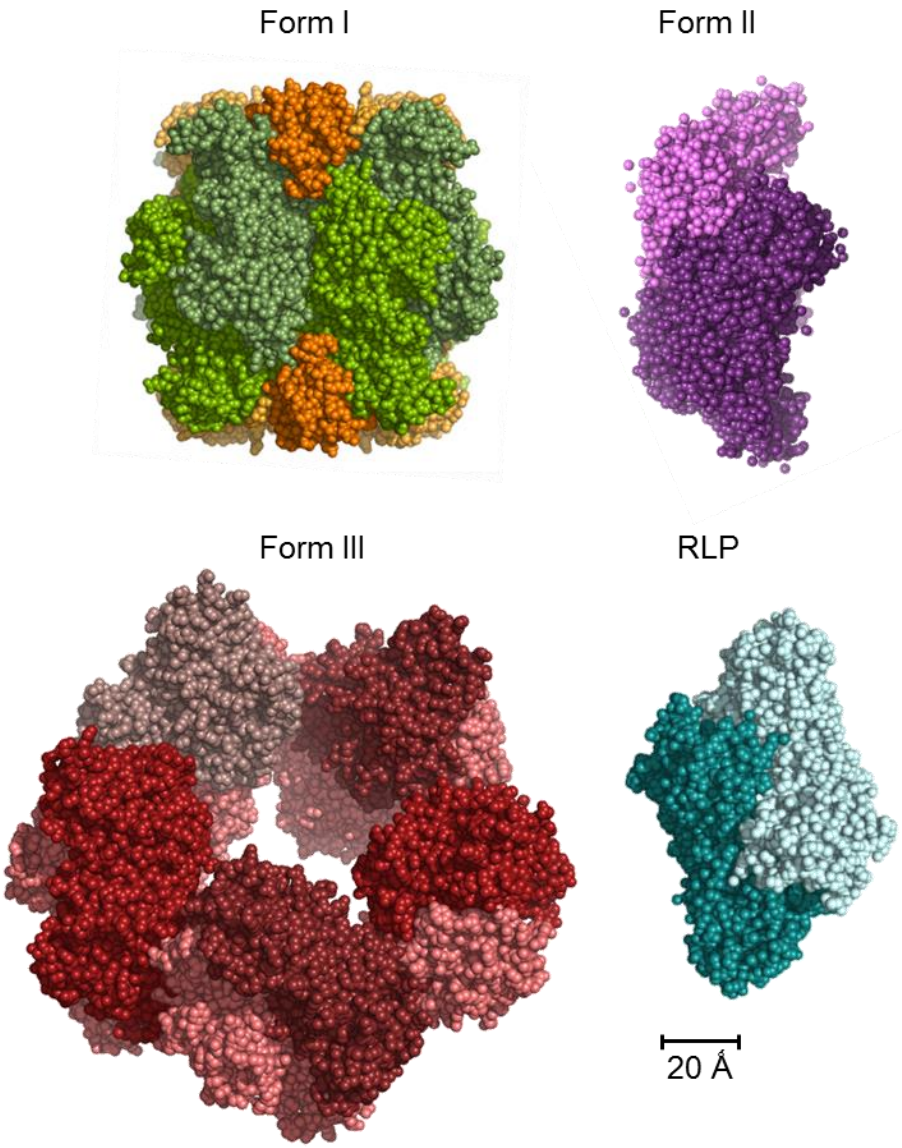

Figure 1.4 Rubisco structural diversity in nature.

The most commonly found oligomer structure of Rubisco is the Form I hexadecamer comprising 8 large (L) and 8 small (S) subunits (*i.e.* L_8S_8) (pdb accession 1RCX). Form II Rubisco comprises a single dimer of L-subunits (L_2) (pdb accession 5RUB) or multiple L_2 units forming tetramer $(L_2)_2$ hexamer $(L_2)_3$ or octamer $(L_2)_4$ configurations (not shown). Rubisco in some Archaea also comprise L_2 Rubisco or pentameric rings of L_2 units (*i.e.* $(L_2)_5$) (pdb accession 1GEH) and are often called Form III Rubisco. A related protein group called Rubisco-like proteins (RLP) (pdb accession 1YKW) arranges similarly to Form II Rubisco dimer but do not function in RuBP catalysis. Each subunit is represented by a different coloured ribbon. Figure adapted from Tabita et al. (2008).

As shown in Figure 1.4, the L_8S_8 conformation of Form I Rubisco comprises a core of eight 50- to 54 kDa L-subunits (L_8) with two tetrads of 12 to 18 kDa S-subunits capping either end (van Lun et al., 2011). S-subunit binding is thought to both stabilise the holoenzyme structure as well as induce conformational changes within the L_8 core to stimulate catalytic viability (Bracher et al., 2011). In nature, the Form I L_8S_8 isoform of Rubisco appears the most prominent as it is the form utilised by plants, algae, cyanobacteria and various proteobacteria (Andersson and Backlund, 2008; Whitney et al., 2011a). Based on the phylogeny of L-subunit sequences, Form I Rubisco comprises of four distinct clades (IA, IB, IC, ID) that generally map to the phylogenetic distribution of other photosynthetic genes and physiological processes (Badger and Bek, 2008). These phylogenies show the clustering of plant, green algae, cyanobacteria and certain proteobacteria Rubisco isoforms (IA and IB) in what is often called the "green-Rubisco" lineage. The Rubisco from non-green algae, other cyanobacteria and different proteobacteria species cluster in a separate "red-Rubisco" lineage (IC and ID) (Delwiche, 1999) (see also Table 1.2). Aligning with these different lineages is the location of *rbcL* and *rbcS* coding the L- and S-subunit genes. The Form I red-Rubisco genes are typically arranged in tandem in a bicistronic operon located in the chloroplast genome (plastome) or prokaryotic chromosome. In some cases these operons include other genes that code for proteins related to Rubisco biogenesis (e.g. rbcX) or catalytic regulation (e.g. cbbX) (Liu et al., 2010; Mueller-Cajar et al., 2011). In contrast, in vascular ("higher") plants and green algae *rbcL* is located in the plastome and multiple *RbcS* copies located in the nucleus (Andersson and Taylor, 2003; Andersson, 2008; Tabita et al., 2008; Whitney et al., 2011a).

Form II Rubisco isoforms exist in proteobacteria and some dinoflagellate algae. The simplest Form II Rubisco structure is the L_2 isoform that is best characterised from the photosynthetic α-proteobacterium *Rhodospirillum rubrum* (Figure 1.4) (Tabita and McFadden, 1974). In dinoflagellates the Form II Rubisco constitutes a more complex oligomeric structure whose stoichiometry is assumed to be L_8, but remains experimentally unclarified (Whitney and Yellowlees, 1995). Study of *R. rubrum* Rubisco has spanned over 40 years by taking advantage of its minimal assembly requirements that have allowed its expression and mutagenesis in hosts such as *E. coli*, cyanobacterium Synechocystis 6803 and leaf chloroplasts (Pierce et al., 1989; Morell et al., 1990; Whitney and Andrews, 2001b; Mueller-Cajar and Badger, 2007). Other Form II Rubisco isoforms produced in species of *Rhodopseudomonas palustris* have been found to form varying oligomeric structures such as $(L_2)_2$ tetramers, $(L_2)_3$ hexamers and

$(L_2)_4$ octamers (Tabita et al., 2008). Common features to Form II Rubisco are the low sequence identity of their L-subunits to Form I Rubisco (typically sharing only 20 to 30% identity) and inferior catalytic properties that comprise 4 to 8-fold reductions in $S_{C/O}$, a >10-fold higher K_m for CO_2 that offset the benefits of the ~2-fold increases in k_{cat} for many Form II Rubisco. Despite these differences however, crystal structure analyses show the quaternary structure of the conserved active site residues within both Form I and II Rubisco are highly superimposable making it difficult to discern structural reasons for their catalytic differences (Tabita et al., 2007; Andersson and Backlund, 2008).

Rubisco isoforms found in Archaea generally show relatively poor sequence similarity (<50%) to Form I and Form II Rubsico (Andersson and Backlund, 2008; Badger and Bek, 2008). This Rubisco type is often called Form III Rubisco and characteristically lacks S-subunits and forms L_2 dimers or decameric complexes (*i.e.* $(L_2)_5$). Unlike the photosynthetic function of Form I and Form II Rubisco, Form III Rubisco appears to function in metabolising the RuBP generated in Archaea during nucleotide (*i.e.* AMP) metabolism (Kitano et al., 2001; Bräsen et al., 2014). Consistent with this function the affinity of Form III Rubisco for RuBP is extremely high; typically having a >10-fold lower K_m for RuBP than Form I and II Rubisco. However Archaea Rubisco typically have slow turnover rates (k_{cat} <1 s^{-1}), a high K_m for CO_2 and $S_{C/O}$ values that are >40-fold lower than Form I Rubisco making them extremely sensitive to O_2 inhibition (Alonso et al., 2009). Despite their different functional role, replacement of Form I Rubisco in tobacco chloroplasts with the Form III Rubisco from *Methanococcus burtonii* produced plants whose photosynthetic growth could be fully supported when grown in air containing elevated levels of CO_2 (Alonso et al., 2009).

Rubisco-like proteins (RLPs) (sometimes referred to as Form IV Rubisco) show structural similarities to conventional Rubisco, but do not retain many of the catalytic residues conserved in all Rubisco forms (Ashida et al., 2005). As a result RLPs are unable to metabolise RuBP, questioning the validity of classifying them as Form IV Rubisco (Table 1.2) (Tabita et al., 2007). Like L_2 Rubisco, RLPs typically comprise a homodimer complex that is thought to function in thiosulfate oxidation as part of sulphur metabolism (Hanson and Tabita, 2001) and methionine salvage pathways such as in *Bacillus subtilis* (Ashida et al., 2005).

Table 1.2 Summary of known Rubisco forms and their properties (adapted with modifications from Tabita et al. [2008]).

Rubisco form	Subunit composition	Rubisco activity	Examples of phylogenetic distribution
IA	L_8S_8	Present	Proteobacteria, cyanobacteria, Prochlorales, Sargasso Sea and global ocean sampling metagenome (Block et al., 1987)
IB	L_8S_8	Present	Cyanobacteria, Eukaryotes (higher plants), Euglenozoa, Sargasso Sea metagenome
IC	L_8S_8	Present	Proteobacteria, chloroflexi
ID	L_8S_8	Present	Proteobacteria, Eukaryotes (stramenopiles), Rhodophyta, Haptophyceae
II	L_2 and L_n	Present	Proteobacteria, Eukaryotes (Dinophyceae)
III	L_2 and $(L_2)_5$	Present	Proteobacteria
RLP	L_2	None	Proteobacteria, chloroflexi, Eukaryotes (*Ostreococcus tauri*) Clostridia, Non-methanogenic euryarchaeota

1.1.6 Activation and regulation of plant Rubisco by Rubisco activase

The catalytic sites within Rubisco can exist in either an inactive (uncarbamylated) or active (carbamylated) state (Figure 1.5). To activate, a conserved lysine residue in the enzyme's active site (Lys-201 in plant L-subunits) first reacts with CO_2 in a reversible reaction forming a carbamate that is stabilised by binding of a Mg^{2+} ion. In this activated state correct binding of RuBP within the active site can proceed which involves structural rearrangements of a flexible loop structure (loop-6 in the L-subunit α/β barrel) and mobile L-subunit C-terminal strand to "close" the active site (van Lun et al., 2011). These movements enable RuBP-enediol formation that then reacts with CO_2 or O_2 to instigate the series of additional partial reactions (hydration, protonation and cleavage) that produce either two 3-PGA molecules (carboxylation) or a 3-PGA and a 2-PG (oxygenation) (Figure 1.3).

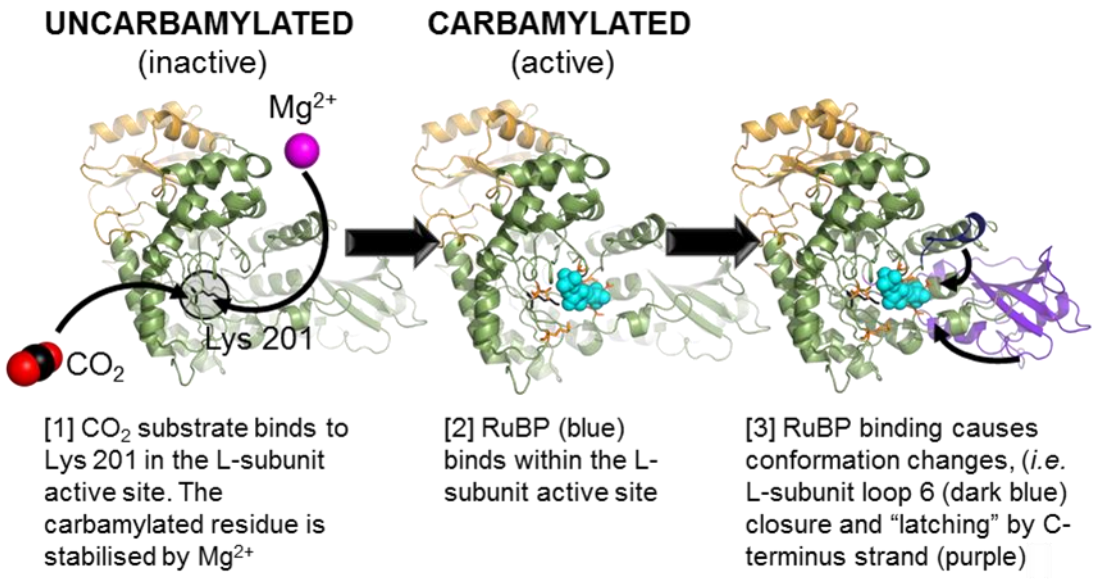

Figure 1.5 Schematic of Rubisco activation.

Lys-201 within each catalytic site of plant Rubisco binds a CO_2 to form a carbamate that facilitates Mg^{2+} binding to form an "activated" catalytic site. In this conformation the catalytic site is able to productively bind RuBP to facilitate structural changes in the L-subunit that include closure of the site by loop 6 and the C-terminal strand. These conformational changes initiate RuBP-enediol formation and the ensuing catalytic chemistry of Rubisco catalysis (Figure 1.3).

Binding of RuBP to non-activated catalytic sites in Rubisco is inhibitory as it binds tightly in a conformation within the active site unsuitable for catalysis. In many plants another inhibitory sugar-phosphate molecule, 2-carboxy-arabinitol 1-phosphate (CA1P), is naturally produced under low illumination as a means to regulate Rubisco activity in response to light. Under illumination, the removal of bound CA1P, inhibitory RuBP as well as other sugar-phosphate inhibitors are facilitated by the protein Rubisco activase (here termed RCA) (Seemann et al., 1985; Robinson and Portis Jr, 1988; Premkumar et al., 2001; Parry et al., 2008) (Figure 1.6). Studies have shown RCA in plants to be species-specific with regards to the Rubisco isoforms it functions with (Wang et al., 1992). RCA is also a heat sensitive protein wherein variations in the thermal stability of photosynthesis in plants correlate with the heat tolerance of their RCA (Kumar et al., 2009). While some plants produce two different sized isoforms of RCA (the α–isoform is ~ 30 amino acids longer than the β–isoform), plants like tobacco produce only β–isoforms of RCA. In plant leaves the activation of RCA function (and thus Rubisco catalytic activity by association) is regulated by the light reactions of photosynthesis. This activation occurs through light dependent up-regulation of the ATP/ADP ratio in the chloroplast stroma as well as activation of α–isoforms of RCA via the electron transport dependent induction of the ferredoxin-thioredoxin reducing system (Figure 1.6) (Eichelmann et al., 2009).

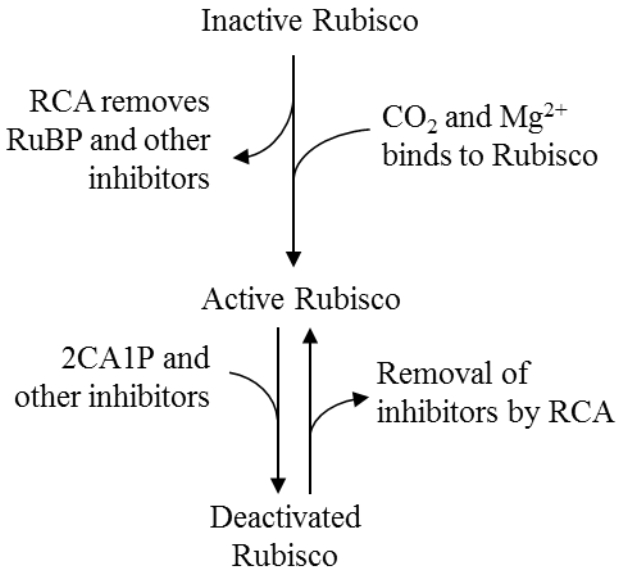

Figure 1.6 Rubisco activation and regulation of its activity by RCA.

Removal of sugar-phosphate bound inhibitors (e.g. RuBP) from the catalytic sites of non-activated Rubisco by RCA enable their activation (carbamylation) with CO_2 and Mg^{2+} to enable catalysis (Figure 1.5). Activated Rubisco can also bind sugar-phosphate inhibitors (e.g. CA1P and the catalytic misfire product XuBP, Table 1.1) whose removal by RCA is critical for enabling/maintaining Rubisco catalysis during photosynthesis.

Similar to other AAA+ (ATPase-Associated Activity) proteins, RCA removes bound inhibitors from the catalytic sites in Rubisco using the energy of ATP hydrolysis (Robinson and Portis Jr, 1989; Portis et al., 2008). Other components involved with inhibitor removal include CbbY, a sugar phosphatase discovered in *Arabidopsis thaliana* that metabolises XuBP to non-inhibitory compounds that can be used for RuBP regeneration (Bracher et al., 2015). Recent success in deriving structural information for tobacco RCA by mass spectrometry (Blayney et al., 2011) and protein crystallography (Stotz et al., 2011) have demonstrated its capacity to form hexameric complexes. These studies also confirm prior mutagenic studies as to the likelihood of a C-terminal "recognition" loop in RCA recognise sequences on the holoenzyme surface in the L-subunit N-domain (between residues 89 and 94) that facilitate conformational changes to the Rubisco L-subunit loop-6 that facilitate sugar-phosphate inhibitor release (Esau et al., 1998). Unfortunately the transitory nature of Rubisco-RCA interactions poses a significant challenge to resolving the influence of the S-subunit and specific mechanistic detail on how RCA interacts with Rubisco to cause these conformational changes (Wachter et al., 2013).

1.2 Higher plant Rubisco

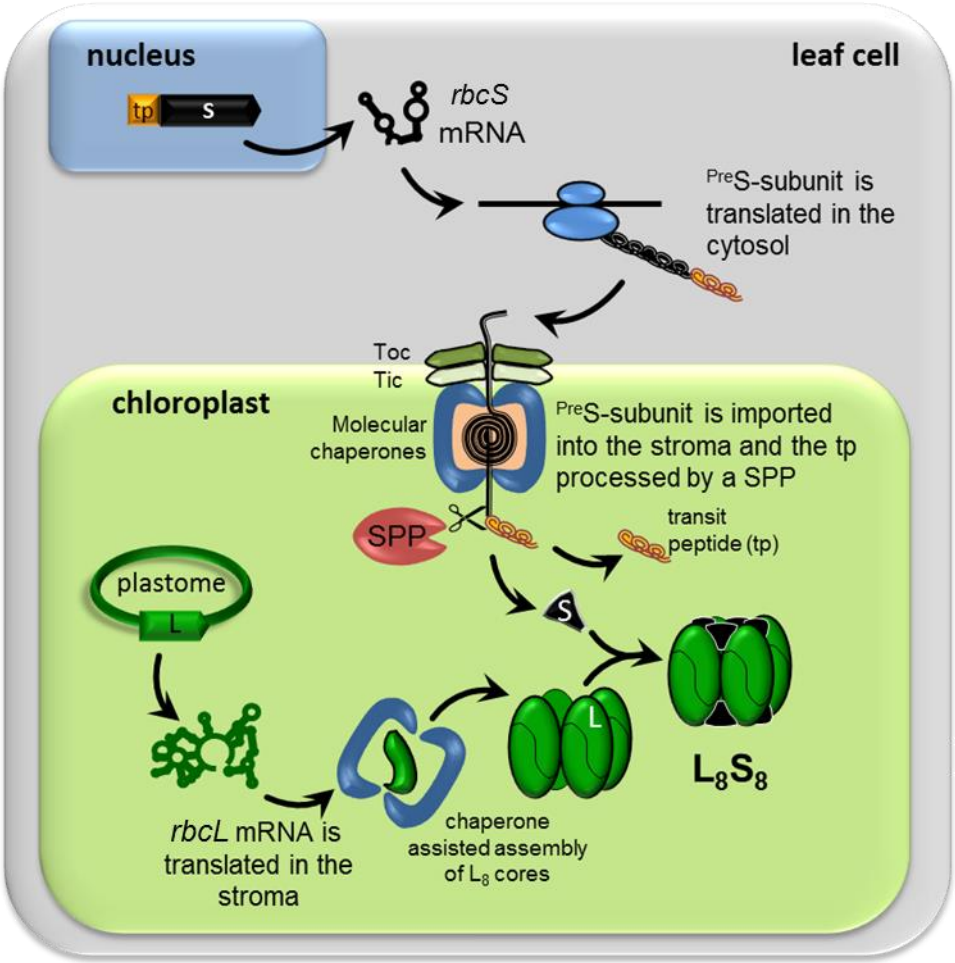

Figure 1.7 General overview of Rubisco biogenesis in leaf cells.

The *rbcL* in the plastome codes for the L-subunits that is synthesised, folded and assembled into L_8 cores with the aid of a range of molecular partners (see Chapter 4 for more detail). The Rubisco S-subunits are made in the cytosol from multiple *RbcS* mRNA transcripts as pre-proteins that contain an N-terminal targeting sequence (transit peptide; tp) that facilitates their transfer into the chloroplast stroma. In the stroma a signal peptide protease (SPP) cleaves off the tp and the new N-terminal Met-1 is methylated prior to the mature S-subunit assembling with L-subunits to form the L_8S_8 holoenzyme.

1.2.1 The biogenesis of L_8S_8 Rubisco in the chloroplast stroma

A single *rbcL* located in the multiple plastome copies in leaf chloroplasts codes for the ~50 kDa L-subunit that harbours the conserved amino acid residues that form the enzyme's active site. In contrast, a family of *RbcS* located in the plant nucleus produce a variety of S-subunit isoforms that are made in the cytosol as pre-proteins before transfer into the chloroplast for assembly with the L-subunits (Figure 1.7) (Nishimura et al., 2008). Synthesis of the S-subunit pre-proteins in the cytosol equips them with an N-terminal targeting sequence (transit peptide) for transfer to and through the translocon outer and inner complexes (Toc/Tic) within the chloroplast double membrane. Within the chloroplast the transit peptide is cleaved by a stromal protein peptidase (SPP) to

produce a ~14 to 15 kDa mature S-subunit whose new Met-1 N-terminus is *N*-methylated by a methyltransferase (Houtz and Mulligan, 1991). Once processed the S-subunit assembles with the L-subunit with the aid of a range of generic and Rubisco-specific chaperones via a process that remains poorly understood (Whitney et al., 2011a; Whitney et al., 2015). Details on the *RbcS* multi-gene family and Rubisco assembly process are given in Chapter 3 and Chapter 4 respectively.

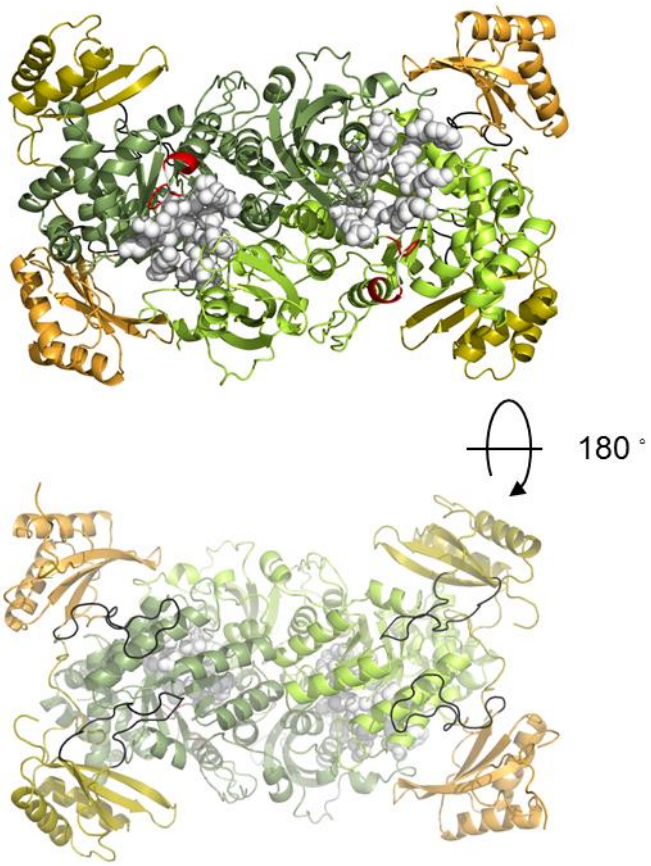

Figure 1.8 Architecture and subunit interactions in a L_2S_4 portion of L_8S_8 Rubisco.

The catalytic (or active) site of Rubisco (white) and Loop 6 (in red) is formed from conserved residues coded in the L-subunit (in green). The S-subunits (in yellow) are able to influence Rubisco catalysis despite their distance from the active site (van Lun et al., 2011). Interactions between the βA/βB loop of the S-subunit (shown in black) and adjoining L-subunit residues within central solvent channel (CSC) are considered key contacts involved in influencing the catalytic properties of Rubisco (Spreitzer et al., 2005)

1.2.2 Higher plant Rubisco subunits and their role in catalysis

The location of the higher plant L_8S_8 Rubisco (Section 1.1.5) catalytic (or 'active') site is positioned at the interface of L-subunits and are dimerised in an antiparallel L_2 fashion (Figure 1.8), where the C-terminal β/α barrel domain of each L-subunit and the N-terminal domain of the other L-subunit contribute conserved His, Gln, Glu, Thr and Lys residues to each active site (Stec, 2012). As the L-subunit harbours the active sites of Rubisco, a significant focus has been made on correlating changes in the L-subunit

sequence with natural catalytic variability measured for Rubisco from different plant, algae and prokaryotic sources (Parry et al., 2003; Galmés et al., 2005; Kapralov et al., 2011; Whitney et al., 2011b; Galmés et al., 2014).

The ability to express and assemble cyanobacteria L_8S_8 Rubisco in *E. coli* proved vital to mutagenic studies of Form I Rubisco in the 80's and 90's, in particular demonstrating the role of the S-subunit on catalysis. Although the S-subunit was found not to be absolutely essential for the assembly and function of cyanobacteria L_8 Rubisco cores, the addition of S-subunits stimulated activity 100-fold and provided structural stability (Andrews and Ballment, 1983; Andrews, 1988). Since these pioneering studies, subsequent mutagenic work using cyanobacteria (Read and Tabita, 1992), *Chlamydomonas* (Genkov and Spreitzer, 2009) and plant (Ishikawa et al., 2011) Rubisco have continued to highlight the pervasive influence of the S-subunit on catalysis. As a consequence of their tetrameric S-subunit arrangements at both apices of the L_8 core in Form I Rubisco (Figure 1.4), each L-subunit makes contact with three separate S-subunits (van Lun et al., 2011). Of particular interest are the interactions between the S-subunit βA/βB loop and residues within its most closely associated L-subunit. Mutations to residues in either subunit around this region have a significant influence on catalysis, despite their substantial distance from the active site (Figure 1.8) (Spreitzer et al., 2001; Spreitzer et al., 2005; Genkov and Spreitzer, 2009). Similar to cyanobacteria and *Chlamydomonas* L_8S_8 enzymes, the S-subunit βA/βB loops of higher plant Rubisco line the circumference at both ends of the central pore that traverses the holoenzyme (Spreitzer and Salvucci, 2002; Spreitzer, 2003; Andersson, 2008; van Lun et al., 2011). Determining the influence of the βA/βB loops and other S-subunit sequences on higher plant Rubisco catalysis remains elusive due to challenges in mutating S-subunits in leaf chloroplasts. Further details of these challenges are considered in Section 1.4.2 below and more thoroughly in Chapter 3.

1.3 CO_2 assimilation in C_3 and C_4 plants

1.3.1 C_3 versus C_4 photosynthesis

The primary distinguishing factor between C_3 and C_4 plants is the initial form or inorganic carbon assimilated into organic carbon. In C_3 plants CO_2 is the initial carbon substrate fixed by Rubisco to produce the 3-C product 3-PGA (Figure 1.1) in model plants species examples include tobacco, *Arabidopsis*, wheat and rice. In contrast C_4 plants are those containing a CCM where carbon assimilation begins with HCO_3^- fixation to phosphoenolpyruvate (PEP) by phosphoenolpyruvate carboxylase (PEPC) to

generate oxaloacetate (OAA). Commonly studied C_4 plants include maize, sorghum and *Brachypodium*.

An important advantage of C_4 photosynthesis is its capacity to improve the resource use of plants through the CCM delivering high CO_2 to Rubisco to avoid the carbon and energy costs of photorespiration (see Section 1.1.3). The shared principle of the varying types of C_4 CCM mechanisms is to fix HCO_3^- by the relatively fast activity of PEPC to produce C_4 acids in the mesophyll cells (MC) (Karki et al., 2013; Ludwig, 2013). These acids diffuse to neighbouring bundle sheath cells (BSC) where they are decarboxylated to release CO_2 either inside, or nearby to Rubisco, thus elevating CO_2 by >10-fold above atmospheric concentrations. This allows Rubisco to operate close to its maximal activity and has also enabled C_4 Rubisco to evolve substantial improvements in k_C^{cat} relative to its C_3 ancestors – albeit at the expense of CO_2 affinity (*i.e.* a higher K_m for CO_2). As a consequence of their CCM and faster Rubisco C_4 plants typically achieve higher photosynthetic rates with less Rubisco (*improving nitrogen use*) and at a lower stomatal conductance, thus reducing H_2O transpiration (*improving water use*) (Bailey et al., 2000; Ghannoum et al., 2005; Ghannoum et al., 2011; Pinto et al., 2014). These features provide C_4 plants with an advantage with respect to water and nitrogen use efficiencies and thus pose a mechanism of potential benefit to the yield potential of C_3 crops like rice (Hibberd et al., 2008). Differences between C_3 and C_4 photosynthesis are summarised in Table 1.3 below.

Table 1.3 Characteristic differences between C_3 and C_4 plants.

References: [(a)](Ludwig, 2013); [(b)](Edwards et al., 2004); [(c)](Furbank and Hatch, 1987); [(d)](Perdomo et al., 2015); [(e)](Schulze et al., 2013); [(f)](Kanai and Edwards, 1999); [(g)](Oaks, 1994).

Trait	C_3	C_4
Initial CO_2- fixing enzyme[(a)]	Rubisco	PEP carboxylase
Carbon product[(a)]	3-PGA (3C)	Oxaloacetate/malate (4C)
Location of CO_2 fixation[(b)]	MC	MC or BSC
Rubisco content[(c)]	90 nmol mg^{-1} chloroplast	22 nmol mg^{-1} chloroplast
Photorespiration[(d)]	Significant	Minimal due to leaf (Kranz) anatomy
Carbon-concentrating mechanisms[(e)]	None present	Present in bundle sheath cells
Cost per CO_2 fixed[(f)]	3 ATP and 2 NADPH	5 ATP and 2 NADPH
Advantages[(g)]	More efficient in cool, moist climates with moderate temperature and low light intensity.	More efficient in warm, dry climates high temperature and high light intensity. Better nitrogen use efficiency.

1.3.2 Modelling C_3 photosynthesis

The net amount of CO_2 present in the cells of C_3 leaves is influenced by three metabolic processes – photosynthetic CO_2 fixation, the rate of CO_2 release by photorespiration (Figure 1.1) and mitochondrial respiration (R_d). CO_2 fluxes through each of these processes are influenced by an array of regulatory mechanisms that all influence accurate modelling the rates of photosynthetic CO_2 assimilation (*A*). The 'industry standard' equations used to model CO_2 assimilation rates in C_3 plants were first derived by Farquhar et al., (1980) based on the basic understanding of photosynthetic biochemistry – in particular that of Rubisco. Essentially the value of *A* is *firstly* determined by Rubisco activity and its response to changes in CO_2 and O_2 levels and *secondly* is also affected by the supply of ATP and NADPH generated by electron flux during the photosynthetic light reactions (Figure 1.1) to fuel RuBP regeneration in the CBB cycle (Figure 1.1). As well *A* can become dependent on the rate of release of inorganic phosphate (P_i) during metabolism of the triose-phosphates produced in the CBB cycle (Bernacchi et al., 2013). The influence of each of the aspects on *A* under varying intercellular CO_2 pressures within the leaf cells (C_i) are shown in Figure 1.9.

Modelling *A* in C_3 plants continues to use the equations of Farquhar et al. (1980). Under low C_i where *A* is limited by Rubisco carboxylase activity the rates for *A* can be calculated using the equation:

$$A = \frac{B(C_i - 0.5xO/S_{C/O})k_C{}^{cat}}{C_i + K_c(1 + O/K_o)} - R_d \qquad \text{(Eq. 1)}$$

where *B* is the Rubisco active site content, C_i and *O* are, respectively, the concentration of CO_2 and O_2 in the chloroplast, $k_C{}^{cat}$ is the maximal rate of carboxylation and K_c and K_o are the Michaelis-Menten (K_m) constants for CO_2 and O_2 respectively (see section 2.5 for detail on how these parameters are measure). In this equation the CO_2 compensation point (typically shown as Γ*, is the C_i where the rate of carboxylation is equal to the rate of photophotorespiratory CO_2 release) is represented by the term (0.5 x *O*)/ $S_{C/O}$ where $S_{C/O}$ represents the Rubisco specificity for CO_2 over O_2 as determined by the equation:

$$S_{C/O} = (K_o \,.\, k_C{}^{cat}) \,/\, (k_O{}^{cat} \,.\, K_c) \qquad \text{(Eq. 2)}$$

When photosynthesis is limited by light dependent regeneration of RuBP the rate of *A* can be modelled by the equation:

$$A = J\,\frac{C_i - 0.5xO/S_{C/O}}{4(C_i + O/S_{C/O})} - R_d \qquad \text{(Eq. 3)}$$

where J is the rate of electron transport (assuming four electrons per reaction of carboxylation/oxygenation) supporting NADPH synthesis for RuBP regeneration. When A is limited by the rate of triose phosphate usage (TPU), A is determined by the equation:

$$A = 3TPU - R_d \qquad \text{(Eq. 4)}$$

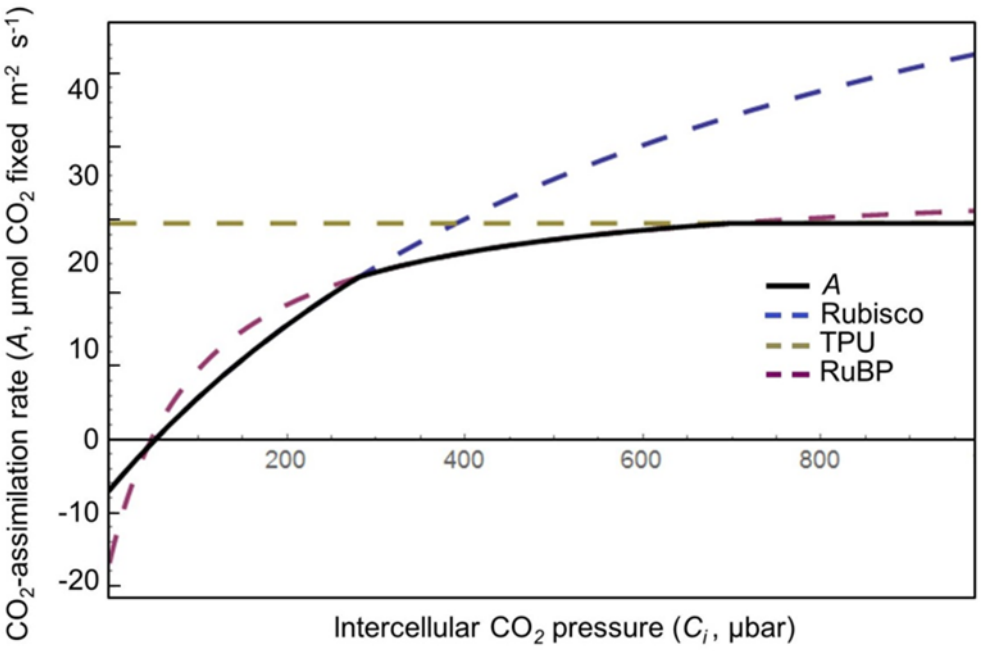

Figure 1.9 Representative *A*-C_i response curve for a C_3 plant.

Figure adapted from Bernacchi et al. (2013) to represent how rates of CO_2 assimilation (A) change in response to varying intercellular CO_2 levels in the leaves at 25°C modelled based on Rubisco carboxylase activity (Eq. 1, blue curve), electron transport rate dependent rates of RuBP regeneration (Eq. 3, red line) and Pi availability (Eq. 4, olive line). The black line represents the minimal rate of A modelled by each equation.

1.4 Rubisco engineering in leaf chloroplasts

1.4.1 Tobacco as a model plant for transgenic studies

Tobacco is a common C_3 plant model for both stable and transient transgenic studies. Of the 64 *Nicotiana* species (Smith, 1968), *N. tabacum* is the world's most common commercial tobacco plant (Figure 1.10). It is an amphiploid species (2n=48) that was produced from an inter-specific cross between *N. sylvestris* Spegazzini and Comes♀ (2n=24) and *N. tomentosiformis* Goodspeed♂ (2n=24) (Gray et al., 1974). In addition to being the first plant species to have its plastome fully sequenced (Shinozaki et al., 1986), *N. tabacum* is also renowned as the preferred species for chloroplast transformation studies due to the high efficiency of successful transformation in cultivars such as Petit Havana (Svab et al., 1990) and Samsun (Mäenpää et al., 2000).

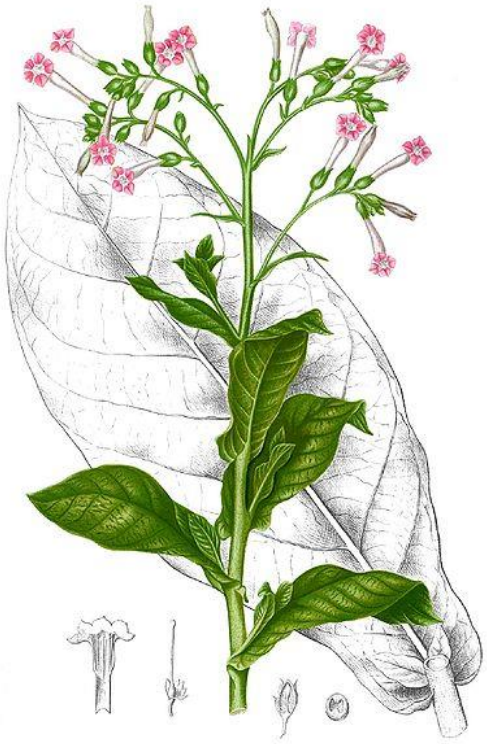

Figure 1.10 Wild-type *Nicotiana tabacum* cv. Petit Havana.

N. tabacum is commonly used as a model system for transgenic studies in higher plants, in particular the application of plastome transformation (Maliga, 2004).

1.4.2 The goals and limitations to bioengineering Rubisco in leaf chloroplasts

Transgenic research on Rubisco over the past 30 years in photosynthetic organisms has highlighted its pivotal influence on photosynthesis. This, along with the finding that Rubisco from non-green algae have better catalytic properties than plant Rubisco (Whitney et al., 2001; Andrews and Whitney, 2003) (detailed further in Chapter 4), have driven Rubisco biologists to identify solutions that improve Rubisco catalysis. On top of this challenge is identifying transgenic approaches to introducing beneficial changes to Rubisco function into plant leaves – in particular crops species. Ultimately by improving Rubisco catalysis it is hoped that photosynthesis can be improved and crop yield increased. In addition, improving Rubisco performance may potentially improve resource-use efficiency by reducing a plants' need for nitrogen (invest less in a more efficient Rubisco), water (lower the C_i levels needed for photosynthesis thereby reducing stomata aperture and water transpiration) or/and light (reduced photorespiration thereby saving energy) (Andrews and Whitney, 2003; Whitney et al., 2011a; Parry et al., 2013). A key limitation to structure-function studies of L_8S_8 Rubisco from higher plants is their inability to assemble in *E. coli* due the incompatibilities in their folding and assembly requirements (Parry et al., 2013). For this reason, genetic

modification of plant Rubisco has been limited by the slower processes associated with generating transgenic plants.

Although the S-subunits of higher plant Rubisco are essential to the enzymes holistic function (see Section 1.2.2), the majority of mutagenic analyses undertaken on higher plant Rubisco have focused on the L-subunit. Primary reasons for this are the location of the catalytic sites within the L-subunit (Figure 1.6), the relative ease of genetically modifying *rbcL* by chloroplast (plastome) transformation (Section 1.4.3) and due to limitations in genetically mutating *RbcS*. The latter limitations stem from there being multiple allelic copies of *RbcS* in the nucleus of plant cells – up to 22 copies in some species (Manzara and Gruissem, 1988; Spreitzer, 2003) – that appear to be differentially expressed in response to growth and environmental cues and code varying degrees of amino acid diversity (Sasanuma, 2001; Ogawa et al., 2011). Such factors complicate mutagenic or replacement strategies targeting *RbcS* (Whitney et al., 2011a). More details on prior S-subunit engineering undertakings are provided in Chapter 3.

1.4.3 Transgenic manipulation of Rubisco by plastome transformation

Plastome transformation was originally developed in *Chlamydomonas* (Boynton et al., 1988) before being applied to modify the small chloroplast genome (plastome; ~160 kb) of higher plant chloroplasts (Svab et al., 1990). The technology is available for a limited range of plant species that includes a few important crop species – tomato, potato soybean and cotton (Daniell et al., 2005; Day and Goldschmidt-Clermont, 2011; Maliga and Bock, 2011). The transformation process remains most efficient in *N. tabacum* (cv Petit Havana SR1) where flanking plastome sequence (typically ~1 kb) included either side of the genetic changes guide their introduction into the plastome with pinpoint accuracy via homologous recombination. Among the genetic modifications introduced is typically the *aadA* selectable marker that confers resistance to the antibiotics spectinomycin and streptomycin. Using this approach a variety of mutations have been made to the tobacco *rbcL* in a bid to examine structure-function relationships and better understand Rubisco biogenesis in plant plastids (Andrews and Whitney, 2003; Sharwood et al., 2008; Whitney et al., 2011b; Whitney et al., 2015). Initial deletion of *rbcL* prevented Rubisco synthesis while the re-introduction of *rbcL* into the nucleus only partially recovered leaf Rubisco content (Kanevski and Maliga, 1994). This confirmed the preferred location of *rbcL* in the plastome. Other plastome transformations have produced site-directed L-subunit mutants (Whitney et al., 1999; Whitney et al., 2011a), shown the folding requirements of marine algae Rubisco

subunits are not met in higher plants (Whitney et al., 2001), demonstrated plastid synthesised S-subunit could partially compete with endogenous cytosol made S-subunit for assembly into L_8S_8 (Whitney and Andrews, 2001a; Dhingra et al., 2004) and confirmed the feasibility of heterologous Rubisco subunit assembly (Kanevski et al., 1999; Whitney et al., 2011a; Zhang et al., 2011; Whitney et al., 2015). Directly replacing *rbcL* with those coding Form II bacterial L_2 Rubisco or Form III Archaea L_{10} Rubisco demonstrated the feasibility that plant photosynthesis could be supported by Rubisco isoforms from divergent evolutionary lineages (Whitney and Andrews, 2001b; Whitney and Andrews, 2003; Sharwood et al., 2008; Alonso et al., 2009).

Since 2008, most of the Rubisco engineering studies in plastids have taken advantage of a higher transformation efficiency tobacco master-line called ^{cm}trL (*i.e.* the (**c**odon-**m**odified **t**obacco-***r****ubrum*** **L**ine) specifically designed for manipulating Rubisco subunits (Figure 1.8) (Whitney and Sharwood, 2008). In ^{cm}trL, the native *rbcL* has been replaced with a codon modified *rbc*M (^{cm}*rbcM*) coding for *R. rubrum* L_2 Rubisco. The *aadA* selectable marker has also been removed in ^{cm}trL permitting its subsequent re-transformation (Whitney and Sharwood, 2008). The lack of sequence similarity between the native tobacco *rbcL* and ^{cm}*rbcM* prevents unwanted recombination events occurring within ^{cm}*rbcM*, ensuring its complete replacement with mutated tobacco or foreign *rbcL*. These salient features of ^{cm}trL makes it a highly useful technological tool for screening the assembly competency and catalytic properties of recombinant Rubisco mutants in plant plastids.

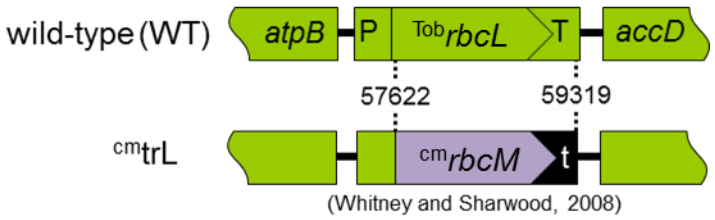

Figure 1.11 Genetic variations between the plastome of the ^{cm}trL and wild-type tobacco genotypes.

Region of genome divergence is indicated by the nucleotide numbering that correlates to the tobacco plastome sequence (Genbank accession number Z00044). P, *rbcL* promoter and 5'UTR sequence; *rbcL*, gene coding the tobacco L-subunit; ^{cm}*rbcM*, codon modified gene coding *R. rubrum* L_2 Rubisco T, *rbcL* 3'UTR sequence; *T*, 112-base pair (bp) of *psbA* 3'UTR sequence (Whitney and Sharwood, 2008).

1.5 Primary objectives of thesis

The ultimate goal of this thesis is to create novel opportunities and technologies that expand the bioengineering potential of higher plant Rubisco. Transformation strategies developed over the past 20 years to surpass nature's attempt at *in vivo* Rubisco evolution have instead realised our incomplete understanding of the enzymes biogenesis requirements and difficulty in improving its catalysis. Being able to produce plant Rubisco complexes comprising homogeneous populations of native and mutated L-subunits and S-subunits is critical to understanding their structure-function interactions and identifying solutions to improve catalysis. This thesis examines the feasibility of using RNA interference (RNAi) to fully silence *RbcS* mRNA synthesis in the ^{cm}trL genotype and then test the efficiency of alternative transgenic approaches for bioengineering recombinant Rubisco comprising chloroplast made L- and S-subunits and their effect on L_8S_8 Rubisco biogenesis, catalysis and leaf photosynthesis.

To assist the reader a summary of the transplastomic tobacco genotypes studied in this thesis and detail of their Rubisco transgenes is provided in Appendix A.

CHAPTER 2 – MATERIAL AND METHODS

2.1 Molecular techniques

2.1.1 E. coli growth and transformation

$CaCl_2$ competent XL1-Blue *E. coli* were made for DNA transformation as described by Sambrook et al., 1989. A 10 mL culture of XL1-Blue *E. coli* cells was grown for 16 h in Luria-Bertani (LB) medium (10 g L^{-1} tryptone, 5 g L^{-1} NaCl, 5 g L^{-1} yeast extract, with the pH adjusted to 7.0 with 1 M NaOH) at 37°C and used to inoculate 1 L of pre-warmed LB medium. After incubating for 4 to 5 h at 37°C the cells reached mid-log phase growth (OD600 of ~0.5 to 0.7) and were immediately dispensed into autoclave sterilised GSA centrifuge tubes and placed on ice. After 10 min the tubes were placed in a pre-chilled (4°C) GSA rotor (SORVALL®) and centrifuged 3000 *g* for 5 min at 4°C. The pelleted cells were gently suspended in 10 mL of ice cold sterile 0.1 M $CaCl_2$ containing 15% (v/v) glycerol. After 20 min on ice 0.6 mL aliquots of the cells were dispensed into sterile 1.8 mL microfuge tubes, snap-frozen in liquid N_2 and stored at -80°C.

E. coli colonies were grown on agar solidified (1.5% [w/v]) LB medium. LB-amp medium contained ampicillin (200 µg mL^{-1}; made from a 1000-fold dilution of 200 mg mL^{-1} stock dissolved in sterile Milli-Q H_2O). Transformed colonies were identified as colonies on the LB-Amp plates grown upside-down at 37°C for 16 h. Single colonies were picked aseptically in a laminar flow cabinet and used to inoculate 1.5 mL (for mini-prep cultures) or 100 mL (for maxi-prep culture) of LB-amp medium and grown for 16-20 h at 37°C in a shaking incubator (set at 180-200 opm).

2.1.2 Plasmid DNA purification

pDNA mini-preps

Plasmid DNA (pDNA) from mini-prep cultures of transformed XL1-Blue *E. coli* cells was extracted and purified using the Wizard® Plus SV Minipreps DNA Purification System Kit (Promega). All steps were carried out at room temperature (RT). Mini-prep cultures were transferred to a sterile 1.8 mL microfuge tube and pelleted by centrifugation (1 min, 10,000 *g*). The cells were suspended in 0.25 mL Cell Resuspension Solution (50 mM Tris-HCL (pH 7.5), 10 mM EDTA, 100 µg mL^{-1} RNase A) prior to adding 0.25 mL Cell Lysis Solution (0.2 M NaOH, 1% SDS) and 10 L of alkaline protease. After 5 min at RT temperature 0.35 mL of neutralization solution (4.09 M guanidine hydrochloride, 0.759 M potassium acetate, 2.12 M glacial acetic acid,

pH ~4.2) was added and the reaction mixed by repeated inversion then centrifuged (5 min, 16,000 *g*). The supernatant was transferred to a spin-column and the pDNA immobilised on the membrane by centrifugation (1 min, 8,000 *g*) and then washed twice with successive 0.4 mL aliquots of wash buffer (60% ethanol, 60 mM potassium acetate, 8.3 mM Tris-HCl pH 7.5, 0.04 mM EDTA pH 8.0) with intermittent centrifugation (3 min, 16,000 *g*). The bound pDNA was eluted from the membrane with 70 µL nuclease-free water by centrifugation (2 min, 8 000 *g*).

pDNA maxi-preps

pDNA purification from 100 mL cultures of *E.coli* was carried out using the Plasmid Maxi Kit (QIAGEN). Cultured cells were pelleted in 50 mL Falcon tubes by centrifugation (4800 *g*, 4°C, 15 min) then suspended in 10 mL buffer (50 mM Tris-Cl, pH 8.0, 10 mM EDTA, 100 µg mL^{-1} RNase A) and transferred to a SS34 centrifuge tube before adding and equal volume of Lysis Buffer (200 mM NaOH, 1% SDS [w/v]). After 5 min at RT, 10 mL of Neutralization Buffer (3.0 M potassium acetate, pH 5.5) pre-chilled to 4°C was added and the tube incubated on ice for 20 min to promote SDS precipitation. The sample was centrifuged at 12,000 *g*, 15 min at 4°C and the supernatant transferred to a QIAGEN-tip 500 column equilibrated with Equilibration Buffer (750 mM NaCl, 50 mM MOPS, 15% isopropanol (v/v), 0.15% Triton® X-100 (v/v), pH 7.0). After sample application the column was rinsed with two amounts of 30 mL Wash Buffer (1.0 M NaCl, 50 mM MOPS, 15% isopropanol (v/v), pH 7.0) before eluting the pDNA with 15 mL of Elution Buffer (1.6 M NaCl, 50 mM MOPS, 15% isopropanol (v/v), pH 7.0) into an SS34 tube. To the pDNA sample was added 10.5 mL isopropanol before centrifuging at 17,000 *g* for 30 min at 4°C. After carefully decanting the supernatant, DNA pellet was washed with 70% ethanol (v/v) and re-centrifuged (17,000 *g*, 10 min, 4°C). The purified pDNA pellet was air dried and resuspended in 500 µL TE buffer (10 mM Tris-Cl pH 8.0 and 1 mM EDTA) then stored at -20°C until use.

2.1.3 Genomic DNA extraction

Cetyltrimethylammonium bromide (CTAB) gDNA extraction

Tobacco leaf samples (0.5 cm^2) were placed in 1.8 mL microfuge tubes and immediately snap-frozen in liquid N_2 and stored at -80°C. Total genomic DNA (gDNA) was extracted using a modified method of Saghai-Maroof et al. (1984). Leaf samples were homogenized in 0.5 mL of 60°C heated CTAB buffer (2 % [w/v] CTAB [hexa-

decyl-trimethyl ammonium bromide], 20 mM Tris-Cl pH 8.0, 1.4 M NaCl, 20 mM EDTA, 1 % [w/v] PVP-40 [polyvinylpyrrolidone] and 0.02 % [w/v] DTT) using a stainless steel pestle attached to an electric drill (MAKITA). The lysed sample was placed in a water bath at 60°C for 20 min before adding 0.5 mL chloroform and then mixing by inverted shaking for 15 s. The sample was centrifuged at 16,000 *g*, 4°C, 15 min to allow phase separation. The upper aqueous phase (~0.45 mL) containing the gDNA was carefully removed by pipette and added to a sterile 1.8 mL microfuge tube containing 1 mL 100% ethanol at RT. The tube was inverted several times to mix and then centrifuged at 16,000 *g* at RT for 1 min to precipitate the gDNA (and RNA). The pelleted gDNA was washed twice with 1 mL 70% (v/v) ethanol and then the ethanol was removed using a pipette. The pellet was left to air dry before dissolving in 0.1 mL TE buffer. Once in solution the gDNA was stored on ice in the short term, or at -20°C for longer storage.

QIAGEN Plant Mini gDNA extraction kit

gDNA was extracted from some leaf tissue samples by lysis with an electric drill in 0.7 mL of DNeasy® (Qiagen) Plant Mini-spin Lysis Solution, followed by further extraction steps as specified by the manufacturer. The purified gDNA was ultimately eluted from the spin-column membrane in 100 µL TE buffer and stored at -20°C until use.

2.1.4 Restriction enzyme digests

DNA digestion with restriction enzymes was performed as described by the various suppliers (Promega; MBI Fermentas; and NEW ENGLAND BioLabs). A standard digest contained 0.5 µL of restriction enzyme(s) (*i.e.* ~5 units) and 2 µL 10× restriction enzyme buffer, made up to final volume of 20 µL using nuclease-free water and the pDNA or gDNA for digest (typically 0.5 to 4µg depending on the application). Digests were incubated at 37°C in an oven for at least 3 h. For digests of vector pDNA, 0.5 µL of alkaline phosphatase (1 unit, Promega) was added for the final 15 min of the 37°C incubation period to prevent self-ligation of the digested vector.

2.1.5 DNA electrophoresis

Digested DNA were analysed using 1% (w/v) agarose (Promega) gels buffered in TAE (40 mM Tris-acetate pH 8.5, 1 mM EDTA) containing 0.01% (v/v) SYBR® Safe DNA Gel Stain (Invitrogen). Digested DNA samples were diluted with 0.2 volume of gel-loading buffer (GLB, 0.25% [w/v] bromophenol blue and 30% [v/v] glycerol) or the

Fermentas 6× loading buffer and electrophoresed along with the 1 kb GeneRuler DNA marker (Fermentas) at 80 V for ~45 min. The separated DNA fragments were visualised with a blue-light illuminator and their sizes estimated relative to the 1 kb ladder bands. Where required, DNA fragments were excised from the gel using a scalpel blade, placed in a sterile microfuge tube and the DNA isolated using the Wizard® SV Gel and PCR Clean-Up System (Promega). This process involved adding 0.4 mL of Membrane Binding Solution (4.5 M guanidine isothiocyanate, 0.5 M potassium acetate pH 5.0) to the excised gel fragment then incubating at 65°C for 10 min. The solution was then transferred to a DNA binding spin-column, centrifuged (8000 *g*, 1 min) and then washed twice with Membrane Wash Solution (10 mM potassium acetate, 80% ethanol, 16.7 µM EDTA). The purified DNA was eluted from the membrane in a final volume of 30 µL sterile H_2O (heated to 65°C to maximise DNA recovery).

2.1.6 DNA ligations

Ligation of gel purified restriction digested fragments of the pDNA vector and DNA insert was achieved with T4 DNA ligase (Promega) according to manufacturer specifications. Ligation reactions with vectors between 3.0 kb and 3.8 kb were undertaken for 1 h at RT whereas reactions with vectors between 3.8 kb and 6.0 kb were ligated overnight at 4°C. The ligation reactions (10 µL total volume) were transformed into $CaCl_2$ competent XL1-Blue cells (see Section 2.1.1)

2.1.7 Primer design and storage

Primers were typically designed to be 20 to 24 nucleotides (nt) in length, with maximal sequence specificity, and incorporated desired restriction sites to assist in the cloning of the amplified products. The synthesized primers (Sigma) were resuspended in nuclease-free 0.1× TE buffer to a final concentration of 100 µM and these stocks stored at -20°C. Working stocks of 10 µM were simultaneously made for use in PCR.

2.1.8 PCR amplification

Genes of interest were amplified using either 2×PCR Master Mix from Promega (low fidelity) or Phusion (high fidelity). The standard thermocycling protocol was carried out with a denaturing step at 94°C for 2 min followed by 35 cycles of three steps; 1) 94°C for 30s (denaturing) 2) 50°C for 30s (primer annealing, with the temperature varied depending on primer G/C content) and 3) 72°C for 1 min per kb of the target gene (elongation). All PCRs were in volumes of 40 µL and were carried out in FTS-960

Thermal Sequencer (Corbett Research). PCR amplification products were separated and visualized using agarose gel electrophoresis and the desired fragments gel purified (see Section 2.1.5) for sequencing (see Section 2.1.9), digestion or cloning into an appropriate vector.

2.1.9 DNA sequencing

DNA sequencing was undertaken using the BigDye® Terminator Cycle Sequencing Kit (Life Technologies) on an ABI 3730 sequencer (Biomolecular Resource Facility (BRF), JCSMR, ANU). A 20 µL reaction contained 1 µL of 100-200 ng of template DNA, 3.5 µL of 5× buffer (400 mM Tris-HCl, pH 9.0; 10 mM $MgCl_2$), 1 µL of BigDye mix and 0.2 µM of a primer specific for the target gene. Sequencing reactions included a denaturing cycle at 94°C for 5 min followed by 30 cycles of three steps; 1) 96°C for 10 s, 2) 50°C for 10 s and 3) 60°C for 4 min. Products from the sequencing reactions were processed for analysis by adding 2 volumes of 100% ethanol and 0.1 volume of 3 M sodium acetate (pH 5.2) to precipitate the DNA. After 15 min on ice the samples were centrifuged (16,200 *g*, 5 min, 4°C) and the DNA pellet washed three times with 300 µL of 70% (v/v) ethanol. The pelleted DNA was vacuum-dried and processed for sequencing by the BRF (ANU).

2.1.10 [^{32}P]-labelled DNA probe synthesis and hybridisation

Appropriate DNA fragments (probes) homologous to target DNA and mRNA sequences for detection were labelled with [^{32}P] by random incorporation of α-[^{32}P]-dATP using the Prime-a-Gene®Labeling System (Promega). DNA template (25 ng) diluted to 10 µL with sterile H_2O was denatured by heating to 95-100°C for 2 min in a dry block heater (Thermoline Scientific) and then rapidly cooled on ice for 1 min before adding to a tube containing 15 µL of reaction mix (5 µL 5 x Labelling Buffer, 2 µL dNTP mix [containing 500 µM dCTP, dGTP and dTTP], 2 µL of 2 mg mL^{-1} nuclease-free BSA, 2.5-5 µL α-[^{32}P]-dATP [50 µCi], 5 U of DNA Polymerase I Large [Klenow] fragment and sterile H_2O up to 15 µL). After incubating at RT for 30-90 min, each [^{32}P]-labelled DNA probe was purified using the Wizard® SV Gel and PCR Clean-Up System (Promega) (see Section 2.1.5) and eluted in 0.1 mL sterile H_2O. The probes were stored at -20°C until use.

The DNA (see Section 2.1.3) or RNA (see Section 2.1.12) bound to nylon membranes were incubated for 3 h at 55ºC in pre-heated 5-10 mL of AlkPhos Direct™ Hybridisation Buffer (GE Healthcare) contained within a hybridisation cylinder

(Hybaid). The [^{32}P]-DNA probe was first denatured at 95^{o}C for 2 min immediately prior to adding ~25 µL into the hybridising membranes at 55^{o}C. After >16 h of hybridisation, the membranes was rinsed twice for 20 min with 200 mL of 0.5× SSC buffer (75 mM NaCl, 7.5 mM tri-sodium citrate, pH 7.0, 0.1% [w/v] SDS) at 55 ^{o}C. The membrane was then blot dried and wrapped in Cling wrap before exposure to a Storage Phosphor Screen GP (Kodak). After 2-96 h the [^{32}P]-DNA hybridisation signals were visualised using a PharosFX Plus Molecular Imager (BIORAD) and analysed using Quantity One software (BioRad).

2.1.11 DNA blot analyses

Extracted leaf gDNA (see Section 2.1.3) was digested at 37°C overnight with restriction enzymes (see Section 2.1.4) and the DNA separated on 0.8% (w/v) TAE agarose gels (see Section 2.1.5). Southern blotting was carried out as described (Sambrook et al., 1989) prior to hybridising with a [^{32}P]- labelled probe (see Section 2.1.10). In summary the separated DNA was denatured by soaking the gel for 20 min in denaturing solution (1.5 M NaCl; 0.5 M NaOH) with slight agitation before briefly rinsing twice in ultrapure H_2O. The cut gDNA was transferred to Hybond^{TM} –N^{+} nylon membrane (GE Healthcare) by placing the agarose gel onto blotting paper on top of an elevated surface (e.g. an upside-down agarose gel tray). The edges of the blotting paper overlapped into a 0.5 L reservoir of transfer buffer (1 M ammonium acetate, 20 mM NaOH). Strips of overhead transparency were overlayed around the edges of the gel to frame the outside of the lanes where the DNA was loaded. Layered on top of the gel was a pre-wetted nylon membrane and 3 layers of blot paper topped with wads of dry paper towelling. DNA transfer from the gel onto the membrane via capillary action was allowed to occur overnight before the membrane was removed and the DNA cross linked to the membrane by UV irradiation using a UV X-linker (Stratagene®). The membrane was stored in Gladwrap at 4^{o}C until ready to probe.

2.1.12 RNA extraction

Tri-Reagent® method

Samples (0.4 cm^2 leaf punches up to 0.8 mg in weight) of healthy tobacco leaves were transferred to sterile microfuge tubes and snap-frozen in liquid N_2 and stored at -80°C. The leaf samples were homogenized into 800 µL of Tri-Reagent (Sigma) using a micro-fuge pestle attached to an electric drill. After 10 min at RT, 160 µL of chloroform was added to the samples and mixed by rapid shaking. RNA extraction by phase separation

was left to occur at RT for 5 min before centrifuging 16,400 *g*, 15 min at 4°C. The aqueous upper-phase (~470 µL) was transferred to a fresh sterile microfuge tubes containing 400 µL isopropanol. The tubes were inverted several times and left at RT for 10 min before pelleting the RNA by centrifugation (16,400 *g*, 10 min, 23°C). The RNA was washed twice with 500 µL 75% (v/v) ethanol before drying for 15 min in a 50°C oven. Dried RNA pellets were resuspended in 30 µL TE buffer and placed on ice for immediate use or snap-frozen in liquid N_2 and stored at -80°C.

QIAGEN RNA extraction kit

Leaf samples (up to 0.8 mg wet weight) were homogenized in 450 µL Buffer RLT (as provided by kit) and vigorously mixed for 10 s by vortex. The sample was then centrifuged (16,400 *g*, 10 min, 23°C) and the supernatant transferred to a QIAshredder spin column and the remaining extraction process carried out according to the manufacturer instructions. The purified RNA was eluted from the RNeasy spin column in two volumes of 30 µL RNase-free water, snap-frozen in liquid N_2 and then stored at -80°C until use. RNA concentrations were quantified by absorbance with a spectrophotometer at 260 nm with an assumed $1A_{260} = 40$ µg mL^{-1} RNA

2.1.13 RNA blot analyses

RNA slot blot /RNA electrophoresis

RNA slot blot analysis was undertaken using the Bio-Dot® SF Cell (Bio-Rad). An Immun-Blot® PVDF Membrane (BIO-RAD) was soaked in sterile water for 10 min prior to assembly of the Bio-Dot® SF Cell apparatus. Once assembled, RNA denaturizing solution (10 mM NaOH, 1 mM EDTA) was added to each well and removed by a gentle vacuum applied to the apparatus. RNA samples were diluted 1:100 with sterile water and ice cold Denaturizing Solution was added to samples immediately before use. RNA samples were added to the wells of the Bio-Dot® SF Cell and bound to the membrane by gentle vacuum. The applied RNA was then washed with RNA Denaturizing Solution, thoroughly dried under vacuum and then the RNA immobilised onto the membrane by UV cross-linking using a UV Stratalinker® 1800 (STRATAGENE). The membrane was wrapped in GladWrap and stored at 4°C until use. RNA samples for analysis by denaturing formaldehyde agarose gel electrophoresis were prepared by adding 39.2 µL gel loading buffer (14 µL formamide, 4.6 µL formaldehyde, 0.6 µL 0.5 M EDTA, 1.1 µL 1 M Na_2HPO_4, pH 6.8; 0.6 10 mg mL^{-1} ethidium bromide, 11.2 µL 6× DNA Loading Dye [Thermo Scientific]) to 5 µg of RNA

in a final volume 67.2 µL. Samples were heated at 65°C for 15 min just prior to electrophoresis, cooled rapidly on ice for >2 min before loading on a 1.2% (w/v) agarose solidified denaturing formaldehyde gel (autoclaved solution of 0.72 g agarose in 55.2 mL of 21.7 mM sodium phosphate buffer (pH 6.8) to which 4.8 mL of formaldehyde solution (37% [w/v] is added once cooled to 55°C). The gel was run at 80 V for 3 h and the gel tank buffer (5.4 mL 1 M $NaHPO_4$, pH 6.8; 41.4 mL formaldehyde [37%]; made up to 500 mL with sterile water) was mixed every 15 min to prevent formation of a pH gradient.

RNA blot hybridisation and visualisation

[^{32}P]-labelled probes were prepared and hyrbidised to the membranes as described in Section 2.1.10. The membranes were left in cassettes for at least 48 h before [^{32}P] signals from labelled probes hybridized to the membrane were visualized using a PharosFX Plus Molecular Imager and analysed using Quantity One software (BioRad).

2.2 Protein analysis techniques

2.2.1 Protein extraction and concentration assay

Leaf disc samples (0.5 cm^2 in area) from either tissue cultured plantlets or soil-grown plants were snap-frozen in liquid N_2 and stored at -80°C in 1.8 mL microcentrifuge tubes. Using 2 mL glass tissue homogenizers (Wheaton® USA) the leaf protein was isolated in 0.5 to 1 mL ice cold extraction buffer (50 mM EPPS-NaOH pH 8.0, 1 mM EDTA, 10 mM $MgCl_2$, 2 mM DTT and 1% [w/v] PVPP, 0.1%

[v/v] plant protease inhibitor [Sigma]) and the soluble protein recovered by centrifugation (16,400 *g*, 5 min, 4°C). Aliquots of the protein were taken for PAGE analysis (see Sections 2.2.2 and 2.2.3), Rubisco content quantification (see Section 2.5.1) and Rubisco catalysis measurements (see Section 2.5.2). The soluble protein content was also determined using the Coomassie Plus Protein Assay Reagent (Pierce) against BSA standards (0, 5 and 10 µg mL^{-1}, Pierce) according to manufacturer instructions.

2.2.2 Non-denaturing (nd)PAGE electrophoresis

An aliquot (160 µL) of each soluble leaf protein was mixed with 40 µL non-denaturing (nd) gel loading buffer (80% [v/v] glycerol; 0.01% [w/v] bromophenol blue) and maintained on ice until analysed by ndPAGE. Samples and appropriate controls were loaded onto 4-12% Tris-Glycine gels (Novex®, Life Technologies) and separated by electrophoresis at 60 V in pre-chilled running buffer (25 mM Tris, 192 mM glycine) at 4°C for 16 h using a XCell SureLock™ Electrophoresis Cell (Novex®). The gel was

removed from its cassette and placed in fixing solution (50% [v/v] methanol, 10% [v/v] glacial acetic acid in Milli-Q water) and gently shaken for 15-45 min using an orbital shaker (BIO-LINE) before washing extensively with repeated changes of 100 mL Milli-Q water every 15 min for 1-2 h. The separated protein bands were then visualised using Gelcode Blue Stain Reagent (Pierce). After incubating for >1 h the excess stain was removed by multiple washes with Milli-Q H_2O. Gel images were scanned at 600 dpi using an Epson dual illumination flatbed scanner.

2.2.3 SDS-PAGE electrophoresis and western blot analyses

SDS-PAGE electrophoresis

Samples of leaf protein (see Section 2.2.1) were also diluted 1:3 with 4× SDS-PAGE gel loading buffer (125 mM Tris-HCl, pH 6.8; 40% [v/v] glycerol; 4% [w/v] SDS; and 75 mM 2-mercaptoethanol). Prior to electrophoresis the samples were boiled for 5 min and then centrifuged (16,400 *g*, 5 min, RT). Each sample and appropriate molecular weight marker standards were loaded onto a 4-12% Bis-Tris gel (Novex®, Life Technologies) and separated using MES buffer (50 mM MES, 50 mM Tris, 0.1% [w/v] SDS, 1 mM EDTA) at 200 V in an XCell SureLock Electrophoresis Cell (Novex®). Gels intended for staining were fixed, washed and stained with Gelcode Blue Stain Reagent as described in Section 2.2.2.

Western blot detection and visualisation

Gels intended for protein (western) blotting were placed in an XCell II Blot Module (Novex®) adjacent to Hybond™-C Extra nitrocellulose membrane (GE Biosciences). Assembly of the blotting "sandwich" incorporated (from the cathode (-) side of the blotting rig) a pre-wetted sponge, a piece of blotting paper, the gel, nitrocellulose membrane, piece of blotting paper and additional wet sponges to fill the blot module. The "sandwich" was submerged in western transfer buffer (25 mM Bicine, 25 mM Bis-Tris, 1 mM EDTA) and the transfer made at a constant 25 V (the current at ~150 mA initially) for 1 h. After transfer the membrane was incubated in appropriate blocking solution (Table 2.1) for 1 hour at room temperature (RT) or overnight at 4°C. The membranes were then rinsed with TBS buffer (50 mM Tris-Cl, 150 mM NaCl, pH 7.6) and appropriate dilutions of a primary (1°) antibody added. After 1 h of gentle shaking at RT the membranes were rinsed with three 5 min washes of TBS buffer before adding the appropriate secondary (2°) antibody (Table 2.1).

Table 2.1 Blocking reagent, primary and secondary antibodies used in western blot analyses.

Antibody type	Blocking reagent	1° antibody	2° antibody
Tobacco Rubisco	milk powder (5% [w/v] dried milk powder in TBS buffer)	5 µL in 15 mL 1× TBS	3 µL BioRad Goat Anti-Rabbit Alkaline Phosphatase Conjugate (BIO-RAD, # 170-6518) in 15 mL 1× TBS
Galdieria sulphuraria Rubisco		15 µL in 15 mL 1× TBS	
Penta-His (QIAGEN, 34460)	15 mL of 3% (w/v) BSA 1× TBS buffer	20 µL in 15 mL 3% BSA (w/v) in 1× TBS	3 µL BioRad Goat Anti-Mouse Conjugate (BIO-RAD, # 170-6520) in 10 mL 10% (w/v) skim milk in 1× TBS

Immunoreactive proteins were visualised using the AttoPhos® AP Fluorescent Substrate System (Promega). Blots were placed protein-side down in a sterile petri-dish containing 0.06 mg mL^{-1} Attophos® substrate with AttoPhos buffer (Promega) for 1-15 min (depending on concentration of protein to be visualised and efficiency of antibody) before being blotted dry with Kimwipes (Kimberly-Clark PROFESSIONAL®), and the immuno-reactive chemi-fluorescent bands imaged using a Pharos FX Plus Molecular imager (BIO-RAD). The digital images were analysed using the Quantity One® (BIO-RAD) software.

2.2.4 Immobilized Metal-Affinity Chromatography (IMAC)

IMAC purification was performed using Ni-NTA Agarose (Qiagen). A 1 mL bed volume of Ni-NTA was prepared in a 10 mL polypropylene Econo column (BioRad) and equilibrated in IMAC buffer (300 mM NaCl, 50 mM Tris-Cl, pH 8.0) by gravity flow. Leaf tissue was ground into a fine powder in a pestle and mortar containing liquid N_2 and then further homogenised in 5-20 mL of ice-cold IMAC extraction buffer (IMAC buffer with 1 mM PMSF, 5 mM Mercaptoethanol, 1% [w/v] PVPP) in pre-chilled 10-40 mL glass homogenisers (Wheaton). Following centrifugation (20,000 x g, 10 min, at 2 ^{o}C) the soluble leaf protein was passed through the column and then washed with 5 column volumes of IMAC wash buffer. His-tagged bound protein was then eluted with 3 successive applications of 0.5× bed volumes of IMAC elution buffer (wash buffer with 200 mM Imidazole). The eluted purified Rubisco was equilibrated with Rubisco assay buffer (see Section 2.5.2) via successive passages and washes through an Amicon® Ultra-15 Centrifugal Filter Device with a nominal molecular weight exclusion size of 100 kDa. The IMAC purified Rubisco samples were analysed by PAGE (see Section 2.2.2) and [^{14}C]-CABP binding (see Section 2.5.1), and used to measure $S_{c/o}$ and CO_2-fixation rate (see Section 2.5.2).

2.3 Plant maintenance, tissue culture techniques

2.3.1 Seed germination

Nicotiana tabacum (cv Petit Havana *N,N*) was the tobacco cultivar used in all transformation experiments. When growing sterile *N. tabacum* plants the seed were germinated on MS medium that contained Macro nutrients (18.5 mM KNO_3, 1.5 mM $MgSO_4 \cdot 7H_2O$, 4.45 mM $CaCl_2 \cdot 6H_2O$, 1.25 mM KH_2PO_4, and 20 mM $(NH_4)NO_3$), Micro nutrients (0.09 mM $MnSO_4 \cdot 2H_2O$, 0.1 mM H_3BO_4, 0.03 mM $ZnSO_4 \cdot 7H2O$, 0.005 mM KI, 0.25 µg mL^{-1} $NaMoO_4 \cdot 2H_2O$, 0.025 µg mL^{-1} $CuSO_4 \cdot 5H_2O$ and 0.025 µg mL^{-1} $CoCl_2 \cdot 6H_2O$), 0.006 mM $FeCl_3 \cdot 6H_2O$ and 0.001 mM Na_2-EDTA$\cdot 2H_2O$. The addition of 1 mg mL^{-1} thiamine, 0.1 mg mL^{-1} α-napthaleneacetic acid [NAA, auxin], 1 mg mL^{-1} 6-benzylaminopurine [BAP, cytokinin]) and 100 g L^{-1} myo-inositol to the MS medium was used to generate Regeneration Media of Plants (RMOP) medium. The pH of both media was adjusted to 5.7 using 1 M NaOH and 0.6% (w/v) agar added to media prior to autoclaving. After sterilization the media was cooled to 50°C. Any required antibiotics (sterilized through 0.2 µ filtration units) were added at this point just prior to pouring the media. Seeds were sterilised by incubating in 1% (v/v) bleach (Na-hypochlorite diluted in Milli-Q water) for 10 min and rinsed with repeated changes of excess sterile water. Floating seeds, indicating a possible lack of embryo, were removed. Once thoroughly rinsed the seeds were sown on a petri-dish containing MS medium and grown at 25°C with 50-100 µmol photons m^{-2} s^{-1} artificial illumination on a 14:10 h L:D cycle.

2.3.2 Maintenance of plants

Seedlings germinated for biolistic transformation were individually transferred under aseptic conditions into sterile 750 mL tissue culture pots (JUPITER INDUSTRIES) containing 150 mL MS medium containing 3% [w/v] sucrose (see Section 2.3.1) with 100 µg mL^{-1} Timentin (ticarcillin disodium and clavunalate potassium; SmithKline and Beecham Phamaceuticals UK) added to prevent fungal contamination. The pots were placed in a 25°C controlled environment growth cabinet with elevated CO_2 conditions (2.5% [v/v] CO_2 in air) and 50-100 µmol photons m^{-2} s^{-1} artificial illumination.

Some Rubisco-deplete tobacco genotypes that were unable to be grown from seed in soil were first germinated on MS medium and grown under elevated CO_2 before transferring to growth in sterile 750 mL tissue culture pots (see above). Once roots and ~4 to 6 true leaves were established the plants were transferred into growth in soil (Green Wizard Premium potting mix, Debco). During transfer care was taken to gently

remove the plants from the tissue culture pots and the roots were carefully massaged in water at RT to remove residual tissue culture media before they were placed in 2-5 L pots of soil. Osmocote® (Scotts Australia) fertiliser pellets were added to the soil every two weeks. Plants were grown in specialised Controlled Environment Rooms (CER) at 25°C, 300-450 µmol photons m^{-2} s^{-1} illumination (14:10 h L:D cycle) in air (0.04% [v/v] CO_2) or air with 1% or 2% (v/v) CO_2.

2.3.3 Floral pollination processes

Care was taken to collect seed from flowers that had been artificially pollinated with pollen from the desired tobacco genotype. Cross-pollination was undertaken by removing the immature anthers from a newly emerging flower and pollinating the stigma with pollen from another tobacco genotype. Pollination using pollen originating from wild-type *N. tabacum* or untransformed plants was termed back-crossing. Self-pollination was undertaken by rubbing the stigma and mature anthers of the same flower together. Manually pollinated flowers were marked with colored strings and other surrounding flowers excised by scalpel before the floral heads were bagged to avoid unwanted pollination events. The resulting seed pods were harvested 4-7 weeks later once they were suitably browned and dried. The pods were excised from the plants, dried at 37°C for 3-5 d and then the seed collected from the pods and stored in 25 mL glass vials at 4°C.

2.4 Plant transformation

2.4.1 Nuclear transformation using Agrobacterium tumefaciens

Growth and transformation of LBA4404 Agrobacterium cells

The psiSS transforming plasmid was a gift from Dr. Katia Wostrikoff, Cornell University, USA following its use in the publication of Wostrikoff and Stern (2007). The genetic details of psiSS are fully described in Chapter 3. *Agrobacterium* strain LB4404 (ElectroMAX™) (Hoekema et al., 1983) cells were grown in autoclave sterilised YM medium (0.04% [w/v] yeast extract; 1.0% [w/v] mannitol; 1.7 mM NaCl; 0.8 mM $MgSO_4 \cdot H_2O$; 2.2 mM $K_2HPO_4 \cdot 3H_2O$, pH 7.0] at 28°C. Electrocompetent LB4404 cell stocks (20 µL aliquot) in 10% (v/v) glycerol provided by Dr. Whitney were transformed with 100 ng of psiSS in a chilled 0.1 cm electroporation cuvette using an *E. coli* Pulser (BIO-RAD) at 2.5 kV, 200 Ω, 25 µF. YM medium (1 mL) was added to the cuvette before transferring to sterile 10 mL round bottom falcon tube and incubating at 28°C for 2 h before plating on agar solidified plates of LB-Kan (30 µg mL^{-1} kanamycin).

After 2 d growth at 28°C a colony of psiSS-transformed LB4404 was used to inoculate 50 mL LB-Kan and grown at 28°C until the turbidity of culture at A600 was ~0.3 before use for leaf transformation.

Agrotransformation and selection of putative transformants

Under aseptic conditions sterile tissue culture grown tobacco leaves were dissected into 0.5 cm × 0.5 cm pieces in a sterile petri dish. Approximately 10 mL of the psiSS-LB4404 cells were added to the leaves for 10 min with constant, gentle agitation. Leaf pieces were then removed, wiped on sterile filter paper and then placed abaxial-side up on MS medium containing Macro nutrients, Micro nutrients, 3 mM $FeSO_4 \cdot 7H_2O$, 10 mM Na_2-EDTA$\cdot 2H_2O$, vitamins (20 mg mL^{-1} inositol, 0.2 mg mL^{-1}, nicotinic acid, 0.2 mg mL^{-1} pyridoxine HCI, 0.2 mg mL^{-1} thiamine HCl, 0.2 mg mL^{-1} glycine), hormones (0.1 µg mL^{-1} NAA, 1 µg mL^{-1} BAP) and 1 mg mL^{-1} glufosinate (Basta) - the non-selective herbicide used to select for tissue stably transformed with the selectable marker *bar* coded in T-DNA region of psiSS. The tissue was grown at 25°C in a growth cabinet in air with 2.5% (v/v) CO_2, and 50-100 µmol photons m^{-2} s^{-1} artificial illumination for up to 2 months. Putative transgenic callus emerged after 3-4 weeks. Callus from different leaf sections (*i.e.* to ensure from independent transformation events) were successively regenerated 5 times on MS medium containing 5 mg L^{-1} Basta before transferring the successfully transformed plantlets to 750 mL pots containing MS medium and timentin (200 mg L^{-1}). Once the plants had established roots they were transplanted to soil and grown to fertile maturity in a controlled environment room (CER) (see Section 2.3) and their flowers pollinated appropriately for segregation analysis and generation of homozygous lines (detailed in Chapter 3).

2.4.2 Biolistic plastome transformation

Preparation of tungsten particles

Tungsten (50 mg, M17 BIO-RAD) was weighed into a 10 mL screw-cap tube containing 2 mL of 100% ethanol and sterilised by heating in a water bath at 90°C for 30 min. The tube was placed on ice and the tungsten sonicated three times for 5 min using a LABSONIC 1510 sonicator (B. BRAUN) to ensure dispersal of tungsten aggregates. The sterilised tungsten was transferred to a sterile 1.8 mL microfuge tube and pelleted by centrifugation at 8000 *g* for 15 s. The ethanol in the tube was removed by pipette and the tungsten suspended in 1 mL of sterile water. This process was

repeated four times to remove all ethanol. The tungsten was finally resuspended in sterile water at a final concentration of 50 µg mL^{-1} and stored on ice until use.

DNA coating of tungsten particles

Prepared tungsten (50 µL) was added to 10 µg of maxiprep-purified plasmid DNA (see Section 2.1.2) in a sterile microfuge tube and flicked to mix. Immediately, 50 µL of 2.5 M $CaCl_2$ then 20 µL of 0.1 M spermidine (Sigma-Aldrich) were sequentially added and mixed by vortex after each addition. The mixture was then mixed at 4°C using an IKA® M51 Minishaker (CROWN SCIENTIFIC) at 1400 opm for 30 min. The DNA coated tungsten were pelleted by centrifugation at 2500 *g* for ~10 s and the supernatant was carefully removed by pipette before rinsing with 200 µL ethanol. The mixture was resuspended by flicking. This process for washing the tungsten-DNA particles with ethanol was repeated 6 more times to remove all spermidine and $CaCl_2$.

Bombardment of DNA into tobacco leaf tissue

Under aseptic conditions young leaves from tissue culture grown tobacco were dissected into ~3 × 3 cm flattened sections and placed abaxial-side up on Whatman paper in a petri-dish of MS medium agar containing 3% (w/v) sucrose (Section 2.3.1). Leaves were bombarded with DNA-coated tungsten using a helium (He) acceleration gun (BioRad) using 1100 psi rupture discs. Bombarded leaves were incubated at 25°C under elevated (2.5% [v/v]) CO_2 conditions at <20 µmol photons m^{-2} s^{-1} artificial illumination for 2 d before dissecting them into 0.5 cm × 0.5 cm pieces and gently embedding them into RMOP-spec selective medium (RMOP containing 500 µg mL^{-1} spectinomycin). After 3-6 weeks the leaf sections bleached white and green spectinomycin resistant plantlets began to emerge. These plantlets were removed and continually passaged though further rounds of growth on RMOP-spec medium until bona-fide transformed lines were identified and viable seed collected.

2.5 Biochemical analyses

2.5.1 [^{14}C]-CABP determination of Rubisco content

Synthesis of RuBP and [^{12}C]- and [^{14}C]-CPBP

Laboratory stocks of RuBP were synthesized and purified according to Kane et al., (1998) by Dr. Whitney and used to synthesise carboxypentitiol-1,5-bisphosphate (CPBP), an isomeric mixture of carboxyribitol-1,5-bisphosphate (CRBP) and the tight binding Rubisco inhibitor carboxyarabinitol-1,5-bisphosphate (CABP). [^{12}C]- and [^{14}C]-

CPBP were made by reacting an appropriate amount of RuBP in 0.1 M Tris-acetate buffer (pH 8.5) with a 1.1-fold molar excess amount of either $K^{12}CN$ or $K^{14}CN$ (GE Biosciences) for 48 h in a sealed vial. The reaction was then filtered through AG50W-X8 (H+ form, BIO-RAD) resin to remove unreacted KCN and the eluent freeze-dried. The dried residue was dissolved in 50 mM Bicine-NaOH (pH 9.3) and stored at -20°C (long term storage) or 4°C (for day to day use). The specific activity of the [^{14}C]-CPBP was 106,667 cpm $nmol^{-1}$.

Rubisco content analysis (per sample)

Rubisco content was determined by chromatographic separation of Rubisco bound [^{14}C]-CABP from unbound [^{14}C]-CPBP using a 12 mL bed volume of Sephadex G50 (Fine grade, GE Biosciences) gel filtration in a glass 0.7 x 30 cm Econo-column (BIO-RAD) equilibrated in column buffer (20 mM Bicine-NaOH, pH 8.0, 75 mM NaCl). Leaf protein samples (see Section 2.2.1, typically 100 µL) were incubated with 10 to 20 mM $NaHCO_3$ and 10 mM $MgCl_2$ for 10 min at RT to "activate" each Rubisco catalytic site (Figure 1.5) before adding 1 µL [^{14}C]-CPBP. After a further 15-30 min at RT the entire sampled was carefully loaded onto the column, followed by 200 µL of column buffer. Three further aliquots of buffer (750 µL) were added to the column before any fractions were collected. The following 7 fractions (750 µL each) were collected into separate 7 mL plastid scintillation vials (16 × 50 mm; Starstedt) and 1 mL of scintillant (Ultima-Flo Gold, Packard) was added and mixed by vortex. Fractions 2 to 4 contained the Rubisco-bound [^{14}C]-CABP peak and fractions 6 and 7 the start of the unbound [^{14}C]-CPBP peak. The radioactivity in each sample was measured using a Tri-Carb 2800TR Liquid Scintillation Analyzer (PerkinElmer).

Rubisco content analysis (per lane) for SDS and ndPAGE

For SDS and ndPAGE samples, Rubisco content per lane was calculated using parameters of Rubisco content analysis per sample (R_s), volume of sample used for SDS or ndPAGE (v_s), volume of gel loading buffer (v_b) and final volume of sample loaded onto the gel (v_f) using the equation

$$\text{Total Rubisco content per lane, } R_l = v_s/(v_s+v_b)*Rc*v \qquad \text{(Eq. 5)}$$

2.5.2 Rubisco catalysis measurements

The Michaelis-Menten constants (K_m) of Rubisco for CO_2 was measured under ambient O_2 concentrations to determine a $K_C^{21\%O2}$ value at 25ºC using RuBP-dependent $^{14}CO_2$ fixation assays using rapidly extracted soluble leaf protein (see Section 2.2.1) (Sharwood et al., 2008). To fully CO_2-Mg^{2+} activate all the Rubisco sites in the sample the soluble protein was diluted with an equal volume 2× Mg-$^{14}CO_2$ buffer (50 mM EPPS-OH, pH 8.0, 20 mM $MgCl_2$, 1 mM EDTA, 20 mM $NaH^{14}CO_3$) and incubated at 25ºC for 7-9 min. The assays were initiated by the addition of 20 µL of the activated enzyme into septum sealed 8 mL glass scintillation vials containing 480 µl of $^{14}CO_2$ fixation assay buffer (50 mM EPPS-OH pH 8.2, 1 mM EDTA, 20 mM $MgCl_2$, 0 to ~4.1 mM $NaH^{14}CO_3$ [*i.e.* 0 to 37.4 µM $^{14}CO_2$, specific activity ~1500-2000 cpm $nmol^{-1}$], 10 µg mL^{-1} carbonic anhydrase, 0.2 mM RuBP). The Henderson-Hasslebach equation used to calculate the CO_2 (*C*) concentration in the assays is

$$[C] = \frac{C_t}{1 + \frac{V}{vqRT} + 10^{(pH-pK_1)} + 10^{(2pH-pK_1-pK_2)}} \qquad \text{(Eq. 6)}$$

where C_t is total organic carbon, the V/v is the ratio of reaction vial headspace (V) to solution volume (v), q is the solubility of CO_2 in water at 1 atm at 25°C (0.03292 Mol L^{-1} atm^{-1}), R is the universal gas constant, T is the reaction temperature (298K). pK_1 and pK_2 values of 6.25 and 10.33, respectively, were used in the calculations.

RuBP-independent $^{14}CO_2$ fixation control assays were run for each sample and contained H_2O in place of RuBP. After adding sample the assays were stopped after one minute by adding 100 µl of 25 % (v/v) formic acid. The mixture was dried at 90ºC using a heating block and the final residue dissolved in 0.5 mL water and mixed with 1 mL of scintillant (Ultima-Gold). Acid stable radioactivity was measured in a scintillation counter. Values for $K_c^{21\%O2}$ (in µM) and substrate saturated carboxylation rates($V_{c\,max}$, in units of mol CO_2 fixed s^{-1} [vol of sample in assay]$^{-1}$) were extrapolated from fitting the data to the Michaelis-Menten equation. The carboxylation turnover rates (k_C^{cat}, in units of s^{-1}) was the determined by dividing $V_{c\,max}$ by the mol Rubisco active sites in the assay as quantified by [^{14}C]-CABP binding (see Section 2.5.1).

2.5.3 $^{14}CO_2$ specific activity determination

To determine the $^{14}CO_2$ specific activity of the reactions, replicate assays (with the highest CO_2 concentrations) containing known amounts of RuBP (typically only 20 nmol) were allowed to proceed for 30-90 min to ensure full RuBP fixation. The specific

activity was calculated by dividing the ^{14}C values measured by the scintillation counter by the 20 nmol of RuBP in the assay to obtain specific activity values for the assays in cpm (nmol CO_2 fixed)$^{-1}$.

2.6 Leaf gas exchange

2.6.1 Optimisation of plant stomatal conditions

Plants were transferred from their growth facility to a laboratory and left overnight in the dark at atmospheric conditions. Gas exchange was performed the next morning on young, fully expanded tobacco leaves (typically mid-way down the canopy of plant 30-40 cm in height) using a Li-COR 6400-02B using a Red / Blue (10%) LED light source and a set leaf temperature of 25°C. Illumination and CO_2 concentrations (C_a) in the leaf chamber were initially set at 110 µmol photons m^{-2} s^{-1}and ~96 µbar C_a respectively to encourage stomatal opening. The apparatus was left for 1 hour prior to measuring how leaf CO_2 assimilation rates (A) responded to changes in intercellular CO_2 concentrations (C_i) (*i.e.* A-C_i response curves comparable to that shown in Figure 1.09).

Once stomatal conductance (g_m) was > 0.25 µmol m^{-2} s^{-1}, the C_a levels in the leaf chamber were raised to 400 ppm, illumination increased to 1200 µmol photons m^{-2} s^{-1} and the chamber air flow rate set at 500 µmol s^{-1}. After 30 min, equilibration measurements of A were then logged in triplicate under varying C_i levels between 50 and 1800 µbar. At the completion of the *A-Ci* measurements the leaf was returned to steady state (i.e. ~400 µbar *Ca*) in the dark a measure of the dark respiration rate (R_d) taken after 15 min before turning the light back on for another 15 min then rapidly taking samples of the leaf for proteomic (see Section 2.2) and biochemical (see Section 2.5) analysis. The data were then compared with the photosynthetic rates predicted using the models of Farquhar et al. (1980) as described in Section 1.3.2.

CHAPTER 3 – GENERATING A ^{CM}TRL$^{RNAi\text{-}S}$ TOBACCO GENOTYPE WHERE S-SUBUNIT SYNTHESIS IS SILENCED BY RNAI

3.1 Introduction

3.1.1 Mutagenic analysis of the RbcS multigene family in leaf chloroplasts

Initial attempts to genetically modify Rubisco in plants utilised an *RbcS* anti-sense (anti-*RbcS*) knockdown of S-subunit synthesis in tobacco (Rodermel et al., 1988; Hudson et al., 1992). This approach was subsequently applied to a number of other species including *Solanum lycopersicum* (tomato) (Kubien and Sage, 2008), *Arabidopsis thaliana* (Izumi et al., 2012), *Flaveria bidentis* (Furbank et al., 1996) and *Oryza sativa* (rice) (Makino et al., 1997). The most potent anti-*RbcS* tobacco (*N. tabacum*) genotype generated had Rubisco levels that were 62% lower than wild-type and therefore struggled to grow under atmospheric CO_2 (Zhang et al., 2002). By using an anti-*RbcS* approach, independent transgenic genotypes have produced varied levels of L_8S_8 Rubisco (Rodermel et al., 1988; Hudson et al., 1992; Andrews et al., 1995). Accordingly the growth and survival becomes increasingly compromised in the genotypes producing lower amounts of Rubisco.

These anti-*RbcS* genotypes proved useful in studying the influence of Rubisco activity on photosynthesis and growth (Stitt et al., 1991; Bernacchi et al., 2001; Kubien et al., 2003) and testing the accuracy of the Farquhar, von Caemmerer and Berry photosynthesis models (Farquhar et al., 1980; von Caemmerer et al., 1994; see also Section 1.3.2). Conversely transgenic studies have also sought to examine the effect of overproducing Rubisco by reciprocal genetic approaches to elevate *RbcS* mRNA levels in leaves (*i.e.* a "sense-*RbcS*" approach). This approach in rice has produced genotypes with up to a 20% increase in L_8S_8 Rubisco, which although influencing the N-partitioning in the plant, did not improve leaf photosynthesis and plant growth (Suzuki et al., 2007; Suzuki et al., 2009). Other analogous nucleus transformation approaches have sought to supplement plants with heterologous *RbcS* to study structural aspects of the S-subunit influence on Rubisco catalysis. For example introducing an *RbcS* from *Pisum sativum* (pea) into *Arabidopsis* resulted in the synthesis of chimeric L_8S_8 enzymes comprising both *Arabidopsis* and pea S-subunits in an average 7:1 molar ratio (Getzoff et al., 1998). Biochemical analyses indicated the Rubisco chimers had ~11% reductions in the carboxylase activity (k_C^{cat}) and reduced catalytic site activation status

(carbamylation status). These findings suggested Rubisco quaternary conformation was adversely affected by structural incompatibilities between the subunits (Getzoff et al., 1998). In contrast a more recent effort to transplant S-subunits from C_4 plant *Sorghum bicolor* into rice successfully produced genotypes with chimeric rice Rubisco where 30-80% of the total S-subunit population were from sorghum (Ishikawa et al., 2011). Consistent with the S-subunits having an influence on catalysis (see Section 1.2.2), the chimeric rice Rubisco isoforms showed 1.3 to 1.5-fold increases in k_C^{cat} and corresponding reductions in CO_2 affinity (*i.e.* an increase in the K_m for CO_2) – reminiscent of the catalytic properties for Rubisco from C_4 plants (see Section 1.3.1). While an exciting step forward in Rubisco bioengineering from the perspective of the S-subunit, these studies demonstrate a glaring limitation in the bioengineering of S-subunits in leaf chloroplasts for structure-function analyses – the population of recombinant L_8S_8 Rubiscos invariably contain varying stoichiometry of heterologous S-subunits. As *RbcS* is a multigene family in plants (for example tobacco has 13 copies (Gong et al., 2014) (see Section 3.2.1), targeted silencing of all *RbcS* mRNA and replacement with a single foreign or modified version has so far been unfeasible.

3.1.2 Relocating RbcS into the tobacco chloroplast

Difficulties in targeted modification of *RbcS* in the nucleus of higher plants led to efforts in engineering the gene in the chloroplast genome (plastome). Initial trials using tobacco introduced native tobacco *RbcS* (coding a hepta-histidine [H_7] C-terminal tag) both with and without its chloroplast transit peptide coding sequence (Whitney and Andrews, 2001a). Both *RbcS* transgenes (tp*RbcS*^{H7} and *RbcS*^{H7}) were inserted into the inverted repeat regions of the tobacco plastome to produce independently transformed RVtpSSuH and RVSSuH tobacco genotypes (discussed in further detail in Section 4.1.4). While it was shown that plastid-synthesized S-subunits could successfully assemble into L_8S_8 Rubisco, only ~1% of plastid made S-subunits assembled despite their chloroplast *RbcS* mRNA levels exceeding endogenous cytosolic *RbcS* mRNA levels by more than 10-fold.

Possible inefficiencies with translation of the plastid made S-subunits or/and strong competition by the endogenous cytosol made S-subunits are possible explanations for the paucity of plastid made S-subunits assembled (Whitney and Andrews, 2001a; Zhang et al., 2002). Consistent with this a comparable transplastomic approach in an anti-*RbcS* tobacco line found no evidence for chloroplast made S-subunits impacting Rubisco production (Zhang et al., 2002). A subsequent attempt

proved more successful when transforming the same anti-*RbcS* tobacco genotype with *RbcS* inserted within a transcriptionally active spacer region between *trnI* and *trnA* of the plastome inverted repeat regions (Dhingra et al., 2004). The resulting transplastomic lines showed significant improvements in Rubisco levels – almost to wild-type levels. Whether this increase in Rubisco levels was solely attributable to plastid made S-subunit synthesis or associated with partial silencing of anti-*RbcS* phenotype was not experimentally examined. Testing for this would be feasible by confirming Rubisco levels were still low in the progeny of wild-type plants pollinated with pollen from the transplastomic lines.

3.1.3 ^{cm}trL - a tobacco genotype for chloroplast-targeted Rubisco bioengineering

An approach to study the role of the S-subunit on Rubisco catalysis by coupling RNAi silencing of *RbcS* mRNA production with transplastomic integration of *RbcS* into the plastome has been proposed (Sharwood et al., 2008). An important consideration is that elimination of Rubisco synthesis in plants by RNAi-*RbcS* would produce progeny of poor viability and unable to grow to fertile maturity outside of tissue culture or via grafting onto wild-type stock. Such genotypes would essentially be comparable to the *rbcL* deletion plants of Kanevski and Maliga (1994). However the ^{cm}trL tobacco genotype (see Section 1.4.3) provides a viable alternative for eliminating tobacco S-subunits synthesis without affecting growth phenotype. In ^{cm}trL the tobacco Rubisco L-subunit gene (*rbcL*) has been replaced with ^{cm}*rbcM* coding for *Rhodospirillum rubrum* L_2 Rubisco (Whitney and Sharwood, 2008) (Figure 3.1A). While the ^{cm}trL line requires growth under high-CO_2 conditions to compensate for the poor catalytic properties of *R. rubrum* Rubisco (see Section 1.1.5) it is readily capable of growing to maturity in soil without detriment to phenotype in air with high-CO_2 (*i.e.* greater than 0.5% [v/v], Figure 3.1C). Of additional benefit is the ^{cm}trL line poses a tailor-made genotype for efficiently introducing *rbcL* coding heterologous Rubisco L-subunits from plants (Whitney et al., 2011b) and Archaea (Alonso et al., 2009), in addition to re-inserting mutated forms of the tobacco *rbcL* (Whitney and Sharwood, 2008; Whitney et al., 2011a). The ^{cm}trL genotype is also advantaged by the size difference between the S-subunit lacking *R. rubrum* L_2 Rubisco (~100 kDa) and larger L_8S_8 Rubisco (~520 kDa) that make identifying L_8S_8 Rubisco transformed lines easily discernible by non-denaturing PAGE (ndPAGE) (Whitney and Sharwood, 2008).

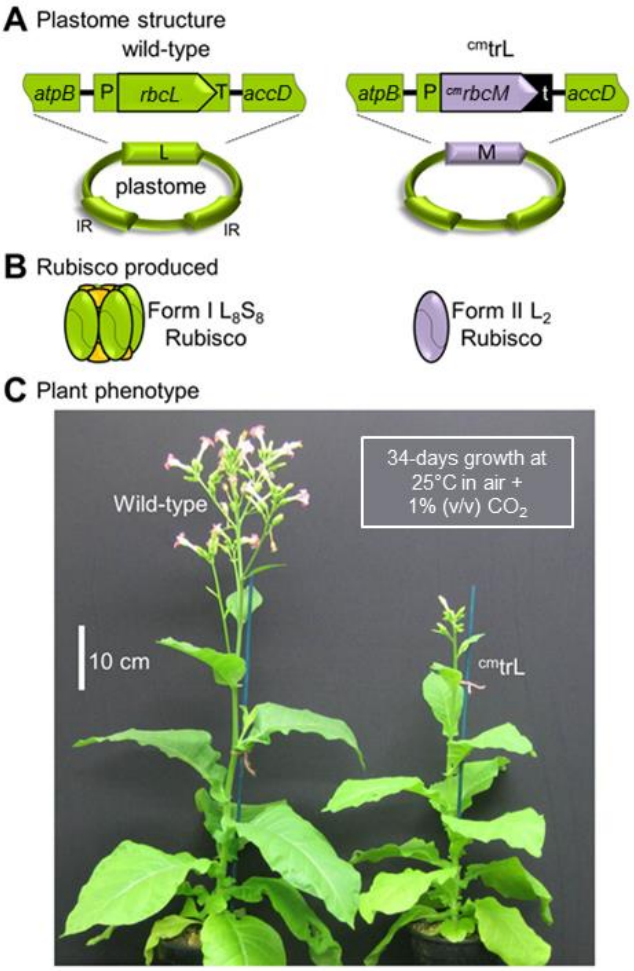

Figure 3.1 Generation and phenotype of the ^{cm}trL tobacco genotype.

As noted in Figure 1.11, plastome transformation was used to (A) replace *rbcL* in tobacco with a codon-modified *rubrum* L-subunit gene (^{cm}*rbcM*) using the p^{cm}trL transforming plasmid (GenBank accession number AY827488). *aadA* in the resulting tobacco line (^{cm}trLA) was excised by CRE recombinase to produce the marker-free ^{cm}trL line (Whitney and Sharwood, 2008). t, 222 bp sequence of the *psbA* 3'-untranslated region (UTR); P, *rbcL* promoter and 5'UTR; T, *rbcL* 3'UTR. (B) The *R. rubrum* L_2 Rubisco produced in ^{cm}trL is structurally simpler and smaller (100 kDa) than the ~520 kDa L_8S_8 produced in wild-type tobacco. (C) When grown under high-CO_2 the phenotype of ^{cm}trL matches wild-type tobacco, albeit slower in growth (Whitney and Sharwood, 2008).

3.1.4 RNAi silencing- a tool of varying success

'RNA silencing' is the suppression of gene expression at the transcriptional and/or post-transcriptional level (Pumplin and Voinnet, 2013). The process uses sequence-specific complementation interactions between RNA sequences of varying length. Variations of RNA silencing have been identified as 'RNA interference' (RNAi) in animals, 'quelling' in fungi and 'post-transcriptional gene silencing' (PTGS) in plants. PTGS in plants was first realized in the 1990s and had been previously referred to as 'co-suppression' (Napoli et al., 1990). It is a regulatory process natural to endogenous genes that functions during plant development as well as protecting the genome against damaging

changes introduced by viruses and mobile DNA elements such as transposons (Voinnet, 2002; Pumplin and Voinnet, 2013).

PTGS regulates cytoplasmic RNA levels through sequence-specific degradation involving a cascade of RNA-interacting proteins (Chen and Aravin, 2015). Degradation is triggered by varying types of small double-stranded RNA (dsRNA) such as microRNA (miRNA) or small-interfering RNA (siRNA). These 21-25 nucleotide RNA molecules are made from the cleavage of dsRNA or hairpin-loop RNA structures by a nuclease complex made of DICER-LIKE1 protein (DCL1) (Blevins et al., 2006; Ahmadovich Bozorov et al., 2012), HYPONASTIC LEAVES1 (HYL1) (Han et al., 2004; Kurihara et al., 2006) and SERRATE (SE) (Yang et al., 2006). As shown in Figure 3.2, the miRNA and siRNA products are recognised by their nucleotide structure and methylated at their 3' ends by HUA ENHANCER1 (HEN1) (Park et al., 2002). HEN1 is a plant miRNA methyltransferase protein that promotes binding of the small RNAs to an RNA-induced silencing complex (RISC). The RISC complex contains an Argonaute-1 (AGO1) protein that helps identify target mRNA for degradation or to inhibit translation by DNA/histone modification (Sunkar and Zhu, 2007). AGO1 also serves as an endonuclease to cleave the targeted mRNA (Martinez and Tuschl, 2004). In addition to AGO1, RISC also has an ATP-dependent helicase-like component that separates the double-stranded RNA at its less stable strand (usually its antisense strand), and retains the antisense strand as a guide to target additional mRNAs for degradation (Khvorova et al., 2003) (Figure 3.2).

3.1.5 The tobacco RbcS multigene family and its potential silencing by RNAi

The *RbcS* multigene family is a result of allopolypoidy and cytonuclear evolution from the two parents (*N. sylvestris*♀ and *N. tomentosiformis*♂) of *N. tabacum* (see Section 1.4.1). *RbcS* expression appears to be light regulated by one or two repeats of a set of light responsive elements (Jiang et al., 1994) sequences approximately 166-149 bp upstream from the TATA box (Gupta, 2009). Differential expression of the *RbcS* mRNAs may also vary due to intrinsic differences in the stability of their transcripts and thus provide inaccurate assessment of difference in transcription rates of the varying *RbcS* alleles (Izumi et al., 2012).

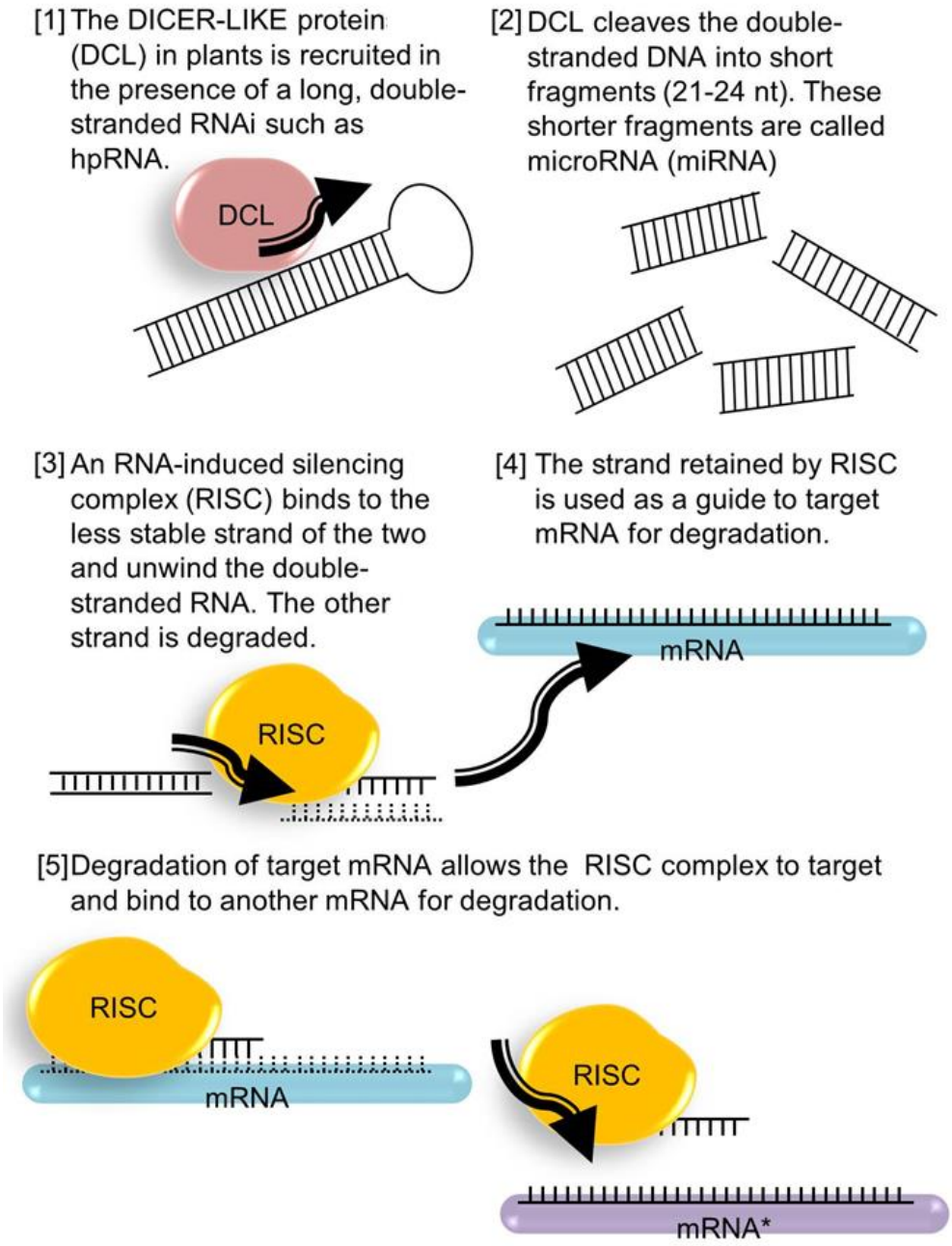

Figure 3.2 Schematic of targeted mRNA degradation by RNAi-silencing.

In tobacco 13 *RbcS* have been identified by genomic sequencing (Gong et al., 2014). This replication has been generated from displacement of gene fragments via gene conversion of tobacco's progenitors. Sequence variation among the gene copies have likely arisen from genome-specific single-nucleotide polymorphism (SNPs), occurring in regions of both the transit peptide, mature protein and the non-coding 5'- and 3' untranslated sequences. Regions in the mature S-subunit that are more highly conserved (e.g. the βA/βB loop that interacts with the L-subunit, Figure 1.8) show very little gene conversion across the varying *RbcS* members in *N. tabacum* (Gong et al., 2014).

RNAi directed silencing of *RbcS* has been successfully performed in tobacco by transient expression using a viral induced gene silencing (VIGS) approach (Wostrikoff and Stern, 2007). Successful knock down of the *RbcS* mRNA pool was accomplished using an inverted hairpin RNAi (ihpRNAi) construct that sought to test how S-subunit availability influenced L-subunit synthesis in tobacco chloroplasts. The silencing construct, phpNtsiSS (in this thesis called psiSS, Figure 3.3A), was generated using the pFGC5941 binary vector (GenBank accession number AY310901.1). The psiSS vector contains the 1353 nucleotide chalcone synthase intron (CSI) into which duplicate regions spanning the first 407 nt of *N. tabacum RbcS* were cloned in opposite orientations (Figure 3.3A). The region of the *N. tabacum RbcS* cloned in psiSS contained sequence spanning the full 171 bp transit peptide coding sequence and first 6 nucleotides of S-subunit coding sequence (*i.e.* the first exon; *Ex1*), the first intron (93 bp), and the second 135 bp exon sequence (*Ex2*) of *RbcS* (Figure 3.3B).

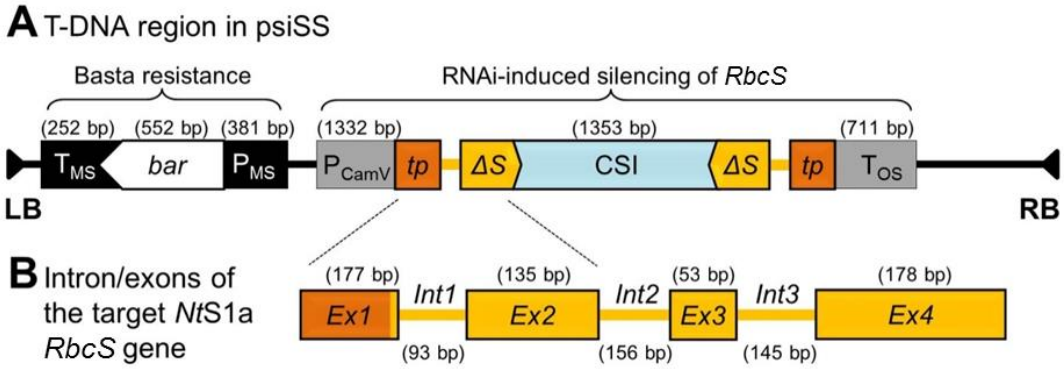

Figure 3.3 The T-DNA sequence of psiSS used to suppress *RbcS* mRNA levels in tobacco.

(A) T-DNA region of the binary vector psiSS and (B) the *N. tabacum RbcS* (from GenBank accession number X02353.1) used to construct the RNAi-*RbcS* ihpRNA region in psiSS. Duplicate copies of 405 bp of *RbcS* gDNA sequence spanning Exon 1 (*Ex1*), Exon 2 (*Ex2*) and the intervening intron (*Int1*) was inserted in either orientation either side of the chalcone synthase intron (CSI). Expression of this RNAi-*RbcS* sequence was regulated by the CaMV 35S promoter (P_{CamV}) and octopine synthase (T_{OS}) terminator. Expression of the selectable *bar* marker (coding Basta resistance) was controlled by the mannopine synthase promoter (P_{MS}) and terminator (T_{MS}). LB, left border; RB, right border; *Ex*, exon; *Int*, intron**.** Figures are not drawn to scale.

3.1.6 Research objective – Silencing S-subunit synthesis in ^{cm}trL by ihpRNAi-RbcS

Being able to study specific protein-protein interactions between the S- and L-subunits of plant Rubisco has remained an elusive goal. As indicated above, partial success has been obtained through introduction of *RbcS* transgenes by nucleus and plastome transformation approaches, although catalytic interpretation of these chimeric enzymes is of limited use given they contain heterologous populations of S-subunits. Fully appreciating the molecular detail of subunit interactions in higher plant Rubisco is stymied by this heterogeneity as it precludes the generation of recombinant Rubisco containing a homogeneous population of S-subunits. Such limitations are avoided in *Chlamydomonas* due to the availability of a mutant strain where both nuclear *RbcS* have been silenced by insertion mutagenesis (Khrebtukova and Spreitzer, 1996). This has allowed for testing of specific sequence changes in both the L- and S-subunits (Karkehabadi et al., 2005; Spreitzer et al., 2005; Genkov and Spreitzer, 2009; Genkov et al., 2010). No comparable system currently exists in plants due to *RbcS* comprising a larger multigene family. The inability to express plant L_8S_8 Rubisco in *E. coli* or other expression host further limits structure-function studies of plant L- and S-subunits.

This chapter describes the generation of a new tobacco genotype where nuclear S-subunit synthesis is eliminated using an RNAi-*RbcS* approach. As summarised in Figure 3.4, the target tobacco genotype for transformation is the ^{cm}trL line where the L_2 *R. rubrum* Rubisco has no requirement for S-subunits and therefore should not be affected by RNAi directed silencing of S-subunit synthesis.

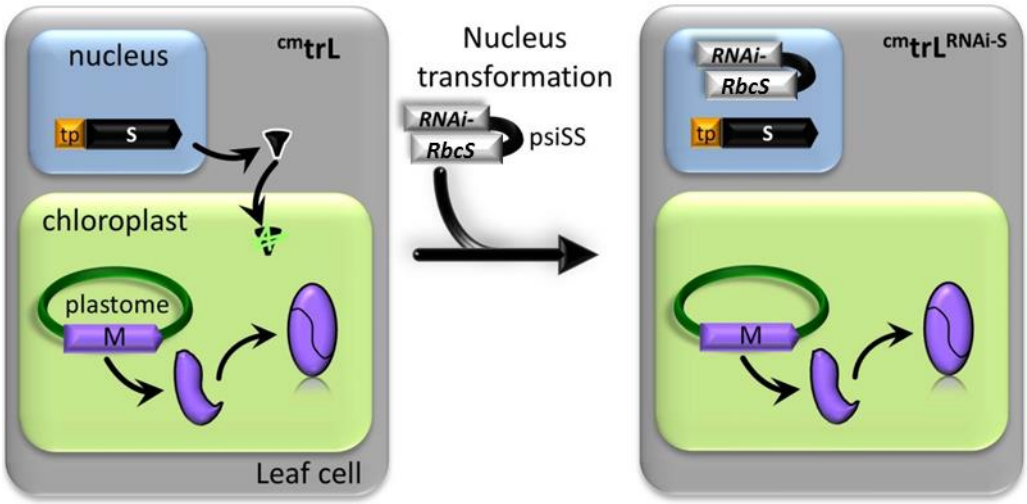

Figure 3.4 Research objective summary – producing an RNAi-*RbcS* silenced tobacco line using the ^{cm}trL genotype.

As the S-subunits have no assembly partner in ^{cm}trL they are rapidly degraded (Whitney and Andrews 2001a). Silencing S-subunit synthesis by RNAi in this tobacco genotype is therefore not expected to disadvantage growth.

3.2 Results

3.2.1 Analysis of the RbcS diversity in tobacco

Since the publication of the full genome sequence for *Arabidopsis* some 15 years ago (Analysis of the genome sequence of the flowering plant *Arabidopsis thaliana*, 2000) there has been an exponential increase in the number of plant genomes sequenced. It is therefore surprising that an entire genome sequence for *N. tabacum* has only recently been publically available (Gong et al., 2014) albeit not annotated. Greater progress has been made with annotating the genome and transcriptome sequence of *N. benthamiana* (http://sydney.edu.au/science/molecular_bioscience/benthamiana/), the variety mostly used in Agro-infiltration experimental transgene applications (Goodin et al., 2008). A bioinformatic analysis of the new *N. tabacum* sequence was undertaken with regard to annotating the genetic information of its *RbcS*. In general, *RbcS* of higher plants typically comprise two or more introns (Wolter et al., 1988). As shown in Figure 3.5, this is also the case for the 13 *RbcS* in *N. tabacum* with 3 alleles having three introns and the other 10 only two introns. In this analysis the genes maternally derived from the *N. sylvestris* genome are represented by the prefix *NtS* and those paternally derived from *N. tomentosiformis* are indicated by *NtT*.

Analysis of the 13 *N. tabacum RbcS* found the *Nt*S5 (***N****icotiana* ***t****abacum* **S**ylvestris parent *RbcS* **5**) and *Nt*T5 (***N****icotiana* ***t****abacum* **T**omentosiformis parent *RbcS* **5**) to be paralogs as they were sufficiently divergent from the other genes by each containing a ~3-fold larger first intron of ~500 bp (Figure 3.5) (Gong et al., 2014). When aligned a number of the *RbcS* alleles were found to share 100% identity in their mature S-subunit coding sequence (*i.e. Nt*S1a & *Nt*S1b; *Nt*S3 & *Nt*T3a & *Nt*S4) (Figure 3.6A). In terms of nucleotide and amino acid sequence identity, all the *RbcS* alleles showed greater variation in the region coding the N-terminal transit peptide pre-sequence that spans 171-174 nucleotides (*i.e.* 57 or 58 amino acids) (Figure 3.6A). As shown in Figure 3.6B, alignment of only the mature S-subunit coding sequence identified several polymorphic residues that constitute 9 different S-subunit isoforms (labelled *Nt*-SS1 to *Nt*-SS9) within *N. tabacum*. In this thesis, the S-subunit isoform studied constitutes the *Nt*-SS1 isoform which is coded by the same *RbcS* inserted into the nuclear transforming plasmid psiSS (Figure 3.3A) (Wostrikoff and Stern, 2007) and transformed into the tobacco plastome to make the RVtpSSuH and RVSSuH genotypes (Whitney and Andrews, 2001a) and described further in Chapter 4.

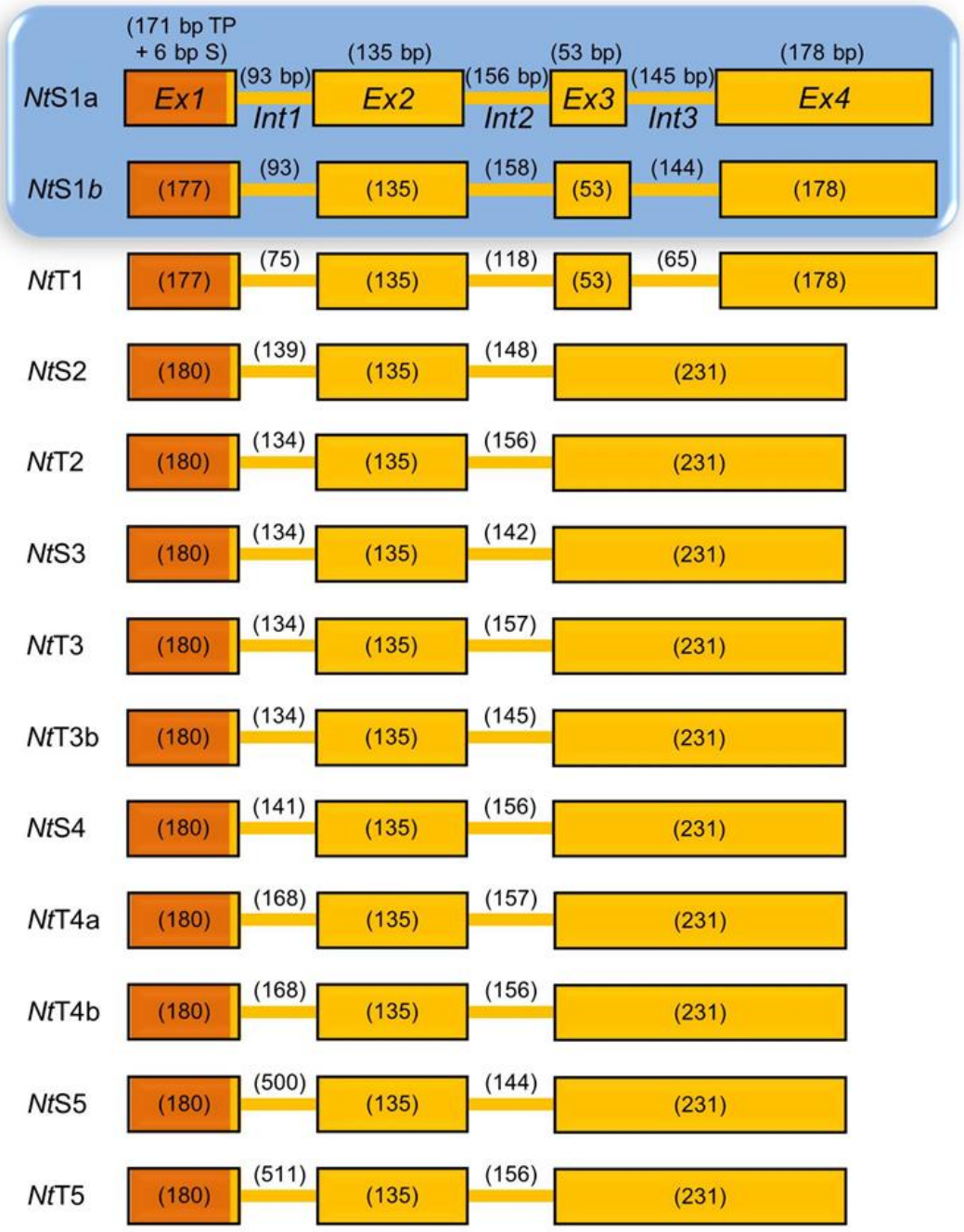

Figure 3.5 The *RBCS* multigene family in *N. tabacum*.

The nucleotide sequence of the 13 *RbcS* in *N. tabacum* vary mainly in their intron sequences. The *Nt*S1a, *Nt*S1b and *Nt*T1 alleles are the only members in the family having 3 introns, the remainder only having 2 introns. *Nt*S1a and *Nt*S1b (highlighted in blue) are the *RbcS* used in the transgenic studies described in this thesis. *Nt*S5 and *Nt*T5 are paralogs that are divergent from the other family members. Genes maternally derived from the *N. sylvestris* genome are represented by the prefix *Nt*S while those paternally derived from *N. tomentosiformis* are indicated by *Nt*T. Genbank accession numbers for each member of the *RbcS* multigene family can be found in Appendix B.

A Full length pre-S-subunit sequences

	*Nt*S1a	*Nt*S1b	*Nt*T1	*Nt*S2	*Nt*T2	*Nt*S3	*Nt*T3a	*Nt*T3b	*Nt*S4	*Nt*T4a	*Nt*T4b	*Nt*S5	*Nt*T5
*Nt*S1a		100.0	95.6	94.5	95.0	92.8	94.5	93.9	93.9	93.9	94.5	94.5	95.0
*Nt*S1b	100.0		95.6	94.5	95.0	92.8	94.5	93.9	93.9	93.9	94.5	94.5	95.0
*Nt*T1	94.3	94.3		90.6	92.3	90.6	91.7	91.7	91.2	91.2	91.7	91.7	91.7
*Nt*S2	98.4	98.4	92.7		97.8	95.0	97.8	97.2	97.8	96.1	96.7	98.3	97.8
*Nt*T2	98.4	98.4	94.3	98.4		97.2	98.9	98.3	97.8	97.8	98.3	99.4	99.4
*Nt*S3	98.4	98.4	94.3	98.4	100.0		96.1	95.6	95.0	95.0	95.6	96.7	96.7
*Nt*T3a	98.4	98.4	94.3	98.4	100.0	100.0		99.4	97.8	97.2	97.8	98.3	98.3
*Nt*T3b	97.6	97.6	94.3	97.6	99.2	99.2	99.2		97.2	96.7	97.2	97.8	97.8
*Nt*S4	98.4	98.4	94.3	98.4	100.0	100.0	100.0	99.2		97.2	97.8	97.2	97.2
*Nt*T4a	96.7	96.7	92.7	96.7	98.4	98.4	98.4	97.6	98.4		99.4	97.2	97.2
*Nt*T4b	97.6	97.6	93.5	97.6	99.2	99.2	99.2	98.4	99.2	99.2		97.8	97.8
*Nt*S5	97.6	97.6	93.5	99.2	99.2	99.2	99.2	98.4	99.2	97.6	98.4		98.9
*Nt*T5	98.4	98.4	93.5	98.4	99.2	99.2	99.2	98.4	99.2	97.6	98.4	98.4	

B Mature S-subunits coding sequences

S-subunit isoform	*RbcS* allele	Amino acid position in the mature S-subunit										
		7	8	23	28	30	31	48	70	88	96	121
Nt-SS1	*Nt*S1a, *Nt*S1b	I	N	Q	S	V	E	H	W	E	Q	E
Nt-SS2	*Nt*T1	Y	G	E	□	I	□	R	□	G	E	□
Nt-SS3	*Nt*S2	□	□	□	R	□	D	□	□	□	□	□
Nt-SS4	*Nt*T2, *Nt*S3, *Nt*T3a, *Nt*S4	□	□	E	R	□	□	□	□	□	□	□
Nt-SS5	*Nt*T3b	□	□	E	R	□	□	□	□	□	R	□
Nt-SS6	*Nt*T4a	□	□	E	R	□	□	□	R	□	□	A
Nt-SS7	*Nt*T4b	□	□	E	R	□	□	□	□	□	□	A
Nt-SS8	*Nt*S5	□	□	E	R	□	D	□	□	□	□	□
Nt-SS9	*Nt*T5	□	□	V	R	□	□	□	□	□	□	□

Figure 3.6 S-subunit sequence comparisons.

(A) Matrix of amino acid sequence identity for the full length pre-S-subunit (*i.e.* including the N-terminal 57 or 58 residue transit peptide; non–shaded data) and mature S-subunit sequences (shaded grey) coded by each of the 13 *RbcS* alleles in *N. tabacum*. Sequences were aligned by the Clustal W algorithm in MegAlign (DNASTAR). See Appendix B for *RbcS* accession information. (B) Summary of the polymorphic amino acids among the *N. tabacum* S-subunits relative to the *Nt*-SS1 isoform (shaded orange) that is used in all transgenic modifications in this thesis.

3.2.2 Generation of the $^{cm}trL^{RNAi\text{-}S}$ tobacco genotypes

The small subunit silencing plasmid (psiSS**;** generously provided by Dr. Katia Wostrikoff, Boyce Thompson Institute for Plant Research, Cornell University) used previously to successfully silence *RbcS* mRNA production in tobacco (Wostrikoff and Stern, 2007) was introduced into ^{cm}trL leaves by *Agrobacterium* transformation (Figure 3.4). A total of 27 independent Basta resistant (Basta^R) calli were collected and passed through successive selection rounds on Basta (1 mg L^{-1}) selective medium. In total 11 individual Basta^R T_0 transgenic plants (called $^{cm}trL^{RNAi\text{-}S1}$ to $^{cm}trL^{RNAi\text{-}S11}$) were successfully propagated and grown to maturity in soil under elevated CO_2 (1.5% [v/v]).

The phenotype of all the $^{cm}trL^{RNAi\text{-}S}$ genotypes matched ^{cm}trL and all eleven T_0 plants were fully fertile. The flowers of each parental T_0 line were self-pollinated and viable seeds obtained. These seeds were germinated to produce the T_1 progeny.

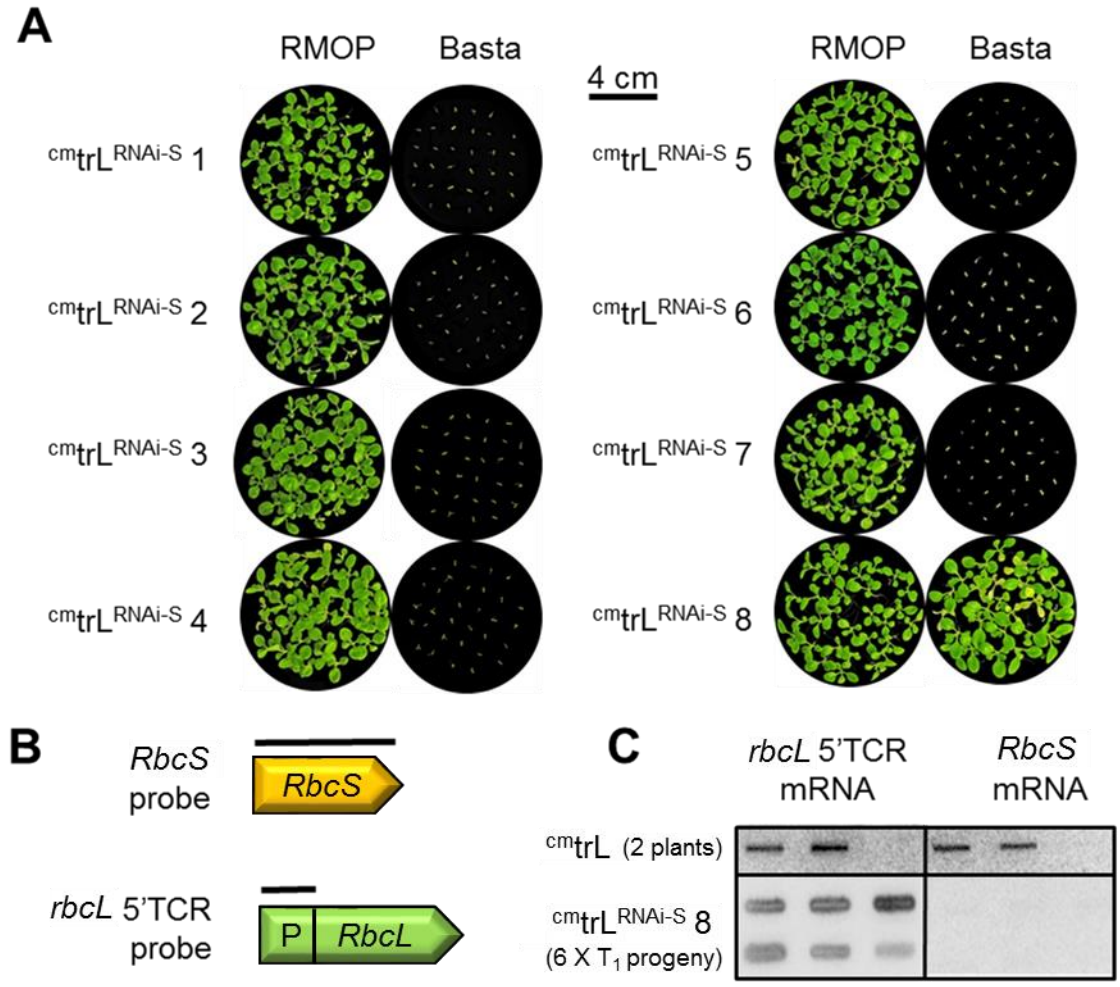

Figure 3.7 Basta^R segregation analysis of $^{cm}trL^{RNAi\text{-}S}$ T_1 progenies and RNA blot screening.

(A) Germination of T_1 progeny for 8 putative $^{cm}trL^{RNAi\text{-}S}$ genotypes on MS medium with 10 µg mL^{-1} Basta. Like ^{cm}trL seedlings, the $^{cm}trL^{RNAi\text{-}S1}$ to $^{cm}trL^{RNAi\text{-}S7}$ genotype progenies were sensitive to Basta (Basta^S) while 75% of the $^{cm}trL^{RNAi\text{-}S8}$ seedlings were Basta^R. (B) DNA probes to the translational control region (TCR) of tobacco *rbcL* (spanning 179 bp of 5'UTR and 42 bp of *rbcL* coding sequence: *rbcL* 5'TCR) or nuclear *RbcS* cDNA were used to hybridise (C) slot blots of total leaf RNA from six T_1 $^{cm}trL^{RNAi\text{-}S8}$ plants and two ^{cm}trL (positive) controls. While all samples produced *rbcL* mRNA, no *RbcS* mRNA was detected in any of the $^{cm}trL^{RNAi\text{-}S8}$ samples.

3.2.3 bar and RbcS mRNA knockout co-segregated in four $^{cm}trL^{RNAi\text{-}S}$ lines

A segregation analysis for Basta^R was performed on the T_1 progeny. Germination and growth analysis of the $^{cm}trL^{RNAi\text{-}S1}$ to $^{cm}trL^{RNAi\text{-}S8}$ genotypes showed that only under the highest Basta concentration (10 mg L^{-1}) did the $^{cm}trL^{RNAi\text{-}S8}$ line showed clear Basta^R (Figure 3.7A). This suggested the concentration of Basta used in the initial screening (1 mg L^{-1}) was insufficient to identify bona-fide transformed lines or those where the

chromosomal T-DNA insertion location was not suited to higher levels of transgene expression.

Analysis of the Basta resistance: sensitive phenotype for the T_1 $^{cm}trL^{RNAi\text{-}S8}$ progeny showed it segregated at a 3:1 ratio, consistent with Mendelian inheritance of a single transgene insertion event. Six of the $Basta^R$ T_1 $^{cm}trL^{RNAi\text{-}S8}$ plants were transferred to grow in soil and the *RbcS* mRNA levels analysed by RNA slot blot. RNA from the ^{cm}trL genotype was analysed as a control. Replica blots were probed with [^{32}P]-labelled DNA to the *rbcL* 5'TCR (that hybridises to 5'**T**ranslational **C**oding **R**egion of the *rbcL* mRNA conserved in both wild type and the ^{cm}trL tobacco genotypes) and to a tobacco *RbcS* (Figure 3.7B). Consistent with the expected co-segregation of the RNAi-*RbcS* sequence and *bar*, no *RbcS* mRNA was detected in all six $Basta^R$ T_1 $^{cm}trL^{RNAi\text{-}S8}$ plants tested but readily apparent in both the ^{cm}trL control plants tested (Figure 3.7C). In the corresponding control *rbcL* 5'TCR blots strong hybridisation signals were found in all the ^{cm}trL and $^{cm}trL^{RNAi\text{-}S8}$ samples. This confirmed equivalent loadings of RNA for each sample in the RNA slot blot analyses.

Slot blot analyses of leaf RNA isolated from the $^{cm}trL^{RNAi\text{-}S1}$ to $^{cm}trL^{RNAi\text{-}S7}$ plants grown on MS medium (no Basta) showed they still produced *RbcS* mRNA at levels similar to wild-type (data not shown) suggesting they were not transformants or produced very low levels of the *bar* and RNAi-*RbcS* transgenes. No further analysis was undertaken on the progeny of these seven lines.

A subsequent $Basta^R$ segregation and *RbcS* mRNA analyses were performed on the remaining three putative $^{cm}trL^{RNAi\text{-}S}$ genotypes (lines 9 to 11). All three genetoype were found to be resistant to Basta concentrations of 10 mg L^{-1} and the segregation of $Basta^R$: $Basta^S$ was again ~3:1 for each line indicative of single T-DNA insertion event (Figure 3.8A). Denaturing formaldehyde agarose gel electrophoresis of the leaf RNA was used to examine the *rbcL* and *RbcS* mRNA contents in four T_1 plants from each $^{cm}trL^{RNAi\text{-}S}$ genotype along with a wild-type control (Figure 3.8B). Unlike the six $^{cm}trL^{RNAi\text{-}S8}$ samples analyzed in Figure 3.7C, RNA blot analyses showed incomplete silencing of *RbcS* mRNA in plants 1 and 4 of $^{cm}trL^{RNAi\text{-}S9}$ and plant 3 of $^{cm}trL^{RNAi\text{-}S11}$. Whether this variation might correlate with these lines being heterozygous for the T-DNA insertion remains to be examined.

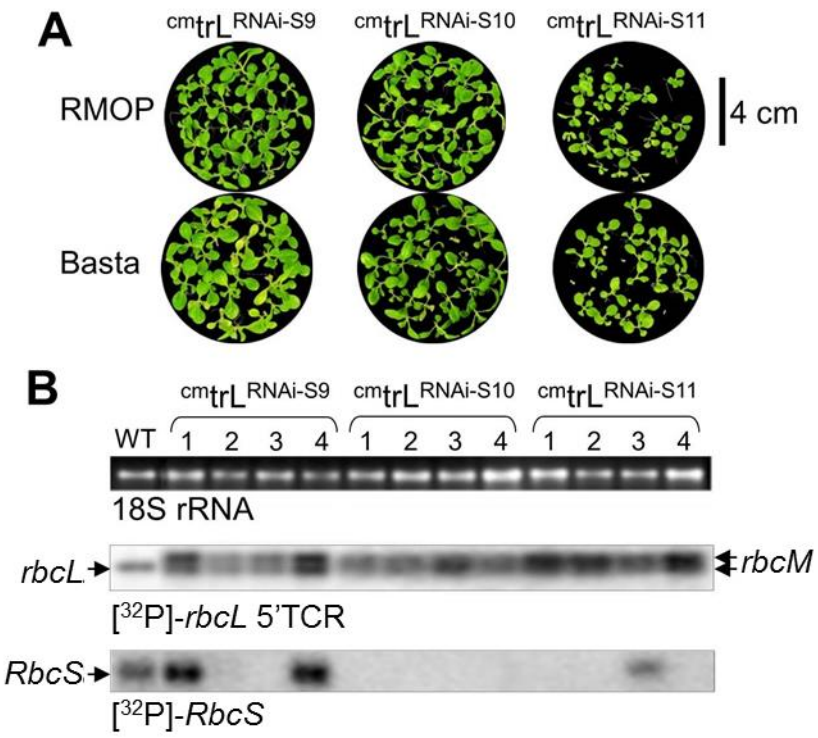

Figure 3.8 Basta^R segregation and RNA blot analysis of the ^{cm}trL$^{RNAi\text{-}S9}$ to ^{cm}trL$^{RNAi\text{-}S11}$ T$_1$ progeny.

(A) Approximately 75% of the T_1 progeny of ^{cm}trL$^{RNAi\text{-}S}$ genotypes 9, 10, and 11 showed Basta resistance. (B) RNA blot probed with the *rbcL* 5'TCR DNA (Figure 3.7B) identified similar levels of *rbcL* in the wild-type (WT) control and ^{cm}*rbcM* mRNAs in each ^{cm}trL$^{RNAi\text{-}S}$ sample. Note that the two *rbc*M transcripts in ^{cm}trL have alternate 3'UTR lengths (Whitney and Sharwood, 2008). The *RbcS* probe detected no *RbcS* mRNA in ^{cm}trL$^{RNAi\text{-}S9}$ plants 2 and 3, all four ^{cm}trL$^{RNAi\text{-}S10}$ plants, and plants 1, 2 and 4 of ^{cm}trL$^{RNAi\text{-}S11}$.

3.2.4 Generation and identification of a homozygous ^{cm}trL$^{RNAi\text{-}S8}$ line

The six T_1 plants from the ^{cm}trL$^{RNAi\text{-}S8}$ genotype examined by RNA blot analysis (Figure 3.7C) were grown to maturity in soil. Their growth phenotype again matched the ^{cm}trL and wild-type controls grown alongside under high-CO_2 growth and produced fully fertile flowers that were self-pollinated. A segregation analysis for Basta^R was undertaken on the resulting T_2 progeny. Assuming this genotype was truly a single T-DNA insertion locus (as suggested by the 3:1 Mendelian inheritance of Basta^R seen in the T_1 ^{cm}trL$^{RNAi\text{-}S8}$ progeny; Figure 3.7A), then the T_2 progeny arising from self-pollination should show a 100% Basta^R phenotype if the T_1 parent was homozygous, and a 75% Basta^R phenotype if heterozygous. As shown in Table 3.1, only the ^{cm}trL$^{RNAi\text{-}S8}$ T_2 progeny from line 4 showed 100% Basta^R indicating the parental T_1 plant was homozygous for the T-DNA allele. In contrast the other five ^{cm}trL$^{RNAi\text{-}S8}$ lines showed only ~75% Basta^R segregation indicating their parental T_1 plants were heterozygous.

Table 3.1 Basta^R segregation analysis of the ^{cm}trL$^{RNAi-S8}$ T_2 progeny

The T_2 progeny from the six T_1 ^{cm}trL$^{RNAi-S8}$ plants following self-pollination were screened for Basta^R as outline in Figure 3.7. Only the progeny from the T_1 plant 4 had a 100% Basta^R phenotype indicating it was homozygous for the T-DNA allele. The Basta^R percentage was obtained from an average of three MS plates containing 15 seedlings per plate.

^{cm}trL^{RNAi-S} line 8 (T_1) progeny	T_2 Basta^R (%)
1	68
2	80
3	71
4	100
5	79
6	77

Seeds from the T_1 progeny of plant 4 of the ^{cm}trL$^{RNAi-S8}$ genotype (or that obtained from its self-pollinated progeny) was used in all subsequent analyses in this thesis and henceforth simply referred to as the ^{cm}trL^{RNAi-S} tobacco genotype. Like its parental ^{cm}trL progenitor, the ^{cm}trL^{RNAi-S} line could be grown to maturity in soil under elevated CO_2 conditions and was fully fertile.

3.2.5 The T-DNA insertion in ^{cm}trL^{RNAi-S} is stably inherited

The stability of RNAi-silencing has shown to be quite variable in the literature, sometimes only lasting a single generation before genetic events that reverse the RNAi effects occur (Kerschen et al., 2004; Travella et al., 2006). The stability of the T-DNA insertion in the ^{cm}trL^{RNAi-S} line was therefore examined over three successive generations for 3 separate plants grown from the T_1 ^{cm}trL^{RNAi-S} seed stock (*i.e.* "plant 4"). Segregation analysis using a Basta^R screen showed the progeny of each generation maintained faithful expression of the *bar* selectable marker (Figure 3.9A). RNA blot analysis of the resulting plant tissue showed their leaves continued to lack *RbcS* mRNA (Figure 3.9B). These findings indicated the RNAi-*RbcS* and *bar* transgenes are stably inherited in successive generations of the ^{cm}trL^{RNAi-S} genotype. As indicated above (see Section 3.2.1) the growth, floral and reproductive phenotype of each ^{cm}trL^{RNAi-S} generation continued to match that of the ^{cm}trL and wild-type controls (Figure 3.10).

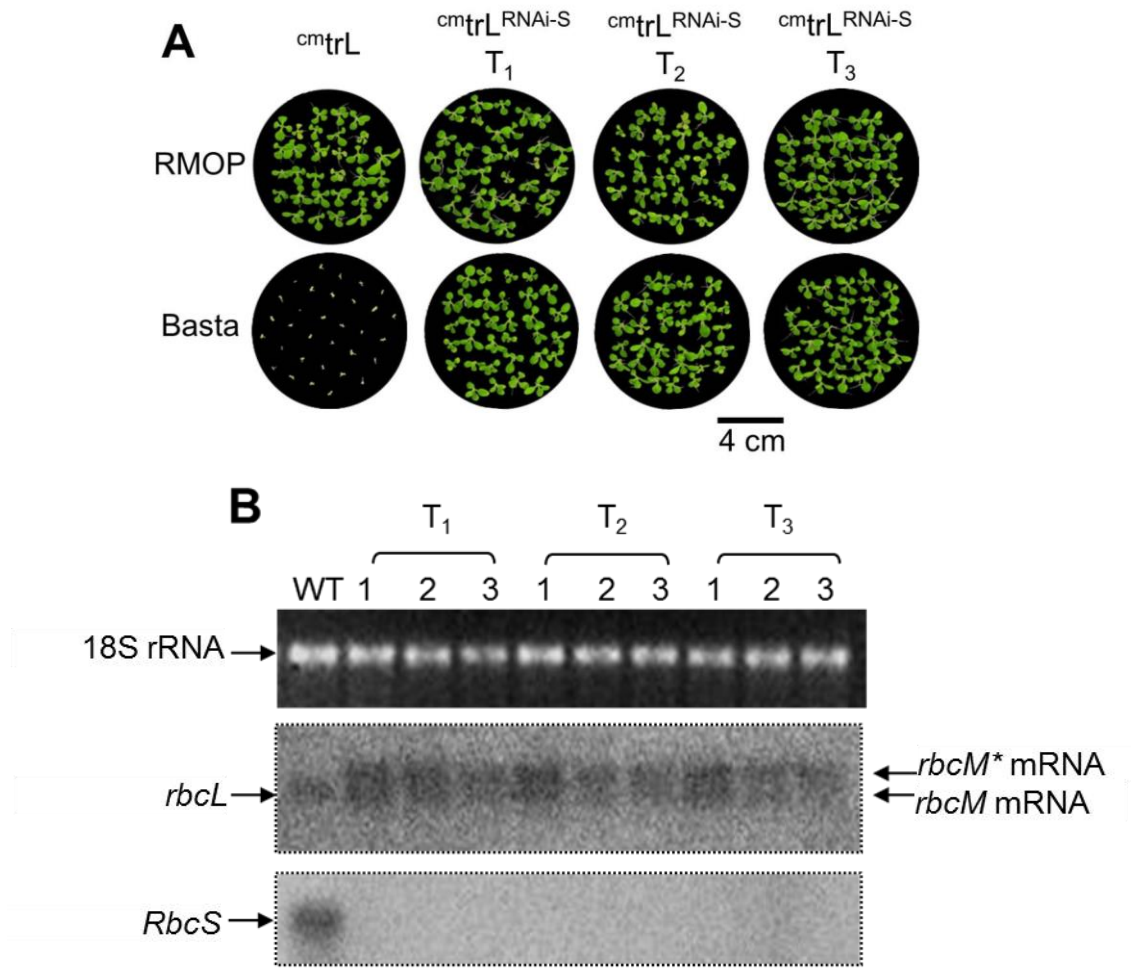

Figure 3.9 Stable inheritance of the Basta^{R} and RNAi-*RbcS* silencing genotypes in three successive generations of the ^{cm}trL^{RNAi-S} genotype.

(A) Segregation analysis of Basta^{R} at four weeks post-germination of ^{cm}trL and ^{cm}trL^{RNAi-S} seedlings on germination medium (with and without 10 µg mL^{-1} Basta). The ^{cm}trL seedlings (as also seen for wildtype, WT) were unable to grow past cotyledon emergence on Basta. In contrast the ^{cm}trL^{RNAi-S} seedlings showed indifference in growth and phenotype when grown on MS medium with or without Basta. (B) Total leaf RNA (3 µg) from three T_1 ^{cm}trL^{RNAi-S} plants and their derived T_2 and T_3 progeny following self-pollination was separated by denaturing agarose gel electrophoresis and probed with [^{32}P]-labelled *rbcL* 5'TCR and *RbcS* probes (Figure 3.7B). RNA from WT was used as a positive control for *RbcS* mRNA levels. *rbcM**, larger ^{cm}*rbcM* mRNA in ^{cm}trL genotypes due to alternative (longer) 3'UTR processing (Whitney and Sharwood, 2008).

3.2.6 The RNAi-RbcS silencing in ^{cm}trL^{RNAi-S} is heritable via cross-pollination

To determine if RNAi-*RbcS* silencing could be effectively introduced by cross-pollination, pollen from the ^{cm}trL^{RNAi-S} line (homozygous for the T-DNA, Section 3.2.4) was used to pollinate the stigma of wild-type (WT) tobacco flowers. The resulting WT♀ × ^{cm}trL^{RNAi-S} ♂ F_1 progeny were sown on MS medium both with and without Basta (10 mg L^{-1}). The MS medium contained 0.5% (w/v) sucrose as a carbohydrate supply under the presumption that the Rubisco content in the heterozygous WT♀ × ^{cm}trL^{RNAi-S} ♂ progenies would be insufficient to support photoautotrophic growth due to the efficacy

of RNAi-*RbcS* silencing. As expected, all the progeny were Basta^{R} and showed a chlorotic phenotype when compared to wild-type (Figure 3.11).

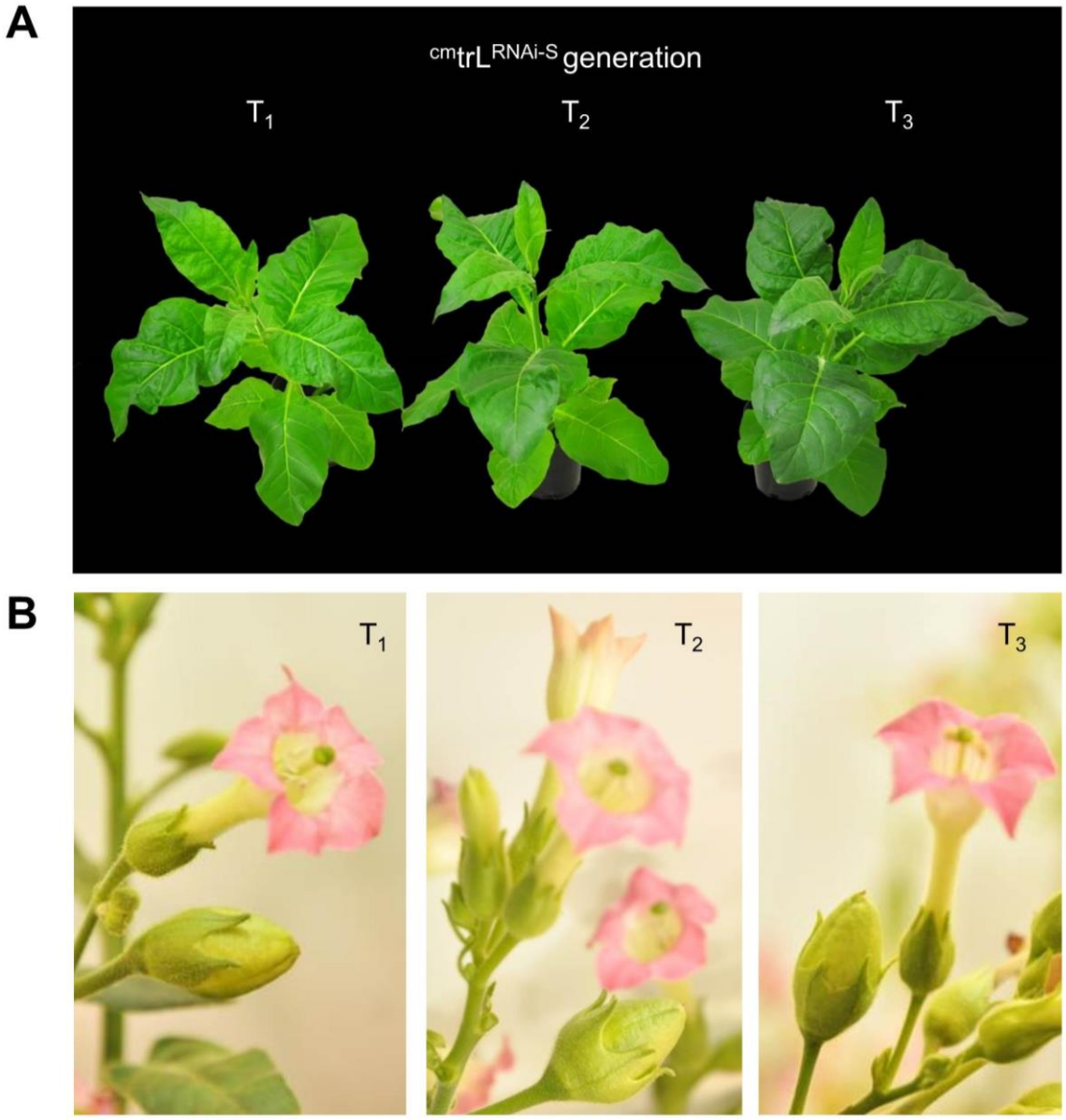

Figure 3.10 The conserved phenotype after successive generations of ^{cm}trL^{RNAi-S}.

Self-pollination of T_0, T_1 and T_2 plants of the ^{cm}trL^{RNAi-S} line gave progenies (T_1, T_2 and T_3 respectively) whose (A) vegetative growth and (B) floral phenotypes under high-CO_2 conditions remained identical to the ^{cm}trL and wild-type tobacco genotypes.

This phenotype matched that found for tobacco genotypes making little or no Rubisco (Whitney and Sharwood, 2008) suggesting effective silencing of *RbcS* mRNA and S-subunit synthesis in the plants that correspondingly depleted L_8S_8 Rubisco biogenesis.

The dependency of the WT♀ × ^{cm}trL^{RNAi-S}♂ F_1 seedlings for sucrose supplementation for survival was tested by transplanting seedlings from the MS medium containing Basta (Figure 3.12A) into medium either

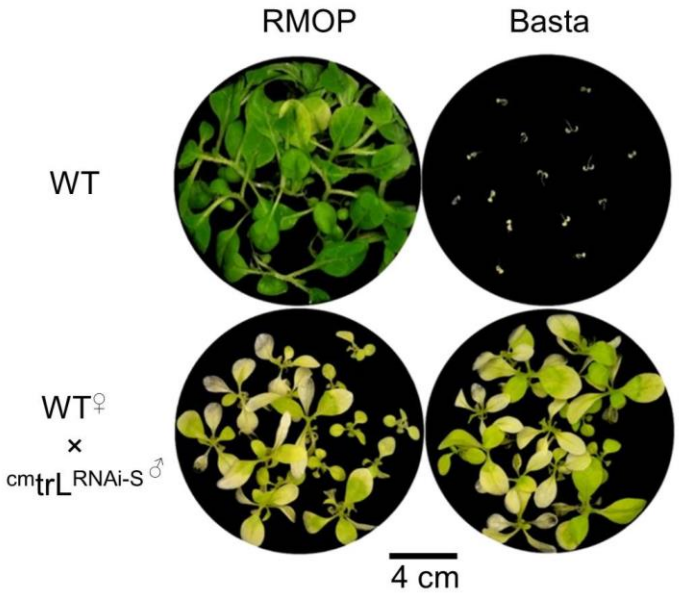

Figure 3.11 The WT♀ × ^{cm}trL^{RNAi-S}♂ progenies are Basta^{R}.

Seedlings from WT♀ × ^{cm}trL^{RNAi-S}♂ showed identical germination and growth phenotypes on MS medium with and without 10 µg mL^{-1} Basta. Their pale green leaf coloration and slow growth contrasted with the dark green, faster growing leaves of WT plants grown on MS medium. The WT seedlings were sensitive to Basta.

lacking sucrose (plants did not survive) or with 3% (w/v) sucrose (Figure 3.12B). Although they grew very slowly, the WT♀ × ^{cm}trL^{RNAi-S}♂ plants growing on MS medium produced roots and were carefully transferred to soil and grown in air with 2% (v/v) CO_2 (Figure 3.12C). Even under high-CO_2 the WT♀ × ^{cm}trL^{RNAi-S}♂ plants were unable to grow in soil (Figure 3.12D) and were fully necrotic 7 weeks after transfer to soil. This work supported the hypothesis that inheritance of the RNAi-*RbcS* genetic trait in the F_1 progenies would render them unable to survive without carbohydrate supplementation or under high-CO_2 levels if their leaves contained insufficient, or no L_8S_8 Rubisco to support photosynthesis and growth. To confirm this, soluble leaf protein from the WT♀ × ^{cm}trL^{RNAi-S}♂ plants grown in tissue culture (Figure 3.12B) was analysed by PAGE (Figure 3.13). By ndPAGE the L_8S_8 Rubisco in WT samples is clearly the most abundant protein that separates at a mass consistent with its size of ~520 kDa. In contrast no equivalent L_8S_8 protein band was evident in the ^{cm}trL^{RNAi-S} (that only produces an abundant amount of *R. ruburm* L_2 Rubisco) and WT♀ × ^{cm}trL^{RNAi-S}♂ samples. This suggested there was little or no L_8S_8 Rubisco made in the WT♀ × ^{cm}trL^{RNAi-S}♂ progeny. Consistent with this [^{14}C]-CABP binding analysis of the same leaf protein detected no appreciable amount of Rubisco in the WT♀ × ^{cm}trL^{RNAi-S}♂ leaf sample (Figure 3.13B).

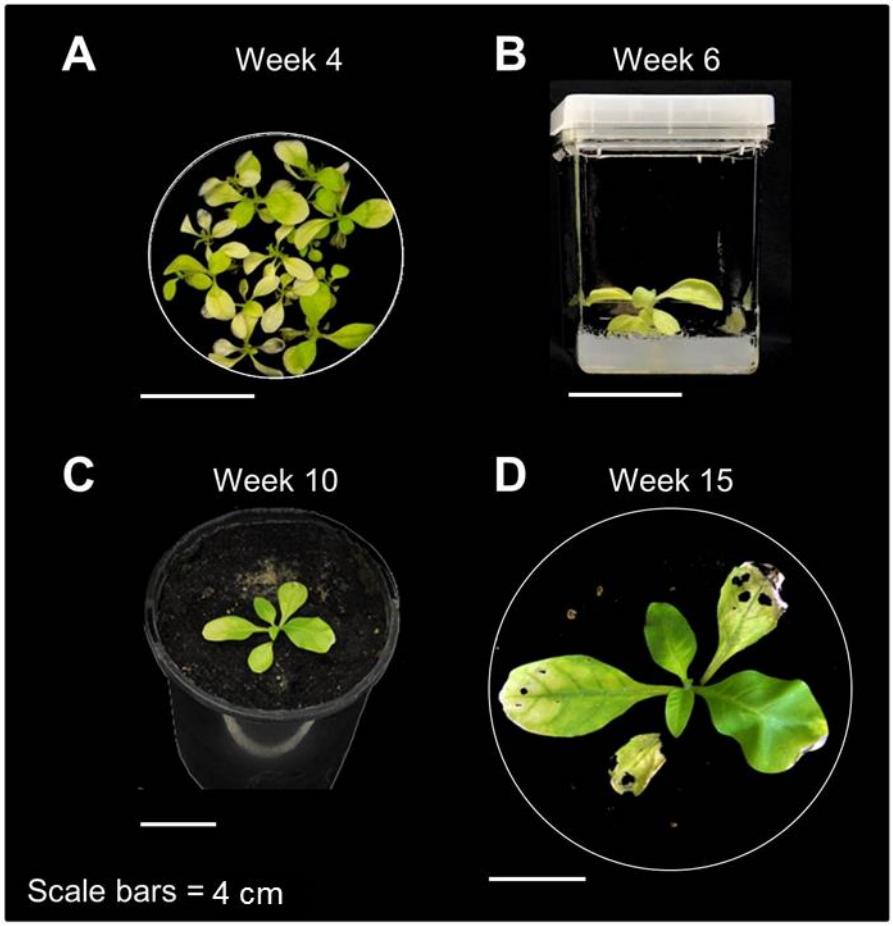

Figure 3.12 The WT♀ × ^{cm}trL$^{RNAi\text{-}S}$♂ progeny are unable to grow autotrophically.

(A) A four-week old WT♀ × ^{cm}trL$^{RNAi\text{-}S}$♂ seedling on MS medium-Basta (0.5% w/v sucrose) was transferred to (B) growth on germination media containing 3% (w/v) sucrose. Although growth was very slow, the WT♀ × ^{cm}trL$^{RNAi\text{-}S}$♂ plant produced roots and was carefully transferred to (C) growth in soil in air with 2% (v/v) CO_2 showed. (D) After four weeks no growth was evident and leaf necrosis was becoming increasing evident.

SDS-PAGE analysis of the same leaf proteins was also undertaken (Figure 3.13C). Both L-subunits and S-subunits were clearly evident by Coomassie staining in the WT sample. However only L-subunits were evident in ^{cm}trL$^{RNAi\text{-}S}$ and no L- or S-subunits were evident in the WT♀ × ^{cm}trL$^{RNAi\text{-}S}$♂ sample. Western blot analysis of the protein with an antibody to tobacco Rubisco detected both subunits in the WT sample, showed no cross-reactivity to the *R. rubrum* Rubisco produced in ^{cm}trL$^{RNAi\text{-}S}$ and detected only trace amounts of soluble L-subunits in the WT♀ × ^{cm}trL$^{RNAi\text{-}S}$♂ sample (Figure 3.13C). Whether this corresponds to nascent, unassembled L-subunits or those assembled in trace levels of L_8S_8 complexes was not clarified in this instance (but were examined in subsequent analyses that are described in Chapter 4).

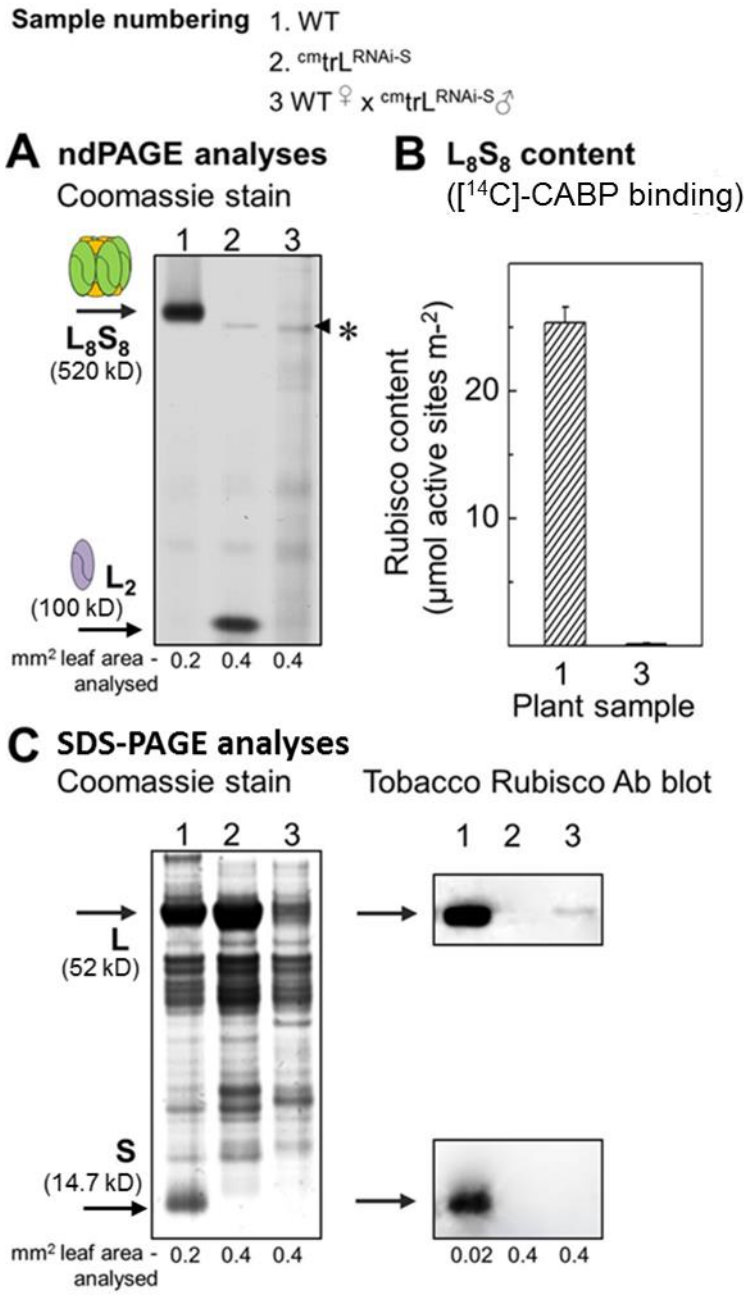

Figure 3.13 PAGE analysis of leaf protein from the different tobacco genotypes.

(A) Non-denaturing PAGE (ndPAGE) analysis identified L_8S_8 Rubisco in wild-type (WT), L_2 Rubisco in ^{cm}trL, and neither Rubisco isoform in WT♀ × ^{cm}trL^{RNAi-S}♂. *non-Rubisco protein made in tobacco (see Whitney and Sharwood, 2008. (B) [^{14}C]-CABP binding no appreciable amount of Rubisco in the WT♀ × ^{cm}trL^{RNAi-S}♂ leaves. (C) Coomassie-stained SDS–PAGE analysis identified the Rubisco L-subunit (L) and S-subunit (S) in WT, only L in ^{cm}trL and neither subunit in WT♀ × ^{cm}trL^{RNAi-S}♂. These findings were confirmed by immunoblot analysis with the tobacco Rubisco Ab that does not recognise the *R. rubrum* L_2 Rubisco (Whitney et al., 2001b). A small amount of soluble L was detected in WT♀ × ^{cm}trL^{RNAi-S}♂.

3.3 Discussion

Since the unravelling of the RNAi-gene silencing phenomenon in plants nearly twenty years ago (Waterhouse et al., 1998) it has emerged as one of the major tools in plant functional genomics. The application of RNAi to study gene function or use in commercial applications to modify metabolic pathways and facilitate resistance to plant pathogens has escalated dramatically over the last decade or so (Duan et al., 2012; Senthil-Kumar and Mysore, 2010). This chapter describes the successful application of RNAi in the generation of genetically stable $^{cm}trL^{RNAi\text{-}S}$ tobacco genotypes where *RbcS* mRNA accumulation has been effectively suppressed to levels that preclude L_8S_8 Rubisco biogenesis.

3.3.1 The potency of the RNAi-RbcS transgene in all the transformed genotypes

While mechanistic detail of the T-DNA insertion process into plant genomes still remains poorly understood, the sites of integration appear to be most frequent in transcriptionally active regions of the genome (Filipenko et al., 2009). It is thought this arises as these chromosome regions are more loosely packed by histones and thus are euchromatic. In each of the transformed $^{cm}trL^{RNAi\text{-}S}$ genotypes selected in this study (*i.e.* lines $^{cm}trL^{RNAi\text{-}S8}$, $^{cm}trL^{RNAi\text{-}S9}$, $^{cm}trL^{RNAi\text{-}S10}$ and $^{cm}trL^{RNAi\text{-}S11}$) segregation analyses for Basta resistance indicated all arose from single T-DNA insertional events (Figures 3.7 and 3.8). Ongoing backcrossing studies within the Whitney laboratory (comparable to that shown in Figure 3.9) are uniformly showing the RNAi-*RbcS* genotype is stably maintained in all the progeny in each of the $^{cm}trL^{RNAi\text{-}S}$ lines. As with the cross-pollination study between $^{cm}trL^{RNAi\text{-}S}$ and wild-type (Figure 3.11), the same crosses with homozygous $^{cm}trL^{RNAi\text{-}S9}$, $^{cm}trL^{RNAi\text{-}S10}$ and $^{cm}trL^{RNAi\text{-}S11}$ plants have recently been reproduced and found to all produce progeny with little or no Rubisco (Whitney, unpublished). These findings attest to the versatility of the RNAi-*RbcS* silencing potential of plasmid psiSS, consistent with that observed by Wostrikoff and Stern (2007) when using the same construct to silence S-subunit synthesis in wild-type tobacco.

The reason for the reproducible genetic stability and efficiency of the RNAi-*RbcS* sequence is uncertain. It is possible that inclusion of the 93 bp Intron 1 sequence in the 405 bp *RbcS* sequence incorporated in psiSS (Figure 3.3B) may suppress gene silencing of the transformed T-DNA RNAi sequence. Consistent with this hypothesis, expression of reporter proteins have shown the inclusion of intron sequences in the transgenes reduced their targeted silencing by more than 4-fold (Christie et al., 2011). Prior RNAi-silencing studies have surmised that for more efficient silencing RNAi

constructs should incorporate 300 bp or more of target sequence, with constructs incorporating the entire target gene sequence likely to have the most efficient silencing (Hily et al., 2007). The efficiency of *RbcS* mRNA silencing in the $^{cm}trL^{RNAi\text{-}S}$ genotypes questions the accuracy of such assumptions given the RNAi-*RbcS* hairpin sequence in the psiSS plasmid comprises only 57% (*i.e.* 312 of the 543 nucleotides) of coding sequence of the varying *RbcS* transcripts found in *N. tabacum* (Figure 3.5).

The relinquished requirement for S-subunits in the ^{cm}trL (Figure 3.4) may also contribute to inherent stability of the RNAi-*RbcS* genotype. As indicated in Figure 3.1, the photosynthetic CO_2 assimilation dependency of ^{cm}trL is supported by *R. rubrum* L_2 Rubisco that does not require S-subunits (Whitney and Andrews, 2001b; Whitney and Andrews, 2003). One method to test this hypothesis would be to transform the tobacco *rbcL* back into the plastome of $^{cm}trL^{RNAi\text{-}S}$. This would reinstate the potential for tobacco L_8S_8 synthesis if silencing of the RNAi-*RbcS* genotype was readily reversible. A reversion of the RNAi-*RbcS* silencing in this genotype however seems unlikely given the WT♀ × $^{cm}trL^{RNAi\text{-}S}$♂ progeny sown on MS medium (no Basta; Figure 3.11) showed no evidence of any progeny having improved growth that would be expected if they re-acquired the capacity for L_8S_8 biogenesis via destabilizing the RNAi-*RbcS* silencing.

3.3.2 Locating the T-DNA insertion position in $^{cm}trL^{RNAi\text{-}S}$ genomes

The recent availability of comprehensive genome sequence for *N. tabacum* (Gong et al., 2014) provides impetus for accurately identifying the T-DNA insertion point within the $^{cm}trL^{RNAi\text{-}S}$ genome. Replicating such analyses in the $^{cm}trL^{RNAi\text{-}S9}$, $^{cm}trL^{RNAi\text{-}S10}$ and $^{cm}trL^{RNAi\text{-}S11}$ is also of merit to compare their chromosomal insertion points and confirm they all arise from independent, single insertion, transformation events (Figure 3.8). Characterising the genome insertional point is also important for identifying potential effects on the expression of gene(s) within inserted region as well as identifying whether the genetic context of their insertional point might explain the potency of the RNAi-*RbcS* genotype (see Section 3.3.1).

Identifying the chromosomal insertion point may prove to be somewhat of a bioinformatic challenge given that the current publically available *N. tabacum* sequence information comprises non-annotated whole genome shotgun contiguous sequences (WGS). Nevertheless, work has now begun in the Whitney laboratory using genome/primer walking to determine the T-DNA insertion site in each of the four $^{cm}trL^{RNAi\text{-}S}$ genotypes produced in this thesis. As outlined in Figure 3.14, the nucleotide template for this PCR based technique is gDNA from each genotype that has been

fragmented by blunt end restriction enzyme digestion prior to ligating on adapter sequences to both ends of the DNA fragment. This template is then used in PCRs using a primer to the adaptor sequence and a Gene Specific Primer (GSP, or a series of nested GSPs) that is unique to the transformed sequence. Typically these primers are designed in close proximity to the left border (LB) and right border (RB) of the inserted T-DNA (Figure 3.14).

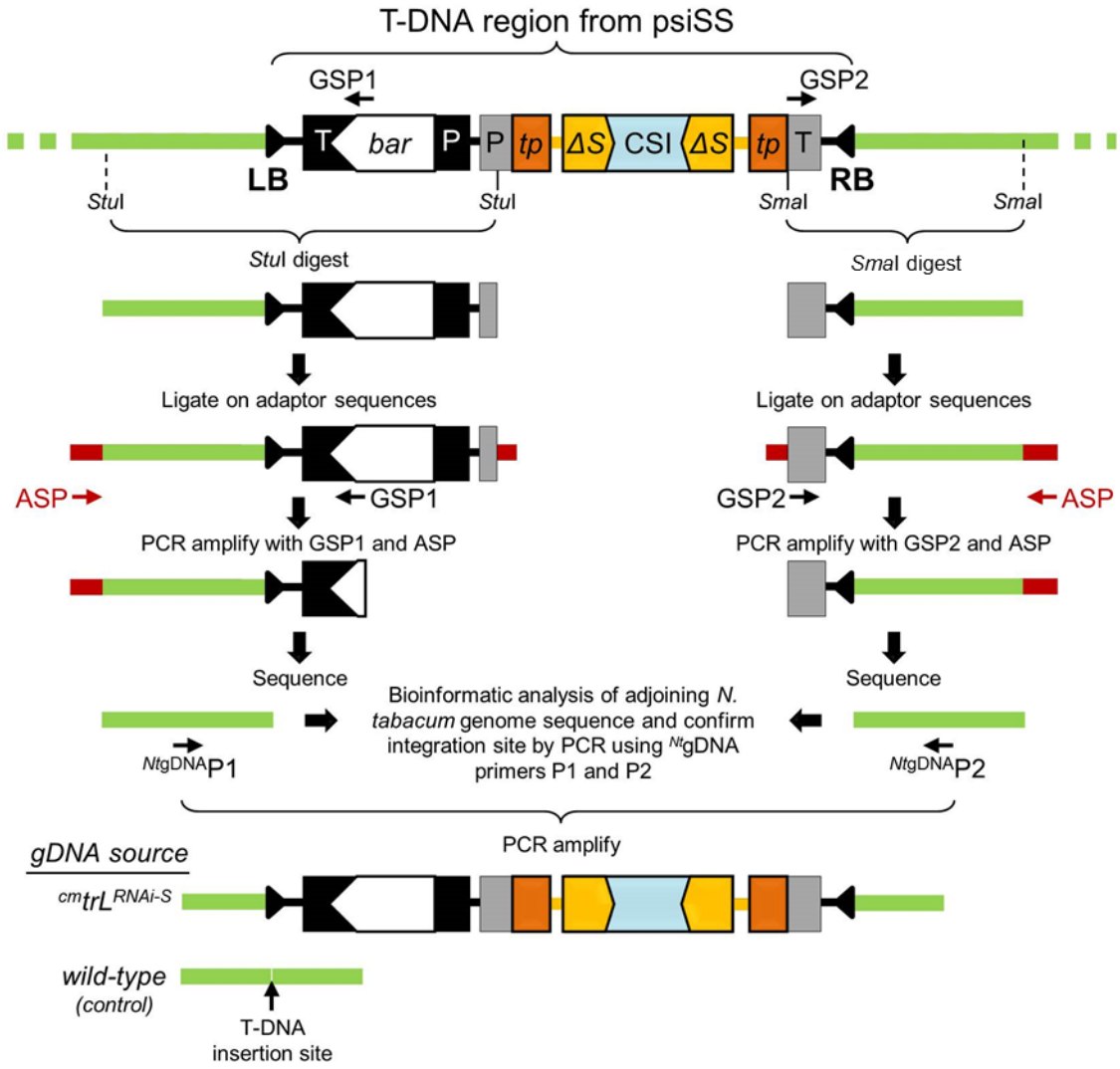

Figure 3.14 Identifying the T-DNA insertion point in the $^{cm}trL^{RNAi\text{-}S}$ genomes by "primer walking".

Summary of the process for primer walking the $^{cm}trL^{RNAi\text{-}S}$ genome to identify the insertion position and amount of the T-DNA sequence in psiSS inserted into the chromosome. Restriction enzymes used to digest the $^{cm}trL^{RNAi\text{-}S}$ gDNA are considered relative to the annealing position of the gene specific primers (GSP-1 and GSP-2) that align to unique sequences near the T-DNA Left Border (LB) and Right Border (RB). Correct mapping of the T-DNA insertion is confirmed by PCR using additional primers (P1, P2) and via computational analysis with the non-annotated whole genome shotgun contiguous sequences (WGS) now available for *N. tabacum* (Gong et al., 2014).

The design of the GSP's used in any genome/primer walking experiment need to take into account the recent finding by deep sequencing that multiple *Agrobacterium* derived cellular T-DNA sequences are already present in the genome of *N.*

tomentosiformis (one of the ancestral progenitors of *N. tabacum*) (Chen et al., 2014; see also Section 1.4.1). This analysis validated the findings of prior genomic PCR analyses that identified varying regions of T-DNA sequence from varying *Agrobacterium* sources in many, but not all, species of *Nicotiana* (Intrieri and Buiatti, 2001; Mohajjel-Shoja et al., 2011). With this in mind, the current GSP's being utilized to analyse the four $^{cm}trL^{RNAi\text{-}S}$ genotypes are specific to the *bar* selectable marker (adjacent to the LB) and the octopine synthase terminator sequence regulating the RNAi-*RbcS* allele (adjacent to the RB Figure 3.14).

3.3.3 Exploiting $^{cm}trL^{RNAi\text{-}S}$ for transplastomic study of Rubisco

Effective silencing of *RbcS* mRNA accumulation in the $^{cm}trL^{RNAi\text{-}S}$ line poses the first report of successful elimination of S-subunit synthesis by RNAi in any species of higher plant. As such the $^{cm}trL^{RNAi\text{-}S}$ lines provided a unique genotype for transgenic studies of S-subunit biochemistry in regard to its role on L_8S_8 biogenesis and catalysis in tobacco leaf chloroplasts. The following chapters describe varying transgenic tests undertaken to test the versatility of $^{cm}trL^{RNAi\text{-}S}$ for bioengineering tobacco and heterologous S-subunits and the development of tailored chloroplast transformation approaches for optimal recombinant Rubisco expression in tobacco leaves.

CHAPTER 4 – ENABLING ASSEMBLY OF RUBISCO COMPRISING CHLOROPLAST MADE SMALL SUBUNITS USING THE ^{CM}TRL$^{RNAi\text{-}S}$ TOBACCO GENOTYPE

4.1 Introduction

4.1.1 Rubisco assembly in higher plants

Approximately 3000 nucleus encoded proteins, including the Rubisco S-subunits, are imported from the cytosol into leaf chloroplasts (Li and Chiu, 2010). The reason why most, but not all, chloroplast genes have been translocated to the nucleus in higher plants remains uncertain. Gene transfer from the chloroplast genome (plastome) to the nucleus during evolution is thought to be facilitated by an improved allowance of gene expansion and adaptive evolution (Coate et al., 2011). The conserved retention of some chloroplast genes is thought to arise from the potential toxicity of their products if produced in the cytosol or an inability to meet the levels needed for chloroplast functioning (Timmis et al., 2004). For Rubisco, relocation of the *rbcL* to the nucleus seems unfavourable with regard to being able to meet the large amounts of L-subunit required in Rubisco biogenesis (Kanevski and Maliga, 1994). In contrast, the evolutionary relocation and duplication of *RbcS* in the nucleus of plant cells has occurred without peril (see Section 3.1.5). Accompanying this relocation has been the incorporation of appropriate *cis* elements necessary for regulating *RbcS* expression and a sequence for chloroplast targeting. As well, appropriate sequence changes have had to evolve to facilitate interaction of the nascent S-subunits with the molecular partners needed during their synthesis, folding and chaperoning to and through the chloroplast envelope. Once in the stroma additional ancillary proteins are also required for chaperoning S-subunit assembly with the Rubisco L-subunits into L_8S_8 holoenzyme (Nishimura et al., 2008).

4.1.2 Synthesis of S-subunits in the cytosol and import into chloroplasts

While the L-subunit undergoes a variety of translational and post-translation processes within the chloroplast stroma, *RbcS* in the nucleus of plant cells have evolved to code a precursor S-subunit peptide of 20 kDa that is synthesized by cytoplasmic ribosomes (Dobberstein et al., 1977). Once translated, the amino (N-) terminal extension (i.e. a ~6 kDa transit peptide) of the S-subunit precursor undergoes a range of post-translational

processes and interactions with a range of energy requiring (*i.e.* GTP, ATP) molecular partners. These interactions include one with a protein kinase to phosphorylate serine amino acids in the tobacco S-subunit precursor (Waegemann and Soll, 1996), followed by interaction with a 14-3-3 protein that recognizes the phosphorylated product and together with an import-associated heat shock protein (Hsp70) forms a 'guidance complex' leading the precursor towards a multi-subunit Translocon at the outer membrane complex of the chloroplast (Toc). The S-subunit precursor is then passed through another multi-subunit translocon complex via a process fuelled by ATP hydrolysis in association with a ubiquitous stromal heat shock protein 93 (Hsp93), also identified as caseinlytic peptidase (ClpC) (Paila et al., 2015). The net positive charge of the precursor (Flores-Pérez and Jarvis, 2013) is also thought to play a shuttling role to the negatively charged chloroplast envelope membrane surface (Kriechbaumer et al., 2012).

Although pictorially a relatively simple process (Figure 4.1), the multiple molecular partners so far known to be involved in S-subunit import into the chloroplast (Table 4.1) underpin the complexity of the chloroplast import requirements. The translocon assemblies in both the outer (Toc) and inner (Tic) membranes of the chloroplast (Justice et al., 2014) comprise super-complexes of numerous components that interact amongst themselves and with cytosolic and stromal proteins during S-subunit processing (Paila et al., 2015). The evolutionary adaptation of the S-subunits with these molecular partners has been hypothesised as a possible reason for why the native cytosolic made S-subunits in leaves appear to assemble with L_8 cores in preference to recombinant S-subunits made in the chloroplast stroma (Whitney and Andrews, 2001a).

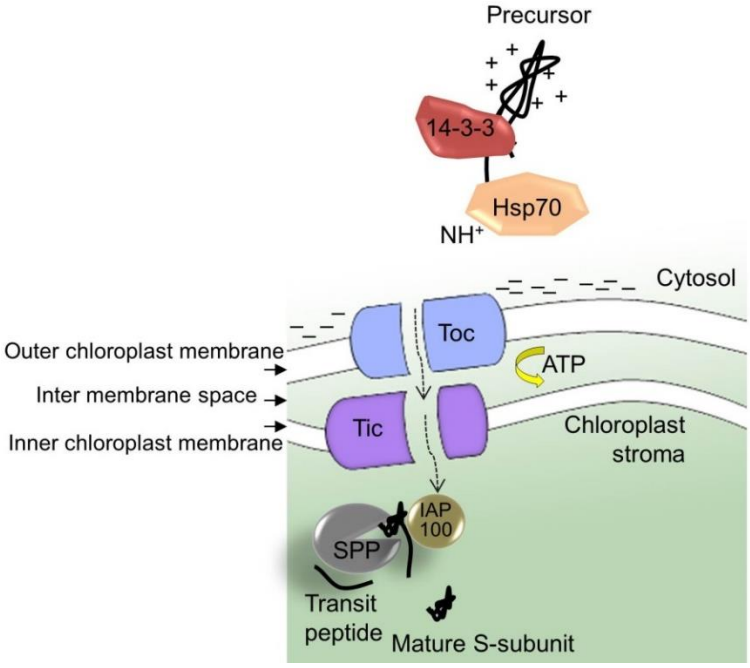

Figure 4.1 S-subunit precursor import into the chloroplast.

Binding of chaperones such as the 14-3-3 proteins and Hsp70 in the cytosol helps target and maintain stable conformation of precursor S-subunits during their transport to the outer chloroplast membrane. Transport of the precursor through the Toc and Tic complexes is driven by nucleotide hydrolysis facilitating their entry into the stroma where they are bound by Tic110/IAP100 chaperones while the transit peptide is cleaved by a generic stromal protein peptidases (SPP). See Table 4.1 below for enzyme details.

Table 4.1 Proteins involved in S-subunit import into the chloroplast.

The members of the S-subunit import mechanisms and L-subunit chaperoning have been determined in various plants and techniques (Waegemann and Soll, 1996; Richter and Lamppa, 2003; Tsai et al., 2012; Shi and Theg, 2013; Paila et al., 2015).

Protein	Location	Function
Kinase	Outer envelope membrane	Phosphorylates Rubisco S-subunit precursor at serine.
Heat shock protein 70 (Hsp70)	Outer envelope membrane	Maintain stability and conformation of precursor, guide translocation by the N-terminal.
14-3-3 protein	Outer envelope membrane	Keeps precursor unfolded, drives translocation and allows recognition of SPP.
Heat shock protein 93 (Hsp93, Clpc)	Outer envelope meembrane	ATP-assisted transportation of Rubisco S-subunit precursor through Toc.
Translocon at the outer membrane of the chloroplast (Toc)	Outer envelope membrane	Consists of Toc160, Toc75, and Toc34. Transports precursor from cytosol into stroma.
Translocon at the inner membrane of the chloroplast (Tic)	Inner envelope membrane	Consists of Tic20, Tic22, Tic40, Tic55, and Tic110. Transports precursor from cytosol into stroma.
Tic110/ Intermediate associated protein 100 (IAP100)	Inner envelope membrane	Binds to precursor
Chloroplast chaperone 60, 20 and 10 (Cpn60, Cpn20/21, Cpn10)	Stroma	Assist folding of L-subunit to facilitate L_8 assembly.
Stromal processing peptide (SPP)	Stroma	Removes and degrades N-terminal transit peptide (maturation of S-subunit precursor).

4.1.3 The S- and L-subunits are post-translationally modified for L_8S_8 assembly

As S-subunit precursors emerge from the Toc/Tic translocation channel into the stroma they are bound by Tic110 (Shi and Theg, 2013) whereupon the transit peptide is removed and degraded by a highly efficient stromal processing peptidase (SPP). Following cleavage the N-terminal Met-1 is methylated by a methyltransferase and requires the cofactor *S*-adenosyl-methionine (SAM) as a methyl-group donor to modify the α-amino group of Met-1 of the mature S-subunit to *N*-methyl-methionine. The significance of *N*-methylation is undetermined but has been proposed to regulate S-subunit expression levels, intracellular targeting and protein stability (Whitney et al., 2011a; Alban et al., 2014). Once correctly folded and post-translationally modified in the stroma the mature S-subunit (of ~14 to 15 kDa) is available for assembly with L-subunit oligomeric complexes to form L_8S_8 holoenzyme (Figure 4.1 and Figure 4.3).

During and after translation of nascent L-subunits in the chloroplasts stroma they interact with an unknown array of chaperones (possibly DnaJ, DnaK and GrpE) (Nishimura et al., 2008) and also undergo post-translational modifications that encompass the removal of the N-terminal Met-1 and Ser-2 residues, followed by the acetylation of Pro-3 (Figure 4.2) (Houtz et al., 1989). The L-subunits are delivered to the cage of chaperonin Cpn60 complexes (Kim et al., 2013) and then capped by Cpn10/20 subunits (Figure 4.3) (Tsai et al., 2012). Folding and release of the L-subunit within the chaperonin cage is powered by ATP hydrolysis, with multiple cycles within the cage likely required for optimal folding (Hartl et al., 2011; Vitlin Gruber et al., 2013). Chaperones such as Rubisco Accumulation Factors 1 (RAF1) and 2 (RAF2) interact with L- and S-subunits to facilitate Rubisco L_8S_8 assembly (Figure 4.3) (Whitney et al., 2015) as well as possible other Rubisco specific chaperones such as BUNDLE SHEATH DEFECTIVE2 (BSD2) and an assembly chaperone for hexadecameric Rubisco, RbcX (Feiz et al., 2012; Feiz et al., 2014). At some stage during L_8S_8 biogenesis the highly conserved Lys-14 in the L-subunit is also tri-methylated by AdoMet:Rubisco LS (lysine) N-methyltransferase (Rubisco LSMT, EC 2.1.1.127) (Figure 4.2). As some plant L-subunits do not undergo this modification, its tentative role in facilitating protection to proteolytic degradation remains uncertain.

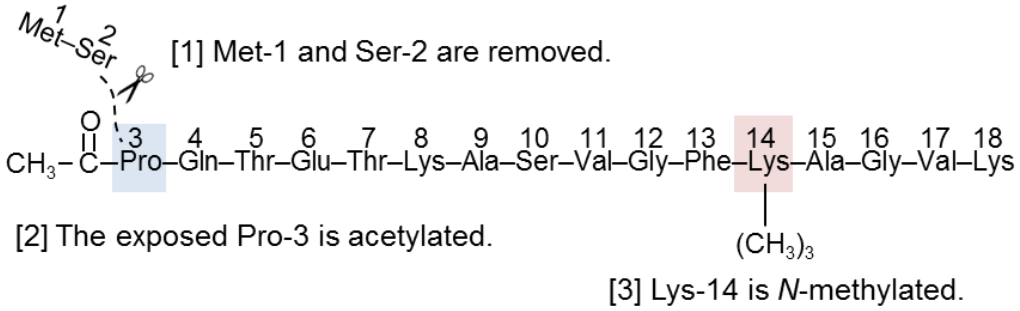

Figure 4.2 Post-translational modification of the L-subunit prior to L_8S_8 assembly.

Modifications were identified by mass spectrometry following partial tryptic proteolysis of Rubisco from plants such as tobacco, wheat and spinach. Figure adapted from Houtz et al. (1989).

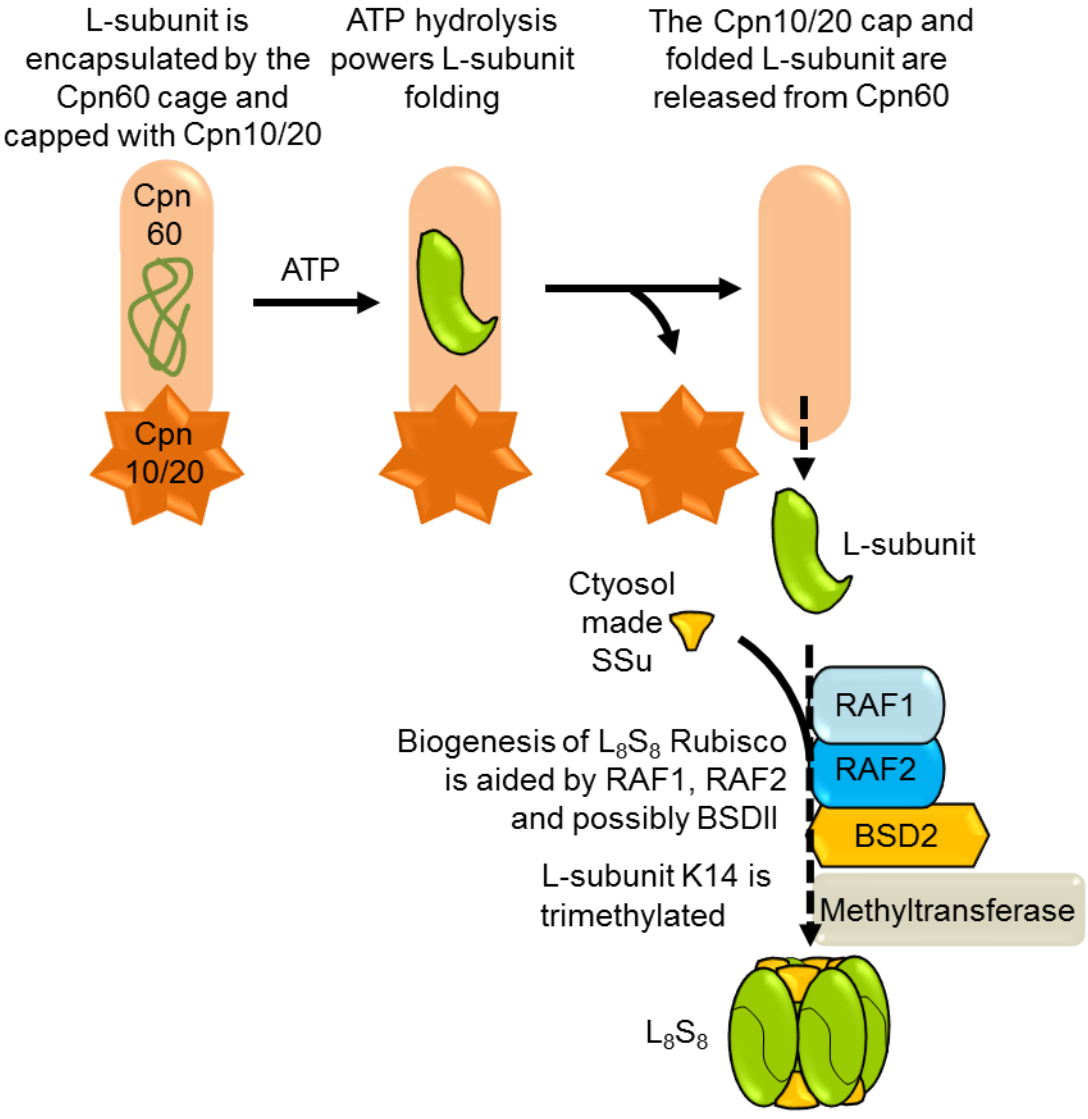

Figure 4.3 Summary of L_8S_8 Rubisco assembly in leaf chloroplasts.

The biogenesis of L_8S_8 Rubisco in leaf chloroplasts involves interactions with a variety of co-evolved molecular partners and a number of post-translation modifications that are thought to provide the enzyme with improved stability and resistance to proteolysis.

4.1.4 Expression of RbcS transformed into the tobacco plastome

Attempts to re-introduce an *RbcS* back into the chloroplast genome (plastome) of tobacco showed that despite large increases in transcript abundance (Figure 4.4) very few chloroplast made S-subunits were incorporated into L_8S_8 complexes (Whitney and Andrews 2001a). The same result was obtained when the same *RbcS* was introduced into anti-*RbcS* tobacco genotypes producing 70 to 80% less Rubisco when compared with WT (Zhang et al., 2002). In both experiments the transplastomic tobacco genotypes contained duplicate copies of a native *N. tabacum RbcS* inserted into the inverted repeat regions of the plastome. In the Whitney and Andrews (2001a) study, the *RbcS* encoded a transit peptide (tp) (RVtpSSuH) or no tp (RVSSuH) (Figure 4.7). Expression of the transgenes was regulated by identical *psbA* promoter and terminator regulatory sequences that had successfully facilitated high levels of recombinant protein expression (Staub and Maliga, 1994; Whitney and Andrews, 2001a). Each *RbcS* transgene included a C-terminal hepta-histidine-encoding sequence (S^{H7}) to allow the identification and purification by nickel-nitrilotriacetic acid (Ni-NTA) of protein complexes comprising chloroplast made S^{H7}-subunits. Analyses revealed the RVtpSSuH genotype produced higher amounts of S^{H7} than the RVSSuH plants (consistent with the higher levels of tp*RbcS* mRNA in RVtpSSuH leaves, Figure 4.4). Despite the >10-fold higher levels of chloroplast *RbcS* mRNAs made relative to the cytosol *RbcS* mRNA levels, the chloroplast made S^{H7}-subunits only accounted for ~1.2% of the total S-subunit pool assembled into Rubisco (Staub and Maliga, 1994; Whitney and Andrews, 2001a).

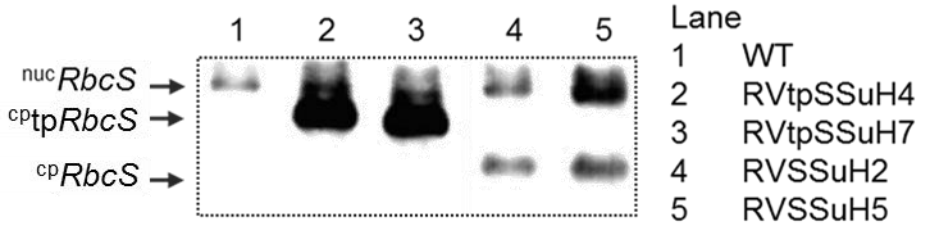

Figure 4.4 RNA blot analyses showing the high abundance of plastome made *RbcS* mRNA in the transplastomic RVtpSSuH and RVSSuH tobacco genotypes relative to wild-type (WT)

RNA hybridized with a [^{32}P]-labelled *RbcS* DNA probe showing the chloroplast made *RbcS* mRNA in the RVtpSSuH (^{pt}tp*RbcS*) and RVSSuH (^{cp}*RbcS*) tobacco lines were more than five-fold higher than the cytosolic *RbcS* mRNA levels (^{nuc}*RbcS*). Figure modified from Whitney and Andrews (2001).

Increasing the incorporation of plastid made S-subunits into L_8S_8 complexes was obtained by directing *RbcS* transgene insertion into a transcriptional hot spot in the plastome inverted repeat region of an anti-*RbcS* tobacco genotype (Dhingra et al., 2004;

see also Section 3.1.2). This posed a significant advance in S-subunit engineering, but was marred by insufficient evidence to confirm the "additional" S-subunits were of chloroplast origin and not from changes in the efficiency of the anti-*RbcS* silencing.

4.1.5 Research Objective –producing L_8S_8 holoenzyme comprising only plastid made S-subunits

As Rubisco catalysis is influenced by sequences in both the L-subunit and S-subunits (see Section 1.2.2), an underpinning goal of Rubisco structure-function studies is to develop tools for mutagenic analysis of both subunits. Such studies are readily feasible for prokaryotic Rubisco isoforms that can be functionally expressed in *E. coli* (Parry et al., 2013). Likewise mutants of the unicellular green algae *Chlamydomonas reinhardtii* where both nuclear *RbcS* are disabled have been used to produce L_8S_8 Rubisco comprising mutated S-subunits either with or without changes to the chloroplast made L-subunits (Khrebtukova and Spreitzer, 1996; Spreitzer et al., 2005; Genkov and Spreitzer, 2009). However such analyses remain elusive in leaf chloroplasts where heterologous *RbcS* expression studies have given conflicting outcomes of impaired catalysis (pea S-subunits expressed in *Arabidopsis*) (Getzoff et al., 1998), no change in catalysis (Fukayama et al., 2015) or catalytic adaptation (Ishikawa et al., 2011) (see Section 5.1.1 for more details).

A key limitation of recombinant S-subunit studies in leaf chloroplasts stems from the multiple *RbcS* copies present in the nucleus. This restricts their capacity for targeted deletion and/or universal mutagenic testing. Targeted silencing of all S-subunit synthesis in leaf chloroplasts may also be considered counter-productive given the reliance of plants on L_8S_8 Rubisco function for autotrophic growth. However, as shown in Chapter 3, the dependence of the $^{cm}trL^{RNAi\text{-}S}$ tobacco genotype on *R. rubrum* L_2 Rubisco for survival has enabled effective silencing of Rubisco S-subunit synthesis by RNAi-*RbcS*. Also demonstrated was the effectiveness of using $^{cm}trL^{RNAi\text{-}S}$ to silence L_8S_8 biogenesis in wild-type tobacco via introduction of the RNAi-*RbcS* transgene by pollination (Figure 3.13).

This chapter describes efforts to qualify the potential for producing Rubisco comprising only chloroplast made small subunits. A pollination approach was used to transfer the RNAi-*RbcS* allele into the transplastomic tobacco genotypes LEVLSSuH, RVSSuH and RVtpSSuH. As summarised in Figure 4.7 these genotypes were chosen as they produce chloroplast S^{H7}-subunits (15.7 kDa) that are larger and readily distinguishable from the endogenous cytosol made S-subunits (14.7 kDa) by SDS-

PAGE (Whitney and Andrews, 2001a). The content and subunit composition of Rubisco in the resulting progeny was analysed to compare the effectiveness of chloroplast made S^{H7}-subunit assembly into L_8S_8 holoenzyme. Such knowledge is pivotal towards developing an optimal transgenic approach for mutagenic study of Rubisco structure and function in leaf chloroplasts.

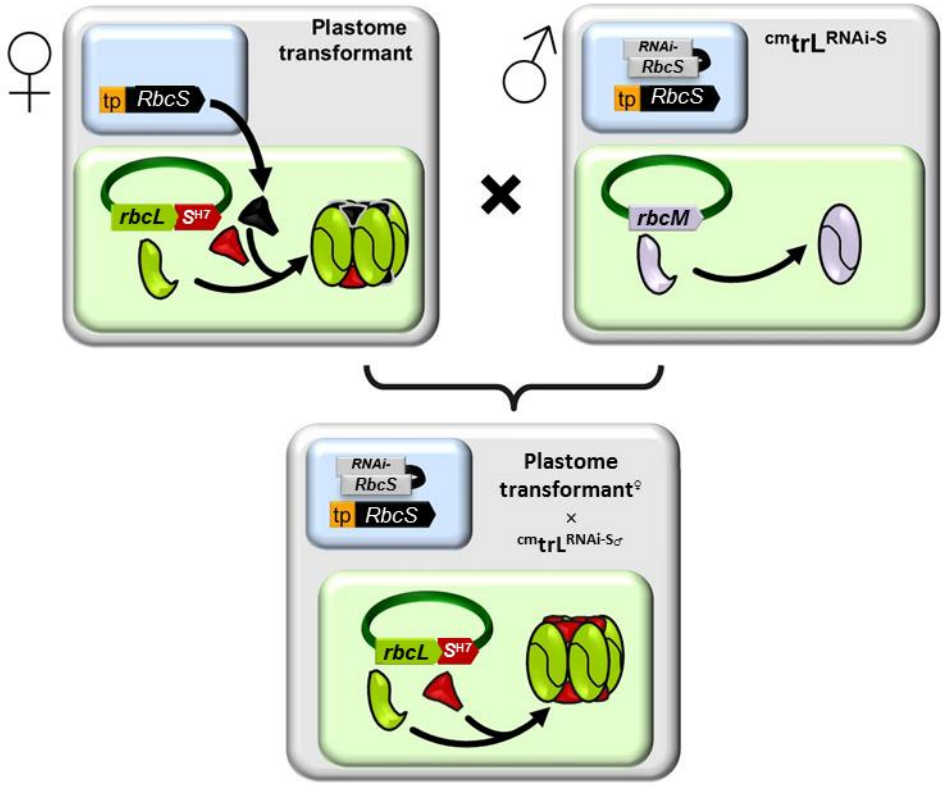

Figure 4.5 Schematic demonstration of the transgenic crosses tested in this study.

Schematic showing the aim of crossed-pollinating $^{cm}trL^{RNAi\text{-}S}$ with varying transplastomic lines producing chloroplast made S-subunits to generate RNAi-*RbcS* progeny where only the chloroplast made S-subunits are available for L_8S_8 biogenesis.

4.2 Results

4.2.1 Generating the LEVLSSuH transplastomic line

The RVSSuH and RVtpSSuH tobacco genotypes used in this study were those previously generated (Whitney and Andrews, 2001a). In contrast the LEVLSSuH tobacco lines are uncharacterised transplastomic genotypes generated by Dr. Whitney where the *N. tabacum RbcS* transgene is inserted downstream of *rbcL* (Figure 4.6). Three homoplasmic LEVLSSuH lines were generated by transforming the ^{cm}trL genotype (Figure 1.11) with plasmid pLevLSSuH, a derivative of the pLEV1 transforming plasmid (Whitney et al., 1999). As indicated in Figure 4.6, the transformed LEVLSSuH tobacco genotypes contained the same tobacco *RbcS* transformed into RVtpSSuH (*i.e.* inclusive of its N-terminal transit peptide coding sequence) that was

cloned downstream of *rbcL* in the large single-copy (LSC) region of the tobacco plastome. In the LEVLSSuH genotype expression of both *rbcL-rbcS* mRNA and *rbcL-rbcS-aadA* mRNA were regulated by the endogenous *rbcL* promoter and 5' untranslated region (5'UTR) (Figure 4.7). The *rbcL* 3'UTR sequence between the *rbcS* and *aadA* genes was used as it has been shown to have sufficient transcriptional read-through for *aadA* mRNA synthesis and translation to facilitate transformant selection on spectinomycin (Whitney and Sharwood, 2008). The T_1 progeny of three independently generated LEVLSSuH lines were found to have identical cellular biochemistry (Whitney, unpublished). This is consistent with each line being genetically identical as a result of the homologous recombination route of plastome transgene transformation (Maliga, 2003). Only one of these lines, annotated as LEVLSSuH, was studied in this thesis.

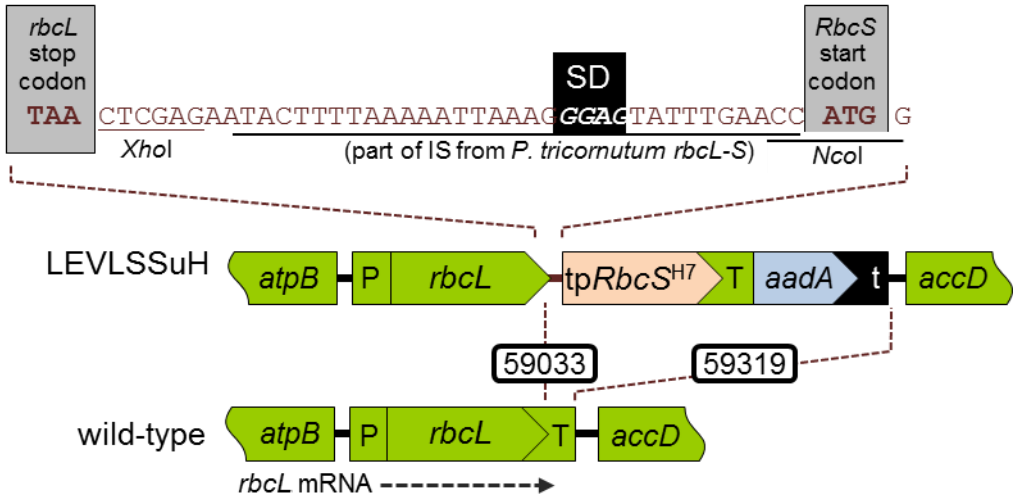

Figure 4.6 Generation of the LEVLSSuH tobacco genotype.

The *RbcS* and transit peptide sequence derived from RVtpSSuH (as a *Nco*I-*Sal*I fragment) were inserted 3' to *rbcL* in plasmid pLEV1 (Whitney et al., 1999) and separated by the shown synthetic 39 bp intergenic sequence (IS) that is similar to that used by Whitney and Sharwood (2008). Expression of the *rbcL*, tp*RbcS*^{H7} and *aadA* genes were regulated by the native *rbcL* promoter and 5'UTR sequence (P). The *rbcL* 3'UTR (terminator, T), *aadA* and *rps16* 3'UTR (t) sequence match those used in pLEV1. The transgene insertion region relative to the wild-type plastome is shown as dashed lines with the nucleotide numbering correlating with GenBank sequence Z00444 for the tobacco plastome.

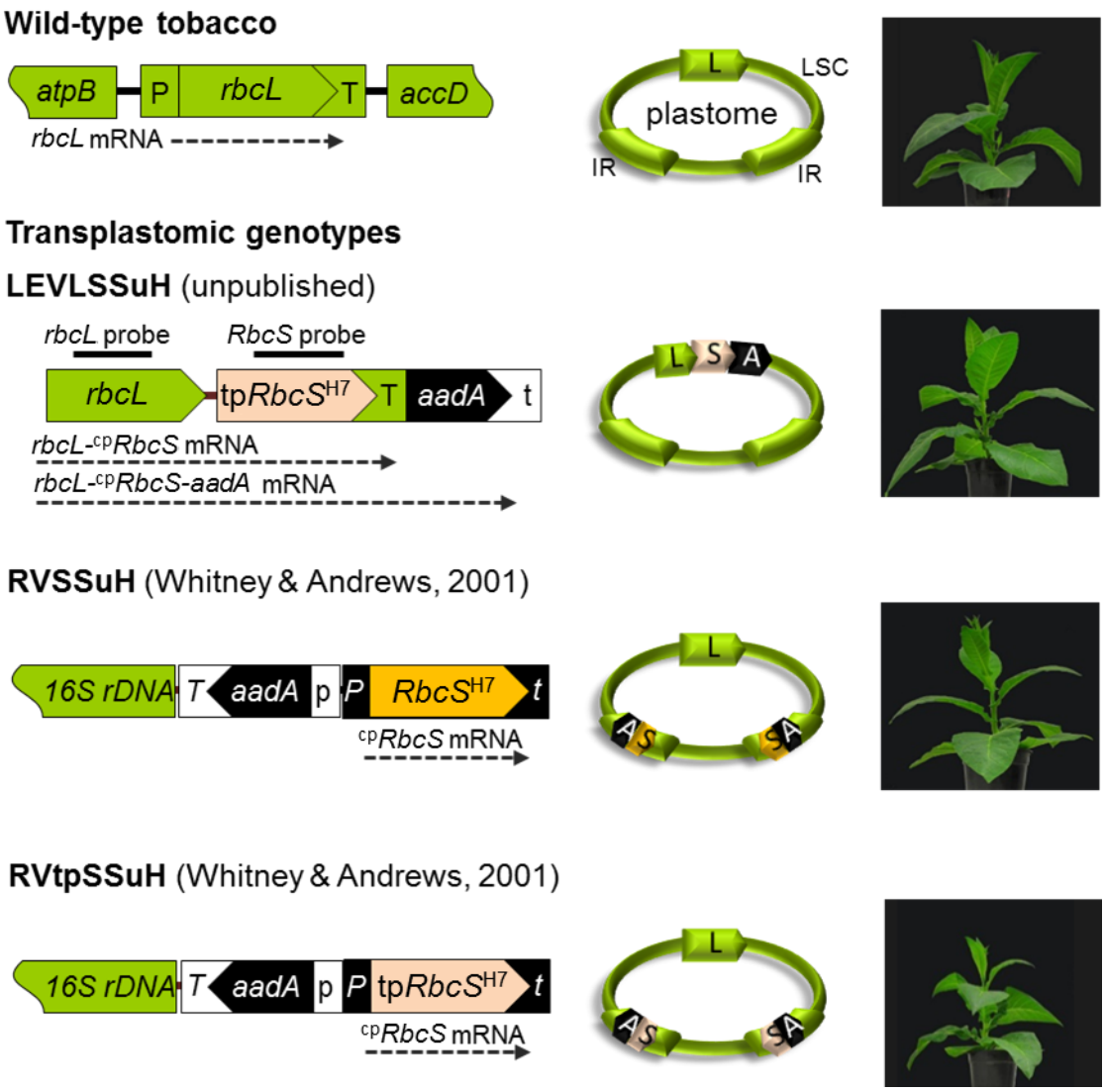

Figure 4.7 Comparative plastomes and phenotypes of the LEVLSSuH, RVSSuH, RVtpSSuH and wild-type tobacco genotypes.

Comparitive location of the native *rbcL* relative to the chloroplast localised *RbcS* (cp*RbcS*) and *aadA* transgenes within the large single copy (LSC) or inverted repeat (IR) regions of the plastome in each tobacco genotype. Shown are the location of the *rbcL* and *RbcS* DNA probes used for RNA blot analyses and the corresponding Rubisco mRNA species produced. After three weeks, the growth and phenotype of all three transplastomic lines matched the wild-type controls (grown in the glasshouse in air). P, tobacco *rbcL* promoter/5'UTR; T, *rbcL* 3'UTR; *P*, *psbA* promoter/5'UTR; *t*, *psbA* 3'UTR; p, *rrn* promoter/*T7g10* 5'UTR; *t*, *rps16* 3'UTR.

4.2.2 Phenotype of LEVLSSuH, RVSSuH and RVtpSSuH transplastomic plants

As seen previously for the RVSSuH and RVtpSSuH lines (Whitney and Andrews, 2001a), the LEVLSSuH line grew to fertile maturity in soil under atmospheric conditions at the same rate as wild-type tobacco controls and without an effect on phenotype (Figure 4.7). While all three lines maintain *rbcL* in the LSC region, they differ in the location of the inserted *RbcS* and *aadA* transgenes (Figure 4.7). Duplicate copies of *RbcS* and *aadA* are present in the plastomes of RVSSuH and RVtpSSuH due to their insertion into the IR region. Despite this difference in gene copy number, the

amount of plastid made S-subunits assembled into Rubisco in LEVLSSuH closely matched that of RVtpSSuH (Whitney unpublished). That is, plastid made S-subunits only accounted for ~1% of the total S-subunit pool assembled into L_8S_8 Rubisco in LEVLSSuH, which is equivalent to the ~1.2% measured in RVtpSSuH (Whitney and Andrews, 2001a).

4.2.3 Inheritance of the RNAi-RbcS T-DNA via pollination with $^{cm}trL^{RNAi\text{-}S}$ pollen

Flowers from RVSSuH, RVtpSSuH and LEVLSSuH T_2 plants were pollinated with pollen from the $^{cm}trL^{RNAi\text{-}S}$ line. The inheritance frequency (segregation analysis) of the *bar* (nuclear transgene) and *aadA* (plastome transgene) selectable markers in the resulting transplastome♀ × $^{cm}trL^{RNAi\text{-}S}$♂ F_1 progenies were examined (Figure 4.8A). Seeds sown on MS medium (*i.e.* with no selection antibiotic or herbicide) showed 100% viability. Compared to the wild-type controls, all the transgenic progeny showed impaired growth on MS medium. In particular the growth of the wild-type (WT)♀ × $^{cm}trL^{RNAi\text{-}S}$♂ progeny was greatly impeded with their survival dependant on the inclusion of sucrose in the MS medium (see also Figure 3.12). All the progeny from the $^{cm}trL^{RNAi\text{-}S}$ crosses survived growth on media containing Basta (10 mg L^{-1}) consistent with Mendelian inheritance of the RNAi-*RbcS* T-DNA (that includes *bar*) from the homozygous $^{cm}trL^{RNAi\text{-}S}$ line. On media containing spectinomycin (500 mg L^{-1}), only progeny of the plastome-transformed lines showed resistance with their growth rate and phenotype mirroring those of the progeny grown on media containing Basta (Figure 4.8A). These findings agree with the nuclear location of *bar* in chromosomes inherited from $^{cm}trL^{RNAi\text{-}S}$♂ and the maternal inheritance of *aadA* in the plastome of the LEVLSSuH, RVSSuH and RVtpSSuH transplastomic genotypes.

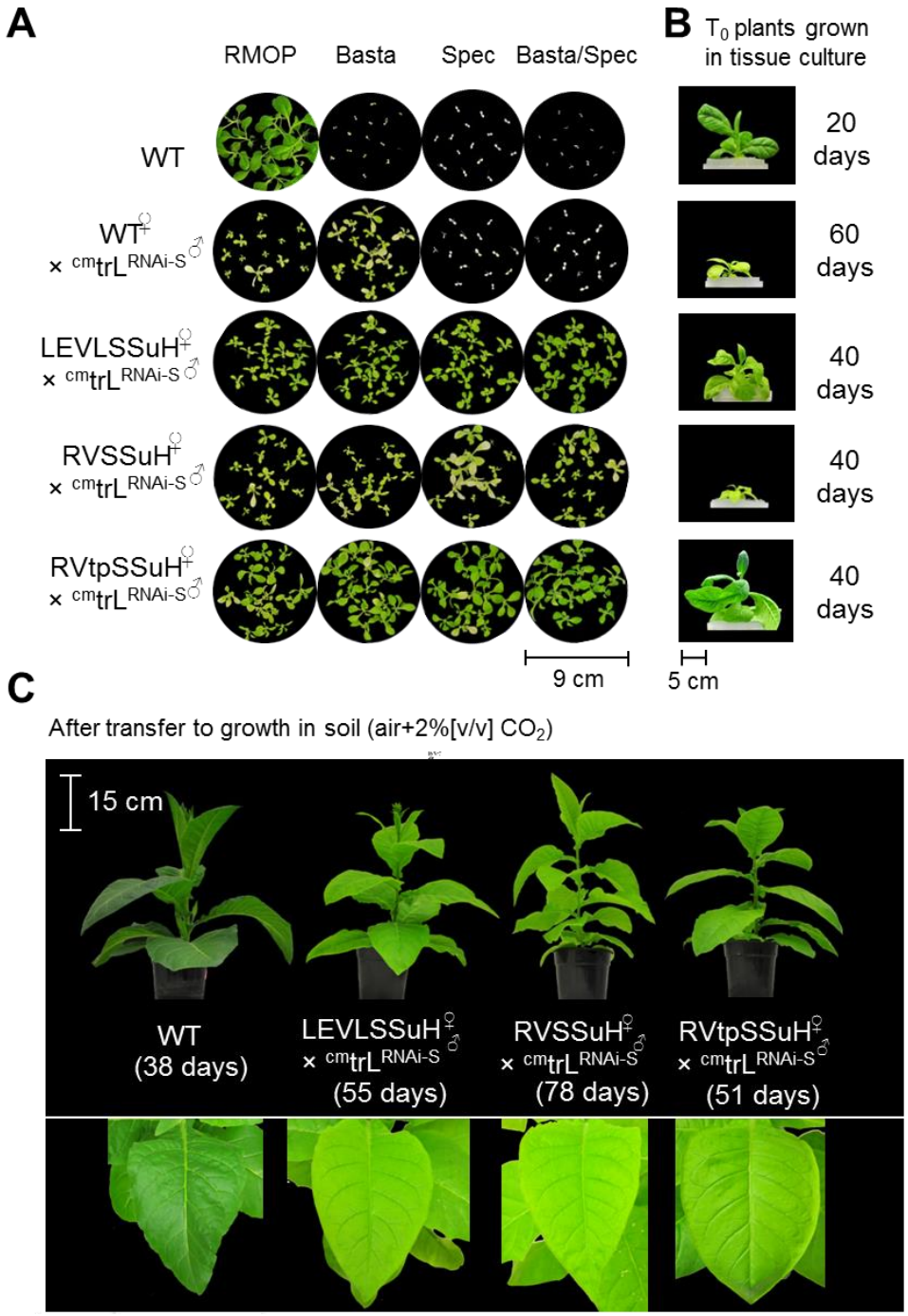

Figure 4.8 All progeny of the transplastomic lines pollinated with pollen from $^{cm}trL^{RNAi-S}$ show resistance to both Basta and spectinomycin.

(A) Segregation analysis of F_1 progeny from wild-type (WT) or the transplastomic tobacco genotypes pollinated with $^{cm}trL^{RNAi-S}♂$ pollen. Seeds were germinated on MS medium with and without spectinomycin or/and Basta. Coupling of the maternally inherited *aadA* in the transplastomic tobacco with the sexual transferral of the single allelic insertion of the RNAi-*RbcS* T-DNA (including *bar*, Figure 3.3) in the pollen from the homozygous $^{cm}trL^{RNAi-S}$ line imparts the F_1 progenies with 100% resistance to both spectinomycin (*aadA*) and Basta (*bar*). In contrast WT is sensitive to both reagents and the WT♀ × $^{cm}trLR^{NAi-S}♂$ seedlings show resistance to Basta but are unable to grow in soil as they lack Rubisco (Chapter 3). (B) After 20 days growth in MS with 3% (w/v) sucrose the T_2 LEVLSSuH, RVSSuH and RVtpSSuH transplastomic genotypes showed matching phenotypes (equal to WT controls, not shown) while after ~40 days the corresponding progeny derived from pollination with $^{cm}trL^{RNAi-S}$ showed growth impediments of increasing levels of severity (RVSSuH > LEVLSSuH >> RVtpSSuH). (C) Progenies from transplastomic plants crossed with $^{cm}trL^{RNAi-S}$ were able to grow to maturity in soil under 1.5% (v/v) CO_2 albeit at different rates and were photographed when approximately 300 mm in height.

4.2.4 Growth, maintenance and resulting phenotype of F_1 progenies

Variations in growth and leaf phenotype among the three transplastome♀ × ^{cm}trL$^{RNAi\text{-}S}$♂ F_1 progenies were evident during their germination in tissue culture on MS medium. The RVtpSSuH♀ × ^{cm}trL$^{RNAi\text{-}S}$♂ progeny showed faster growth and darker green leaves than the LEVLSSuH♀ and RVSSuH♀ × ^{cm}trL$^{RNAi\text{-}S}$♂ progenies (Figure 4.8A). In MS supplemented with 3% (w/v) sucrose the phenotype of the LEVLSSuH♀ and RVtpSSuH♀ × ^{cm}trL$^{RNAi\text{-}S}$♂ progenies were more similar to wild-type while the RVSSuH♀ × ^{cm}trL$^{RNAi\text{-}S}$♂ progeny showed impaired growth rate and a thinner, pale green leaf phenotype (Figure 4.8B).

The tissue culture grown plants were transferred into pots of soil and maintained in growth chambers at 25°C in air containing 2% (v/v) CO_2 under ~400 ± 100 µmol photons m^2 s^{-1} illumination. Under these elevated CO_2 growth conditions all the transplastome♀ × ^{cm}trL$^{RNAi\text{-}S}$♂ F_1 progenies survived to reproductive maturity, albeit at slower, varying rates to wild-type (Figure 4.8C). While the general plant and canopy architecture of the mature F_1 plants were comparable to wild-type, the leaf phenotype of each transplastomic genotype was more pale green, thinner and with dimpling and/or curling around the leaf margins (Figure 4.8C). In general these phenotypes were more prevalent in the RVSSuH♀ × ^{cm}trL$^{RNAi\text{-}S}$♂ genotype whose growth rate was accordingly much slower.

4.2.5 Rubisco content analysis

The varied growth capacity of the LEVLSSuH, RVtpSSuH and RVSSuH (transplastome) genotypes and their transplastome♀ × ^{cm}trL$^{RNAi\text{-}S}$♂ F_1 progenies correlated with the varying levels of Rubisco biogenesis in their leaves. Rubisco content was first examined by ndPAGE analysis of soluble protein from leaves from a comparable canopy position (except those grown in tissue culture). The plants were grown either at ambient CO_2 in the glasshouse (*i.e.* WT and the parental transplastomic genotypes), under elevated (1.5% [v/v]) CO_2 (*i.e.* the transplastome♀ × ^{cm}trL$^{RNAi\text{-}S}$♂ F_1 progenies) or in tissue culture (*i.e.* the WT♀ × ^{cm}trL$^{RNAi\text{-}S}$♂ F_1 control progeny). Coomassie-stained analysis of soluble leaf protein separated by ndPAGE showed the Rubisco content in the three parental transplastomic genotypes mirrored the wild-type control (Figure 4.10A). This finding matches that observed previously for RVtpSSuH and RVSSuH (Whitney and Andrews, 2001a). In contrast $L_8(S^{H7})_8$ Rubisco levels in the transplastome♀ × ^{cm}trL$^{RNAi\text{-}S}$♂ samples were > -1 fold compared to wild-type (i.e. 1.10-

1.65 µmol catalytic sites m^{-2}, Figure 4.9B). This correlates with the high-CO_2 requirement of these plants for growth in soil. Their impaired growth phenotype matches that observed in prior transplastomic tobacco lines similarly deficient in Rubisco (Sharwood et al., 2008).

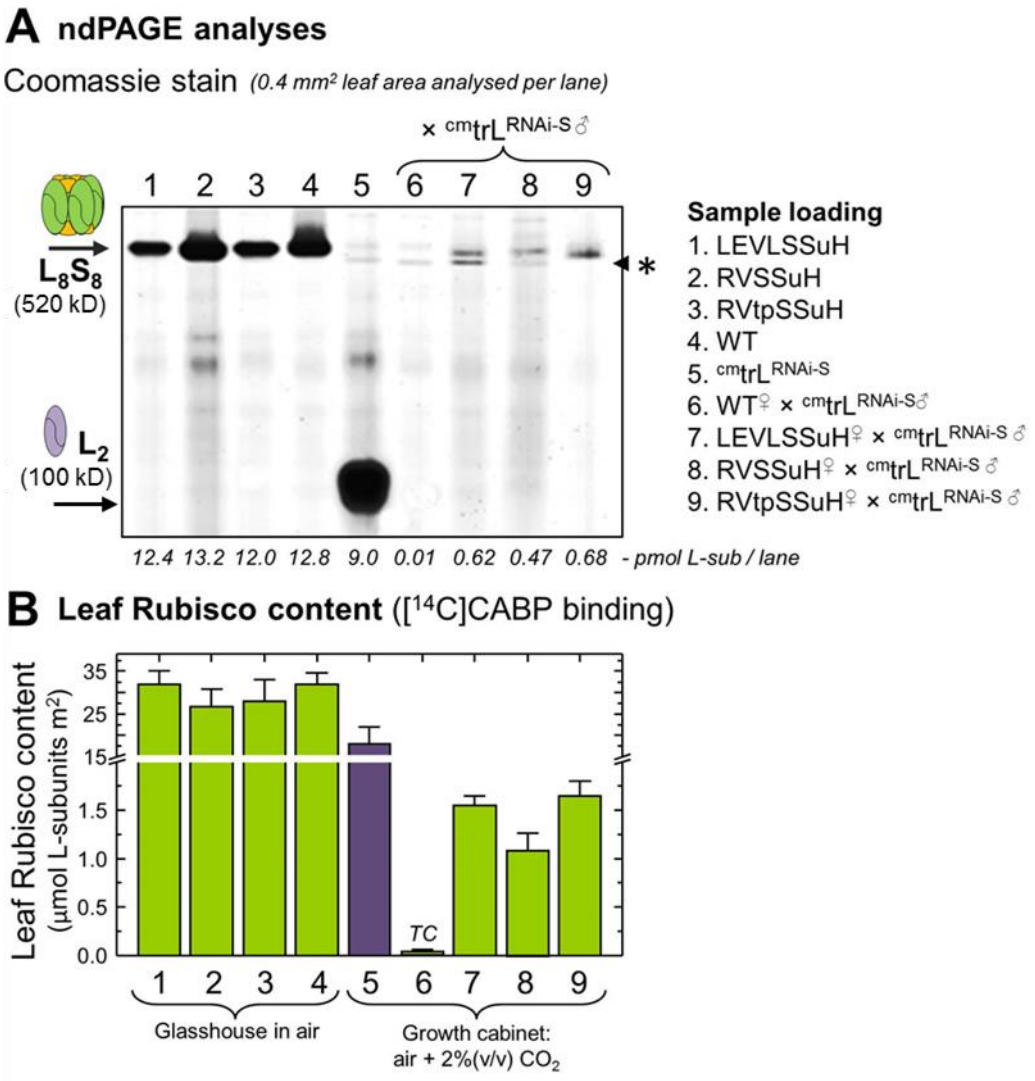

Figure 4.9 ndPAGE and [^{14}C]-CABP analysis of leaf Rubisco contents

(A) Non-denaturing PAGE (ndPAGE) analysis of soluble leaf protein from wild-type (WT) and transplastome plants grown in air (0.04% [v/v] CO_2) and their $^{cm}trL^{RNAi\text{-}S}♂$ crossed F_1 progenies grown in air with 2% (v/v) CO_2 or tissue culture (*TC*, for WT♀ × $^{cm}trL^{RNAi\text{-}S}♂$). Positions of the separated *R. rubrum* L_2, tobacco L_8S_8 and transplastomic $L_8(S^{H7})_8$ complexes are shown. (B) Rubisco content quantified by [^{14}C]-CABP (± S.D) in 3 plant samples for each genotype.* denotes a non-Rubisco band.

A comparison of the $L_8(S^{H7})_8$ levels produced in each transplastome♀ × $^{cm}trL^{RNAi\text{-}S}♂$ F_1 progeny showed higher amounts were produced in the RVtpSSuH♀ × $^{cm}trL^{RNAi\text{-}S}♂$ and LEVSSuH♀ × $^{cm}trL^{RNAi\text{-}S}♂$ F_1 progeny (~1.65 and 1.55 µmol catalytic sites m^2 respectively) relative to that produced in the RVSSuH♀ × $^{cm}trL^{RNAi\text{-}S}♂$ F_1 progenies (~1.1 µmol catalytic sites m^2) (Figure 4.10B). This variation accords with the

slower growth of the RVSSuH♀ × ^{cm}trL^{RNAi-S}♂ plants (Figure 4.8C). Only L_2 Rubisco was evident in ^{cm}trL^{RNAi-S} (Figure 4.10A, Lane 1) and the wild-type♀ × ^{cm}trL^{RNAi-S}♂ plants were Rubisco deficient (Figure 4.10A, Lane 9) as shown in Figure 3.13.

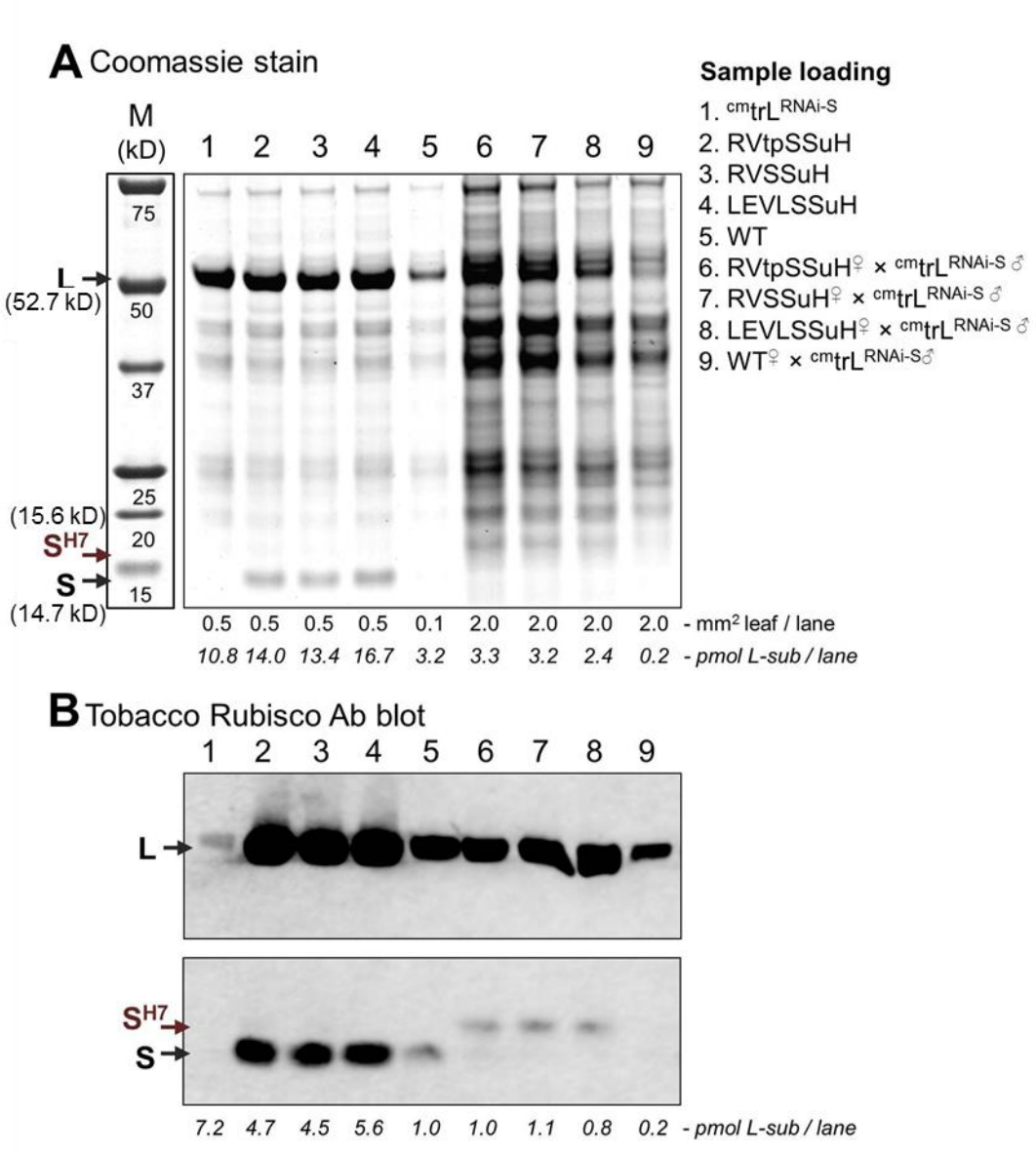

Figure 4.10 SDS-PAGE and immunoblot analysis Rubisco subunit synthesis.

(A) SDS-PAGE and (B) immunoblot analysis of the same samples analysed in Figure 4.9. The antibody to tobacco Rubisco did not recognize *R. rubrum* Rubisco produced in ^{cm}trL^{RNAi-S} but readily detected the Rubisco L-subunit (L) in all other samples, the cytosol made S-subunits (S) in wild-type (WT) and transplastome genotype and only the larger chloroplast made hepta-histidine tagged S-subunits (S^{H7}) in their ^{cm}trL^{RNAi-S}♂ crossed F_1 progenies. Rubisco content quantified by [^{14}C]-CABP-binding.

SDS-PAGE and immunoblot analyses of the same leaf protein samples confirmed the varied Rubisco content for each genotype (Figure 4.10A) and the production of chloroplast made S^{H7}-subunits (Figure 4.10B). As seen previously in the RVtpSSuH and RVSSuH genotypes, the small population of the 15.7 kDa chloroplast made S^{H7}-subunits produced in their leaves (that account for <1.2% of the endogenous 14.7 kDa S-subunits made; Whitney and Andrews, 2001a) could not be detected by

Coomassie staining or by immunoblot analysis using a tobacco Rubisco antibody. This was also the case for LEVLSSuH. In contrast, the immunoblot analyses only detected the 15.7 kDa chloroplast made S^{H7}-subunits in all three transplastome♀ × $^{cm}trL^{RNAi\text{-}S}$♂ F_1 progeny (Figure 4.10B). This finding is consistent with the effective RNAi-silencing of cytosolic S-subunit synthesis that was also observed in the wild-type♀ × $^{cm}trL^{RNAi\text{-}S}$♂ sample (Figure 4.10B, Lane 9) where only some soluble L-subunit was detected (noting the amount of sample loaded was 3-fold higher than the other transplastome♀ × $^{cm}trL^{RNAi\text{-}S}$♂ samples).

4.2.6 Rubisco in the transplastome♀ × $^{cm}trL^{RNAi\text{-}S}$♂ progeny comprises only plastome made S-subunits

The absence of wild-type S-subunits in each transplastome♀ × $^{cm}trL^{RNAi\text{-}S}$♂ genotype suggested their Rubisco subunit stoichiometry was $L_8(S^{H7})_8$ – that is, comprising a homogeneous population of chloroplast made S^{H7}-subunits. This was further tested by purifying the S^{H7} containing Rubisco complexes from the RVtpSSuH and LEVLSSuH genotypes and each transplastome♀ × $^{cm}trL^{RNAi\text{-}S}$♂ by immobilized metal affinity chromatography (IMAC: Ni-NTA agarose, see Section 2.2.4). The Rubisco purified from each sample was quantified by [^{14}C]-CABP binding with only trace amounts of Rubisco detected in the Ni-NTA bound protein from the WT (non-transformed) control. Equivalent amounts of the purified Rubisco were then analyzed by SDS-PAGE (Figure 4.11). By Coomassie staining, the cytosolic S-subunits were most predominant in the Ni-NTA purified Rubisco from RVtpSSuH and LEVLSSuH (Figure 4.11A, Lanes 1 and 2). Immunoblot analysis however confirmed the presence of S^{H7} in these samples, consistent with the Ni-NTA purified Rubisco having a 7:1 S:S^{H7}-subunit stoichiometry as seen previously by Whitney and Andrews (2001). In contrast to this $L_8S_7(S^{H7})_1$ structure, S^{H7}-subunits were almost exclusively detected by Coomassie staining and immunoblot analysis of the Ni-NTA purified Rubisco from the transplastome♀ × $^{cm}trL^{RNAi\text{-}S}$♂ plants (Figure 4.11). This confirmed the prevalent Rubisco stoichiometry as $L_8(S^{H7})_8$ in these plants.

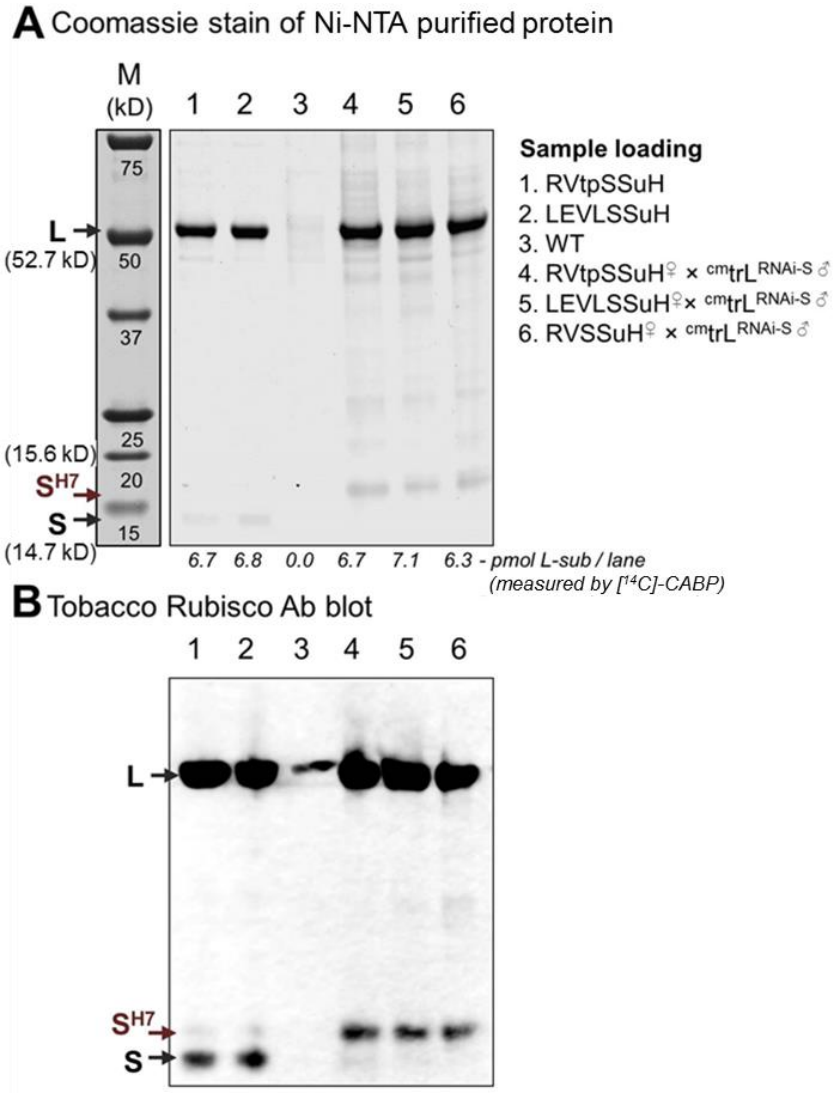

Figure 4.11 SDS-PAGE and immunoblot analysis of Ni-NTA purified Rubisco.

Leaf protein was purified by Ni-NTA (see Section 2.2.4), the Rubisco content quantified by [^{14}C]-CABP and ~6.5 pmol L-subunits (actual amounts loaded are indicated) were separated by SDS-PAGE and visualized by (A) Coomassie staining and (B) immunoblot analysis with a tobacco Rubisco antibody. Equivalent banding intensities were found for the Rubisco L-subunit (L) in all samples (except the WT control where no binding to Ni-NTA was expected), with both cytosol made S-subunits (S) and hepta-histidine tagged S-subunits (S^{H7}) identified in the RVtpSSuH and LEVLSSuH samples and almost exclusively S^{H7}-subunits in the purified protein from all three transplastome$^{♀}$ × ^{cm}trL$^{RNAi\text{-}S♂}$ F_1 progenies.

4.2.7 Rubisco mRNA content

Leaf RNA blot analyses were performed to better appreciate how variations in *rbcL* and *rbcS* mRNA levels contributed to the differing levels of Rubisco made in each genotype. Total RNA isolated from the same leaves analysed in Figure 4.10 was separated through denaturing formaldehyde gels and visualized by ethidium bromide (Figure 4.12). The separated RNA from replica gels were blotted onto nylon membrane and probed with [^{32}P]-labelled DNA fragments that hybridized to either the tobacco *rbcL* (*rbcL* probe, Figure 4.12B) or to the endogenous nuclear and chloroplast *RbcS* mRNAs (Figure 4.12C).

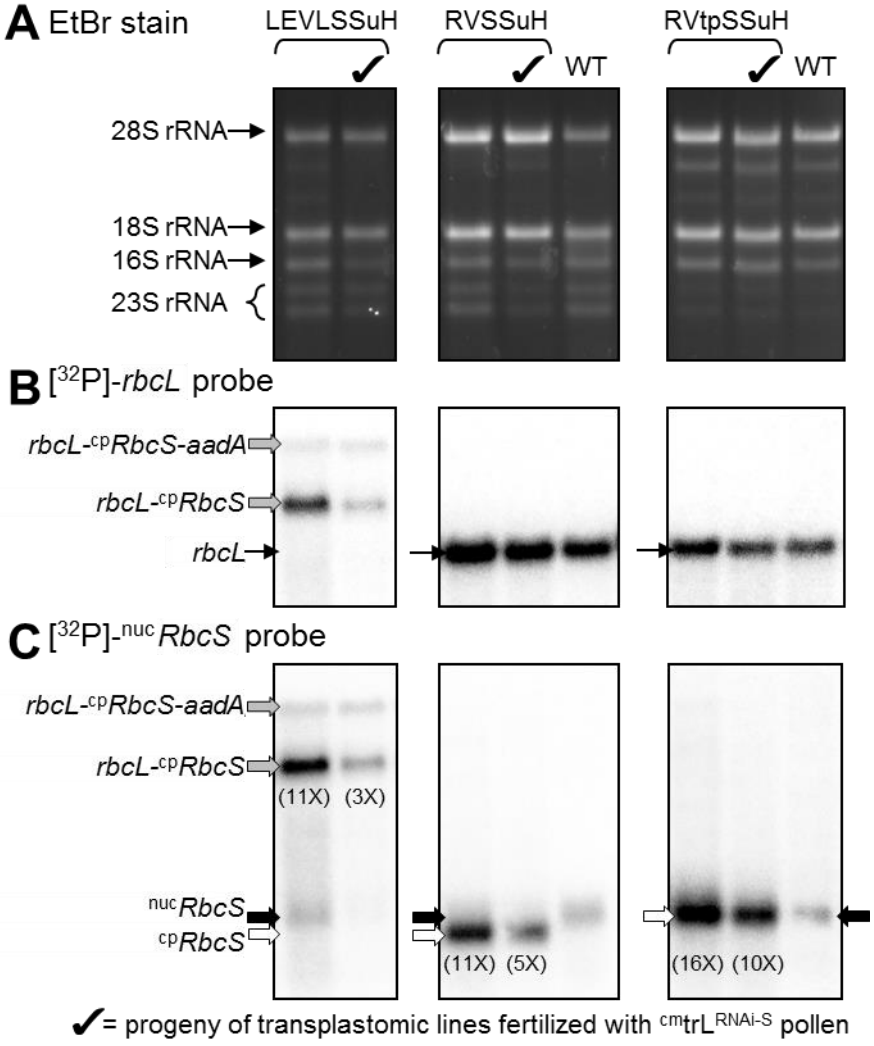

Figure 4.12 RNA blot analysis of *rbcL*, ^{nuc}*RbcS* and plastid made ^{cp}*rbcS*^{H7} mRNA levels.

Total leaf RNA (3 µg) was separated by denaturing RNA gel electrophoresis and the RNA (A) visualised by ethidium bromide and then blotted onto nylon membrane, then hybridised with either a [^{32}P]-labelled (B) *rbcL* probe or (C) *RbcS* probe (see figure 4.7 for location of probes and the expected hybridising mRNA). The signal intensities for the chloroplast *RbcS* mRNA (^{cp}*RbcS*) relative to the endogenous cytosolic *RbcS* mRNA (^{nuc}*RbcS*) in WT control and in LEVLSSuH are shown in parentheses.

The origin of both DNA probes is shown in Figure 4.7. Similar *rbcL* mRNA contents were found in WT, RVtpSSuH, and RVSSuH (Figure 4.12B). In the LEVLSSuH genotypes no *rbcL* monocistronic mRNA was detected. Consistent with that, the LEVLSSuH genotype produced both an *rbcL-RbcS* bicistronic mRNA and ~10-fold less abundant *rbcL-RbcS-aadA* tricistronic mRNA. Lower amounts of the *rbcL* transcripts were detected in the transplastome♀ × ^{cm}trL^{RNAi-S}♂ leaves, with LEVLSSuH *rbcL* transcripts being notably lower relative to other transplastomic lines. This may possibly be due to the reduced photosynthetic capacity of these lines (even under high-CO_2), slowed growth and altered leaf phenotype and ontogeny (Figure 4.8C). Nevertheless, the *rbcL* mRNA levels were still high in these genotypes indicating the severe

limitations to $L_8S^{H7}{}_8$ biogenesis in these plants is unlikely to be prompted by *rbcL* transcription impediments. Analysis of the *RbcS* mRNA found that relative to the endogenous ^{nuc}*RbcS* mRNA the chloroplast *RbcS* mRNA levels (^{cp}*RbcS*) were 11 to 16-fold higher in RVtpSSuH, RVSSuH and LEVLSSuH and similarly 3 to 10-fold higher in their $^{cm}trL^{RNAi\text{-}S}$♂ crossed progeny (Figure 4.12C). These elevated levels of ^{cp}*RbcS* mRNA match those reported previously (Figure 4.4) (Whitney and Andrews, 2001a). In combination these Rubisco mRNA analyses demonstrate that the abundance of *rbcL* is sustained in all three transplastome♀ × $^{cm}trL^{RNAi\text{-}S}$♂ genotypes relative to their maternal transplastomic genotypes, however pollination with $^{cm}trL^{RNAi\text{-}S}$ reduced ^{cp}*RbcS* mRNA to varying degrees in all three transplastome♀ × $^{cm}trL^{RNAi\text{-}S}$♂ genotypes. This implies that limitations in one or more post-transcriptional events are primarily impeding $L_8(S^{H7})_8$ biogenesis in these F_1 plants.

4.2.8 Rubisco catalysis is affected by the S-subunit C-terminal hepta-histidine tag

As the RVtpSSuH♀ × $^{cm}trL^{RNAi\text{-}S}$♂ plants produced the most $L_8(S^{H7})_8$ Rubisco (Figure 4.9B), it was chosen as the source material for measuring the k_C^{cat} and K_m for CO_2 under ambient O_2 levels ($K_C^{21\%O2}$). Measurements were made using rapidly extracted leaf protein as described by Sharwood et al. (2008) and compared against tobacco wild-type (Table 4.2). The $L_8(S^{H7})_8$ enzyme showed 30-35% reductions in both k_C^{cat} and in $K_C^{21\%O2}$. This correlates to both $L_8(S^{H7})_8$ and native L_8S_8 Rubisco sharing comparable carboxylation efficiencies ($k_C^{cat}/K_C^{21\%O2}$), consistent with the $S_{C/O}$ for the Ni-NTA purified $L_8(S^{H7})_8$ showing no significant difference to wild-type L_8S_8 Rubisco.

Table 4.2 Rubisco catalysis comparison

Catalytic parameter	Plant source	
	tobacco (n=6)	RVtpSSuH♀ × $^{cm}trL^{RNAi\text{-}S}$♂ (n=4)
k_C^{cat} (s^{-1})	3.0 ± 0.1	2.1 ± 0.3*
$K_C^{21\%O2}$ (μM)	18.3 ± 2.1	11.9 ± 2.3*
$k_C^{cat}/K_C^{21\%O2}$ (mM^{-1} s^{-1})	163	176
$S_{C/O}$ (mol mol^{-1})	82 ± 2	80 ± 2

*Significance variation ($p<0.01$) relative to tobacco Rubisco determined by T-test. $K_C^{21\%O2}$, the apparent K_m for CO_2 (K_C) at atmospheric [O_2] (assumed 252 μM at 25°C).

4.3 Discussion

The research of this chapter demonstrates the suitability of pollinating chloroplast S-subunit producing transplastomic tobacco genotypes with pollen from $^{cm}trL^{RNAi\text{-}S}$ to effectively eliminate cytosolic S-subunit synthesis in the resulting F_1 progeny. This approach enabled, for the first time, the synthesis of tobacco Rubisco comprising solely chloroplast made S^{H7}-subunits (*i.e.* $L_8(S^{H7})_8$ holoenzyme). Each F_1 line however showed limitations in their growth and viability in soil, even when grown under elevated CO_2. This restriction stems from low photosynthetic CO_2 assimilation rates as a result of limitations in $L_8(S^{H7})_8$ biogenesis that accumulated in young upper-canopy leaves at levels approximately 3-5% that produced in wild-type (Figure 4.9B). Indeed similar perturbations to tobacco growth and phenotype have been found in tobacco genotypes producing such low levels of Rubisco (Whitney and Andrews, 2001a; Whitney et al., 2001; Whitney et al., 2009) as well as those producing mutated/foreign Rubisco isoforms with impaired catalysis (Whitney et al., 1999; Whitney and Andrews, 2003).

The restrictions to $L_8(S^{H7})_8$ synthesis in the transplastome$^{♀}$ × $^{cm}trL^{RNAi\text{-}S♂}$ F_1 genotypes appear to be primarily influenced by post-transcriptional limitations (Figure 4.12). In each F_1 progeny, high levels of *rbcL* and ^{cp}*RbcS* mRNA were maintained. The 5 to 16-fold higher abundance of ^{cp}*RbcS* mRNA relative to the endogenous ^{nuc}*RbcS* levels correlates with the ~10 to 100-fold higher molar abundance of plastome copies per nucleus in a leaf cell (Kabeya and Miyagishima, 2013). The sustained Rubisco mRNA abundance in the F_1 progeny indicated the synthesis, assembly and/or stability of the recombinant S^{H7}-subunits are somehow impeded in these genotypes. This correlates with the previous hypothesized limitations to S^{H7}-subunit incorporation into L_8S_8 Rubisco within the maternal RVtpSSuH and RVSSuH (and apparently also LEVLSSuH) genotypes (Whitney and Andrews, 2001a). Notably the absence of endogenous ^{nuc}*RbcS* mRNA in these lines confirmed the effectiveness of introducing the RNAi-*RbcS* silencing allele by cross-pollination with $^{cm}trL^{RNAi\text{-}S}$ pollen (Figure 4.12C).

4.3.1 Possible limitations to plastid made S-subunit production and/or assembly into L_8S_8 Rubisco in leaf chloroplasts

The approach of engineering the *RbcS* in the plastome appears to be impeded by either translational and/or post-translational events in the chloroplast. As summarised in Figure 4.13, the low levels of $L_8(S^{H7})_8$ produced in the $^{cm}trL^{RNAi\text{-}S♂}$ crossed F_1 genotypes may arise from perturbations to one or more post-transcriptional processes.

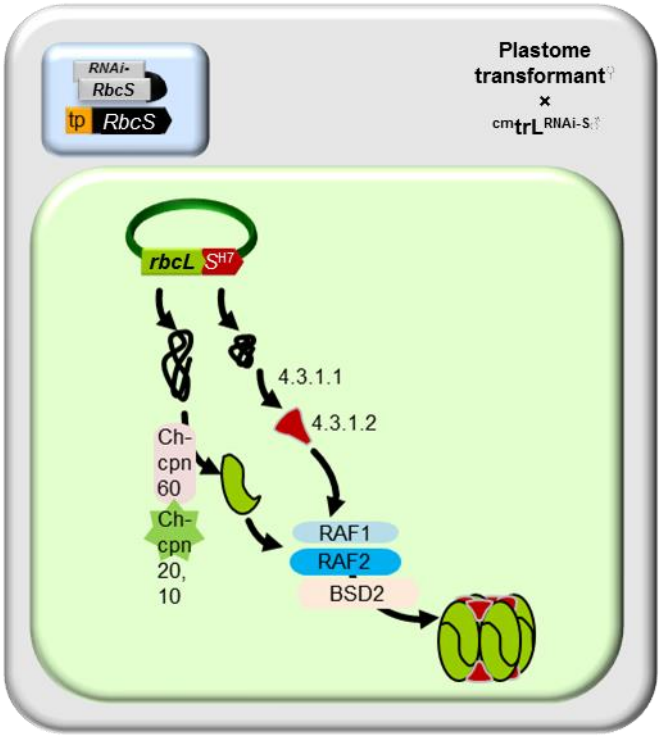

Figure 4.13 Summary of Rubisco subunit expression in $^{cm}trL^{RNAi\text{-}S♂}$ crossed F_1 genotypes and unknown limitations in subunit processing in the chloroplast.

Possible limitations imposed by the additional C-terminal hepta-histidine (H7) tag on the capacity of S^{H7}-subunits to assemble into L_8S_8 holoenzyme seem unlikely. A prior comparison of tranplastomic tobacco producing plastid made S-subunits without H7 tags showed they shared the same assembly limitations as the S^{H7}-subunits (Whitney and Andrews, 2001a). This would suggest limitations in translational processing of chloroplast made S-subunits (see Section 4.3.1.1) or an increased propensity for their proteolytic degradation (see Section 4.3.1.2) in explaining their limited capacity for incorporation during L_8S_8 biogenesis.

4.3.1.1 Limitations to translational processing of the RbcS^{H7} mRNA

Translational processing of chloroplast mRNA's is highly influenced by the structure and stability of the mRNA, its capacity to engage a wide range of regulatory mRNA elements and a host of requisite protein translation factors coded by genes in both the chloroplast and nucleus (Yamaguchi et al., 2000; Zerges, 2000). RNA elements identified as regulatory components in the translation of chloroplast messages are primarily located in the 5′UTR. These elements include Shine-Dalgarno (SD) sequences, stem-loop structures, and A/U rich elements. While nearly all bacterial mRNAs use base pairing between a SD sequence and a complementary sequence located near the 3′ end of the 16S rRNA, the positioning of the SD sequence in chloroplast mRNA 5'UTR is highly variable. For example the SD in the tobacco *psbA* mRNA is 33-36 nt upstream of the D1 protein initiator AUG codon (Bonham-Smith and Bourque, 1989). A common impediment to reliably expressing recombinant proteins in leaf chloroplasts is the pervasive influence the introduced gene coding sequence has on mRNA structure and its translational processing (Maliga, 2004). Significant variations in recombinant protein

expression have been observed for different genes using the same chloroplast gene regulatory sequences (*i.e.* promoter, 5'- and 3'UTR) (Maliga, 2003). For example, the same *psbA* gene elements used in this thesis to regulate *RbcS*^{H7} translation in the RVSSuH and RVtpSSuH genotypes (Figure 4.7) have been used to drive the production of the cyanobacterial BicA membrane protein (Pengelly et al., 2014), GUS (Staub and Maliga, 1993) and *rbcL-S* operons of *Galdieria sulphuraria* (red algae) and *Phaeodactylum tricornutum* (diatom) Rubisco (Whitney et al., 2001) in tobacco chloroplasts. Each protein was produced in differing amounts ranging from 0.1%, 2% and 35% of the leaf soluble cellular protein respectively. Similarly the use of the same *rrn* promoter, *T7g10* 5'UTR and *rps16* 3'UTR sequences have produced up to 30-fold differences in the levels of recombinant protein expression (Maliga, 2003). These examples highlight the necessity to better understand promoter and terminator element function and their translation machineries in greater molecular detail. Such information is critical if we are to more reliably modulate recombinant protein translation initiation and elongation rates in the chloroplast (Mayfield et al., 1995; Somanchi and Mayfield, 1999; Maliga and Bock, 2011).

The structural similarity between the translation machinery of chloroplasts and prokaryotes has led to the belief that the patterns of codon usage in chloroplasts might show evidence of bias that can be linked to levels of protein expression (Sugiura, 1992). Understanding the biased usage of synonymous codons has been of particular benefit for optimising recombinant protein expression in *E. coli* (Angov, 2011). For *E. coli*, the codon usage efficiency closely reflects the differential composition of the genomic tRNA pool. In chloroplasts, only around 30 tRNA species are coded by the plastome. Highly translated proteins in the chloroplasts therefore tend to show strong codon use preference for these tRNA (Alkatib et al., 2012). Increasing evidence from plastome transformation studies seems to increasingly support this assertion. By incorporating the biased usage of particular synonymous codons comparable to those used by highly expressed chloroplast genes the production of recombinant proteins such as *R. rubrum* Rubisco (Whitney and Sharwood, 2008), *S. verticillus* Ble (Heitzer et al., 2007), *B. thuringiensis* cryIA(b) (Perlak et al., 1991) and *C. tetani* TetC (Tregoning et al., 2003) have been enhanced by 3 to 10-fold. This enhancement is presumed to occur as a consequence of faster rates of translation elongation. With regard to this current study, the higher GC content of nuclear tobacco *RbcS* incorporated into each transplastomic line produces a codon use that varies considerably from the AT rich tobacco *rbcL* (Table 4.3). Examination of the differential codon use however sees the CUC (coding

leucine) as the only codon uniquely used by the ^{cp}*RbcS* transgene. The frequency usage of the CUC codon by all 79 proteins coded in the tobacco plastome is noticeably very low, only 0.069 (Nakamura and Sugiura, 2009). Whether the single use of the CUC codon in the ^{cp}*RbcS* transgene significantly impairs translation of the S^{H7}-subunits in the chloroplast remains experimentally untested. Further details on the potential importance and testing the role of codon use in chloroplast protein expression is described in Chapter 5.

Table 4.3 Comparative codon use of the tobacco *rbcL* and ^{cp}*RbcS* transgene

Highlighted are the preferred codons used in *rbcL* (pink) and ^{WT}*RbcS** (green)

Amino acid	codon	*rbcL*		^{cp}*RbcS*	
		No.	%	No.	%
Ala (A)	GCA	13	2.7	1	0.8
	GCC	5	1.0	3	2.4
	GCG	4	0.8	1	0.8
	GCU	23	4.8	1	0.8
Arg (R)	AGA	7	1.5	1	0.8
	AGG	0	0.0	0	0.0
	CGA	6	1.3	0	0.0
	CGC	5	1.0	0	0.0
	CGG	1	0.2	0	0.0
	CGU	11	2.3	3	2.4
Asn (N)	AAC	6	1.3	4	3.3
	AAU	9	1.9	1	0.8
Asp (D)	GAC	4	0.8	1	0.8
	GAU	23	4.8	3	2.4
Cysl	UGC	4	0.8	3	2.4
	UGU	5	1.0	0	0.0
Gln (Q)	CAA	9	1.9	3	2.4
	CAG	4	0.8	4	3.3
Glu (E)	GAA	24	5.0	5	4.1
	GAG	8	1.7	7	5.7
Gly (G)	GGA	13	2.7	5	4.1
	GGC	2	0.4	2	1.6
	GGG	8	1.7	0	0.0
	GGU	23	4.8	0	0.0
His (H)	CAC	5	1.0	1	0.8
	CAU	9	1.9	0	0.0
Ile (I)	AUA	2	0.4	0	0.0
	AUC	10	2.1	3	2.4
	AUU	9	1.9	3	2.4
Lys (K)	AAA	21	4.4	1	0.8
	AAG	4	0.8	8	6.5

Amino acid	codon	*rbcL*		^{cp}*RbcS*	
		No.	%	No.	%
Leu (L)	CUA	6	1.3	1	0.8
	CUC	0	0.0	1	0.8
	CUG	6	1.3	0	0.0
	CUU	10	2.1	3	2.4
	UUA	9	1.9	0	0.0
	UUG	10	2.1	5	4.1
Met(M)	AUG	8	1.7	3	2.4
Phe (F)	UUC	9	1.9	4	3.3
	UUU	12	2.5	1	0.8
Pro (P)	CCA	5	1.0	5	4.1
	CCC	2	0.4	0	0.0
	CCG	3	0.6	0	0.0
	CCU	11	2.3	3	2.4
Ser (S)	AGC	3	0.6	1	0.8
	AGU	2	0.4	2	1.6
	UCA	3	0.6	2	1.6
	UCC	2	0.4	0	0.0
	UCG	0	0.0	0	0.0
	UCU	7	1.5	0	0.0
Term	UAA	1	0.2	0	0.0
Thr (T)	ACA	5	1.0	0	0.0
	ACC	8	1.7	2	1.6
	ACG	1	0.2	0	0.0
	ACU	15	3.1	3	2.4
Trp(W)	UGG	8	1.7	5	4.1
Tyr (Y)	UAC	8	1.7	9	7.3
	UAU	10	2.1	1	0.8
Val (V)	GUA	17	3.6	0	0.0
	GUC	1	0.2	1	0.8
	GUG	3	0.6	5	4.1
	GUU	16	3.3	2	1.6

4.3.1.2 Are the translated S^{H7}-subunits prone to proteolysis?

As the *R. rubrum* L_2 Rubisco in the ^{cm}trL tobacco genotype has no requirements for S-subunits, it is assumed the cytosolic made S-subunits are still made but are quickly degraded in the chloroplast stroma as no evidence for their accumulation has been found (Whitney and Andrews, 2001a; Whitney and Andrews, 2003; Whitney and Sharwood, 2008). The same is also assumed for L-subunits in anti-*RbcS* genotypes where the detection of unassembled L-subunits or oligomeric assemblies of L-subunits have not been observed (Hudson et al., 1992; Andrews et al., 1995b; Wostrikoff and Stern, 2007; Kubien and Sage, 2008). This apparent rapid degradation of "unused" proteins in the stroma likely stems from the highly efficient degradation pathways that exist in chloroplasts (Xie et al., 2015). The most notable proteases are DegP (a serine protease) and the multi-subunit ClpP and FtsH homologs. These proteases function via ATPase hydrolysis with varying levels of substrate recognition specificity (Kuroda and Maliga, 2003; Adam et al., 2011). Overall chloroplast proteases play critical roles in chloroplast biogenesis and maintaining homeostasis and function. Their roles in maintaining homeostasis are particularly important in response to cellular stresses (e.g. heat, high light) where the requirement for degradation and recycling of damaged proteins, such as the D1 protein of photosystem II, is elevated (Haußühl et al., 2001).

In the chloroplast, is the assumed co-translational formylation of the nascent peptide Met-1. Peptide deformylase subsequently removes this modification to facilitate direct post-translational modification of Met-1 by *N*-acetyltransferase (NAT) activity, N-methylation or its removal by methionine amino peptidase (MAP) before modification of the new N-terminal amino acid (*i.e.* amino acid at position 2). The capacity of MAP to undertake this process is thought to be dependent on the size and charge of the amino acid at position 2. For cytosol made proteins targeted to the stroma, processing of the transit peptide leader sequence (see Section 4.1.2) is facilitated by a ~140 kDa stromal processing peptidase (SPP; a metalloprotease) (Richter et al., 2005). Consistent with that seen previously by Whitney and Andrews (2001) none of the chloroplast made S^{H7}-subunits in RVtpSSuH, LEVLSSuH or their $^{cm}trL^{RNAi\text{-}S♂}$ crossed F_1 progeny contained the 57 amino acid leader sequence (Figure 4.10) reaffirming SPP processing of transit peptides occurs within the chloroplast stroma.

An underpinning question is whether the limited capacity to incorporate stroma synthesized S^{H7}-subunit into L_8S_8 complexes stems from their spatial segregation away from the co-evolved chaperone-facilitated S-subunit assembly pathway? As indicated in Figure 4.1, for cytosol made S-subunits this pathway begins near the Tic entry point of

the chloroplast envelope where a range of evolved molecular partners are located. In contrast the S^{H7}-subunits are likely synthesized by thylakoid-bound or stroma-located chloroplast polysomes. This places the S^{H7}-subunits spatially remote from the envelope-associated molecular partners, likely exposing the S^{H7}-subunits to heightened rates of proteolysis. Prior [^{35}S]-Met pulse-chase analyses however showed no significant difference in the synthesis or degradation of the S^{H7}-subunits in either RVtpSSuH or LEVLSSuH (Whitney and Andrews, 2001a). Admittedly the nature of these analyses only detected the S^{H7}-subunits that successfully assembled into $L_8S_7(S^{H7})_1$ complexes as the low levels of S^{H7}-subunits measurable necessitated selective enrichment by IMAC (using Ni-NTA). Repeating this [^{35}S]-Met pulse-chase analysis in the transplastome♀ × $^{cm}trL^{RNAi\text{-}S}$♂ F_1 progeny would unlikely require IMAC enrichment given the higher (and homogeneous) population of S^{H7}-subunits incorporate the $L_8(S^{H7})_8$ Rubisco made. This would improve the accuracy and sensitivity of measuring whether the S^{H7}-subunits show differences in their synthesis, assembly or stability relative to the cytosol made S-subunits in wild-type controls. Such [^{35}S]-Met pulse-chase analyses remain to be undertaken.

A key difference between the cytosol made S-subunits and stroma made S^{H7}-subunits are the post-translational modification of their mature Met-1 residue. As indicated in Section 4.1.3, following import of cytosol made precursor S-subunits into the stroma, their tp sequence is removed and the exposed Met-1 is *N*-methylated. The function of this modification remains unknown (Houtz et al., 2008). In contrast, the Met-1 of the chloroplast made S^{H7}-subunits are acetylated (Whitney, unpublished) presumably via NAT activity for which there are multiple isoforms in chloroplasts. N-terminal acetylation is considered a modification that provides chloroplast proteins (such as the L-subunit) protection from proteolysis (Houtz et al., 2008) (Figure 4.2). With this in mind one might speculate there may be limitations to the post-translational acetylation of stromal made S^{H7}-subunits by NAT – with only a limited population of S^{H7}-subunits correctly modified and able to resist proteolysis and assemble into L_8S_8 complexes. The future [^{35}S]-Met pulse-chase analyses proposed above for the transplastome♀ × $^{cm}trL^{RNAi\text{-}S}$♂ F_1 progeny will enable experimental testing of this hypothesis.

4.3.2 The RNAi-S genotype is stably inherited

A key deficiency of many RNAi studies has been the instability of T-DNA integration. As shown in Chapter 3, the heritable *bar* conferring Basta resistance in the ^{cm}trL$^{RNAi\text{-}S}$ line has proven an ideal marker gene for nuclear transformation and the identification in transplastome♀ × ^{cm}trL$^{RNAi\text{-}S}$♂ F_1 progeny inheriting the paternal chromosome containing *bar* (Figure 4.8A) and RNAi-*RbcS* silencing T-DNA (Figure 4.12C). Subsequent selfing of the F_1 genotypes studied in this chapter have shown that the RNAi-*RbcS* silencing phenotype is stably inherited in F_3 progeny (data not shown).

4.3.3 The RNAi-processing machinery is not present in chloroplasts

A key finding of this chapter is the RVtpSSuH, RVSSuH and LEVLSSuH (where it is primarily an *rbcL*-^{cp}*RbcS* transcript) and their corresponding ^{cm}trL$^{RNAi\text{-}S}$ crossed F_1 progeny produced comparable levels of ^{cp}*RbcS* mRNA (Figure 4.12). Notably the codon use of the plastome ^{cp}*RbcS* transgene matches the region of ^{nuc}*RbcS* sequence used in the RNAi-*RbcS* T-DNA (Figure 3.5). This provides strong evidence that the efficient RNAi-processing machinery present in the cytosol (Figure 3.2) does not function in the chloroplast stroma. This supports the findings of Zhang et al. (2015) who found no evidence of RNAi silencing of recombinant double-stranded RNAs (dsRNAs) in potato chloroplasts. This is somewhat not unexpected as the genes coding the dicer enzymes or/and other protein components of the RNA-induced silencing complexes do not code for appropriate N-terminal chloroplast targeting sequences. The discovery that chloroplast gene expression is immune to RNAi-silencing may pose an advantage in chloroplast bioengineering applications where silencing of cytosolic enzymes/pathways may be beneficial. For example, many subunits of the protein complexes involved in photosynthetic electron transport are coded in the nucleus (Leister, 2012). Future structure-function studies of these protein components via a plastome transformation approach would necessitate silencing of the nucleus genes by RNAi – a goal that is now clearly achievable.

4.3.4 Future directions

The data presented in this chapter represent experiments undertaken to qualify the potential for producing Rubisco complexes fully comprising plastome made S-subunits. This poses a significant step forward with regard to being able to modify Rubisco catalysis through co-ordinated changes to both the L- and S-subunits. Limitations in the capacity to produce and assemble chloroplast made S-subunits continue to hinder

progress toward such goals. Identifying the causes and potential solutions to these challenges are addressed in the following two chapters.

CHAPTER 5 – TRANSPLASTOMIC PRODUCTION OF HYBRID RUBISCO COMPRISING TOBACCO L-SUBUNITS AND ALTERNATIVE S-SUBUNITS

5.1 Introduction

During the evolution of plants and green algae multiple *RbcS* copies in the nucleus have been acquired as a consequence of gene transfer and duplication from the *rbcL-rbcS* operon within the genome of the cyanobacterial progenitor of plastids (Martin and Kowallik, 1999; Bogorad, 2012). Within the nucleus, the numbers of *RbcS* copies have multiplied and with ensuing mutagenic events, led to plants and algae producing varying numbers of *RbcS* copies that typically code different S-subunit sequences. Differential expression of the varying S-subunit isoforms in response to environmental cues are hypothesised to potentially modulate Rubisco catalysis in some plant species (Morita et al., 2014). In support of this are the rising numbers of studies on Rubisco L_8S_8 chimeras comprising alternative mixtures of heterologous S-subunits that lead to varying effects on catalysis (Table 5.1). Clearly the goals of being able to modulate Rubisco catalysis through directed amino acid changes necessitates a better understanding of interactions between the L- and S-subunit. This goal, hampered by the nuclear location and multiple *RbcS* copies in plants have prevented their directed deletion and mutagenesis (Whitney et al., 2011a; Parry et al., 2013). As evident from Chapter 3 and Chapter 4, the $^{cm}trL^{RNAi\text{-}S}$ genotype has the potential to circumvent these limitations.

5.1.1 Expression of rbcL-rbcS operons in higher plants chloroplasts

The Rubisco genes in proteobacteria, non-green algae and cyanobacteria remain encoded as a single, co-transcribed dicistronic *rbcL-rbcS* (*rbcL-S*) mRNA (Assali et al., 1991; Badger and Bek, 2008). In the non-green algae the Rubisco operon still resides in the plastome with the genes separated by an intergenic region (IR) of varying lengths (typically between 30-60 nucleotides in length). The IR typically contains a Shine-Dalgarno (SD) sequence 7-10 nucleotides upstream of the *rbcS* initiator codon to facilitate ribosome engagement for S-subunit translation (Whitney and Andrews, 2001b). These genetic elements in the IR are readily recognised by the translational machinery within *E .coli*. For example the native *rbcL-S* sequences from proteobacteria (e.g. *Rhodobacter sphaeroides*, *Alcaligenes eutrophus*), cyanobacteria (e.g.

Synechococcus elongatus PCC7942), diatom (*Phaeodactylum tricornutum*), and red algae (*Galdieria sulphuraria*) have led to high levels of both L-subunit and S-subunit production in *E. coli* (Andersen and Caton, 1987; Whitney et al., 2001; Whitney et al., 2011a; Lin et al., 2014). In many cases however, the folding and assembly requirements of these subunits into L_8S_8 complexes are not met in *E. coli.* This is particularly the case for Rubisco from non-green algae (Whitney et al., 2001).

Reminiscent of the LEVLSSuH tobacco genotype described in Chapter 4 that codes a synthetic tobacco *rbcL-RbcS* operon in the plastome, other studies have transplanted *rbcL-rbcS* from algae and cyanobacteria into the tobacco plastome. The first study introduced the native *rbcL-rbcS* operon from *P. tricornutum* and *G. sulphuraria* into the inverted repeat region of the tobacco plastome under the control of the *psbA* promoter and terminator elements (Figure 5.1). In these lines the tobacco *rbcL* remained unmodified enabling normal tobacco L_8S_8 Rubisco biogenesis. The resulting transplastomic Pt and Gs tobacco genotypes generated were found to make abundant amounts of the foreign L- and S-subunits, sometimes at levels matching the amount of tobacco L_8S_8 Rubisco made (Whitney et al., 2001) (Table 5.1). As seen in *E. coli* however, the algae Rubisco subunits were almost entirely insoluble with no evidence of assembly into functional Rubisco. This finding suggested there were differences in the assembly requirements of Rubisco from algae and plants, with no evidence that algae subunits were able to assemble with the tobacco L or S-subunits into L_8S_8 complexes.

A more recent study successfully showed the folding and assembly requirements of *S. elongatus* PCC7942 L_8S_8 Rubisco could be met by tobacco chloroplasts (Lin et al., 2014). Here the tobacco *rbcL* was directly replaced with a genetically altered version of the *S. elongatus* PCC7942 *rbcL-rbcS* operon (Figure 5.1). An intercistronic expression element (IEE) and SD sequence was included in the IR between *rbcL* and *rbcS* to promote cleavage of the dicistronic mRNA as a means to enhance S-subunit translation (Scharff and Bock, 2014; Zhou et al., 2007). Included in the operons were additional genes coding either the RbcX chaperone or a CcmM35 carboxysome shell protein (*ccmM35*) (Lin et al., 2014). The CcmM35 protein contains 3 repeats of S-subunit like sequences that are thought to be part of the Rubisco holoenzyme assembly in carboxysomes (Price et al., 1998; Long et al., 2005).

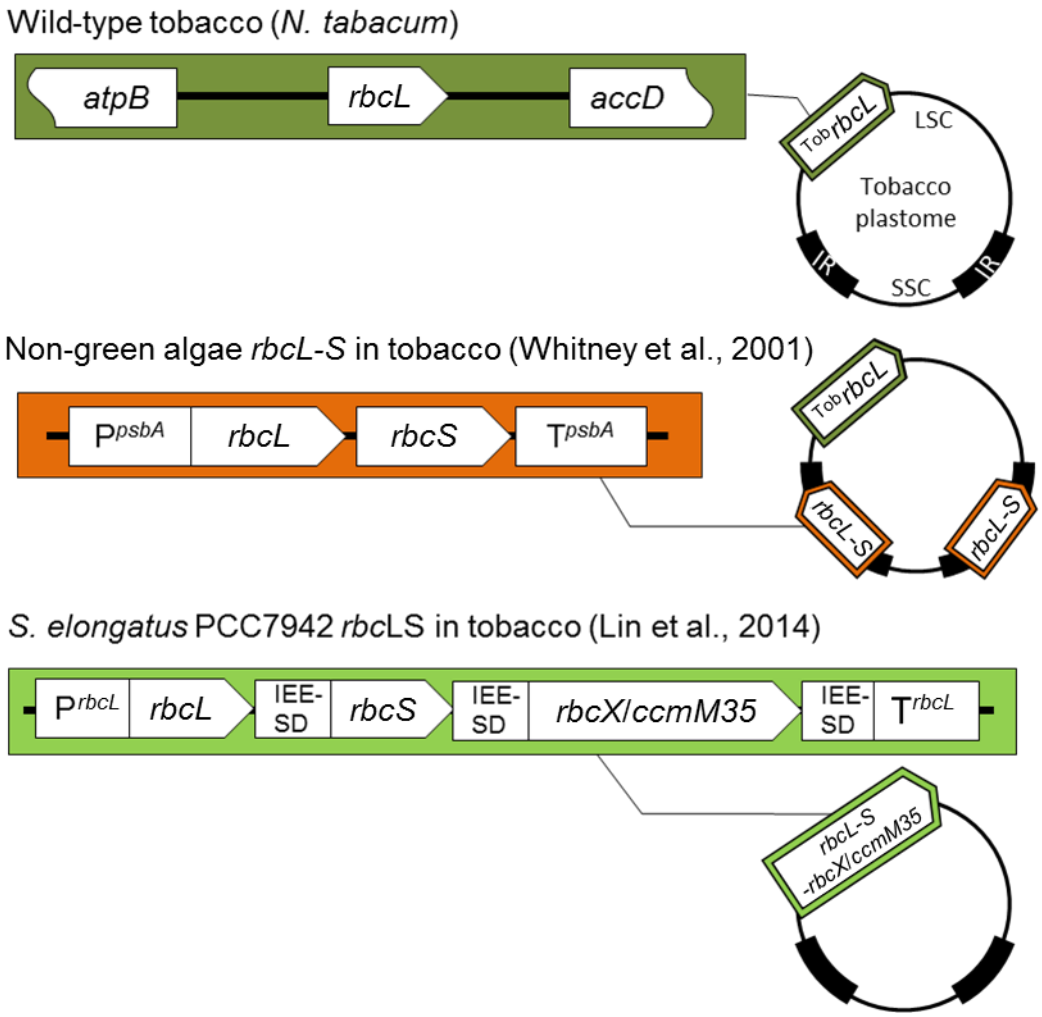

Figure 5.1 Transformation of *rbcL-S* operons coding heterologous Rubisco in the tobacco plastome.

Non-green algal *rbcL* and *rbcS* from *P. tricornutum* and *G. sulphuraria* were introduced into the inverted repeat (IR) region of the *N. tabacum* plastome using *psbA* regulatory elements (Whitney et al., 2001). Lin et al. (2014) introduced the *S. elongatus* PCC7942 Rubisco genes into *N. tabacum* by replacing the tobacco *rbcL* with a genetic cassette expressing *S. elongatus* PCC7942 *rbcL*, *rbcS* and either the *rbc*X or *ccmM35* gene. The *S. elongatus* PCC7942 operon was regulated by the tobacco Rubisco *rbcL* promoter and terminator with each gene separated by a heterologous 3'UTR sequences and repeated IEE-SD sequences (Lin et al., 2014).

Table 5.1 Summary of Rubisco properties from native and recombinant hybrid or foreign L_8S_8 complexes produced in plant leaves.

Comparison of catalysis by red- and green-type Rubiscos (upper panels in table) whose subunits were targeted for recombinant enzyme studies in plant leaves by nucleus (‡) and plastome (†) transformation approaches. References: [(a)]Whitney et al. (2001); [(b)]Whitney et al. (2011); [(c)]Ishikawa et al. (2011); [(d)]Sharwood et al. (2008); [(e)]Getzoff et al. (1998); [(f)]Zhang et al. (2010); [(g)]Lin et al. (2014); [(h)]Sharwood and Whitney (2010); [(i)]Fukayama et al. (2015); [(j)]Whitney et al. (2015); [(z)]Mueller-Cajar and Whitney (2008). In examples 11 and 12 the algae genes were transformed into the inverted repeat region of the tobacco plastome (Figure 5.1) without replacing tobacco L_8S_8 Rubisco production.

(table on next page)

Native L_8S_8 Rubisco

Rubisco type	Organism type	Plant/algae species[reference]	Catalysis			
			k_C^{cat}	K_c	$K_c^{21\%O2}$	$S_{c/o}$
			(s^{-1})	(μM)	(μM)	(mol mol^{-1})
Red	Red algae	*Griffithsia monilis* [a]	2.6	9.3	12.6	167
		Galdieria sulphuraria [a]	1.2	3.3	5.5	166
	Diatom	*Phaeodactylum tricornutum* [a]	3.4	27.9	42.9	133
Green	cyanobacteria	*Synechococcus elongatus* PCC 7942 [z]	11.8	200.0	250.8	42
	C_3	*Nicotiana tabacum* (tobacco) [b]	3.0	12.6	18.3	82
	C_3	*Oryza sativa* (rice) [c]	1.7	17.3	N/A	117
	C_3	*Helianthus annuus* (sunflower) [d]	2.9	8.2	23.9	84
	C_4	*Flaveria bidentis* [b]	4.8	20.4	33	81
	C_4	*Sorghum bicolor* (sorghum) [c]	4.1	41.5	N/A	N/A

Hybrid or foreign L_8S_8 Rubisco

Example	Name of plant genotype[reference]	Rubisco subunit source		recombinant mRNA content*		Rubisco content	Catalysis			
							k_C^{cat}	K_c	$K_c^{21\%O2}$	$S_{c/o}$
		L-subunit	S-subunit	*rbcL*	*RbcS*	(% of WT)	(s^{-1})	(μM)	(μM)	(mol mol^{-1})
1‡	T7.3 [e]	*A. thaliana*	*P. sativum*	native	18%	89%	~85% WT	n.m	n.m	n.m
2†	LLS4 [f]	*S. lycopersicum*	*N. tabacum*	n.m	native	<20%	2.8	n.m	n.m	n.m
3†	Se7942 [g]	*Synechococcus* PCC7942	*N. tabacum*	n.m. (*rbcL-S* mRNA)		<15%	>8.0	n.m	n.m	n.m
4†	tob^{pring} [b]	*F. pringlei*	*N. tabacum*	80-100%	native	20%	3.5	13.0	23.3	80
5†	tob^{flo} [b]	*F. floridana*	*N. tabacum*	80-100%	native	50%	3.7	14.5	24.7	81
6†	tob^{bid} [b]	*F. bidentis*	*N. tabacum*	80-100%	native	35%	4.7	19.9	32.2	79
7†	tob^{Rst} [d]	*H. annuus*	*N. tabacum*	15%	native	11%	3.3	N/A	20.8	84
8†	$t^{Rst}L7$ [h]	*H. annuus*	*N. tabacum*	60%	native	17%				
9†	tob^{AtL} [j]	*A. thaliana*	*N. tabacum*	70-75%	native	25%	2.3	8.6	18.4	80
10‡	SS5 [c]	*O. sativa*	*S. bicolor*	native	79%	124%	2.5	24.0	N/A	103
11‡	PS23 [i]	*O. sativa*	*P. pratense*	native	33%	~107%	1.8	22.4	N/A	126
12†	Pt2 [a]	*P. tricornutum*	*P. tricornutum*	38% (*rbcL*-S mRNA)		8-30%	The algae Rubisco subunits produced were insoluble			
13†	Gs [a]	*G. sulphuraria*	*G. sulphuraria*	3% (*rbcL*-S mRNA)		5%	The algae Rubisco subunits produced were insoluble			

The resulting SeLSX and SeLSM35 tobacco genotypes produced by Lin et al., (2014) accumulated low and varying amounts of *S. elongatus* PCC7942 Rubisco. At most the cyanobacteria Rubisco accumulated to only ~15% that of the wild-type tobacco controls (Table 5.1). Due to these low levels and *S. elongatus* PCC7942 Rubisco's poor affinity and specificity for CO_2, the SeLSX and SeLSM35 genotypes required high-CO_2 supplementation to support growth in soil. Apparent structural incompatibilities between the *S. elongatus* PCC7942 S-subunits and the endogenous tobacco S-subunits precluded assembly of the latter in the Rubisco complexes made in SeLSX and SeLSM35. This incompatibility may explain the observation of a prior transplastomic study where replacement of the tobacco *rbcL* with only the *S. elongatus* PCC7942 *rbcL* resulted in no Rubisco production (Kanevski et al., 1999).

5.1.2 Catalytic variability of higher plant hybrid Rubisco

While generally it is evident the S-subunit can influence catalysis, the greater sequence diversity between S-subunits (relative to L-subunits) appears to produce unpredictable patterns as to the potential for S-subunits to assemble with heterologous L_8 cores and their influence on holoenzyme catalysis. For example, different algae S-subunits were able to assemble with *Rhodobacter sphaeroides* L-subunits into "red"-type L_8S_8 complexes, however the carboxylation rate (k_C^{cat}) of each hybrid enzyme was slowed >100-fold (Joshi et al., 2015). In contrast, assembly of tobacco S-subunits with L-subunits from sunflower, tomato and various *Flaveria* species has no significant influence on catalysis (Sharwood et al., 2008; Sharwood and Whitney, 2010), but slow down the carboxylation rate of *Arabidopsis* Rubisco (Whitney et al., 2011b; Zhang et al., 2011; Whitney et al., 2015) (see Section 5.1.2). Likewise, the assembly of Sorghum S-subunits into rice Rubisco produced L_8S_8 chimers with increased k_C^{cat} and K_m for CO_2 (K_C) (Ishikawa et al., 2011), while assembly of pea S-subunits into *Arabidopsis* Rubisco decreased k_C^{cat} (Getzoff et al., 1998).

The inability to assemble vascular plant Rubisco in *E. coli* has also led to numerous structure-function studies by bioengineering hybrid higher plant Rubisco (*i.e.* complexes comprising heterologous subunit compositions) via plastome and nuclear transformation approaches (Table 5.1). While the catalytic properties of some hybrid enzymes suggest some S-subunits have little or no influence on catalysis, others can evince a dramatic change. For example, assembly of pea Rubisco S-subunits into *A. thaliana* Rubisco generated a hybrid enzyme where k_C^{cat} was reduced by ~12% (Getzoff et al., 1998) while a S-subunit from *Phleum pratense* had no effect on rice Rubisco

catalysis (Fukayama et al., 2015). In contrast, introducing a S-subunit from the C_4 plant sorghum into rice had a significant effect on Rubisco catalysis – raising k_C^{cat} and K_C by 47% and 39% respectively (Ishikawa et al., 2011).

Targeted changes to the L-subunit source in tobacco via chloroplast transformation has also led to varying effects on catalysis. Replacement of the tobacco *rbcL* with the gene from sunflower (Sharwood et al., 2008), tomato (Zhang et al., 2011) and different *Flaveria* species (Whitney et al., 2011b) had little effect on the catalytic properties of the hybrid enzymes that closely matched that of the Rubisco from which the L-subunit originated. This suggests the tobacco S-subunits although having little influence on hybrid enzyme catalysis, are required to maintain functional Rubisco catalysis. However, recent work by Whitney et al. (2015) show that the k_C^{cat} of hybrid Rubisco comprising *Arabidopsis* L-subunits and tobacco S-subunits is impaired by ~25%. Identifying how sequences with the Rubisco L- and S-subunits from different plant sources interact to affect catalysis poses a critical avenue for further study if we are to identify ways in which to reliably bioengineer improved forms of Rubisco (Parry et al., 2013).

5.1.3 Differential assembly of hybrid Rubisco in tobacco chloroplasts

As highlighted in Table 5.1, the biogenesis of hybrid Rubisco comprising tobacco S-subunits and different plant L-subunits varies considerably. In genotypes producing sunflower L-subunits the hybrid enzyme accumulated in tissue culture grown plants to levels of ~30% that of wild-type (Kanevski et al., 1999). In soil, this genotype required elevated CO_2 to survive where hybrid Rubisco levels were only ~10% that of wild-type (Sharwood et al., 2008). The reduced levels of hybrid Rubisco resulted in unique leaf phenotypes in the juvenile plants. Even in genotypes producing 4-fold higher levels of sunflower *rbcL*, the level of hybrid Rubisco produced only increased by ~70% (Sharwood and Whitney, 2010) indicating biogenesis of the hybrid L_8S_8 complex was primarily impeded by limitations in the folding and/or assembly of the sunflower L-subunits with the tobacco S-subunits. A parallel study of Whitney et al. (2011) using L-subunits from 3 different *Flaveria* species also showed 20-50% limitations in hybrid Rubisco production compared to wild-type (Table 5.1). Although the transplanted L-subunits only varied in 3 amino acid residues, the level of hybrid Rubisco produced varied more than 2-fold – attesting to how single amino acid changes in the L-subunit can strongly influence holoenzyme biogenesis.

The limited capacity of tobacco genotypes producing tomato L-subunit to assemble hybrid Rubisco poses a conundrum (Zhang et al., 2011) as both tobacco and tomato are Solanaceae species with L-subunits that vary only by 4 amino acid residues (Genbank accession numbers ABC56308.1 and CAA77361.1). The use of the *rrn* promoter by Zhang et al. (2011) in place of the native *rbcL* promoter/5'UTR sequence was found to perturb tobacco Rubisco biogenesis dramatically as shown by a control genotype where the native tobacco *rbcL* is controlled by the *rrn* genetic elements (Whitney, unpublished). The cause of this unexpected result has yet to be determined.

As indicated in Table 5.1, common to all current heterologous *rbcL* replacement studies has been impediments to the biogenesis of the hybrid or foreign Rubisco complexes. In general this deficiency appears attributable to incompatibilities in the chloroplast such as inefficiencies in mRNA translation, subunit misfolding and/or incompatible assembly requirements. As a consequence no foreign or hybrid L_8S_8 Rubisco has been produced in amounts nearing wild-type levels. This has typically necessitated additional CO_2 to support autotrophic growth of these transplastomic lines.

5.1.4 Research Objective – Producing hybrid Rubisco comprising tobacco L-subunits and heterologous S-subunits

As indicated above, technological limitations in the capacity to effectively engineer the Rubisco S-subunits *in planta* and the puzzling variability in the catalytic properties of the recombinant hybrid enzymes produced has so far frustrated Rubisco S-subunit mutagenic studies. The surgical precision of plastome transformation provides a tantalizing opportunity to use the $^{cm}trL^{RNAi\text{-}S}$ genotype as a vector to produce Rubisco complexes by transplanting in an *rbcL-rbcS* operon to replace *rbcM*. The strategy is summarised in Figure 5.2.

By this approach the assembled Rubisco would comprise a homogenous population of L- and S-subunits and avoid the need for propagating and testing multiple transgenic lines currently undertaken following nucleus transformation approaches (Suzuki et al., 2007; Suzuki et al., 2009; Suzuki and Makino, 2012). Research described in this chapter was aimed at determining the capacity of phylogenetically different S-subunit isoforms to assemble with tobacco L_8 cores and their consequence on catalysis. Using chloroplast transformation in $^{cm}trL^{RNAi\text{-}S}$, *rbcM* was replaced with synthetic *rbcL-rbcS* operons comprising tobacco *rbcL* and *rbcS* coding Rubisco S-subunits from tobacco (control), *Sorghum bicolor*, *Flaveria bidentis* (both C_4 plants) and the red algae *Griffithsia monilis* (Figure 5.2). Transforming plasmid design, the transforming process

and identification of transplastomic genotypes followed by an analysis of the Rubisco biochemistry in each genotype is examined to explain their growth phenotype.

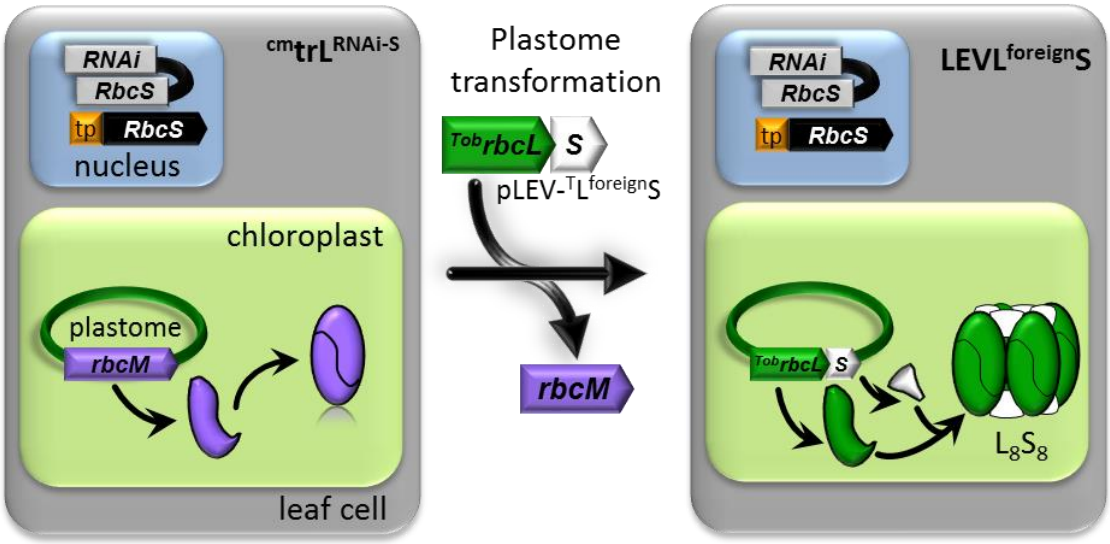

Figure 5.2 Strategy for introducing *rbcL-rbcS* operons into $^{cm}trL^{RNAi-S}$ via plastome transformation.

5.2 Results

5.2.1 Choice of S-subunits for transformation

S-subunits of varying structural compatibility to tobacco Rubisco were used in this study to test how they influenced catalysis if capable of assembly with tobacco L_8 cores. The S-subunit from *Griffithsia monilis* was chosen as the Rubisco from this filamentous red algae possesses the most efficient L_8S_8 enzyme characterised so far (Table 5.1). *G. monilis* Rubisco has a 2-fold higher CO_2/O_2 specificity ($S_{c/o}$) and 26% higher carboxylation efficiency ($k_C^{cat}/K_C^{21\%O2}$; 206 $mM^{-1}\ s^{-1}$) relative to tobacco Rubisco (176 $mM^{-1}\ s^{-1}$) (Whitney et al., 2001). Typical of S-subunits from non-green algae, the βA/βB loop of *G. monilis* S-subunits (10 amino acids) is shorter than higher plant S-subunits (22 amino acids) and has an extended C-terminus that includes a βE-βF loop that is unique to "red"-type Rubisco (Spreitzer, 2003) (Figure 5.3A). The S-subunits from the C_4 species *Flaveria bidentis* is studied as its Rubisco shows differential increases of 57% and 76% in k_C^{cat} and $K_C^{21\%O2}$ respectively, relative to tobacco Rubisco (Table 5.1). Of particular interest was whether the increases in K_C observed for rice Rubisco incorporating sorghum S-subunits (Ishikawa et al., 2011) (Table 5.1) were emulated when assembled with tobacco L-subunits. A comparison of the vascular plant S-subunit identities showed all three isoforms shared ~71-78% identity while only having 36-39% identity to the *G. monilis* S-subunit (Figure 5.3B).

5.2.2 Modifying the codon use of the transplanted RbcS

The objectives of this work were run in parallel with efforts to transform the nucleus of ^{cm}trL$^{RNAi\text{-}S}$ with a synthetic tobacco *RbcS* (^{Tob}*RbcS*) (Birch and Whitney, unpublished). To ensure ^{Tob}*RbcS* was not also a substrate for the introduced RNAi-*RbcS* silencing in ^{cm}trL$^{RNAi\text{-}S}$ its codon use was modified to diverge from the native *RbcS* mRNA transcripts. As shown in Table 5.2, the codon use of ^{Tob}*RbcS* varied significantly from the native nuclear *RbcS* (^{WT}*RbcS*) previously transformed into tobacco (Whitney and Andrews, 2001a) (Figure 4.7). As a result of the altered codon use the ^{Tob}*RbcS* and ^{WT}*RbcS* shared only 71% identity (Figure 5.4B) compared to the >94% homology shared by the varied *RbcS* mRNAs in tobacco (Figure 3.6A). While analyses of the ^{cm}trL$^{RNAi\text{-}S}$ cross-pollinated with RVSSuH, RVtpSSuH and LEVLSSuH genotypes showed the chloroplasts are immune to cytosol directed RNAi-*RbcS* silencing (see Section 4.3.3), this was not known prior to initiation of this project.

The synthetic *RbcS* for the *F. bidentis*, *S. bicolor* and *G. monilis* S-subunit were generated using the ^{Tob}*RbcS* as a template (Table 5.2). Where possible, identical nucleotide sequences were incorporated. The goal of maintaining maximum sequence identity was to minimise potential variations in the stability of each mRNA and their translational potential. As shown in Figure 5.4B, resulting synthetic ^{Sorg}*RbcS* and ^{Bid}*RbcS* showed high levels of identity with ^{Tob}*RbcS* (82-89%), consistent with their high level of amino acid homology (72-78%) (Figure 5.3B). In contrast the high amino acid divergence between the *G. monilis* S-subunit and the plant S-subunits (only 36-38% identity) (Figure 5.3B) led to low identities (only 36-40%) between ^{Gm}*RbcS* and synthetic plant *RbcS* (Figure 5.4B, noting that due to the extensive structural and sequence divergence of the ^{Gm}S-subunit in Figure 5.3, the alignment of ^{Gm}*RbcS* is not provided in Figure 5.4A).

5.2.3 Transforming RbcS into the plastome as an rbcL-rbcS operon

Introducing the ^{Tob}*RbcS* into the transforming plasmid pLEV4 took advantage of a unique *Nde*I cloning site in tobacco *rbcL* (Figure 5.5A). A GenScript synthetic gene cloned into pUC57 was made that coded the 3'end of tobacco *rbcL* (starting at the *Nde*I site) and an adjoining 52 bp intergenic sequence (IS). This sequence is 19 bp longer than that used in LEVLSSuH (Whitney and Sharwood, 2008) and incorporates less of the native *P. tricornutum rbcL-S* intergenic sequence (Figure 5.5B). The IS sequence also varied with the SD sequence positioned at nucleotides -10 to -7 upstream of the ^{Tob}*RbcS* AUG initiator codon compared with its position at -15 to -11 in LEVLSSuH.

This variation was introduced to facilitate the incorporation of a unique *Sph*I cloning site found naturally in the tobacco *RbcS* at the transit peptide scission site. A *Sal*I site was introduced adjacent to the TAA stop codon in synthetic ^{Tob}*RbcS* to enable cloning of the 720 bp Δ^{tob}L-IS- ^{Tob}*RbcS* sequence directly into the *Nde*I-*Sal*I sites of pLEV4 to make the transforming plasmids pLEVL-TobS^{H6} (Figure 5.5). The synthesized ^{Sorg}*RbcS*, ^{Bid}*RbcS* and ^{Gm}*RbcS* (Figure 5.5A) that coded a S-subunit for Rubisco from *S. bicolor, F. bidentis*, and *G. monilis* (Figure 5.4A) incorporated complementary *Sph*I and *Sal*I sites to facilitate their cloning into pLEVL-TobS^{H6} to generate the transforming plasmids pLEVL-SorgS^{H6}, pLEVL-BidS^{H6} and pLEVL-GmS^{H6}, respectively. Each *RbcS* coded a C-terminal 6×His-tag so they were readily distinguishable from endogenous tobacco S-subunits.

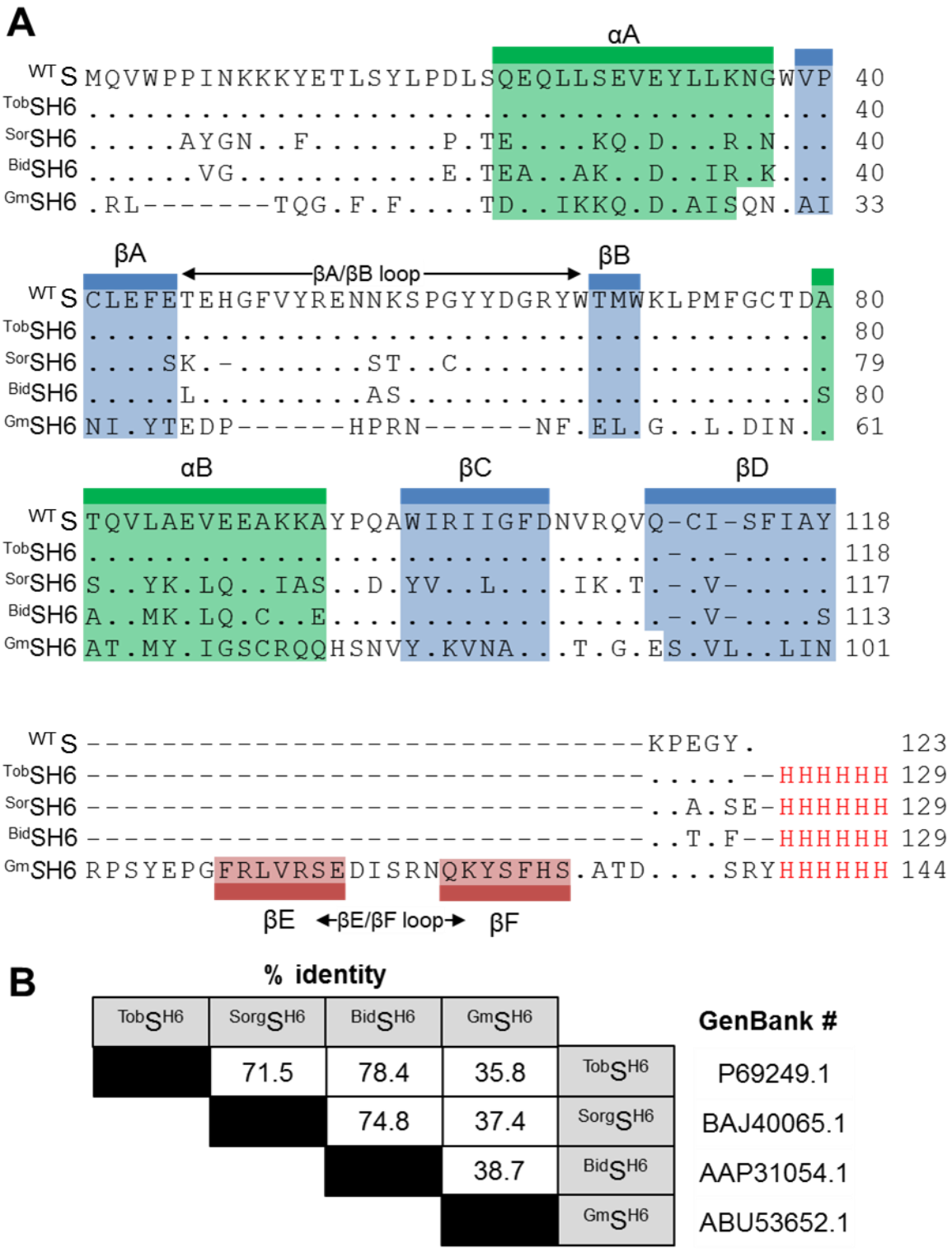

Figure 5.3 Comparative alignment and structure of the S-subunits studied.

(A) Alignment of the translated amino acid sequences of the synthetic *RbcS* designed to code Rubisco S-subunits from *N. tabacum* ($^{Tob}S^{H6}$), *S. bicolor* ($^{Sorg}S^{H6}$), *F. bidentis* ($^{Bid}S^{H6}$) and *G. monilis* ($^{Gm}S^{H6}$). These are aligned relative to the S-subunits encoded by the *Nt*S1a and *Nt*S1b *RbcS* alleles (here called ^{WT}S) in Figure 3.5. Sequences were aligned using MegALIGN. Dots represent residues identical to ^{WT}S. Dashes indicate gaps that were introduced to maximise the alignment. α helices A and B are shaded green, the β strands A-D in blue and the βE/F stands and loops in $^{Gm}S^{H6}$ are in red. (B) Percentage sequence identity between the different S-subunits (excluding the C-terminal 6×His-tag). The GenBank accession numbers for the corresponding natural S-subunit homologs are shown.

Table 5.2 Comparative codon use of tobacco *rbcL*, the tobacco *Nt*S1a/ *Nt*S1b *RbcS* mRNAs (*) and synthetic *rbcS* genes made for this study.

Highlighted are the preferred codons used in *rbcL* (pink), ^{WT}*RbcS** (green) and others in the synthetic genes (grey)

Amino acid	codon	*rbcL*		^{WT}*RbcS*		^{Tob}*RbcS*		^{Sorg}*RbcS*		^{Bid}*RbcS*		^{Gm}*RbcS*	
		No.	%	No.	%	No.	%	No.	%	No.	%	No.	%
Ala	GCA	13	2.7	1	0.8	2	1.5	3	2.3	2	1.5	6	4.1
(A)	GCC	5	1.0	3	2.4	2	1.5	1	0.8	1	0.8	0	0.0
	GCG	4	0.8	1	0.8	0	0.0	0	0.0	0	0.0	0	0.0
	GCU	23	4.8	1	0.8	2	1.5	3	2.3	3	2.3	0	0.0
Arg	AGA	7	1.5	1	0.8	3	2.3	2	1.5	3	2.3	7	4.8
(R)	AGG	0	0.0	0	0.0	1	0.8	2	1.5	2	1.5	0	0.0
	CGA	6	1.3	0	0.0	0	0.0	0	0.0	0	0.0	1	0.7
	CGC	5	1.0	0	0.0	0	0.0	0	0.0	0	0.0	0	0.0
	CGG	1	0.2	0	0.0	0	0.0	0	0.0	0	0.0	0	0.0
	CGU	11	2.3	3	2.4	0	0.0	0	0.0	0	0.0	1	0.7
Asn	AAC	6	1.3	4	3.3	1	0.8	4	3.1	1	0.8	1	0.7
(N)	AAU	9	1.9	1	0.8	4	3.1	1	0.8	2	1.5	9	6.2
Asp	GAC	4	0.8	1	0.8	3	2.3	3	2.3	3	2.3	4	2.8
(D)	GAU	23	4.8	3	2.4	1	0.8	2	1.5	1	0.8	5	3.4
CysI	UGC	4	0.8	3	2.4	1	0.8	2	1.5	2	1.5	1	0.7
	UGU	5	1.0	0	0.0	2	1.5	2	1.5	2	1.5	1	0.7
Gln	CAA	9	1.9	3	2.4	3	2.3	1	0.8	2	1.5	7	4.8
(Q)	CAG	4	0.8	4	3.3	4	3.1	6	4.6	5	3.8	0	0.0
Glu	GAA	24	5.0	5	4.1	6	4.6	4	3.1	5	3.8	8	5.5
(E)	GAG	8	1.7	7	5.7	6	4.6	5	3.8	6	4.6	1	0.7
Gly	GGA	13	2.7	5	4.1	2	1.5	3	2.3	3	2.3	3	2.1
(G)	GGC	2	0.4	2	1.6	5	3.8	3	2.3	4	3.1	1	0.7
	GGG	8	1.7	0	0.0	0	0.0	0	0.0	0	0.0	0	0.0
	GGU	23	4.8	0	0.0	0	0.0	0	0.0	0	0.0	2	1.4
His	CAC	5	1.0	1	0.8	2	1.5	2	1.5	2	1.5	3	2.1
(H)	CAU	9	1.9	0	0.0	5	3.8	4	3.1	5	3.8	6	4.1
Ile	AUA	2	0.4		0.0	0	0.0	0	0.0	0	0.0	1	0.7
(I)	AUC	10	2.1	3	2.4	3	2.3	3	2.3	2	1.5	4	2.8
	AUU	9	1.9	3	2.4	3	2.3	1	0.8	3	2.3	4	2.8
Lys	AAA	21	4.4	1	0.8	4	3.1	2	1.5	3	2.3	3	2.1
(K)	AAG	4	0.8	8	6.5	5	3.8	6	4.6	7	5.4	2	1.4

Amino acid	codon	*rbcL*		^{WT}*RbcS*		^{Tob}*RbcS*		^{Sorg}*RbcS*		^{Bid}*RbcS*		^{Gm}*RbcS*	
		No.	%	No.	%	No.	%	No.	%	No.	%	No.	%
Leu	CUA	6	1.3	1	0.8	0	0.0	0	0.0	0	0.0	1	0.7
(L)	CUC	0	0.0	1	0.8	1	0.8	2	1.5	1	0.8	0	0.0
	CUG	6	1.3	0	0.0	0	0.0	0	0.0	0	0.0	0	0.0
	CUU	10	2.1	3	2.4	6	4.6	7	5.4	5	3.8	2	1.4
	UUA	9	1.9	0	0.0	0	0.0	0	0.0	0	0.0	6	4.1
	UUG	10	2.1	5	4.1	3	2.3	2	1.5	3	2.3	0	0.0
Met(M)	AUG	8	1.7	3	2.4	3	2.3	3	2.3	4	3.1	2	1.4
Phe	UUC	9	1.9	4	3.3	2	1.5	3	2.3	3	2.3	3	2.1
(F)	UUU	12	2.5	1	0.8	3	2.3	3	2.3	3	2.3	5	3.4
Pro	CCA	5	1.0	5	4.1	3	2.3	3	2.3	3	2.3	7	4.8
(P)	CCC	2	0.4	0	0.0	0	0.0	0	0.0	0	0.0	0	0.0
	CCG	3	0.6	0	0.0	0	0.0	0	0.0	0	0.0	0	0.0
	CCU	11	2.3	3	2.4	5	3.8	5	3.8	5	3.8	0	0.0
Ser	AGC	3	0.6	1	0.8	4	3.1	4	3.1	3	2.3	3	2.1
(S)	AGU	2	0.4	2	1.6	0	0.0	1	0.8	1	0.8	3	2.1
	UCA	3	0.6	2	1.6	1	0.8	3	2.3	1	0.8	1	0.7
	UCC	2	0.4	0	0.0	0	0.0	0	0.0	0	0.0	0	0.0
	UCG	0	0.0	0	0.0	0	0.0	0	0.0	0	0.0	1	0.7
	UCU	7	1.5	0	0.0	0	0.0	0	0.0	1	0.8	4	2.8
Term	UAA	1	0.2	0	0.0	1	0.8	1	0.8	1	0.8	1	0.7
Thr	ACA	5	1.0	0	0.0	0	0.0	0	0.0	0	0.0	3	2.1
(T)	ACC	8	1.7	2	1.6	3	2.3	2	1.5	2	1.5	0	0.0
	ACG	1	0.2	0	0.0	0	0.0	0	0.0	0	0.0	0	0.0
	ACU	15	3.1	3	2.4	2	1.5	4	3.1	3	2.3	4	2.8
Trp(W)	UGG	8	1.7	5	4.1	5	3.8	4	3.1	5	3.8	3	2.1
Tyr	UAC	8	1.7	9	7.3	4	3.1	7	5.4	3	2.3	0	0.0
(Y)	UAU	10	2.1	1	0.8	6	4.6	4	3.1	5	3.8	8	5.5
Val	GUA	17	3.6	0	0.0	0	0.0	0	0.0	0	0.0	2	1.4
(V)	GUC	1	0.2	1	0.8	0	0.0	0	0.0	0	0.0	0	0.0
	GUG	3	0.6	5	4.1	3	2.3	3	2.3	3	2.3	1	0.7
	GUU	16	3.3	2	1.6	5	3.8	4	3.1	6	4.6	4	2.8

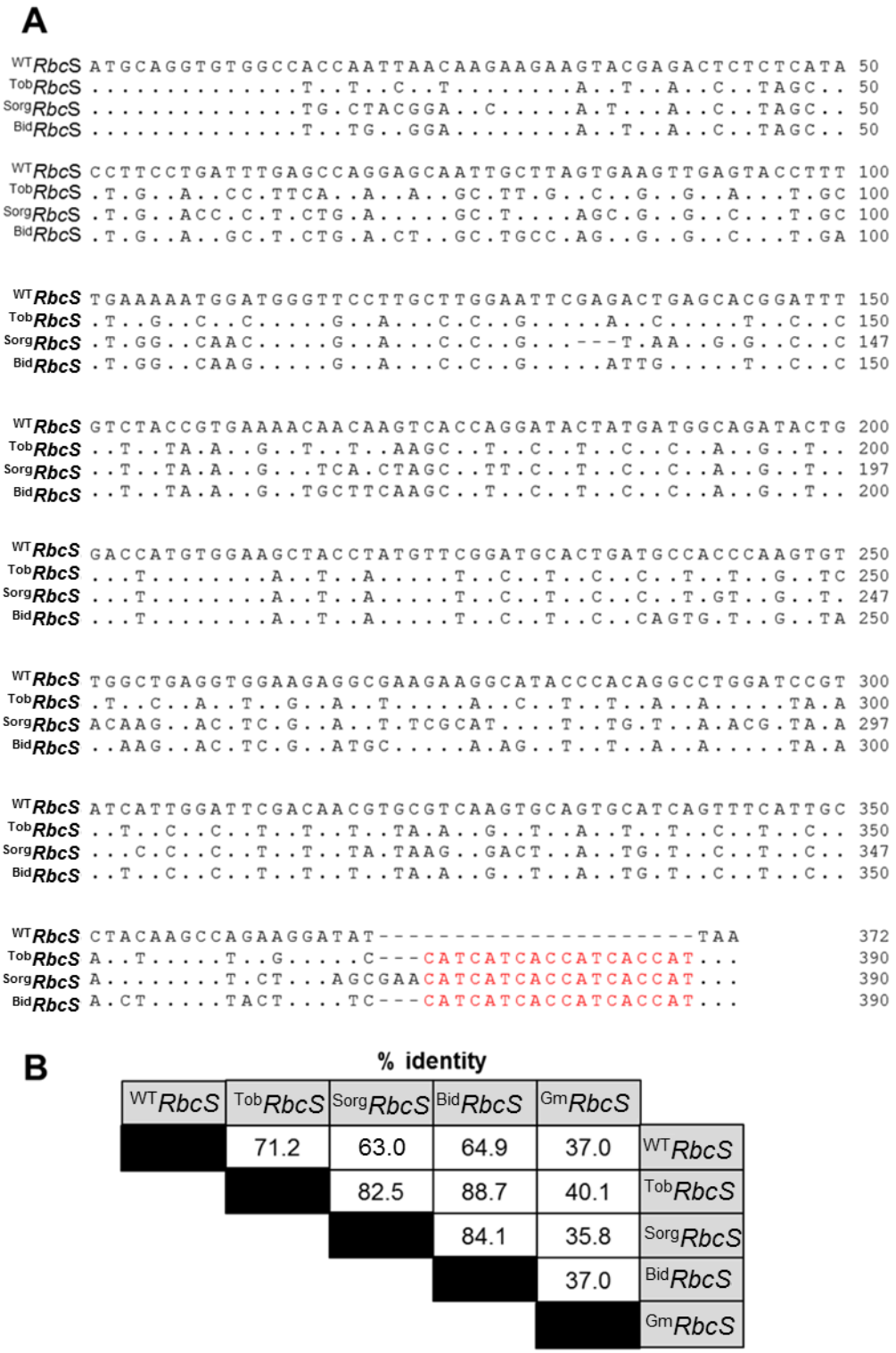

Figure 5.4 Alignment of the *RbcS* genes studied

(A) Alignment of a wild-type *N. tabacum RbcS* (^{WT}*RbcS*; GenBank accession number AY220079.1) and codon modified versions for the same gene (^{Tob}*RbcS*) and a S-subunit from *S. bicolor* ($^{Sorg}S^{H6}$), *F. bidentis* ($^{Bid}S^{H6}$) and *G. monilis* ($^{Gm}S^{H6}$). Sequences were aligned using MegALIGN. Dots represent residues identical to ^{WT}*RbcS*. Dashes indicate gaps introduced to maximise the alignment. Due to the extensive structural and sequence divergence of the ^{Gm}S-subunit (Figure 5.3) the alignment of ^{Gm}*RbcS* is not shown. (B) Percentage sequence identity between the different *RbcS* genes (excluding the C-terminal 6×His-tag sequence highlighted in red).

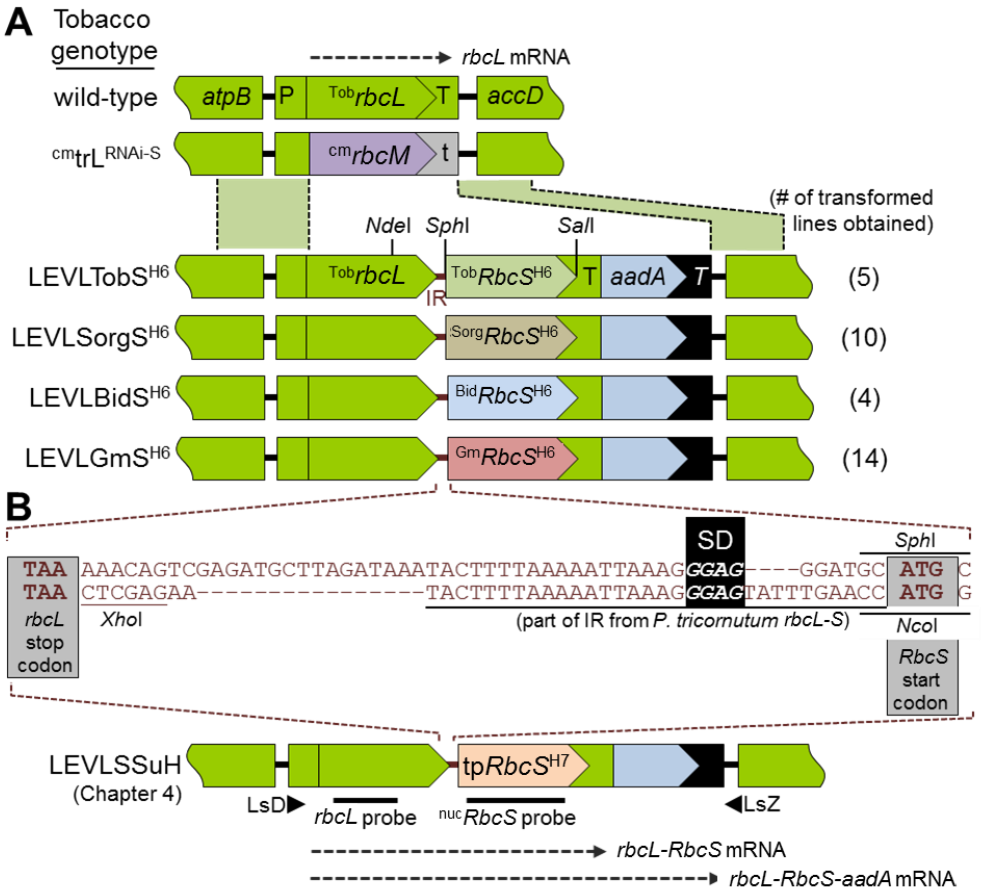

Figure 5.5 Design and detail of the LEVL-S^{H6} plastome transforming plasmids.

(A) Comparison of the gene organisation in the plastome of wild-type, ^{cm}trL^{RNAi-S} (GenBank accession number AY827488) and the four variant LEVL-S^{H6} tobacco genotypes generated by homologous recombination integration (dashed lines, green shading) into ^{cm}trL^{RNAi-S} of genetic material coding the tobacco L-subunit gene (^{Tob}*rbcL*), the different *RbcS*^{H6} genes (Figure 5.4) and the *aadA* selectable marker. Expression of all three genes is under the control of the *rbcL* promoter/5'UTR sequence (P). The number of independent lines obtained for each genotype is shown. T, tobacco *rbcL* terminator (3'UTR) region; *t*, *psbA* 3'UTR; *T*, *rps16* 3'UTR ^{tob}*rbcL*, tobacco Rubisco large subunit gene; (B) Comparative sequence of the intergenic-region (IR) in the LEVL-S^{H6} genotypes and that used in LEVLSSuH (Chapter 4). Shown are the regions of DNA used to make the tobacco *rbcL* probe and *RbcS* probe (recognising the cytosolic *RbcS* mRNA) in addition to the chloroplast mRNA species in each genotype expected to hybridise with the *rbcL* probe (dashed arrows). Positioning of primers LsD and LsZ are shown.

The transforming plasmids made were each introduced into 10 leaf sections from sterile, tissue culture grown ^{cm}trL^{RNAi-S} plants by biolistic bombardment (Figure 5.6A). As shown in Figure 5.5A, each pLEVL-S^{H6} transforming plasmid contained flanking tobacco plastome sequence incorporating regions of the *atpB* and *accD* genes to facilitate replacement of ^{cm}*rbcM* with the *rbcL-rbcS* and *aadA* (selectable marker) transgenes by homologous recombination. In each genotype all three transgenes were controlled by the native tobacco *rbcL* promoter and 5'UTR regulatory elements (Figure 5.5A). Transformed leaf material was selected in RMOP tissue culture medium containing 0.5 g L^{-1} spectinomycin (RMOP^{spec}) (Section 2.4.2). During the transfer of green spectinomycin resistant plantlets (Figure 5.6A) to fresh RMOP^{spec} some of the

soluble leaf protein was analysed by ndPAGE (Figure 5.6B). Correctly transformed lines were identified as those making L_8S_8 Rubisco and/or those no longer making the *R. rubrum* L_2 Rubisco encoded by the displaced ^{cm}*rbcM* in ^{cm}trL$^{RNAi\text{-}S}$ (Figure 5.5A). Four to 14 independently transformed lines were obtained for each genotype. After two to four rounds of further selection on RMOP^{spec} the transformed region of the plastome was PCR amplified (using primers LsD and LsZ, Figure 5.5B) from three lines of each genotype and fully sequenced (results obtained not shown). As expected from the precision of homologous recombination no unwanted nucleotide differences were identified in any of the genotypes. The three lines for each genotype were therefore genetically identical and accordingly showed matching growth phenotypes and cellular biochemistry. The following data depicts that measured for a representative T_0 line of each genotype.

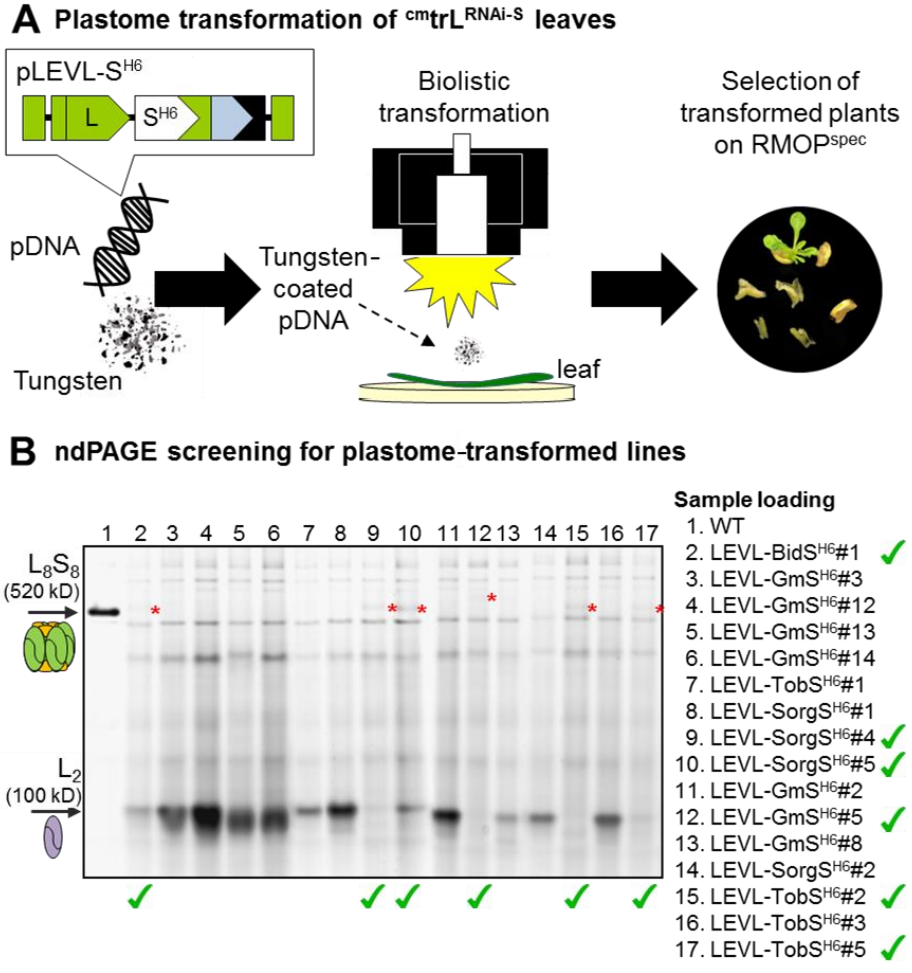

Figure 5.6 Transforming ^{cm}trL$^{RNAi\text{-}S}$ and selecting for the transplastomic genotypes.

(A) The variant pLEVL-S^{H6} transforming plasmids were coated onto tungsten and introduced into ^{cm}trL$^{RNAi\text{-}S}$ chloroplasts by biolistic transformation. The bombarded leaves were embedded into selective RMOP^{spec} medium and after ~4-7 weeks at 25℃ under ~20-60 µmol photons m^2 s^{-1} illumination in air containing 1.5% (v/v) CO_2, green plantlet tissues emerged from the bleached white leaf sections. (B) Example of ndPAGE screening of soluble leaf protein from the spectinomycin resistant plantlets. Correctly transformed lines (green ticks) were identified as those making (small amounts of) recombinant L_8S_8 Rubisco (red asterix) or less/no *R. rubrum* L_2 Rubisco.

5.2.4 All four LEVL-S^{H6} genotypes were unable to grow in soil

Significant attempts were made to propagate the T_0 plants through to maturation for the production of seed. When grown in tissue culture on MS medium all four LEVL-S^{H6} genotypes required sucrose in the medium (3% [w/v]) for development (Figure 5.7). Under these conditions the plants grew very slowly taking twice as long as ^{cm}trL^{RNAi-S} (*i.e.* ~7 weeks) to reach ~6-8 cm in height and develop adequate root mass suitable for transferring to soil. Each plant shared a similar fragile growth phenotype, producing thin, pale green leaves when compared with WT or ^{cm}trL^{RNAi-S} plants grown under the same conditions. Despite repeated attempts, none of the genotypes were able to survive autotrophic growth in soil, even under elevated CO_2 (Figure 5.7). Although initially capable of maintaining leaf and stem turgor and green coloration, after 2 weeks the onset of necrotic lesions became evident in the leaves. After 3 weeks the leaves had succumbed to total necrosis.

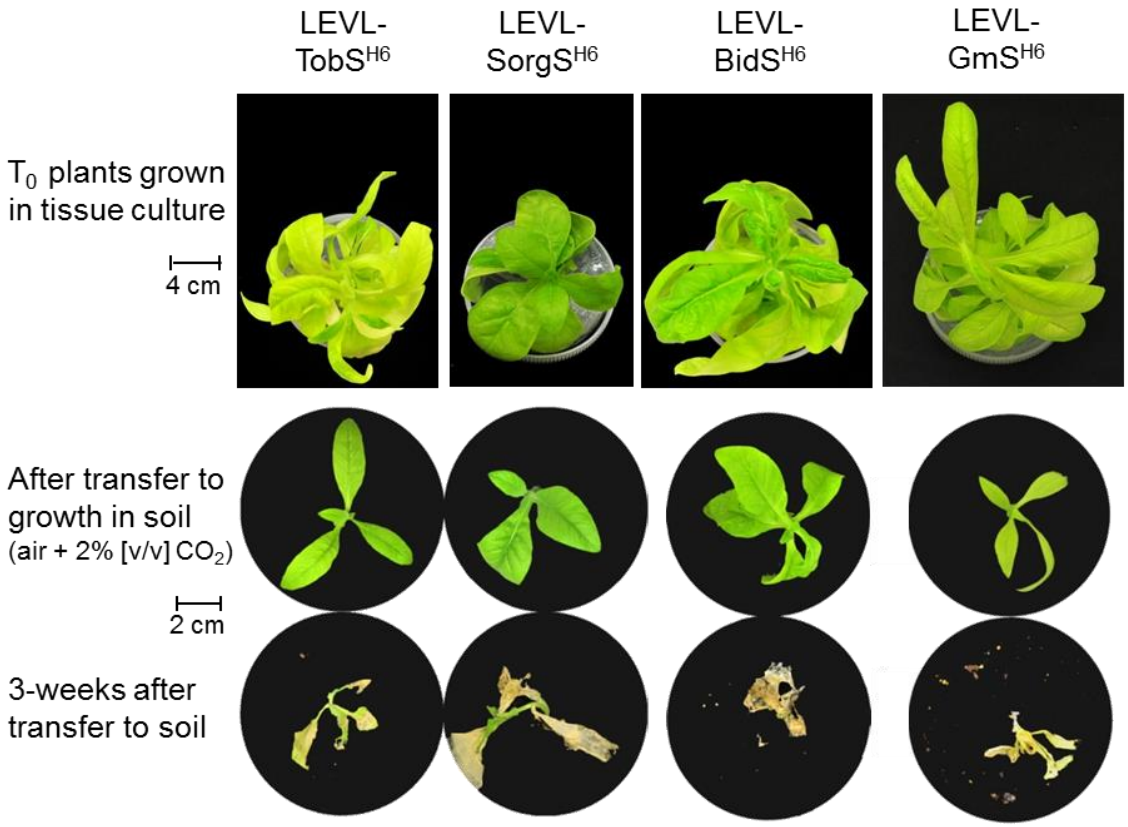

Figure 5.7 The LEVL-S^{H6} genotypes could only survive in tissue culture.

The LEVL-S^{H6} T_0 plantlets were able to produce roots and survive on MS medium (with 3% w/v sucrose), but all shared an unhealthy pale green phenotype. Plantlets with adequately developed roots were transferred to 2 litre pots of soil and maintained at 25℃, ~40-60 µmol photons m^2 s^{-1} illumination and high-CO_2. After 2-weeks growth in soil all plants showed the onset of severe necrosis, with full mortality after 3 weeks.

5.2.5 The LEVL-S^{H6} genotypes produce very little L_8S_8 Rubisco

Very little L_8S_8 Rubisco was evident in the LEVL-S^{H6} genotypes during the ndPAGE screening used to identify each transformed line (Figure 5.6B). It was therefore hypothesized that the inability of the plants to survive in soil stemmed from insufficient levels of Rubisco in their leaves. This was confirmed by PAGE and [^{14}C]-CABP-binding analyses of Rubisco levels in the soluble protein from leaves of duplicate plants grown in tissue culture (Figure 5.8). The L_8S_8 complexes produced in the LEVL-S^{H6} genotypes separated more slowly than tobacco Rubisco through ndPAGE (Figure 5.8A). The relative Coomassie staining intensity of each Rubisco suggests Rubisco levels in the LEVL-S^{H6} genotypes were >100-fold lower than in the leaves of wild-type and ^{cm}trL^{RNAi-S} control plants grown under elevated CO_2. This was confirmed by [^{14}C]-CABP-binding that quantified Rubisco levels in the LEVL-S^{H6} genotypes to be only 0.1 to 0.3 μmol Rubisco active sites m^2 compared with 22 ± 3 μmol Rubisco active sites m^2 in young upper canopy leaves from soil grown wild-type (Figure 5.8B). As seen previously (Figure 4.9B) the Rubisco content in the tissue culture grown LEVLSSuH♀ × ^{cm}trL^{RNAi-S}♂ controls produced ~1.5 μmol Rubisco active sites m^2, more than 5-fold higher than the LEVL-S^{H6} genotypes.

Coomassie staining of soluble leaf protein separated by SDS-PAGE showed a high abundance of both L- or S-subunits in wild-type tobacco, only *R. rubrum* L-subunits in ^{cm}trL^{RNAi-S}, but no distinct Rubisco subunits in the LEVL-S^{H6} genotypes (Figure 5.9). Production of tobacco L-subunits was however confirmed by immunoblot analysis using a tobacco Rubisco antibody (Figure 5.9B). While the antibody was able to detect the endogenous S-subunit in WT and the chloroplast S^{H7}-subunit made in LEVLSSuH♀ × ^{cm}trL^{RNAi-S}♂, its sensitivity was not enough to detect the small amount of recombinant S^{H6}-subunits in any of the LEVL-S^{H6} genotypes. As the tobacco Rubisco antibody does not recognise the S-subunits of sorghum or *G. monilis* Rubisco (Whitney, unpublished) duplicate blots were probed with a Penta-His antibody (Qiagen) used to detect polyhistidine tagged proteins. In this instance the S^{H7}-subunits in LEVLSSuH♀ × ^{cm}trL^{RNAi-S}♂ and the S^{H6}-subunits made in LEVL-BidS^{H6} and LEVL-GmS^{H6} were detected, but the sensitivity of the antibody was insufficient to detect the lower amounts produced in LEVL-TobS^{H6} and LEVL-SorgS^{H6} (Figure 5.9C). The diminished Rubisco content in the LEVL-TobS^{H6} lines suggests L_8S_8 biogenesis in all four LEVL-S^{H6} genotypes was primarily impacted by limitations in the synthesis/stability of one or both subunits, not perturbations in subunit assembly capacity.

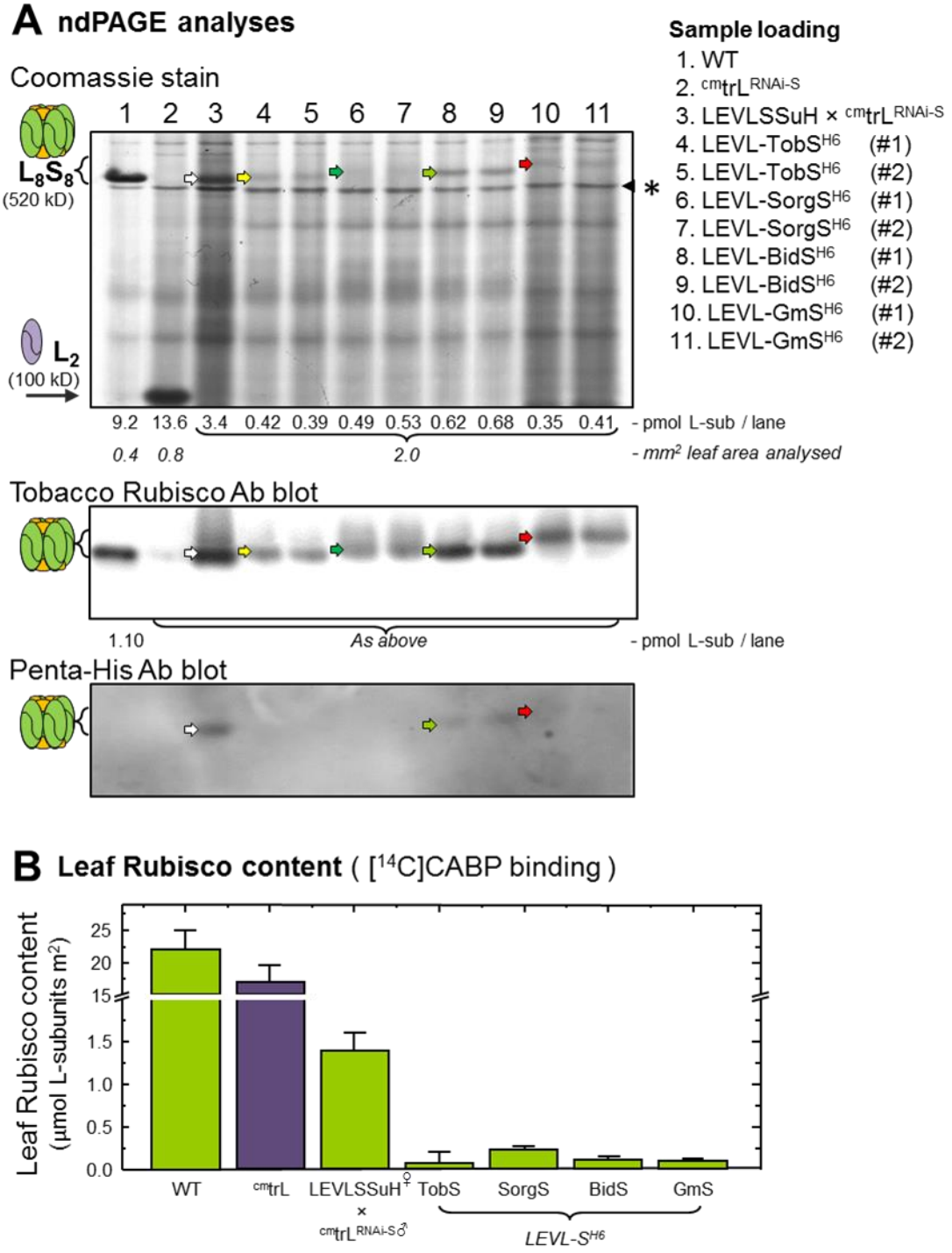

Figure 5.8 Rubisco content in the LEVL-S^{H6} genotypes.

The Rubisco content in the soluble protein from the leaves of each LEVL-S^{H6} genotype grown in tissue culture (Figure 5.7) was compared by (A) ndPAGE and quantified by (B) [^{14}C]-CABP binding relative to that made in tobacco (WT) and ^{cm}trL^{RNAi-S} plants grown in soil in air with 1% (v/v) CO_2. (*) non-Rubisco protein that separates by ndPAGE slightly faster than tobacco Rubisco. The ndPAGE-separated leaf protein was analysed by immunoblotting using antibodies to tobacco Rubisco and a penta-histidine epitope (Qiagen). The area of leaf protein separated by PAGE is shown. The different colored arrows indicate the positioning of the separated recombinant Rubisco complexes in each LEVL-S^{H6} genotype based on their location in the Coomassie-stained gel.

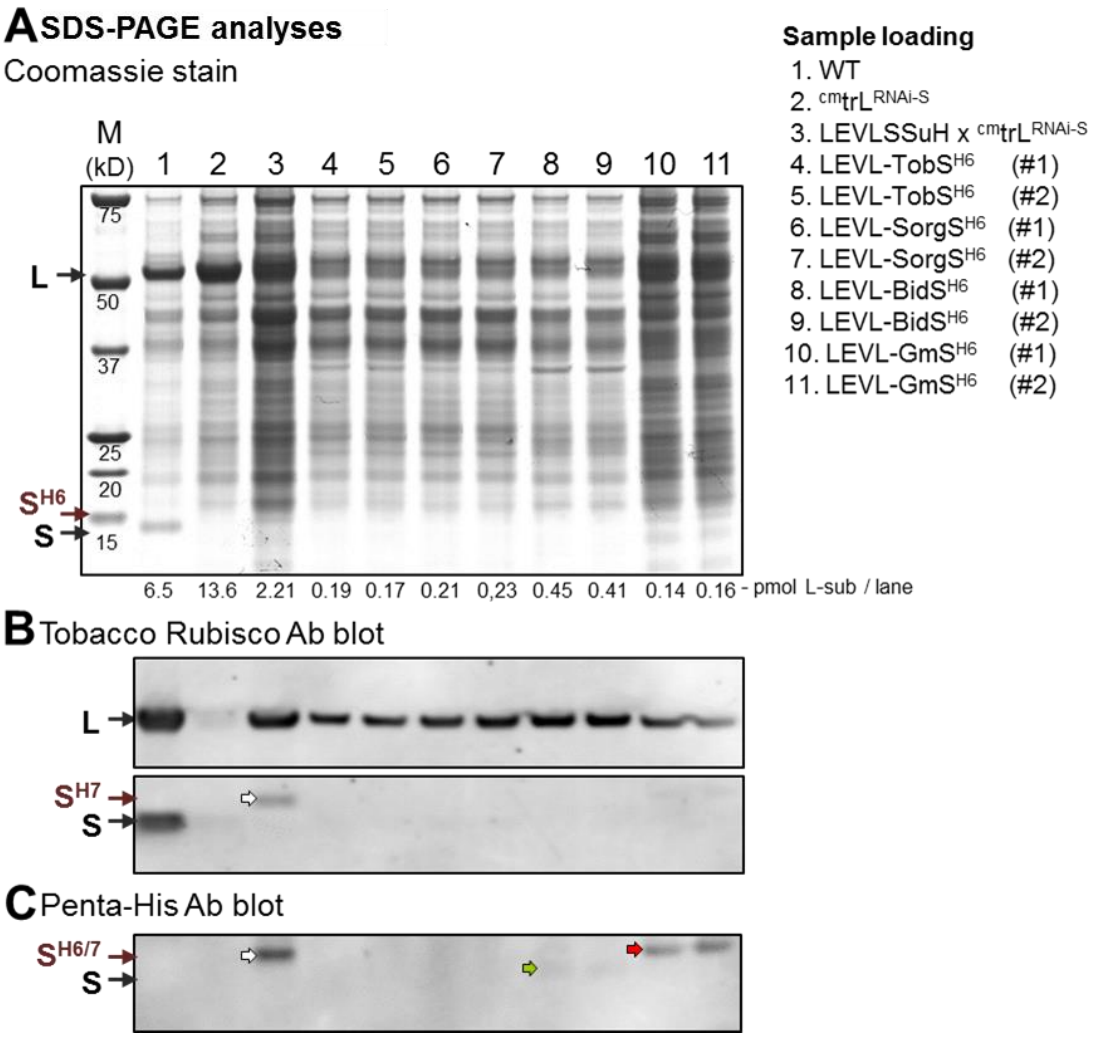

Figure 5.9 Rubisco subunit composition in the LEVL-S^{H6} genotypes.

The Rubisco content in the soluble protein from the same leaves analysed in Figure 5.8 were analysed by SDS-PAGE and (A) Coomassie-stained or analysed by immunoblotting using antibodies to (B) tobacco Rubisco or (C) a penta-histidine epitope (Qiagen). The area of leaf protein separated in each PAGE analysis is shown. M, protein marker (sizes shown); L, L-subunits; S$^{H6/7}$, C-terminal 6×- or 7×His-tagged chloroplast made S-subunits; S, endogenous cytosol made tobacco S-subunits.

5.2.6 Post-transcriptional limitations also impact Rubisco biogenesis in each LEVL-S^{H6} genotype

Despite the fragile phenotype of the LEVL-S^{H6} genotypes, good quality RNA could still be extracted from leaves of the tissue culture grown plants. Compared with the total RNA from soil-grown WT and ^{cm}trL^{RNAi-S} leaves, the LEVL-S^{H6} genotypes had comparable ribosomal RNA (rRNA) patterning (Figure 5.10A). One exception was the lower level of 23S rRNA precursors detected in the LEVL-S^{H6} genotypes presumably an effect of glucose starvation and/or pleotropic effects from a reduction in chloroplast protein translation potential (Barkan et al., 1994; Basturea et al., 2011).

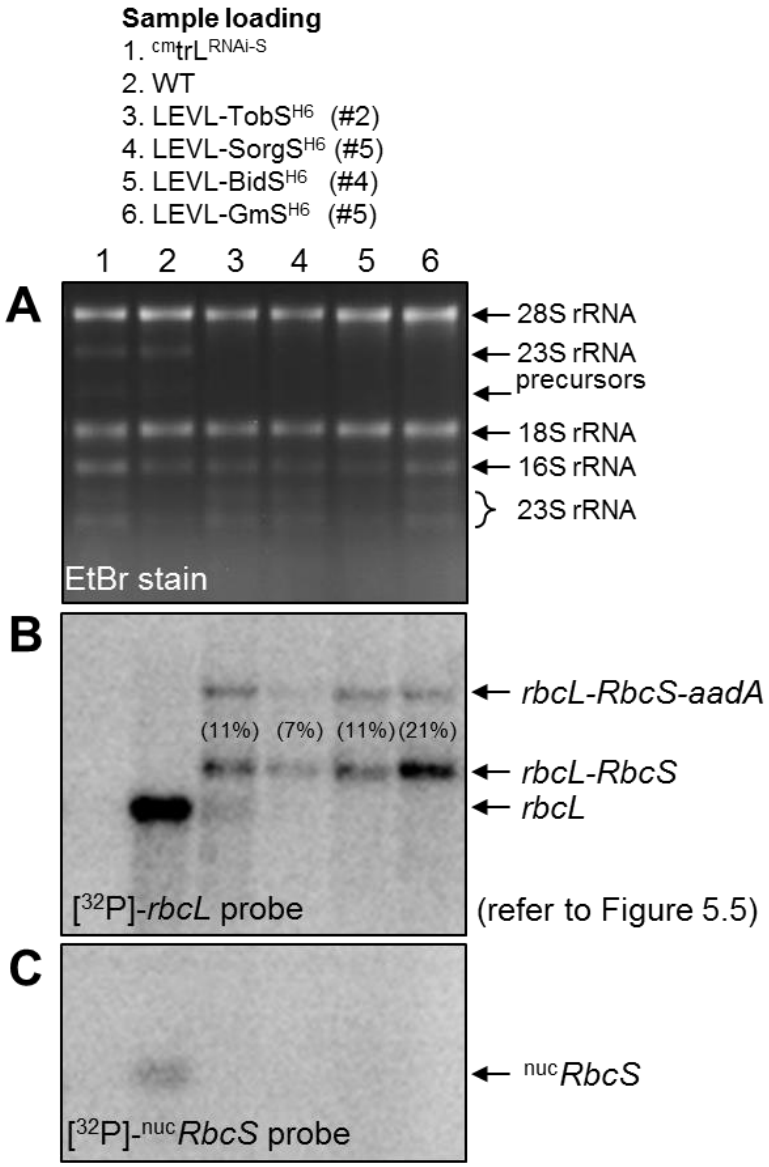

Figure 5.10 The LEVL-S^{H6} genotypes produce plastid Rubisco mRNA.

Rubisco mRNA in total RNA (2 µg) from the same leaves of each tobacco genotype analysed in Figure 5.8 were separated through denaturing formaldehyde agarose gels. (A) The separated RNA was visualised by ethidium bromide (EtBr) staining and the RNA (rRNA) banding annotated according to Claros et al. (1999). Duplicate RNA gels were blotted onto nylon membrane and hybridized with either (B) [^{32}P]-*rbcL* or (C) [^{32}P]-*RbcS* probes (Figure 5.5B). The native cytosolic ^{nuc}*RbcS* mRNA was only detected in wild-type tobacco (WT). Two chloroplast *rbcL* transcripts were detected in each LEVL-S^{H6} genotype (*rbcL-RbcS* and *rbcL-RbcS-aadA*), the native *rbcL* mRNA in WT, and nothing in ^{cm}trL^{RNAi-S} as it codes ^{cm}*rbcM*. The relative amount of both *rbcL* mRNAs in each LEVL-S^{H6} genotype relative to that in WT are shown in parentheses.

As depicted in Figure 5.5B, each LEVL-S^{H6} genotypes produced two *rbcL* mRNA species. These included a prominent dicistronic *rbcL-rbcS* operon and a less abundant tricistronic *rbcL-rbcS-aadA* mRNA. Although the steady state pool of these transcripts in the LEVL-S^{H6} plants were 5 to 14-fold lower than *rbcL* mRNA in WT (Figure 5.10B), they were clearly in sufficient abundance to enable aminoglycoside-3-adenyltransferase production from *aadA* at levels suitable to facilitate spectinomycin

resistance during selection. Importantly the reduced abundance of these mRNA levels are less severe than the 100-fold lower levels of Rubisco produced in the LEVL-S^{H6} genotypes (Figure 5.8B). This implies post-transcriptional limitations are likely the key factor impeding L_8S_8 biogenesis in the LEVL-S^{H6} genotypes. Consistent with the efficient RNAi-*RbcS* targeted silencing in the paternal $^{cm}trL^{RNAi\text{-}S}$ genotype (Chapter 3) no cytosolic *RbcS* mRNA was detected in the LEVL-S^{H6} genotypes (Figure 5.10C).

5.3 Discussion

Comparable to the high plastome transformation efficiency of the "tobacco master line" ^{cm}trL (Whitney and Sharwood, 2008), the $^{cm}trL^{RNAi\text{-}S}$ line was found to be similarly efficient for deriving independently transformed lines (Figure 5.5A). This efficiency appears independent of photosynthetic viability as all LEVL-S^{H6} genotypes produced very little hybrid L_8S_8 enzyme (Figure 5.8) and was incapable of supporting autotrophic plant growth (Figure 5.7). This finding matches that observed by Sharwood and Whitney (2008) who readily produced tobacco genotypes that made no Rubisco or non-catalytic tobacco Rubisco via plastome transformation of ^{cm}trL. Despite only producing low levels of Rubisco, the LEVL-S^{H6} genotypes produced provide the first examples of transgenic plant producing functional hybrid Rubisco comprising tobacco L-subunits assembled with a homogenous population of S-subunits from either *S. bicolor*, *F. bidentis* or the red algae *G. monilis*. Rubisco production via this *rbcL-rbcS* transplantation approach however appears predominantly impeded by one or more post-transcriptional events. As discussed below, the confronting challenge is to identify the post-transcriptional process(es) impeding hybrid Rubisco biogenesis and design solutions to circumvent them.

5.3.1 Lower Rubisco mRNA levels in LEVL-S^{H6} – cause or effect of low hybrid enzyme biogenesis?

The limitation to hybrid Rubisco levels in the LEVL-S^{H6} genotypes accorded with their inability to survive without carbohydrate supplementation (*e.g.* sucrose) in tissue culture. All the LEVL-S^{H6} progeny produced low levels of Rubisco mRNA. These steady state mRNA pools comprised a *rbcL-rbcS-aadA* transcript and a >2-fold more abundant shorter *rbcL-rbcS* transcript. In total these bi- and tricistronic mRNAs were more than 5-fold lower in relative abundance than the *rbcL* mRNA content in wild-type (Figure 5.10). As shown previously in transplastomic tobacco genotypes where Rubisco content is adversely limited, the steady state levels of *rbcL* mRNA can be reduced (e.g. 2 to 5-

fold in the tob^{RSt} and t^{Rst}L7 genotypes) (Sharwood et al., 2008; Sharwood and Whitney, 2010) (Table 5.1). Plausible causes of this reduction are variations in mRNA synthesis and/or stability – both of which are likely sensitive to cellular homeostasis which appears highly compromised in Rubisco deficient transgenic plants, even when grown in tissue culture media supplemented with sucrose (Figure 5.7).

The mRNA's sequence strongly influences its quaternary folding and capacity to interact with molecular factors that are essential to its correct, stabilising maturation and translation. One example of Rubisco mRNA maturation includes the pentatricopeptide repeat protein (PPR) MRL1 that processes the *rbcL* 5'UTR sequence to produce a shortened transcript with higher stability to 5'-3' degradation (Johnson et al., 2010). Likewise, equipping *rbcL* with its native *rbcL* 3'UTR appears important for maintaining wild-type *rbcL* mRNA abundance (Whitney and Andrews, 2003). The *rbcL* 3'UTR is maintained in the LEVL-S^{H6} genotypes and is located downstream of *RbcS*. Use of this gene organisation seems practical as it had little impact on the *rbcL*-^{cp}*RbcS* mRNA levels produced in the LEVLSSuH genotype (Figure 4.10). Only in the LEVLSSuH♀ × ^{cm}trL$^{RNAi\text{-}S}$♂ F_1 progeny where photosynthesis and growth were perturbed was a 4-fold reduction in Rubisco mRNA observed. Recent work has also found 5-fold reductions in the levels of Rubisco chloroplast mRNA in tob$^{AtL\text{-}R1}$ genotypes (Whitney et al., 2015). In this genotype, a gene coding RAF1 from *Arabidopsis* is situated in a comparable place to *RbcS* in the LEVL-S^{H6} genotypes. The growth of the tob$^{AtL\text{-}R1}$ plants was also slowed relative to wild-type due to reductions in Rubisco content.

The variation in Rubisco transcript levels in the LEVL-S^{H6} genotypes and prior transplastomic lines highlights two issues in the context of the ongoing challenges in plastome transformation studies. Firstly, it emphasises the unpredictable influence of changes to the 5'UTR, coding and 3'UTR sequences on mRNA synthesis and stability. This uncertainty often necessitates optimisation via trialling different sequence combinations (Maliga, 2004). Secondly, it questions the extent to which changes in the cell of transplastomic genotypes influence mRNA transcription and stability. This appears particularly pertinent to genotypes where photosynthesis (and thus growth) have been perturbed. For example, the diminished cellular viability of the LEVL-S^{H6} genotypes likely contributes strongly to their low Rubisco mRNA levels. This contrasts with other genotypes with Rubisco activity limitations where the *rbcL* mRNA levels can be increased by enhancing cellular viability by growing the plants under elevated CO_2 or in tissue culture. As seen in Table 5.1, such growth conditions enabled near wild-type *rbcL* mRNA levels to be produced in the tob^{pring}, tob^{flo} and tob^{bid} genotypes grown

under high-CO_2 (Whitney et al., 2011b). Improving the growth potential of the LEVL-S^{H6} genotypes by such approaches proved untenable as the level of hybrid Rubisco biogenesis was too low to attain suitable levels of autotrophic growth by high-CO_2 or tissue culture (Figure 5.7).

The application of exogenous hormones such as cytokinin, auxin or gibberellin (GA_3) have been used to rescue perturbed growth development and fertility in tobacco transgenes (Abbasourr et al., 2012; Huang et al., 2003; Reutter et al., 1998) however the relationship between exogenous and plant endogenous hormones is complex (Black et al., 1994). To what extent such hormone treatments can rescue, if at all, the carbohydrate limitated growth of plants lacking Rubisco activity remains untested. Certainly the slow growth of Rubisco deficient plants can be partially mitigated when grown in medium containing 0.5% sucrose (Figure 5.7), but to what extent their growth can be improved by growing *in vitro* in media with higher carbohydrate (e.g 2% glucose (Chen et al., 2016)) has yet to be examined.

Pale green leaves are commonly attributed to a reduced leaf chlorophyll content that may or may not be related to photosynthethic efficiency (Havaux & Tardy, 1999). Chloroplast genes such as *EGY1* that control's leaf senescence (Chen et al., 2016) as well as genes like *RBD1* (Wang et al., 2016), *S6K1* (Sun et al., 2016) and *RPS5* (Zhang et al., 2016) that regulate protein translation when manipulated have produced plants showcasing low chlorophyll content with pale green phenotype. The quest to pinpoint specific genes affected by engineering the LEVL-S^{H6} genotypes and their relative levels in an induced chlorophyll-limited environment remains to be embarked upon.

5.3.2 Post-transcriptional limitations to hybrid Rubisco biogenesis in LEVL-S^{H6}

While the lower *rbcL* mRNA levels in the LEVL-S^{H6} genotypes likely contribute to the scarcity of hybrid Rubisco produced, it appears perturbations to one or more post-transcriptional processes further limit the enzymes' production. As evident from the growing plastome transformation literature, driving expression of different transgenes with a common promoter/5'UTR regulatory does not guarantee reproducible levels of recombinant protein production (Maliga, 2003; Maliga, 2004; Scharff and Koop, 2007). For example, experiments using the same rRNA operon promoter (P*rrn*) have led to more than a 10,000-fold variation in the levels of recombinant protein produced due to varying post-transcriptional issues (Maliga, 2003). In the case of the LEVL-S^{H6} genotypes it seems unlikely the impediment to Rubisco biogenesis arises from an

obstruction to tobacco L-subunit synthesis, in particular since L_8S_8 Rubisco biogenesis in the genetically similar LEVLSSuH genotype matches wild-type (Figure 4.9B).

The versatility of the pLEV vectors in successfully bioengineering Rubisco is well documented (Whitney et al., 2011a) (Table 5.1). Using pLEV the expression of *rbcL* transgenes (and promoter-less *aadA*) is regulated by the native tobacco *rbcL* promoter and 5'UTR sequences (Figure 5.5). The resulting genotypes have all succeeded in producing L-subunits for L_8S_8 biogenesis, but with varying levels of success (Table 5.1). For example, tobacco lines transformed with pLEV4 (that generated the genotype tob^{LEV4}) produced wild-type levels of Rubisco and *rbcL* mRNA (Whitney et al., 2011b). In contrast, introducing sunflower *rbcL* (*rbcL*^{sun}) produced the tob^{Rst} genotype where the total *rbcL*^{sun} mRNA pool and hybrid $(^{sun}L)_8(^{tob}S)_8$ Rubisco levels were both reduced ~9-fold (Sharwood et al., 2008). In a subsequent $t^{Rst}L7$ genotype the *rbcL*^{sun} mRNA pool was increased 4-fold, but the level of $(^{sun}L)_8(^{tob}S)_8$ Rubisco made only increased 50% (Sharwood and Whitney, 2010) (Table 5.1). Clearly post-transcriptional issues can influence heterologous L-subunit synthesis in tobacco chloroplasts. However these issues are likely dampened in each LEVL-S^{H6} genotype as they share the native tobacco *rbcL* coding and promoter/5'UTR regulatory sequences. It therefore seems unlikely that problems with translation of the tobacco L-subunit are causing the >100-fold lower levels of L_8S_8 production in the LEVL-S^{H6} genotypes.

The spectinomycin resistant phenotype of the LEVL-S^{H6} lines implies sufficient levels of aminoglycoside-3-adenyltransferase (aadA) are produced. That is, translation processing of the *aadA* component of the larger, less abundant *rbcL-rbcS-aadA* mRNA is feasible. Questions arise however as to how much aadA protein was made in each of the LEVL-S^{H6} genotypes and what amount is needed to confer a spectinomycin resistant phenotype? These issues remain to be quantified in all pLEV-derived genotypes, and in all tobacco plastome transformation events in general. One approach would be to quantify and compare aadA levels in varying transplastomic lines using a new antibody from Agrisera. This is an objective for future consideration.

Taken together, these justifications suggest a significant impediment to hybrid Rubisco production in the LEVL-S^{H6} lines arising from a heightened hindrance in the synthesis of the heterologous Rubisco S-subunits or/and their capacity to assemble with the tobacco L-subunits. The efficient functioning of proteases within chloroplasts may also contribute to the paucity of hybrid Rubisco biogenesis, in particular if problems with Rubisco subunit production, folding or assembly into stable L_8S_8 complexes increase their propensity for proteolysis.

5.3.2.1 Problems with initiating chloroplast S-subunit synthesis in the LEVL-S^{H6} lines

As in bacterial systems, protein translation in chloroplasts requires the successful assembly of a ribosome on an mRNA (initiation) before synthesis of a polypeptide can proceed (elongation) and reach its full length and trigger protein release (termination). Impeding any of these three phases slows the translational processing of a protein (Woodson and Chory, 2008). In bacteria the rate-limiting step often occurs at the point of initiation with the strength of ribosome binding strongly correlating with the amount of protein synthesis (O'Connor et al., 2013). In particular, changes to the Shine-Dalgarno (SD) sequence (*i.e.* the ribosome binding site) have a dramatic influence on the strength (*i.e.* effectiveness) of ribosome engagement with the mRNA. Using a *gfp* marker the mechanistic differences in the SD recognition machinery between *E. coli* and tobacco chloroplasts has been tested by modifying the position and number of SD sequences placed upstream of the AUG initiator codon (Drechsel and Bock, 2011). The results suggested that closely located SD sequences upstream of an AUG initiation codon in a plastome impede translation initiation by competitively impeding 30S ribosomal subunit engagement. A key finding was that the 30S ribosome preferentially bound to the most 5' SD sequence, suggesting that the chloroplast translational machinery may be inefficient at recognising SD sequences within polycistronic transcripts – in direct contrast to *E. coli* (Drechsel and Bock, 2011). This finding provided reasoning for the hypothesis that many chloroplast polycistronic mRNA's undergo inter-cistronic cleavage into monocistronic mRNAs to increase their translation efficiency. This requirement for this cleavage however does not appear to be absolute as some chloroplast oligocistronic mRNAs do not undergo scission (e.g. the *psa*A-*psa*B mRNA) and neither do some transgenes (e.g. *rbcL-rbcS* operon from algae) which can still produce very high levels of L- and S-subunit synthesis in tobacco chloroplasts (Whitney and Andrews, 2001a) (example 12 and 13, Table 5.1).

Similarly, other elements such as mRNA secondary structure, small RNA (sRNA) binding sites and start codon positioning all strongly influence translation initiation (Storz et al., 2011). Compared with bacterial systems however, chloroplast mRNA's show significant variation in the positioning of their SD sequence within the 5'UTR relative to the AUG initiator codon (typically 12-7 nucleotides upstream of AUG [Maliga, 2003]). At the extreme is the *psbA* mRNA where the SD sequence (GGAG) is located 33 nt upstream of the AUG start codon (Kim and Mullet, 1994). In this instance the chloroplast S1 ribosomal protein binds to the *psbA* 5'UTR to fold the mRNA and bring the SD sequence to the consensus position for ribosome engagement

and initiation. In most instances the plastid mRNAs share SD sequences that are complementary to the 3' end of the 16S rRNA.

Table 5.3 Variation in the intergenic sequences used in *rbcL-rbcS* transgene studies in the tobacco plastome.

Details of Rubisco mRNA and L_8S_8 contents are summarised in Table 5.1. The Shine-Dalgarno (SD) GGAG and ATG/GTG initiator codons for the *rbcS* transgenes are shown in bold.{1} Whitney and Sharwood, 2008; {2} Whitney and Andrews, 2001; {3} Lin et al., 2014. Part of the 5'UTR sequence and SD for *rbcL* is provided as a comparison.

Tobacco genotype	(*reference*)	3' end of intergenic sequence
LEVL-S^{H6}	(*this study*)	..AG**GGAG**----GGATGC **ATG** -10 -7
LEVLSSuH $LEVL^{Ub}S$	(*Chapter 4*) *{1}*	..AG**GGAG**TATTTGAACC **ATG** -14 -11
Pt2	*{2}*	..AG**GGAG**TATTTGAATA **GTG** -14 -11
Gs2	*{2}*	..AG**GGAG**-TATAAAACA **GTG** -13 -10
Se7942	*{3}*	..AA**GGAG**--ATATACCC **ATG** -12 -9
Wild-type *rbcL*		..AA**GGAG**----GGATTT **ATG** -10 -7

An examination of prior *rbcL-rbcS* operons transformed into the tobacco plastome shows variation in the positioning of the SD sequence relative to the AUG codon of the *rbcS* transgene (Table 5.3). A distinct difference in the LEVL-S^{H6} genotypes is the closer location of the SD sequence to the AUG start codon of the synthetic ^{cp}*RbcS* transgenes. However the position of the SD -11 to -7 nucleotides in the LEVL-S^{H6} lines matches that used by the tobacco *rbcL* (Figure 5.10). As noted by Kuroda and Maliga (2001), the translational control region (TCR) of the *rbcL* mRNA is dependent on sequence within the 5'UTR and adjoining coding sequence. Work within the Whitney lab has found synonymous single nucleotide changes within the first three codons of the coding sequence (*i.e.* nucleotide changes that maintain amino acid sequence) that were predicted to alter mRNA folding ("secondary structure") leading to significant perturbations in L-subunit synthesis (Orr, 2013). Work in this thesis

demonstrated that maintaining mRNA folding, and not amino acid sequence, was important for maintaining L-subunit synthesis.

This finding has little relevance on most of the *rbcL* transgene substitution studies so far undertaken as they have generally maintained the wild-type tobacco *rbcL* sequence for up to 42 nucleotides downstream of the AUG codon. As indicated in Whitney et al. (2011), the first 50 nucleotides of 5' coding sequence of plant *rbcL* are highly conserved. This suggests the differences observed in the capacity for foreign Rubisco biogenesis in tobacco chloroplasts (Table 5.1) is independent of recombinant L-subunit translation initiation.

Problems with the mRNA quaternary structure of the ^{cp}*RbcS* transgenes in the LEVL-S^{H6} therefore seem a likely contributor to the low amount of hybrid Rubisco produced if S-subunit translation initiation and/or elongation is impeded. Potential problems with initiation could be tested by altering the SD location and intervening sequence to the AUG to match that used naturally by other chloroplast transcripts. As with tobacco *rbcL*, this may need to include a short region of the native sequence downstream of the AUG codon that naturally facilitates translation (a possibility experimentally tested in Chapter 6). As discussed in Section 5.3.2.2, problems with translation elongation might be examined by altering the ^{cp} *RbcS* sequence to match the codon use of other chloroplast genes (also tested in Chapter 6).

5.3.2.2 Synthesis of the S-subunit is slowed by poor codon use

Slowing the elongation process of translation would expectantly also influence the levels of protein synthesis in chloroplasts. Extensive analyses in bacterial systems have highlighted how the use, clustering, and repetition of rare codons in an mRNA can slow the elongation rate (Gustafsson et al., 2004; Proshkin et al., 2010). This slowing typically correlates with impediments in the cellular availability of cognate transfer RNA (tRNA) that trigger pausing of ribosomes on the mRNA (Buchan and Stansfield, 2007). Sucrose gradient centrifugation analysis of mRNA-polysome associations (*i.e.* mRNA's with multiple ribosomes bound) is often used to gauge how well an mRNA is being translated. Efficiently translated mRNAs typically have higher numbers of ribosomes attached and therefore sediment further down the gradient (Mašek et al., 2011). A comparison of the polysome sedimentation profile for the *rbcL-RbcS* and *rbcL-RbcS-aadA* mRNA's in the LEVLSSuH$^{♀}$ × ^{cm}trL$^{RNAi\text{-}S♂}$ and LEVL-TobS^{H6} genotypes may therefore prove useful in identifying differences in S-subunit translation. For example, if translational processing of the mRNA's was more impeded in LEVL-

TobS^{H6} then a higher proportion of the *rbcL-RbcS* and *rbcL-RbcS-aadA* mRNA's would be found in fractions collected further up the sucrose gradient.

The importance of codon use on recombinant protein expression in tobacco chloroplasts remains uncertain (Ullrich et al., 2015). Interestingly chloroplasts have 56 tRNA genes, but lack tRNA genes recognising some codons for alanine (GCU, GCC) arginine (CGC, CGA, CGG), leucine (CUU, CUC) or proline (CCU, CCC) (Nakamura and Sugiura, 2007). As indicated in Table 5.4 however, some of these codons have a high frequency of use by chloroplast mRNA's (e.g. Ala, GCU; Arg, CGA; Leu, CUC and Pro, CCU) demonstrating the supply of these tRNA species from the cytosol may not be limiting in leaf cells. Interestingly *in vitro* assays used to measure translation rates in isolated tobacco chloroplast extracts (Yukawa et al., 2005) suggest translation efficiency does not necessarily correlate with codon use (Nakamura and Sugiura, 2007, 2009). This coincides with the expression of a bacterial *bar* in tobacco chloroplasts that produced high levels of protein expression (~7% of the soluble leaf protein) despite its high (69%) GC content (Lutz et al., 2001). Similarly, changes to the AT bias of a *gfp* have no discernible effect on the amount of GFP produced (Reed et al., 2001). These findings are somewhat unexpected considering the base composition of the 79 protein coding genes in the tobacco plastome have a >60% AT content (Nakamura and Sugiura, 2009), largely as a result of the third base in the codons showing a ~75% AT bias. This AT preference is evident in the *rbcL* codon use frequency (Table 5.2) and the consensus codon usage by all the tobacco plastome mRNA transcripts (Table 5.4).

When compared with the codon use of the synthetic *RbcS* transgenes in the LEVL-S^{H6} genotypes, alanine (GCG), arginine (CGC, CGG, AGG), serine (AGC, UCG) and threonine (ACG) were generally excluded except for the preferential use of AGC (Ser) by most of the *RbcS* transgenes and the AGG (Arg) codon incorporated twice in ^{Sorg}*RbcS* and ^{Bid}*RbcS* (Table 5.2). Whether use of these codons in the genes is unfavourable to the translation of each S^{H6}-subunit remains to be experimentally tested (see Chapter 6). One must keep in mind however the merit of looking individually at specific codon use frequencies as a measure of the translational potential for a gene. For example the *rbcL* mRNA makes use of the rare CGC (Arg) codon (whose tRNA is nucleus encoded) at a relatively high frequency – somewhat in conflict with the high levels of L-subunits translated in tobacco chloroplasts.

Table 5.4 Codon use by the 79 mRNAs produced in tobacco chloroplasts (Nakamura and Sugiura, 2009)

An examination of the codon preferences for the tobacco chloroplast genes showed the lowest frequencies of use are for alanine (GCG), arginine (CGC, CGG, AGG), serine (AGC, UCG) and threonine (ACG).

	Codon	Fraction		Codon	Fraction		Codon	Fraction		Codon	Fraction
Phe	UUU	0.667	Ser	UCU	0.299	Tyr	UAU	0.804	Cys	UGU	0.752
Phe	UUC	0.333	Ser	UCC	0.152	Tyr	UAC	0.196	Cys	UGC	0.248
Leu	UUA	0.328	Ser	UCA	0.188	STOP	UAA	0.519	STOP	UGA	0.228
Leu	UUG	0.200	Ser	UCG	0.059	STOP	UAG	0.253	Trp	UGG	1.000
Leu	CUU	0.214	Pro	CCU	0.393	His	CAU	0.770	Arg	CGU	0.219
Leu	CUC	0.069	Pro	CCC	0.187	His	CAC	0.230	Arg	CGC	0.063
Leu	CUA	0.128	Pro	CCA	0.286	Gln	CAA	0.756	Arg	CGA	0.251
Leu	CUG	0.062	Pro	CCG	0.135	Gln	CAG	0.244	Arg	CGG	0.074
Ile	AUU	0.495	Thr	ACU	0.392	Asn	AAU	0.768	Ser	AGU	0.209
Ile	AUC	0.200	Thr	ACC	0.197	Asn	AAC	0.232	Ser	AGC	0.059
Ile	AUA	0.306	Thr	ACA	0.304	Lys	AAA	0.754	Arg	AGA	0.289
Met	AUG	0.853	Thr	ACG	0.107	Lys	AAG	0.246	Arg	AGG	0.104
fMet	AUG	0.141									
Val	GUU	0.372	Ala	GCU	0.448	Asp	GAU	0.797	Gly	GGU	0.322
Val	GUC	0.120	Ala	GCC	0.172	Asp	GAC	0.203	Gly	GGC	0.118
Val	GUA	0.380	Ala	GCA	0.280	G1 u	GAA	0.757	Gly	GGA	0.389
Val	GUG	0.128	Ala	GCG	0.100	Glu	GAG	0.243	Gly	GGG	0.171
fMet	GUG	0.006									

5.3.2.3 An increased propensity for recombinant Rubisco subunit proteolysis?

Proteases are active in all regions of the chloroplast to assist in protein maturation, damaged protein recycling and general maintenance of protein quality control (van Wijk, 2015). While a dozen or so types of protease are known to operate in different compartments of chloroplasts, their mechanisms for substrate selection remain poorly understood, despite many showing evolutionary linkages with well-studied bacterial proteases (Olinares et al., 2011). The absence of detectable S-subunits in $^{cm}trL^{RNAi\text{-}S}$ (Figure 5.9B) attests to efficiency of stromal proteases for degrading unassembled proteins. As discussed above, the use of atypical codons in the *RbcS* transgenes tested in this study (see Section 5.3.2.2) and possible problems arising from unfavourable mRNA folding (see Section 5.3.2.1) likely impeded translational processing of the recombinant S-subunits in the LEVL-TobS^{H6} genotypes. A consequence of this may be a slowing of S-subunit translational processing that, hypothetically, may increase exposure of the emerging nascent peptides as substrates for protease attack. A technique often employed to measure protein translation, maturation, modification and stability is pulse-chase with [^{35}S]-Met/unlabelled-Met (Pohl and Hasilik, 2015; Whitney et al., 2015). This has previously been used to measure the stability of plastid made S^{H7}-subunits incorporated into L_8S_8 complexes in the RVSSuH and RVtpSSuH genotypes (Whitney and Andrews, 2001a) (Figure 4.7). The method was however not sensitive enough to measure the synthesis and degradation of the nascent chloroplast made S^{H7}-peptides, especially considering the efficiency of proteolysis in chloroplasts. This approach would therefore

be even more ineffective in the LEVL-S^{H6} genotypes given they produce even lower levels of plastid made S-subunits.

Prior attempts to express non-green algae Rubisco in tobacco chloroplasts found no evidence for "red"-L_8S_8 assembly, however the heterologous L- and S-subunits were found to accumulate as insoluble protein in the Pt2 and Gs tobacco genotypes (Whitney et al., 2001) (Table 5.1). Notably this finding prompted comparative SDS-PAGE and immunoblot analysis of the soluble and the total cellular protein (*i.e.* both soluble and insoluble protein) in the LEVL-S^{H6} leaves to confirm tobacco L-subunits and varied S-subunits were not accumulating as insoluble protein (data not shown). In another PhD project in the Whitney lab, the flowers of both Pt2 and Gs tobacco genotypes were pollinated with pollen from $^{cm}trL^{RNAi-S}$ to knock out tobacco L_8S_8 production (analogous to the process used in Chapter 4). As expected the resulting Pt2♀ × $^{cm}trL^{RNAi-S}$♂ and Gs♀ × $^{cm}trL^{RNAi-S}$♂ progeny produced no tobacco Rubisco resulting in plants that could only grow slowly in tissue culture (i.e. comparable to the LEVL-S^{H6} genotypes) (Figure 5.7). Curiously, despite the high levels of insoluble algae L- and S-subunit units made in the parental Pt2 and Gs genotypes, none were detected in the $^{cm}trL^{RNAi-S}$ crossed progeny except for trace levels of soluble algal S-subunits (Gunn, 2014). This finding demonstrates the efficiency of protease activity in tobacco chloroplasts, especially in plants where growth and resource availability are greatly impeded. It also demonstrates that algae S-subunits seem less prone to chloroplast protease degradation, as also reported by Whitney et al. (2001). This improved stability might explain why the GmS^{H6}-subunit levels detected in the soluble protein of LEVL-GmS^{H6} leaves appears to accumulate at higher than the S-subunits in the other LEVL-S^{H6} genotypes (Figure 5.9C), that did not correlate with the amount of hybrid $(^{Tob}L)_8(^{Gm}S)_8$ Rubisco made in the same protein sample (Figure 5.8).

The role of proteolysis in the effect of low Rubisco contents in the LEVL-S^{H6} genotypes remains unclear. As shown in Chapter 4, the LEVLSSuH♀ × $^{cm}trL^{RNAi-S}$♂ plants make ~1.5 μmol L-subunits m^2 of $L_8(S^{H7})_8$ Rubisco (Figures 4.9 and Figure 5.8) which can support autotrophic growth to full maturity in soil under high-CO_2 (Figure 4.8C). In contrast the LEVL-$TobS^{H6}$ genotype only managed to produce <0.4 μmol L-subunits m^2 which relegated their survival dependency to growth in tissue culture (Figure 5.7). When considering the identical subunit amino acid sequence analogies between the LEVL-$TobS^{H6}$ and LEVLSSuH♀ × $^{cm}trL^{RNAi-S}$♂ genotypes it seems hard to envisage that variations in proteolytic activity or reduced S-subunit chaperoning can entirely account for their >4-fold differences in Rubisco content (Figure 5.8).

5.3.3 Varying structural incompatibilities between heterologous L- and S-subunit effect on holoenzyme assembly and catalysis

There is an extensive number of amino acid interactions between the S- and L-subunit in an L_8S_8 complex (Figure 1.8). As demonstrated in the example alignment in Figure 5.3, there is significant divergence among S-subunit sequences, especially between the "green" and "red" Rubisco lineages (Andersson, 2008). An important structural differentiation in the S-subunits between these lineages is the extended C-terminal β-hairpin extension (*i.e.* the βE/βF loop) that structurally occupies the ends of the central solvent channel that traverses the centre of L_8S_8 complexes (Spreitzer, 2003). Expression studies in *E. coli* demonstrated the red-type Rubisco S-subunits from a diatom could assemble with L_8 cores of cyanobacteria Rubisco (Joshi et al., 2015). The level of the hybrid L_8S_8 enzyme made was however extremely low. This might be explained by the recent demonstration by Joshi et al. (2015) as to the role of the C-terminal β-hairpin extension in "red" S-subunits in forming critical interactions in the holoenzyme central channel that are necessary for stable L_8S_8 assembly and activity. Despite these apparent subunit compatibility issues, the LEVL-GmS^{H6} progeny successfully demonstrated for the first time the biogenesis of L_8S_8 complexes comprising tobacco L-subunits and the *G. monilis* S-subunits (Figure 5.8). Notably, the catalytic viability of this hybrid enzyme is totally compromised – further attesting to the influence of the S-subunit on Rubisco catalysis. This finding is in agreement with the results of Joshi et al. (2015) that showed hybrid L_8S_8 comprising the L-subunits of the "red"-type Rubisco from *Rhodobacter sphaeroides* and the S-subunits from red algae Rubisco were also catalytically inactive.

Incompatibilities in amino acid sequences between L- and S-subunits from heterologous higher plant sources seem less impactful on hybrid L_8S_8 assembly. As shown in Table 5.1, hybrid Rubisco holoenzyme comprising cytosol made heterologous plant S-subunits (e.g. from *Arabidopsis*, *S. bicolor* or *P. pratense* Rubisco) or tobacco S-subunits and alternative plant L-subunits (e.g. sunflower, tomato, *Flaveria* and *Arabidopsis*) can be readily produced in leaf chloroplasts, although with varying effects on catalysis. Prior analysis of rice Rubisco containing varying stoichiometries of rice and sorghum S-subunits showed, respectively 50% and 40% increases in k_C^{cat} and K_C relative to wild-type rice Rubisco (Ishikawa et al., 2011) (see also Table 5.1). Unfortunately the low amounts of Rubisco produced in the LEVL-S^{H6} genotypes in this thesis prevented rapid extraction methods typically undertaken to accurately measure k_C^{cat} and K_C (Sharwood et al., 2008). Consistent with this need for rapid analysis of

freshly extracted Rubisco, the measured k_C^{cat} rates for the Ni-NTA purified enzymes from the LEVL-S^{H6} genotypes are low (results not shown) and likely are compromised by the inclusion of a polyhistidine tag on the S-subunits that appears to result in ambiguous changes to the catalytic properties of Rubisco (Table 4.2). Nevertheless the activity measurements serve to highlight that the Rubisco L_8S_8 hybrid enzymes comprising *S. bicolor* or *F. bidentis* S-subunits retained catalytic activity while those comprising *G. monilis* S-subunits did not.

The synthesis of cytosolic made S-subunits appears to be stably and efficiently silenced in the $^{cm}trL^{RNAi\text{-}S}$ line and its plastome-transformed progeny. This brings into question the necessity for including distinguishable peptide tags on the re-introduced S-subunit transgenes. Exclusion of tags would help to better understand the influence of S-subunits on the catalytic properties – a consideration for future S-subunit engineering in $^{cm}trL^{RNAi\text{-}S}$ (discussed in Chapter 7).

5.3.4 Future goals – increasing incorporation of plastid made S-subunits into L_8S_8 Rubisco

As hypothesized by Whitney and Andrews (2001) the relocation of *RbcS* to the nucleus appears to have led to adaptive changes in S-subunit evolution that influence the biogenesis pathway of Rubisco that appear to limit the incorporation of chloroplast made S-subunits. The validity of this hypothesis requires further testing using plastome transformation to identify solutions for increasing S-subunit synthesis in the plastid. As indicated in Section 5.3.2 above, one potential solution may be to increase translational processing of the plastid S-subunits through modification of its codon use to match that of other chloroplast made proteins – an objective tested in Chapter 6. An overall critical component of engineering the S-subunit is better understanding the natural import and chaperoning processes of cytosol made S-subunits. This understanding may provide clues as to why they may be preferentially incorporated during L_8S_8 biogenesis in leaf chloroplasts. Such considerations are important if transformations of heterologous S-subunits into other plant species are to be effectively undertaken as a means to bioengineer changes to Rubisco catalysis. Future possibilities for utilising the $^{cm}trL^{RNAi\text{-}S}$ genotype to study components of the cytosolic S-subunit maturation process are discussed in Chapter 7.

CHAPTER 6 – ENHANCING HYBRID RUBISCO PRODUCTION IN TOBACCO CHLOROPLASTS

6.1 Introduction

The prior chapters of this thesis have highlighted the potential utility of the $^{cm}trL^{RNAi\text{-}S}$ master line for engineering both the Rubisco L- and S-subunits simultaneously in higher plants chloroplasts. Pollinating transplastomic lines producing chloroplast made S-subunit with pollen from the $^{cm}trL^{RNAi\text{-}S}$ genotype was successful in producing Rubisco isoforms comprising solely chloroplast made L- and S-subunits (Chapter 4). An initial attempt to directly transform the $^{cm}trL^{RNAi\text{-}S}$ plastome with synthetic Rubisco operons comprising tobacco *rbcL* and heterologous *rbcS* genes proved less effective at producing hybrid, recombinant Rubisco (Chapter 5). Such anomalies in the differential expression potential of transgenes is common to chloroplast transformation applications as the technology remains encumbered by uncertainties on how to reliably predict recombinant protein production (Ullrich et al., 2015). As indicated in Section 4.3.1.1 and Section 5.3.2, expression of different proteins driven only recorded by identical regulatory elements (*e.g.* the *rrn* promoter and *T7g10* 5'UTR) can differ by as much as 10,000-fold in their levels of expression (Maliga, 2003). To counter these uncertainties it is common practice for transplastomic application to pursue a try-it-and-see approach by testing the effect of different regulatory sequences or modifications in codon use on transgene expression (see Section 5.3.2.2).

6.1.1 Chaperone incompatibilities and proteolysis influence Rubisco biogenesis in E. coli and in chloroplasts

In any recombinant protein expression system both the intrinsic folding potential of the target protein and its requirements for compatible molecular partners (e.g. chaperones, chaperonin, accessory proteins and subunits) for folding and assembly strongly influence the level of functional protein expression (*i.e.* its biogenesis). As a result of folding and assembly incompatibilities the expression of the Rubisco subunits from any plant or algae in *E. coli* results in the accumulation of mis-folded, insoluble L- and S-subunits that aggregate as insoluble inclusion bodies (Whitney et al., 2011a; Parry et al., 2013). With regard to recombinant protein expression in leaf chloroplasts however, the detection of insoluble red algae Rubisco L- and S-subunits in the tobacco Pt and tobacco Gs genotypes (Table 5.1) poses the only recorded instance identifying insoluble photosynthetic recombinant protein accumulation in chloroplasts (Whitney et al., 2001).

Importantly no insoluble red algae Rubisco subunits are evident in the progeny of the tobacco Pt and tobacco Gs genotypes pollinated with $^{cm}trL^{RNAi\text{-}S}$ pollen (Gunn, 2014). In these plants tobacco Rubisco synthesis is eliminated via integration of an RNAi-*RbcS* allele resulting in chlorotic, Rubisco depleted plants that only survive in tissue culture. This provides important evidence for the efficiency of chloroplasts mechanisms for recycling cellular resources – especially when these resources become limiting such as in tissue that is aging or exposed to environmental stress (Feller et al., 2008). The mechanism of this recycling involves the diverse and efficient range of proteolytic enzymes residing in chloroplasts that function to help maintain cellular homeostasis (Sakamoto, 2006; as discussed in Section 5.3.2.3). The avidity of this proteolytic "recycling" activity may necessitate protective chaperoning of proteins within the chloroplast during their biogenesis, thus explaining why unassembled Rubisco subunits are very difficult to detect (Whitney and Sharwood, 2008). Indeed, improving the expression of recombinant proteins introduced into chloroplasts may necessitate the co-introduction of complementary assembly partners that not only improve the folding and assembly of a protein, but also avoid proteolysis of misfolded products. The importance of chaperone complementation has a significant influence on foreign Rubisco biogenesis (Whitney et al., 2015) (Section 6.1.2) and the bio-insecticide from *Bacillus thuringiensis* in leaf chloroplasts (de Cosa et al., 2001) (Section 6.1.3).

6.1.2 A popular transplastomic target – hybrid Rubisco of sunflower L-subunits and tobacco S-subunits

A number of transplastomic studies have examined the production of hybrid $^{s}L_8{}^{t}S_8$ Rubisco (*i.e.* that comprising chloroplast made sunflower L-subunits [^{S}L] and cytosol made tobacco S-subunits [^{t}S]) in tobacco chloroplasts (Kanevski et al., 1999; Sharwood et al., 2008; Sharwood and Whitney, 2010). Common to each study was the replacement of tobacco *rbcL* with the gene from sunflower (^{sun}*rbcL*), albeit each regulating ^{sun}*rbcL* mRNA synthesis via varying 3' regulatory sequences (Figure 6.1A). The initial focus of these transplantation studies stemmed from the perceived catalytic superiority of sunflower Rubisco over tobacco Rubisco (Kanevski et al., 1999) which proved to be incorrect (Sharwood et al., 2008). The catalytic properties for the hybrid $^{s}L_8{}^{t}S_8$ produced in the initial Nt-pIK83-1 tobacco genotype were first reported to be significantly impaired (Kanevski et al., 1999). Subsequent analysis of this genotype (renamed tob^{Rst} to signify *tob*acco producing *R*ubisco comprising *s*unflower L and *t*obacco S-subunits) however showed the catalytic properties of the hybrid $^{s}L_8{}^{t}S_8$ enzyme match those of

sunflower Rubisco (Table 5.1) in accordance with the measured leaf gas exchange properties of the plant (Sharwood et al., 2008).

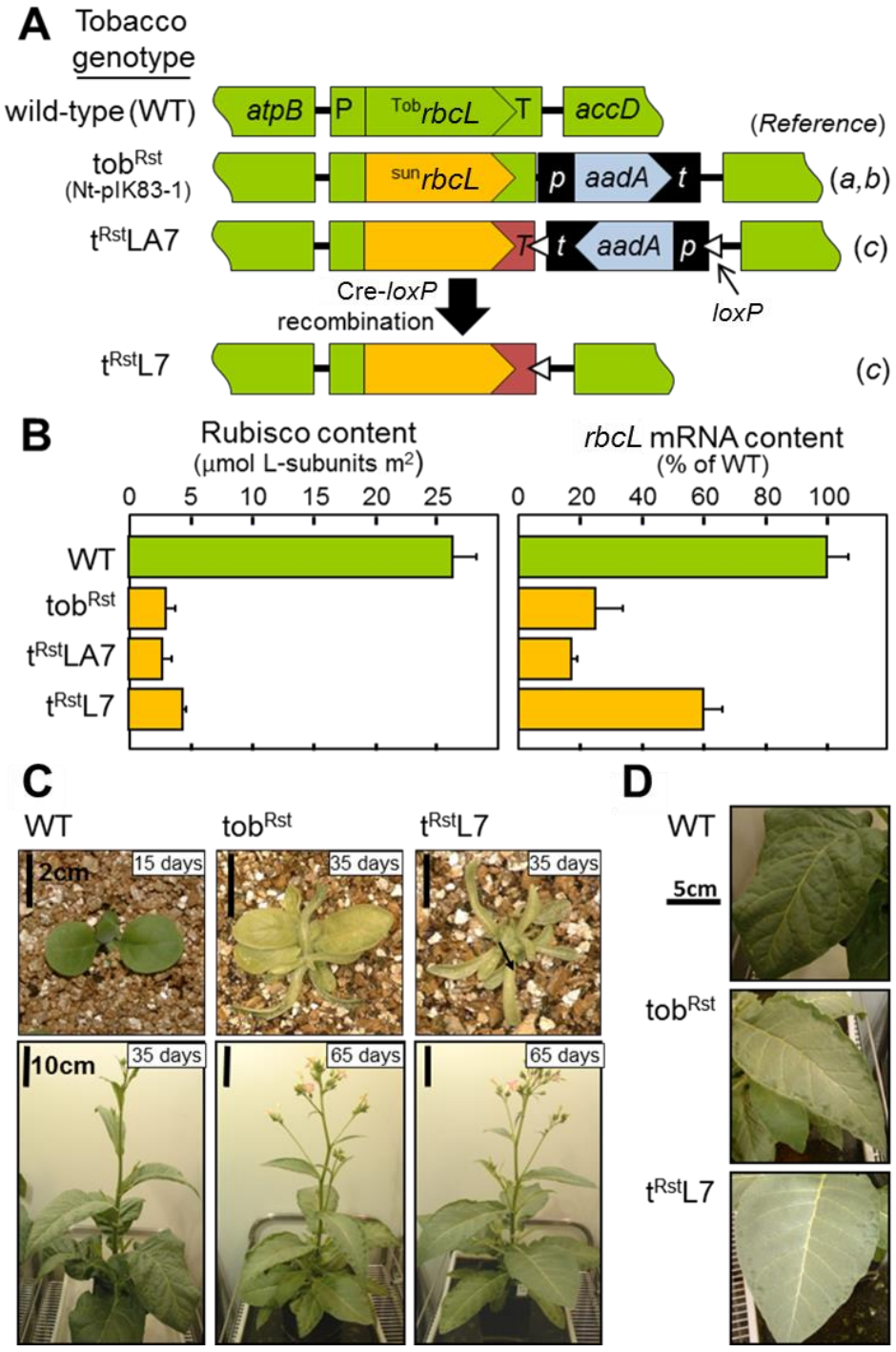

Figure 6.1 Key features of tobacco genotypes producing sunflower L-subunits.

(A) Different transplastomic replacement strategies have replaced the tobacco *rbcL* with the sunflower *rbcL* to produce the genotypes Nt-pIK83-1 ([a]Kanevski et al, 1999 – renamed tob^{Rst} by [b]Sharwood et al., 2008), t^{Rst}LA7 and t^{Rst}L ([c]Sharwood and Whitney 2010). P, *rbcL* promoter/5'UTR sequence; T, tobacco *rbcL* 3'UTR; *T*, *psbA* 3'UTR; *t*, *rps16* 3'UTR; *p*, *rrn* promoter/*T7g10* 5'UTR; white triangles, 34 nt *loxP* sequences. (B) Only low levels of hybrid $^{S}L_8{}^{t}S_8$ Rubisco (comprising sunflower L-subunits and tobacco S-subunits) were made in each genotype, even in the t^{Rst}L lines where ^{sun}*rbcL* mRNA levels were increased 4-fold. (C) Each genotype could be grown to maturity in air with 0.5% (v/v) CO_2 producing slower growing plants with pale green leaves with (D) abnormal curling around the edges that was more prominent in lines producing less $^{S}L_8{}^{t}S_8$ Rubisco. Figure adapted from Sharwood et al. (2008, 2010).

All the transplastomic tobacco genotypes producing hybrid $^{s}L_8{}^{t}S_8$ enzyme showed significant limitations on the enzyme's biogenesis in tobacco chloroplasts (Figure 6.1B). At best the amount of $^{s}L_8{}^{t}S_8$ produced was only ~17% the Rubisco levels made in tobacco (wild-type) controls. Even increasing the ^{sun}*rbcL* mRNA content 4-fold only led to a modest 40-50% increase in $^{s}L_8{}^{t}S_8$ production (when comparing the t^{Rst}LA7 and t^{Rst}L7 genotypes in Figure 6.1B) suggesting hybrid $^{s}L_8{}^{t}S_8$ synthesis was primarily impeded during one or more post-transcriptional events. As a result of the reduced Rubisco levels, the growth of each $^{s}L_8{}^{t}S_8$ producing genotype was slower than wild-type, necessitating high-CO_2 for growth in soil. Even under high-CO_2 all the genotypes shared a pale green leaf phenotype and their juvenile progeny produced abnormal, thin, strap-like shaped leaves (Figure 6.1C). The leaves of more mature plants were of similar shape to the wild-type controls, but were thinner with pronounced dimpling around the leaf margins (Figure 6.1D). The severity of this dimpling phenotype was less evident in the t^{Rst}L7 genotype that produced the most $^{s}L_8{}^{t}S_8$ enzyme and thus had improved leaf CO_2 assimilation rates and grew more quickly than the t^{Rst} and t^{Rst}LA7 genotypes (Sharwood et al., 2008; Sharwood and Whitney, 2010).

The reason(s) for the low levels of $^{s}L_8{}^{t}S_8$ biogenesis remain speculative. The finding that $^{s}L_8{}^{t}S_8$ levels were not greatly enhanced by increasing ^{sun}*rbcL* mRNA levels strongly favours limitations to one or more events limiting synthesis of the hybrid enzyme. Analyses of [^{35}S]-Methionine labelled $^{s}L_8{}^{t}S_8$ complexes showed their turnover rates matched that of wild-type tobacco Rubisco (Sharwood et al., 2008). This indicated the hybrid $^{s}L_8{}^{t}S_8$ enzyme was not susceptible to a higher rate of proteolysis. As both the ^{tob}*rbcL* and ^{sun}*rbcL* share >92% sequence identity (with their 5' sequences being identical for the first 56 bp) it was difficult to advocate that incompatibility in translation initiation or elongation significantly impeded ^{S}L-subunit synthesis. It was proposed that structural incompatibilities in the quaternary conformations of the assembled ^{S}L-subunit octameric cores (*i.e.* $^{S}L_8$) may hinder ^{t}S-subunit assembly into L_8S_8 complexes (Sharwood and Whitney, 2010). It was also hypothesized this impediment may also increase the susceptibility of the subunits to proteolysis. Overall it was postulated the compounding limitation impeding hybrid $^{s}L_8{}^{t}S_8$ biogenesis in tobacco chloroplasts resulted from incompatibilities in the chaperoning requirements of the ^{S}L-subunit (Sharwood et al., 2008; Sharwood and Whitney, 2010). This conclusion is now supported by recent work demonstrating the importance of chaperone compatibility on hybrid Rubisco biogenesis in leaf chloroplasts (Whitney et al., 2015) (see also Section 6.1.3)

6.1.3 Considerations for increasing recombinant protein production in chloroplasts

As emulated in hybrid $^{s}L_8{}^{t}S_8$ studies and other recombinant protein expression work using chloroplast transformation, it is not simply a case that the steady state pool of a transgene mRNA levels reflects the amount of recombinant protein produced (Maliga, 2003). A number of early plastome transformation studies in particular paid close attention to the high levels of transgene mRNA production with little consideration to the level of recombinant protein made (Ohtani et al., 1991; Richter et al., 2000; Outchkourov et al., 2003). Deciphering the underpinning reason(s) for this mismatch in the abundance of transgene transcript and protein is rarely scrutinized experimentally due to the costs (in both time and money) of chloroplast transformation. For example, as discussed in Chapter 5, a comprehensive study on the relative importance of codon use on transgene expression in chloroplasts remains incomplete (see Section 5.3.2.2). The potential influence of the highly efficient proteolytic mechanisms in chloroplasts to recombinant protein synthesis in leaf chloroplasts is also poorly understood (see Section 5.3.2.3 and paragraph above). Although some appreciation is required for the necessity for genetic complementarity of an mRNA and the translational machinery for efficient initiation and elongation processes of translation (see Section 5.3.2.1), these rules do not appear absolute as there is significant natural variation found among the endogenous chloroplast mRNA species (Choquet and Wollman, 2002; Peeters and Hanson, 2002; Juszczak et al., 2012).

As first hypothesised by Whitney and Andrews (2001), problems with the production of recombinant Rubisco in leaf chloroplasts likely stem from incompatibilities with their folding and assembly requirements. This is now supported by recent tests on comparable tobacco genotypes transformed with the *Arabidopsis rbcL* with and without *Arabidopsis raf1*. In the transformed lines making the *Arabidopsis* RAF1 Rubisco chaperone, the levels of hybrid $^{A}L^{t}S$ enzyme (comprising *Arabidopsis* L-subunits and ^{t}S) were increased more than 7-fold. The RAF1 chaperone forms a homo-dimer complex and functions to assemble the post-chaperonin folded L-subunits into Rubisco complexes (Feiz et al., 2014). The benefits of chaperone co-expression were also seen in tobacco genotypes expressing recombinant Bt-protein where inclusion of the putative chaperone, ORF 2, in the transformed cry2Aa2 operon helped attain Bt expression levels of ~40% (w/w) of the leaf protein (de Cosa et al., 2001).

6.1.4 New insights into polycistronic mRNA design

There is increasing interest to exploit the inherent capacity of chloroplasts to produce polycistronic mRNA's in recombinant protein studies. A favoured application of this approach has been to try and introduce novel metabolic pathways to enable the synthesis of a particular product of metabolic or commercial interest. For example to synthesize the biodegradable polyester polyhydroxybutyrate (PHB) in tobacco chloroplasts, a polycistron encoding the enzymes phbC, phbA and phbB was successfully introduced into the plastome (Nakashita et al., 2001). Similarly, expression of the insecticide *Bacillus thuringiensis* (*Bt*) in *Btcry*2Aa2 as a three-gene operon in tobacco resulted in the production of high levels of *Bt* toxin and accompanying chaperones (de Cosa et al., 2001). With regard to recombinant Rubisco engineering, the use of the IEE element was used in the synthetic polycistronic mRNA driving expression of *Synechococcus* PCC7942 L-subunit, S-subunit and CcmM35/RbcX synthesis in tobacco leaves (Lin et al., 2014; see also Figure 5.1). Unfortunately, quantitative analyses of the mRNA levels of the cyanobacteria transgenes in the Se7942 tobacco genotypes was not examined (Table 5.1) making it difficult to meaningfully gauge the effectiveness of incorporating the IEE sequences.

6.1.5 Research Objective – testing alternative transgene structures to modulate hybrid Rubisco synthesis in $^{cm}trL^{RNAi\text{-}S}$

Difficulties in engineering Rubisco S-subunits *in planta* have thus limited the feasibility of studying S-subunit interactions with chaperones and elements upon entry into the chloroplast stroma, and as to the dependency of these interactions for assembly with L-subunits into L_8S_8 holoenzyme. Furthermore, the inability to produce plant or algae L_8S_8 Rubisco in *E. coli* (Nishimura et al., 2008; Parry et al., 2013) or efficiently manipulate the S-subunit in leaf chloroplasts (see Section 4.1.4) has impaired meaningful study on the structural complementarity between plant Rubisco L- and S-subunits and its consequences to Rubisco catalysis. In a bid to begin addressing the former issue, this chapter describes utilisation of a unified chloroplast transforming plasmid design to introduce into the plastome of $^{cm}trL^{RNAi\text{-}S}$ with varying combinations of tobacco and sunflower L- and S-subunits. Rubisco production and catalysis in the resulting four transplastomic genotypes is examined and the corresponding effects on leaf photosynthesis, plant growth and phenotype tested. The outcomes are examined in the context of better understanding the constraints to Rubisco biogenesis when using

chloroplast made S-subunits and the extent to which L_8S_8 assembly and catalysis is influenced by the supply of cognate versus heterologous S-subunits.

6.2 Results

6.2.1 Laying the experimental foundation with tobacco and sunflower Rubisco

An extensive amount of work has already been undertaken with transplastomic modification of sunflower L-subunits in tobacco leaves with suggestions that structural incompatibilities between tobacco S-subunits (^{t}S) and sunflower L-subunits (^{s}L) may limit hybrid $(^{s}L)_8(^{t}S)_8$ Rubisco biogenesis (Kanevski et al., 1999; Sharwood et al., 2008; Sharwood and Whitney, 2010) (see also Section 6.1.2). With this in mind, a second generation of plastome-transformed $^{cm}trL^{RNAi\text{-}S}$ genotypes were made that focused on engineering tobacco ($^{T}L_8{}^{T}S_8$) Rubisco, sunflower Rubisco ($^{S}L_8{}^{S}S_8$) and two hybrid variants – $(^{S}L)_8(^{T}S)_8$ and $(^{T}L)_8(^{S}S)_8$ in $^{cm}trL^{RNAi\text{-}S}$ chloroplasts. This was deemed a versatile way to test the inter-subunit compatibility requirement of Form I Rubisco. As shown in Figure 6.2, a comparison of tobacco and sunflower Rubisco show their L-subunits share 94% identity while the S-subunits tested in this study were 77% identical.

6.2.2 Modifying the codon use of the plastome-transformed ^{Tob}RbcS and ^{Sun}RbcS

A new ^{Tob}*RbcS* was synthesized for this study (called ^{Tob}*RbcS**) whose codon use was modified to match tobacco *rbcL* (Table 6.1). As a result of the altered codon use the ^{Tob}*RbcS** shared only 70% and 81% identity with the ^{WT}*RbcS* and original synthetic ^{Tob}*RbcS* respectively (Figure 6.3). Where possible the nucleotide sequence of a synthetic ^{Sun}*RbcS* was designed to match the ^{Tob}*RbcS** mRNA. As indicated for the LEVL-S^{H6} constructs examined in Chapter 5, the objective of maintaining maximum sequence identity between the ^{Sun}*RbcS* and ^{Tob}*RbcS** was to minimise potential variations in their translational potential and their mRNA stability. The efforts to keep the nucleotide sequences of the ^{Sun}*RbcS* and ^{Tob}*RbcS** as similar as possible resulted in them sharing 84% identity (Figure 6.3B). The codon use of both these synthetic genes closely matched that of both the tobacco and sunflower *rbcL* (Table 6.1).

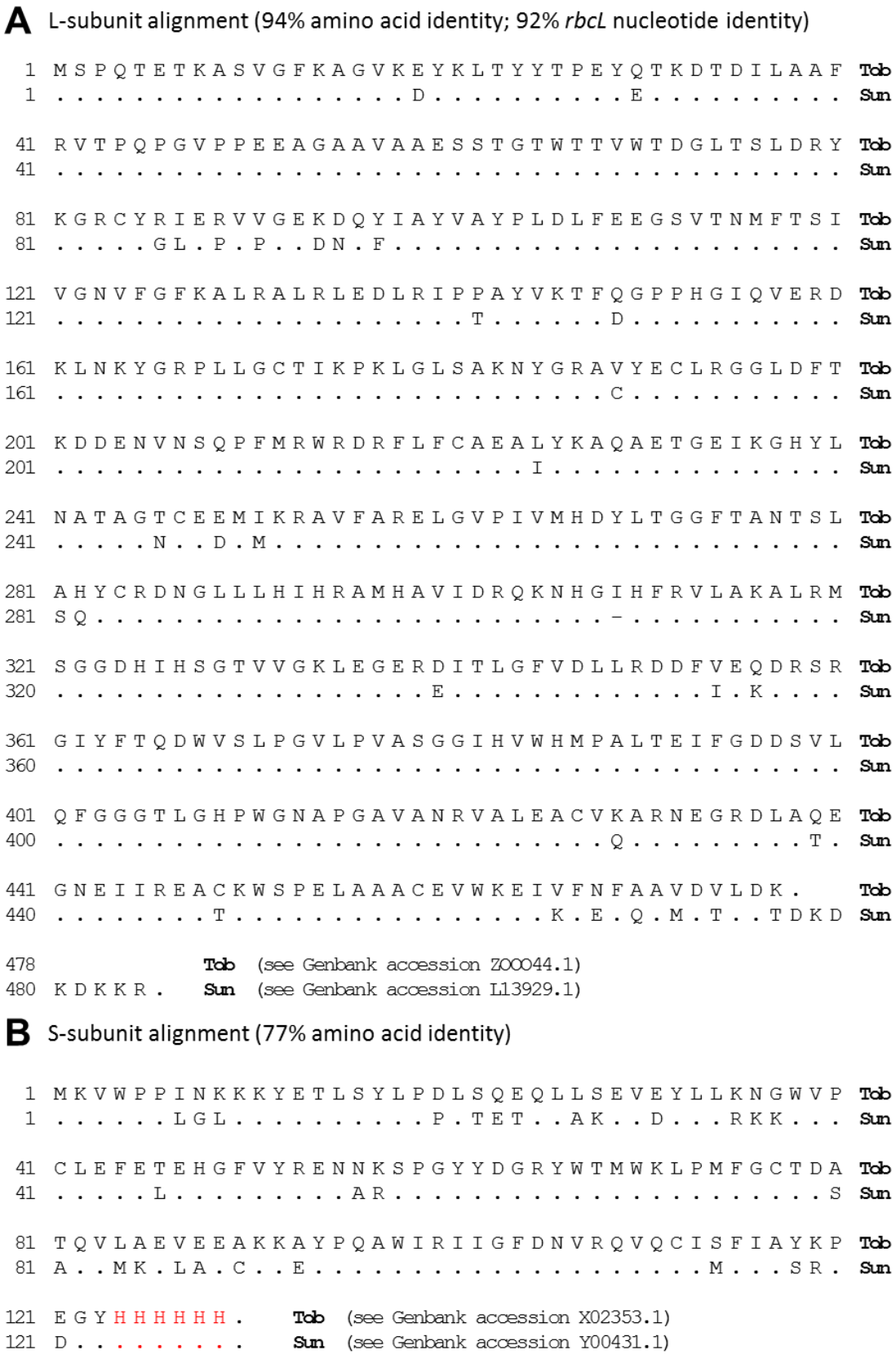

Figure 6.2 Alignment of the sunflower and tobacco Rubisco subunits.

Alignment of the tobacco and sunflower Rubisco (A) L-subunits and the (B) S-subunit isoforms transplanted into the plastome of ^{cm}trL^{RNAi-S}. The sequence identity calculations exclude the S-subunit C-terminal hexa-histidine sequence (shown in red).

Table 6.1 Comparative codon use of the native tobacco and sunflower *rbcL* and synthetic ^{Tob}*RbcS and ^{Sun}*RbcS*.**
Highlighted in pink are the preferred codons used in each.

Amino acid	codon	^{Tob}*rbcL*		^{Sun}*rbcL*		^{Tob}*RbcS**		^{Sun}*RbcS*	
		No.	%	No.	%	No.	%	No.	%
Ala (A)	GCA	13	2.7	11	2.3	2	1.6	2	1.6
	GCC	5	1.0	4	0.8	1	0.8	1	0.8
	GCG	4	0.8	4	0.8	0	0.0	0	0.0
	GCU	23	4.8	21	4.3	3	2.4	3	2.4
Arg (R)	AGA	7	1.5	8	1.6	1	0.8	2	1.6
	AGG	0	0.0	1	0.2	0	0.0	0	0.0
	CGA	6	1.3	5	1.0	1	0.8	1	0.8
	CGC	5	1.0	3	0.6	0	0.0	0	0.0
	CGG	1	0.2	0	0.0	0	0.0	0	0.0
	CGU	11	2.3	12	2.5	2	1.6	4	3.2
Asn (N)	AAC	6	1.3	6	1.2	2	1.6	1	0.8
	AAU	9	1.9	10	2.1	3	2.4	1	0.8
Asp (D)	GAC	4	0.8	6	1.2	1	0.8	1	0.8
	GAU	23	4.8	26	5.3	3	2.4	4	3.2
Cysl	UGC	4	0.8	3	0.6	1	0.8	2	1.6
	UGU	5	1.0	6	1.2	2	1.6	2	1.6
Gln (Q)	CAA	9	1.9	8	1.6	5	4.0	5	4.0
	CAG	4	0.8	4	0.8	2	1.6	1	0.8
Glu (E)	GAA	24	5.0	25	5.1	9	7.2	7	5.6
	GAG	8	1.7	9	1.9	3	2.4	3	2.4
Gly (G)	GGA	13	2.7	12	2.5	2	1.6	2	1.6
	GGC	2	0.4	3	0.6	0	0.0	0	0.0
	GGG	8	1.7	8	1.6	1	0.8	1	0.8
	GGU	23	4.8	22	4.5	4	3.2	4	3.2
His (H)	CAC	5	1.0	7	1.4	0	0.0	0	0.0
	CAU	9	1.9	7	1.4	1	0.8	1	0.8
Ile (I)	AUA	2	0.4	0	0.0	1	0.8	0	0.0
	AUC	10	2.1	10	2.1	3	2.4	3	2.4
	AUU	9	1.9	9	1.9	2	1.6	2	1.6
Lys (K)	AAA	21	4.4	21	4.3	8	6.4	7	5.6
	AAG	4	0.8	7	1.4	1	0.8	2	1.6
Leu (L)	CUA	6	1.3	9	1.9	1	0.8	3	2.4
	CUC	0	0.0	0	0.0	0	0.0	0	0.0
	CUG	6	1.3	5	1.0	1	0.8	1	0.8
	CUU	10	2.1	11	2.3	3	2.4	3	2.4
	UUA	9	1.9	6	1.2	3	2.4	2	1.6
	UUG	10	2.1	11	2.3	2	1.6	3	2.4
Met(M)	AUG	8	1.7	11	2.3	3	2.4	5	4.0
Phe (F)	UUC	9	1.9	9	1.9	2	1.6	2	1.6
	UUU	12	2.5	13	2.7	3	2.4	3	2.4
Pro (P)	CCA	5	1.0	4	0.8	2	1.6	2	1.6
	CCC	2	0.4	1	0.2	1	0.8	1	0.8
	CCG	3	0.6	4	0.8	1	0.8	1	0.8
	CCU	11	2.3	14	2.9	5	4.0	6	4.8
Ser (S)	AGC	3	0.6	3	0.6	1	0.8	1	0.8
	AGU	2	0.4	3	0.6	0	0.0	0	0.0
	UCA	3	0.6	1	0.2	2	1.6	1	0.8
	UCC	2	0.4	6	1.2	0	0.0	0	0.0
	UCG	0	0.0	1	0.2	0	0.0	0	0.0
	UCU	7	1.5	5	1.0	3	2.4	2	1.6
Term	UAA	1	0.2	1	0.2	1	0.8	1	0.8
Thr (T)	ACA	5	1.0	5	1.0	1	0.8	0	0.0
	ACC	8	1.7	6	1.2	1	0.8	1	0.8
	ACG	1	0.2	2	0.4	0	0.0	0	0.0
	ACU	15	3.1	19	3.9	4	3.2	5	4.0
Trp(W)	UGG	8	1.7	8	1.6	5	4.0	5	4.0
Tyr (Y)	UAC	8	1.7	5	1.0	4	3.2	4	3.2
	UAU	10	2.1	12	2.5	6	4.8	5	4.0
Val (V)	GUA	17	3.6	17	3.5	3	2.4	3	2.4
	GUC	1	0.2	3	0.6	0	0.0	0	0.0
	GUG	3	0.6	1	0.2	0	0.0	0	0.0
	GUU	16	3.3	12	2.5	4	3.2	3	2.4

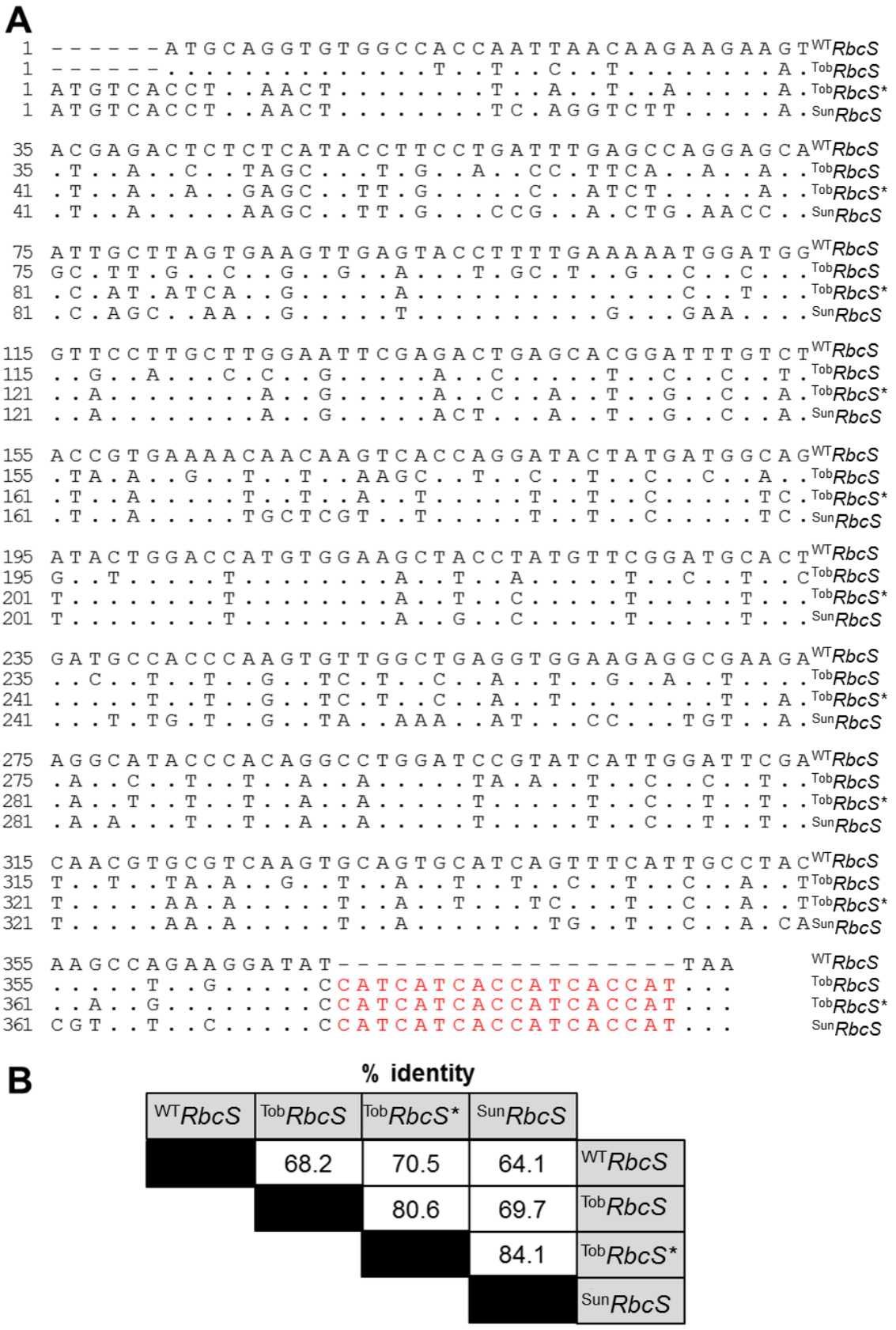

Figure 6.3 Sequence comparison of the *RbcS* transgenes transformed into the tobacco plastome.

(see next page for figure legend)

Figure 6.3 Sequence comparison of the *RbcS* transgenes transformed into the tobacco plastome.

(figure on prior page)
(A) Alignment of the mature S-subunit coding sequence (aligned in Figure 6.2B) for a wild-type *N. tabacum RbcS* (^{WT}*RbcS*, same as alleles *Nt*S1a/b, Figure 3.5) and the synthetic *RbcS* in pLEVL-TobS^{H6} (^{Tob}*RbcS*, Figure 5.5A) and in pLEV^{T}L^{T}S and pLEV^{S}L^{T}S (^{Tob}*RbcS**, Figure 6.4B). ^{Sun}*RbcS*, synthetic gene coding for the sunflower S-subunit sequence in Figure 6.2B. Sequences were aligned using MegALIGN. Dots represent residues identical to ^{WT}*RbcS*. Dashes indicate gaps introduced to maximise the alignment. (B) Percentage sequence identity between the different *RbcS*' (excluding the C-terminal 6×His-tag sequence highlighted in red).

6.2.3 Modifying the translation initiation sequence of ^{Tob}RbcS and ^{Sun}RbcS in the intergenic region

As discussed in Section 5.3.2.1, problems with S-subunit synthesis in the LEVL-S^{H6} lines may have stemmed from complications with translation initiation as a consequence of impediments to ribosome binding. To test the importance of this relationship, new synthetic transforming plasmids were made that replicated part of the *rbcL* 5'UTR sequence in the *rbcL-RbcS* intergenic sequence (IS) upstream of the AUG codons for the synthetic ^{Tob}*RbcS* and ^{Sun}*RbcS* transgenes (Figure 6.4). The replicated sequence spanned nucleotides -12 to -1 of the *rbcL* 5'UTR (which included the SD sequence GGAG at -7 to -10) (Figure 6.4A). Also replicated were the *rbcL* AUG Met-1, UCA Ser-2, CCA Pro-3, CAA Gln-4 and ACT Thr-5 codons. These were appended to the N-terminus of the ^{Tob}*RbcS* and ^{Sun}*RbcS* transgenes to replace sequences coding their natural MQV and MKV N-termini, respectively. The appended L-subunit N-terminal sequence was included based on prior observations that TCR of the *rbcL* mRNA is dependent on sequence within the 5'UTR and adjoining coding sequence (Kuroda and Maliga, 2001a), and that single changes to the nucleotide sequence in this region can perturb L-subunit translation initiation (Orr, 2013). An additional potential benefit to S-subunit synthesis was the proposed role of this N-terminal sequence in facilitating protection from proteolysis following its co-translational removal of Met-1, Ser-2 and acetylation of Pro-3 (Houtz et al., 1989) (Figure 4.2; see also Section 4.1.3).

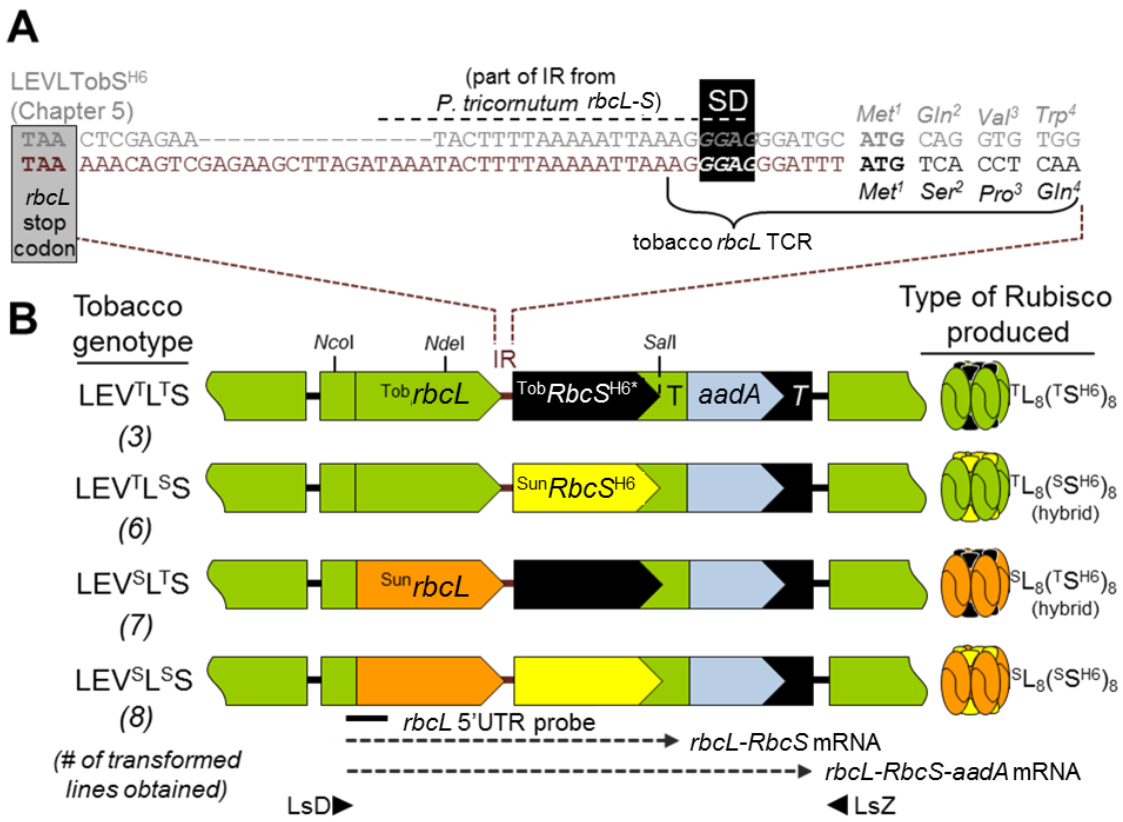

Figure 6.4 Design and detail of the plastome transforming plasmids.

(A) Comparative sequence of the intergenic-sequence (IS) in the LEVL-TobS^{H6} genotype (Chapter 5, shown in grey) and that used in (B) the transforming plasmids studied in this chapter. Each transforming plasmid contains flanking plastome sequence (see Figure 5.5A for detail) to facilitate homologous recombination integration of the transgenes into the ^{cm}trL$^{RNAi\text{-}S}$ plastome. The transgenes included the *aadA* selectable marker and either the tobacco or sunflower *rbcL* genes (^{Tob}*rbcL* in green, ^{Sun}*rbcL* in orange) and the synthetic ^{Tob}*RbcS** (black) or ^{Sun}*RbcS* (yellow) genes (Figure 6.3). The number of independent lines obtained for each genotype and the corresponding subunit stoichiometry of their L_8S_8 Rubisco are shown. Expression of all three transgenes was regulated by the *rbcL* promoter/5'UTR sequence (P). The 5' end of each *RbcS* shares sequence spanning the TCR of ^{tob}*rbcL*. T, tobacco *rbcL* terminator [3'UTR]; *T*, *rps16* 3'UTR. The *rbcL* 5'UTR probe region spans 220 bp of 5'UTR and 42 nt of *rbcL* coding sequence that was shared by all four genotypes and therefore equally recognises the two chloroplast *rbcL* mRNA species indicated (dashed arrows). Positioning of primers LsD and LsZ and the unique cloning restriction sites *Nco*I, *Nde*I and *Sal*I are shown.

6.2.4 Transforming the RbcS into the ^{cm}trL$^{RNAi\text{-}S}$ plastome as an rbcL-rbcS operon

Included at the 3' end of each *RbcS* was the nucleotide sequence CAT CAT CAC CAT CAC CAT coding a C-terminal hexa-histidine (H6) tag for each S-subunit. Each synthetic gene construct also share an identical 52 bp of intergenic sequence (Figure 6.4). The intergenic sequence (IS) separating the *rbcL* and *RbcS* again incorporated part of the native *P. tricornutum rbcL-S* IS sequence and 12 nt of the *rbcL* 5'UTR (Figure 6.4A, see also Section 6.2.3). A *Sal*I site was introduced adjacent to the TAA stop codon of the synthetic ^{Sun}*rbcS* and ^{Tob}*rbcS**. To make the pLEV^{T}L^{T}S and pLEV^{T}L^{S}S transforming plasmids the 1317 bp *Nco*I-*Nde*I fragment from pLEV4 spanning part of the tobacco *rbcL* and 5'UTR sequence was first cloned into the respective pUC57-

^{Sun}*rbcS* or pUC57- ^{Tob}*rbcS** plasmids (made by GenScript that contained the *rbcL* sequence downstream of the *Nde*I site and the appropriate IS sequence) before cloning the 2046 bp *Nco*I-*Sal*I ^{Tob}*rbcL*-^{Tob}*RbcS** or ^{Tob}*rbcL*-^{Sun}*RbcS* back into pLEV4 (Whitney et al., 2011b) (Figure 6.4B). Similarly the pLEV^{S}L^{T}S and pLEV^{S}L^{S}S transforming plasmids were made using the 1317 bp *Nco*I-*Nde*I fragment from the transforming plasmid used to make the t^{Rst}LA tobacco genotype (Sharwood et al., 2008) (Figure 6.1A). This fragment spanned part of the tobacco 5'UTR and sunflower *rbcL* and was ligated into the appropriate pUC57-*RbcS* plasmids before cloning the 2070 bp *Nco*I-*Sal*I ^{Sun}*rbcL*-^{Tob}*RbcS** or ^{Sun}*rbcL*-^{Sun}*RbcS* back into pLEV4.

The transforming plasmids were each introduced by biolistic bombardment into five sterile leaf sections from tissue culture grown ^{cm}trL^{RNAi-S} plants. ndPAGE of soluble leaf protein from spectinomycin resistant plantlets was used to identify the plastome-transformed lines where the *rbcL-S-aadA* transgenes had replaced *rbcM* by homologous recombination (Figure 6.5; for an overview of the transformation and screening process see Figure 5.6). The presence of L_8S_8 or the lack of L_2 is used as an indication of a successful transformation event. Not all L_8S_8 are detected at 520 kD (Lane 7, LEV^{T}L^{S}S#2 and Lane 14, LEV^{S}L^{S}S#1) and some bands such as those found in Lane 1, ^{cm}trL$^{S\text{-}RNAi}$, remain unidentified as an artefact from the ^{cm}trL genotype (data not shown) (Figure 6.5).

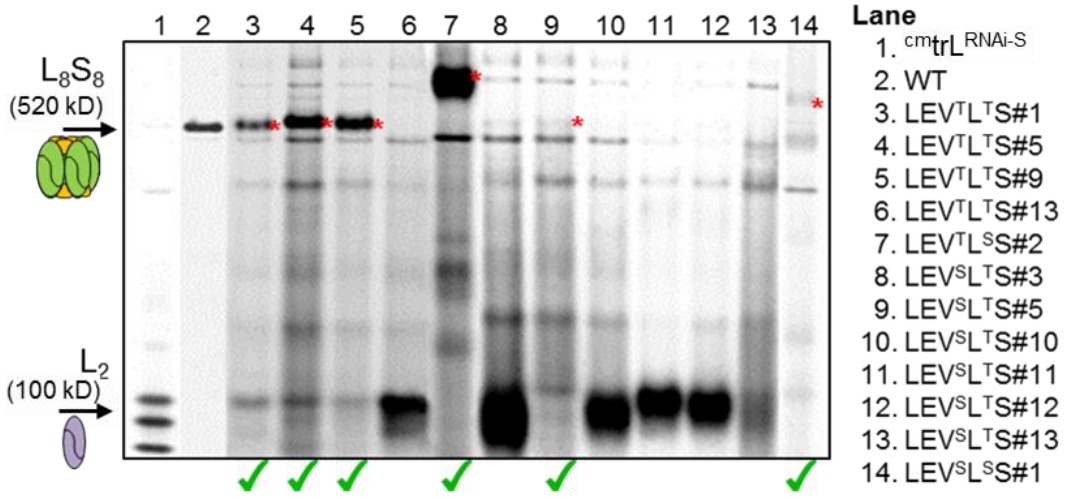

Figure 6.5 ndPAGE screening for the transplastomic lines.

Soluble leaf protein from spectinomycin resistant plantlets were separated by ndPAGE and the correctly transformed lines (green ticks) identified as those making recombinant L_8S_8 Rubisco (red asterix) and less/no *R. rubrum* L_2 Rubisco.

Similar to the LEVL-S^{H6} genotypes made in Chapter 5, the three transgenes (*rbcL*, *RbcS* and *aadA*) that were transformed into the resulting $LEV^{T}L^{T}S$, $LEV^{T}L^{S}S$, $LEV^{S}L^{T}S$ and $LEV^{S}L^{S}S$ genotypes were all controlled by the native tobacco *rbcL* promoter, 5'UTR and 3'UTR regulatory elements (Figure 5.5A). Three to eight independently transformed lines were obtained for each genotype (Figure 6.4B).

6.2.5 Growth, maintenance and resulting phenotype the different tobacco genotypes

After 2-4 rounds of further selection on $RMOP^{spec}$ the transformed region of the plastome was PCR amplified (using primers LsD and LsZ, Figure 6.4) from three lines of each genotype and fully sequenced to confirm each independently transformed line was genetically identical (data not shown). At least three T_0 lines for each genotype were transferred from $RMOP^{spec}$ regeneration medium into tissue culture pots containing MS medium (with 3% [w/v] sucrose and 500 mg L^{-1} spectinomycin) to stimulate normal root and shoot development. After five weeks growing at 25°C under 2% (v/v) CO_2 and ~40 µmol photons m^2 s^{-1} illumination, the phenotype of the $LEV^{T}L^{T}S$ and $LEV^{T}L^{S}S$ genotypes resembled wild-type. In contrast, the sunflower L-subunit producing $LEV^{S}L^{T}S$ and $LEV^{S}L^{S}S$ lines struggled to grow despite sucrose supplement in MS medium (Figure 6.6). These lines shared a pale green phenotype, had fragile, thin leaves and grew very slowly – even more impaired than that observed previously for the tob^{Rst}, $t^{Rst}LA$ and $t^{Rst}L7$ genotypes grown in tissue culture (Whitney and Sharwood, 2008; Sharwood and Whitney, 2010).

After developing suitable root mass in tissue culture, the plants were transferred into soil to grow to maturity in air containing 2% (v/v) CO_2. In soil, the $LEV^{T}L^{T}S$ and $LEV^{T}L^{S}S$ lines maintained their wild-type like phenotype and were able to produce normal flowers that were pollinated with wild-type pollen. The resulting seeds were collected for further study of the T_1 progeny. Despite repeated attempts the $LEV^{S}L^{T}S$ and $LEV^{S}L^{S}S$ lines were however unable to grow in soil under elevated CO_2. This restricted subsequent studies of their leaf biochemistry to material from T_0 plants grown after several rounds of selection and regeneration in RMOP-spec medium.

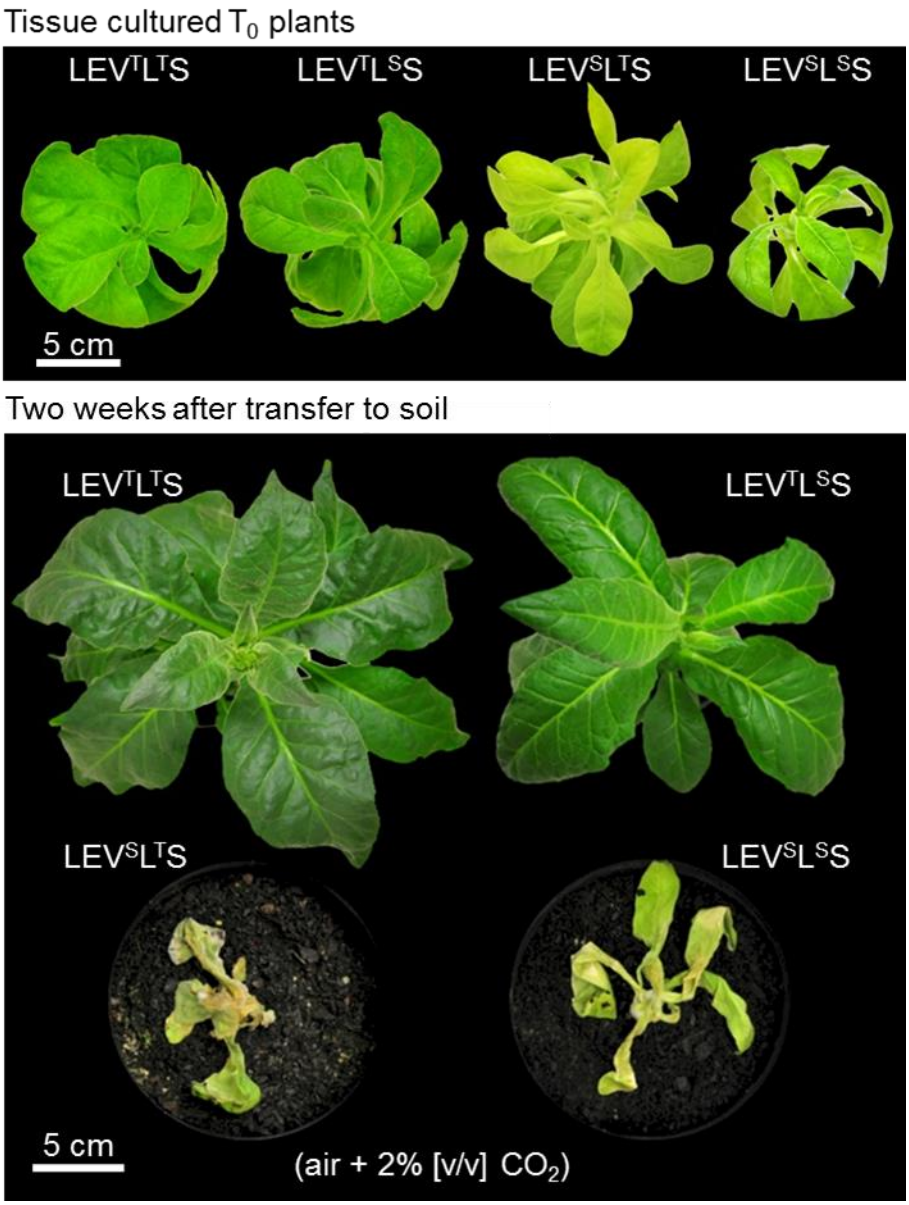

Figure 6.6 Comparative growth phenotypes of the transplastomic genotypes.

All the T_0 genotypes were able to produce roots and survive on MS medium (with 3% [w/v] sucrose). The sunflower L-subunit producing LEV^{S}L^{T}S and LEV^{S}L^{S}S genotypes shared a distinctly unhealthy pale green phenotype. Once plantlets had developed adequate root mass the plants were transferred to two litre pots of soil and maintained at 25℃, ~100-200 µmol photons m^2 s^{-1} illumination and air enriched with 2% (v/v) CO_2. After 2 weeks growth the phenotype of the tobacco L-subunit producing LEV^{T}L^{T}S and LEV^{T}L^{S}S genotypes resembled wild-type, while the LEV^{S}L^{T}S and LEV^{S}L^{S}S plants showed the onset of severe necrosis and full mortality after 3 weeks.

6.2.6 Recombinant L_8S_8 Rubisco production was dependent on the L-subunit source

Analyses of Rubisco content in three independently obtained lines for each genotype were undertaken. The T_1 LEV^TL^TS and LEV^TL^SS progeny were grown in a growth cabinet (25°C under ambient CO_2 and 400 ± 100 μmol photons m^2 s^{-1} illumination, 14:10h L:D cycle) and at 35 cm in height leaf #5 from the apical meristem (*i.e.* the youngest near fully expanded leaf) was sampled for protein analyses. Leaf samples from the LEV^SL^TS and LEV^SL^SS lines were obtained from T_0 tissue culture plants growing in MS containing 3% (w/v) sucrose. Analysis of the soluble leaf protein by ndPAGE showed abundant levels of Rubisco were produced in the LEV^TL^TS and LEV^TL^SS genotypes and very little in the sunflower L-subunit (^SL) producing LEV^SL^TS and LEV^SL^SS lines (Figure 6.7A). The identities of the Rubisco complexes were confirmed by immunoblot analysis using antibodies to tobacco Rubisco and a penta-histidine antigen. Only the Rubisco in the transplastomic lines reacted with the latter antibody, confirming they incorporated the chloroplast made recombinant sunflower ($^SS^{H6}$) or tobacco ($^TS^{H6}$) S-subunits.

A comparison of the separation rates through ndPAGE for the different Rubisco isoforms showed those incorporating the sunflower $^SS^{H6}$-subunits migrated substantially slower. In contrast, the $^TL_8(^TS^{H6})_8$ and $^SL_8(^TS^{H6})_8$ complexes produced in the LEV^TL^TS and LEV^SL^TS genotypes separated at the same rate as wild-type tobacco Rubisco. This suggests the sunflower $^SS^{H6}$-subunits impart differences in the quaternary packing when assembled with either the tobacco L-subunits (^TL) or sunflower L-subunits (^SL). In all the lines analysed, no *R. rubrum* L_2 Rubisco was detectable by ndPAGE confirming their homoplasmicity (Figure 6.7A).

The Rubisco levels in each genotype were quantified by [^{14}C]-CABP binding analyses (Figure 6.7B). Relative to the Rubisco content in control wild-type (WT) tobacco leaves, the Rubisco levels in LEV^TL^TS and LEV^TL^SS was reduced approximately 40% and 70% respectively. In contrast the Rubisco content in LEV^SL^TS and LEV^SL^SS leaves were reduced by more than 96% resembling those produced in the LEVL-S^{H6} progeny (*i.e.* <1 μmol active sites m^2, Figure 5.8B).

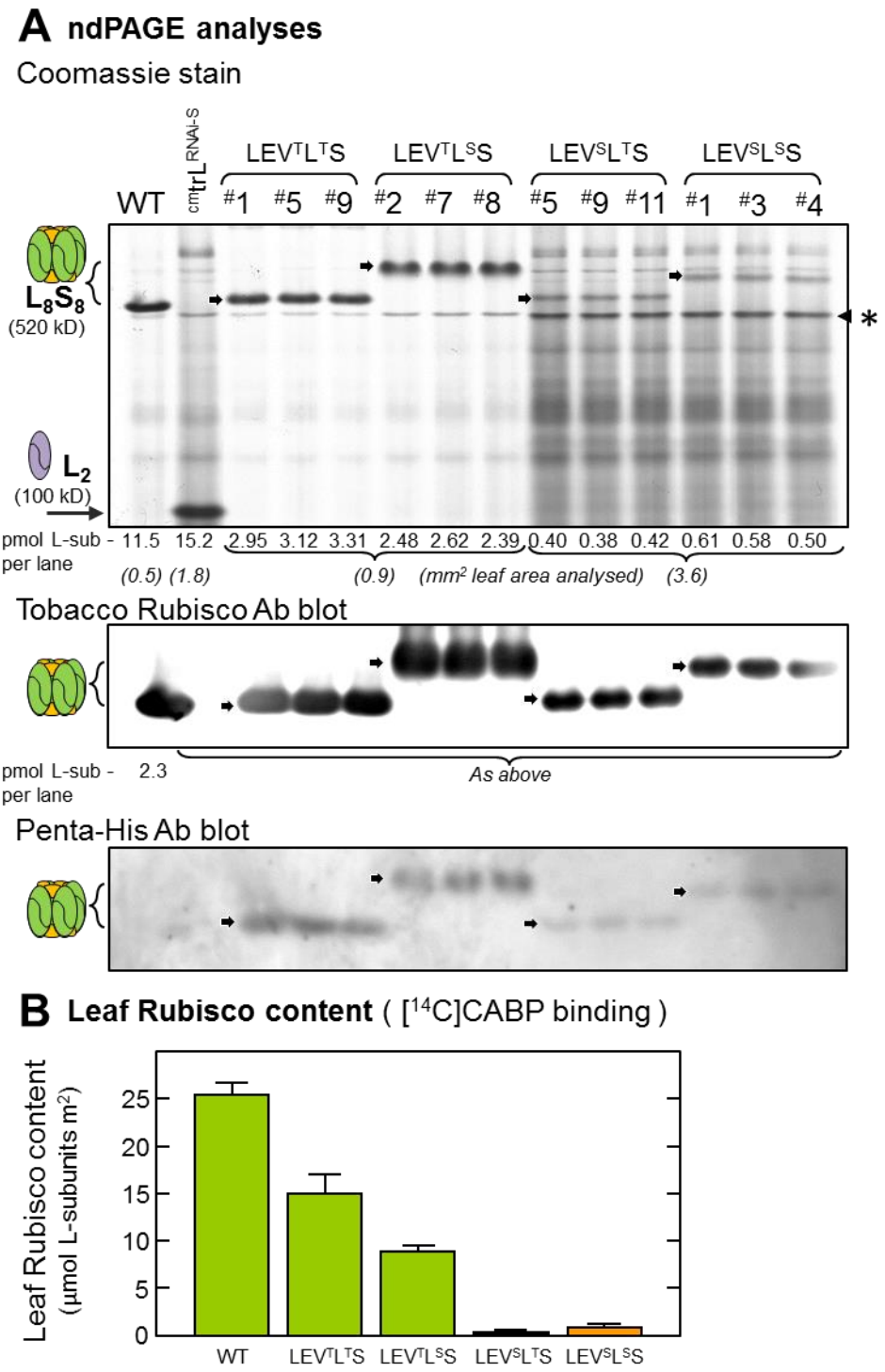

Figure 6.7 ndPAGE analysis and CABP quantification of Rubisco content.

The leaf soluble protein from tissue culture grown LEV^{S}L^{T}S and LEV^{S}L^{S}S plants and in the young mature leaves (leaf #5) of 35 cm tall tobacco (WT), ^{cm}trL$^{RNAi\text{-}S}$, LEV^{T}L^{T}S and LEV^{T}L^{S}S plants grown in soil in air with 1% (v/v) CO_2 were compared by (A) ndPAGE and the Rubisco content quantified by (B) [^{14}C]-CABP binding. (*) non-Rubisco protein. The area of leaf protein separated in each PAGE analysis is shown. M, protein marker (sizes shown); L, L-subunits; S^{H6}, C-terminal 6×His-tagged chloroplast made S-subunits; S, endogenous cytosol made tobacco S-subunits.

SDS-PAGE analysis of the leaf protein confirmed the differential levels of Rubisco produced in each genotype (Figure 6.8). Coomassie-stained gels and immunoblot analysis with an antibody to tobacco Rubisco did not detect cytosolic made tobacco S-subunits in any of the transplastomic lines (Figure 6.8A and B respectively). This is consistent with the continued efficiency of the S-subunit silencing phenotype of the parental $^{cm}trL^{RNAi\text{-}S}$ genotype (Chapters 3, 4 and 5). The tobacco Rubisco antibody successfully detected the production of L-subunits in each line and the chloroplast made $^{Tob}S^{H6}$-subunits in the $LEV^{T}L^{T}S$ and $LEV^{S}L^{T}S$ lines. The antibody however only poorly cross-reacted with the chloroplast made sunflower $^{S}S^{H6}$-subunits produced in the $LEV^{T}L^{S}S$ and $LEV^{S}L^{S}S$ genotypes. The production of $^{S}S^{H6}$-subunits was however confirmed using penta-histidine antibody (Figure 6.8C). The relative intensities of the antibody hybridisation signals correlated with the varying levels of Rubisco made in each genotype.

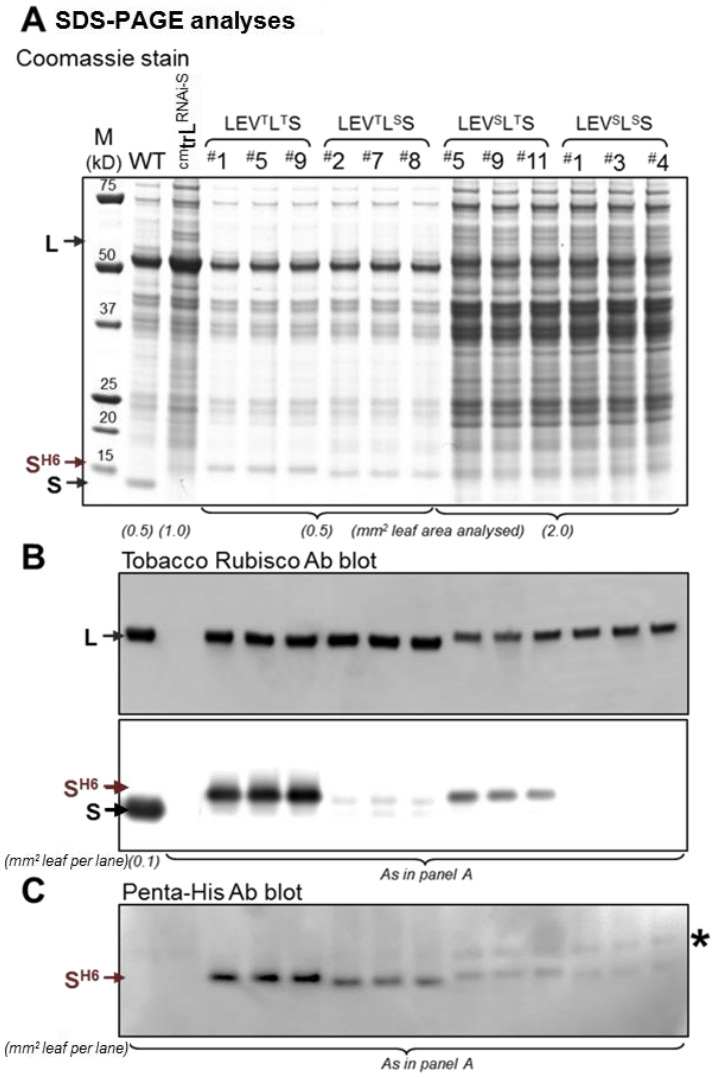

Figure 6.8 SDS-PAGE analysis of Rubisco subunit composition.

(see next page for figure legend)

Figure 6.8 SDS-PAGE analysis of Rubisco subunit composition.

(figure on prior page)
The leaf soluble protein from Figure 6.7 was analysed by SDS-PAGE and (A) Coomassie-stained or immunoblotted against antibodies to (B) tobacco Rubisco or (C) a penta-histidine epitope (Qiagen). The area of leaf protein separated in each PAGE analysis is shown. M, protein marker (sizes shown); L, L-subunits; S^{H6}, C-terminal 6×His-tagged chloroplast made tobacco or sunflower S-subunits; S, endogenous cytosol made tobacco S-subunits. Asterix (*) indicates a protein in tobacco leaves at ~16.5 kDa that cross-reacts with the penta-histidine antibody.

6.2.7 Post-transcriptional limitations to Rubisco biogenesis in LEV^{S}L^{T}S and LEV^{S}L^{S}S

After transferral to nylon membrane the RNA was probed with the [^{32}P]-labelled *rbcL* 5'UTR probe that hybridises to the 5' sequence conserved in both the ^{Tob}*rbcL* and ^{Sun}*rbcL* mRNA (Figure 6.4B). Each transplastomic genotype produced two *rbcL* mRNA species; a prominent *rbcL-rbcS* (dicistronic) operon and a ~50% less abundant *rbcL-rbcS-aadA* (tricistronic) mRNA. The latter transcript is produced as a consequence of inefficient termination by the *rbcL* 3'UTR located between *RbcS* and *aadA* (Whitney and Sharwood, 2008).

Analysis of levels of both endogenous chloroplast *rbcL* mRNA (Figure 6.9B) and nuclear *RbcS* mRNAs (Figure 6.9C) in the tissue culture grown wild-type showed reduction by ~10% relative to that in the high-CO_2 sample. In contrast no *RbcS* mRNAs were detected in any of the transplastomic lines, consistent with the efficiency of the RNAi-targeted silencing of these transcripts in the maternal ^{cm}trL$^{RNAi\text{-}S}$ genotype (Chapter 3). The same probe did not hybridise with the abundant chloroplast made *rbcL-RbcS* transcripts comprising either the ^{tob}*RbcS** or ^{sun}*RbcS* due to their <70% sequence identity with ^{WT}*RbcS* (Figure 6.3).

The total pool of *rbcL-RbcS* transcripts in the LEV^{T}L^{T}S and LEV^{T}L^{S}S lines were both reduced by around one-third relative to the *rbcL* mRNA levels in WT. This implies that limitations in transcript abundance likely contribute to the ~40% and ~70% lower levels of Rubisco made, respectively, in the LEV^{T}L^{T}S and LEV^{T}L^{S}S genotypes (Figure 6.7B). In contrast the ^{Sun}*rbcL-RbcS* mRNA levels in the LEV^{S}L^{T}S and LEV^{S}L^{S}S genotypes were, respectively, ~80% and ~90% lower than the *rbcL* transcript content in WT (Figure 6.9B). While these mRNA levels are low, they do not match the more than 25-fold lower levels of Rubisco produced in these genotypes (Figure 6.7B). This implies that further limitations during the post-transcriptional processing of the ^{Sun}*rbcL* mRNA are impeding L_8S_8 biogenesis in the LEV^{S}L^{T}S and LEV^{S}L^{S}S genotypes.

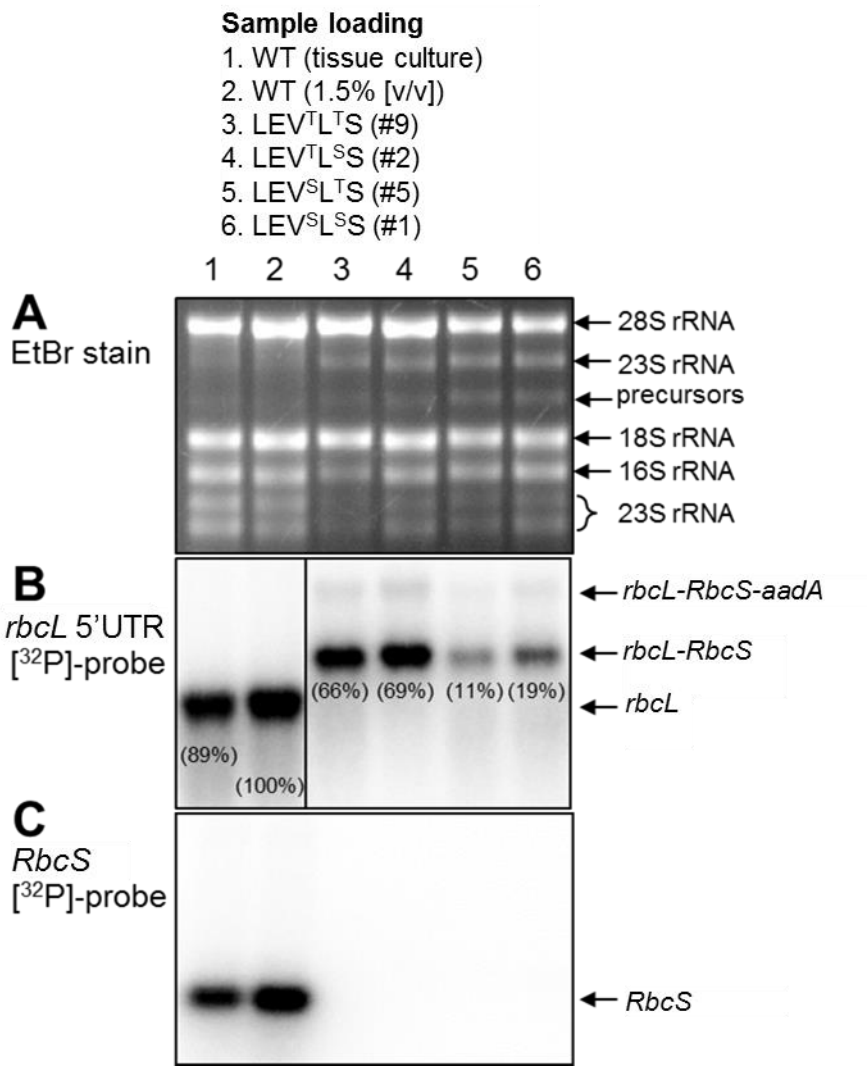

Figure 6.9 RNA blot analyses.

Rubisco mRNA in total RNA (2 µg) from the same leaves of each tobacco genotype analysed in Figure 6.7 were separated under denaturing conditions. The RNA was (A) visualised by ethidium bromide (EtBr) staining and then blotted onto nylon membrane and hybridized with either the (B) [^{32}P]-*rbcL* 5'UTR probe (Figure 6.4B) or (C) a [^{32}P]-*RbcS* probe (Figure 5.5B). The native cytosolic ^{nuc}*RbcS* mRNA was only detected in wild-type tobacco (WT). Two chloroplast *rbcL* transcripts *rbcL-RbcS* and *rbcL-RbcS-aadA* were detected in each transplastomic genotype (see Figure 6.4B for map) and the native *rbcL* mRNA in WT. The ^{cm}*rbcM* in ^{cm}trL^{RNAi-S} shares the sequence comprised in the *rbcL* 5'UTR probe. The relative amount of each Rubisco mRNA relative to the *rbcL* steady state pool in WT are shown in parentheses.

6.2.8 Tobacco Rubisco containing tobacco or sunflower S^{H6}-subunits are catalytically identical

The higher levels of Rubisco produced in the leaves of the LEV^{T}L^{T}S and LEV^{T}L^{S}S enabled assaying of carboxylation turnover rate (k_C^{cat}) and K_m for CO_2 under ambient O_2 levels ($K_C^{21\%O2}$) using rapidly extracted soluble leaf protein. This approach mirrors that used by Sharwood et al. (2008) which proved highly accurate in measuring these parameters relative to the slower, error-prone methods using protein purification steps. Measurements of CO_2/O_2 specificity ($S_{C/O}$) (Kane et al., 1994) however necessitates

purified Rubisco which was undertaken by IMAC (Section 2.2.4) prior to desalting the Ni-NTA purified protein by gel filtration (Sharwood et al., 2008).

As shown in Table 6.2, the measured k_C^{cat} and $S_{C/O}$ values for both the ${}^{T}L_8({}^{T}S^{H6})_8$ and hybrid ${}^{T}L_8({}^{S}S^{H6})_8$ enzymes match those measured for the $L_8(S^{H7})_8$ produced in the RVtpSSuH♀ × ${}^{cm}trL^{RNAi\text{-}S}$♂ progeny (2.1 ± 0.3 s^{-1}, Table 4.2). In contrast the comparable $K_C^{21\%O2}$ values for the ${}^{T}L_8({}^{T}S^{H6})_8$ and hybrid ${}^{T}L_8({}^{S}S^{H6})_8$ Rubisco isoforms were ~70% higher than that measured for the $L_8(S^{H7})_8$ enzyme made in RVtpSSuH♀ × ${}^{cm}trL^{RNAi\text{-}S}$♂ (11.9 ± 2.3 μM, Table 4.2). This variation may stem from differences in the length of their C-terminal polyhistidine tags or/and the N-terminal sequence of the tobacco S-subunits in the ${}^{T}L_8({}^{T}S^{H6})_8$ (MSPQWPP, Figure 6.4A) and $L_8(S^{H7})_8$ (MQVWPP, Figure 5.3A) Rubisco isoforms. The catalytic parameters measured for both wild-type tobacco and sunflower Rubisco were again found to be highly comparable (Sharwood et al., 2008; Sharwood and Whitney, 2010) and matched those measured previously (Table 4.2).

Table 6.2 Rubisco catalysis comparison.

Catalytic parameter	Plant source			
	tobacco (n=4)	sunflower (n=2)	$LEV^{T}L^{T}S$ (n=4)	$LEV^{T}L^{S}S$ (n=3)
k_C^{cat} (s^{-1})	3.1 ± 0.1	3.3 ± 0.1	2.1 ± 0.2*	2.0 ± 0.1*
$K_C^{21\%O2}$ (μM)	18.8 ± 2.3	18.3 ± 2.1	20.1 ± 3.2	19.8 ± 0.5
$k_C^{cat}/K_C^{21\%O2}$ (mM^{-1} s^{-1})	166	163	105	98
$S_{C/O}$ (mol mol^{-1})	82 ± 2	83 ± 2	82 ± 1	81 ± 2

*Significance variation ($p<0.01$) relative to tobacco Rubisco determined by T-test. $K_C^{21\%O2}$, the apparent K_m for CO_2 (K_C) at atmospheric [O_2].

6.2.9 The altered catalysis of the plastome engineered Rubisco isoforms match that predicted by leaf gas exchange

Leaf gas exchange measurements of $LEV^{T}L^{T}S$, $LEV^{T}L^{S}S$ and wild type tobacco plants during their exponential growth phase after reaching 35-40 cm in height were compared. Measurements were made on the youngest, near fully expanded fifth leaf (14-16 cm in width) located at comparable positions in the upper canopy. Consistent with their lower Rubisco contents (Figure 6.7) the rates of photosynthetic CO_2 assimilation (*A*) in the $LEV^{T}L^{T}S$ and $LEV^{T}L^{S}S$ genotypes were slower than wild-type over the range of intercellular CO_2 pressures (pC_i) tested (Figure 6.10). For the wild-type plants the rates of *A* showed the expected response to varying pC_i (Figure 1.9, see also Section 1.3.2). This differential biphasic response stems from CO_2 assimilation being limited by

Rubisco activity under lower pC_i (e.g. below ~400 μbar for wild-type) and then increasingly restricted by the rate of electron transport through the light reactions of photosynthesis as the pC_i exceeds ~500 μbar (Farquhar et al., 1980) as shown in Figure 6.10. In the LEV^TL^TS and LEV^TL^SS leaves however the CO_2 assimilation rates remained limited by Rubisco activity over the pC_i range tested (Figure 6.10). This occurs due to the lower Rubisco content in their leaves (Figure 6.7) and slower Rubisco carboxylation rates (Table 6.2).

The *A*-pC_i data for each genotype was compared with those predicted using the Michaelis-Menten rate equation from Farquhar et al. (1980) fitted with the catalytic parameters measured for each Rubisco isoform (Table 6.2) and the measured Rubisco content (quantified by [^{14}C]-CABP binding). As shown in Figure 6.10, for the LEV^TL^TS and LEV^TL^SS genotypes the modelled CO_2 assimilation rates closely match those measured, confirming the accuracy of the slower carboxylation properties (*i.e.* k_C^{cat} and $k_C^{cat}/K_C^{21\%O2}$) measured for both the $^TL_8(^TS^{H6})_8$ and hybrid $^TL_8(^SS^{H6})_8$ Rubisco isoforms.

For the wild-type samples the measured carboxylase limiting CO_2 assimilation rates (*i.e.* under low pC_i) were lower than those modelled (Figure 6.10). This overestimation likely stems from the rates of the CO_2 assimilation model not taking into account variations in the activation status of Rubisco in wild-type plants grown under elevated CO_2 – which can be reduced by up to 40% (Whitney et al., 1999; Whitney and Andrews, 2001b; Sharwood et al., 2008), as well as light limitations that impaired CO_2 assimilation beyond 400 pC_i of CO_2. Unfortunately the leaf discs taken for analysis following leaf gas exchange in this study were not analysed for Rubisco activation status – a critical oversight considering how Rubisco catalytic content has a pervasive influence on modelling predictions using the equations of Farquhar et al. (1980) as depicted by the *B* term in the equation in the legend to Figure 6.10.

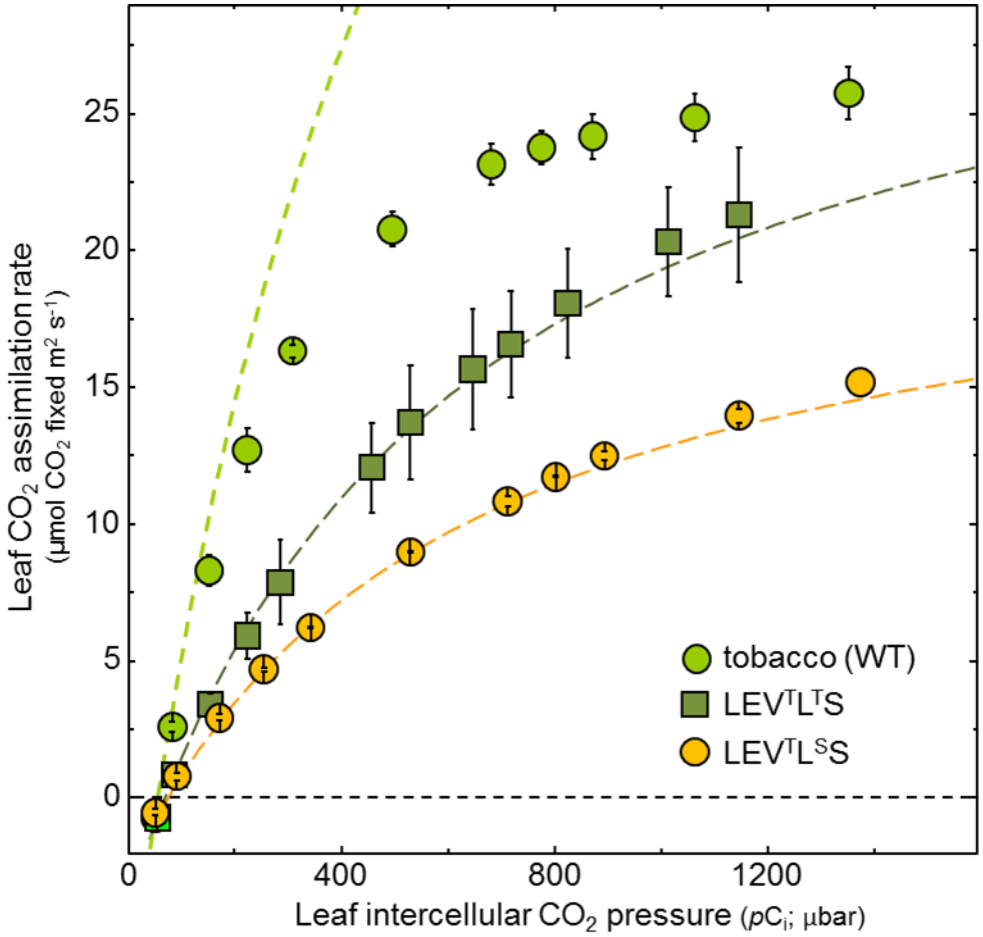

Figure 6.10 CO_2 assimilation rates in response to varying intercellular CO_2 pressures.

Photosynthetic CO_2 assimilation rates were measured under varying intercellular CO_2 pressures (pC_i) in the fifth leaf of 35-40 cm in height tobacco (wild-type, n=2), LEV^{T}L^{T}S (n=3) and LEV^{T}L^{S}S (n=2) plants. Measurements were made using a LiCor 6400 gas exchange system at a constant leaf temperate of 25˚C and at the growth illumination of 400 µmol photons m^2 s^{-1} using a red/blue LED light source. The average leaf Rubisco contents in the leaves analysed were 25.2, 16.4 and 11 µmol L-subunit active sites m^{-2} s^{-1}, respectively, for the wild-type, LEV^{T}L^{T}S and LEV^{T}L^{S}S leaves. The corresponding rates of CO_2 release by leaf mitochondrial respiration (R_d) measured in darkened leaves at 400 ppm CO_2 were 1.6, 1.2 and 1.2 µmol CO_2 released m^2 s^{-1}. The dashed lines shown are those modelled using the catalysis measurements listed in Table 6.2 fitted to the Michaelis-Menten rate equation of Farquhar et al. (1980)

$$A = \frac{B(C_c - \Gamma^*)k_C{}^{cat}}{C_c + K_c(1 + O/K_o)} - R_d \qquad \text{(Eq. 7)}$$

where B is the Rubisco active site content, C_c and O are the CO_2 and O_2 partial pressures in the chloroplast, respectively, $k_C{}^{cat}$ is the maximal rate of carboxylation and K_c and K_o are the Michaelis-Menten (K_m) constants for CO_2 and O_2, respectively. Under ambient levels of O the value for $K_c(1+O/K_o)$ equates to the $K_C{}^{21\%O2}$ measurement listed in Table 6.2. Γ* is the CO_2 compensation point in the absence of R_d (*i.e.* the pC_i where the rate of carboxylation is equal to the rate of respiratory CO_2 release) and is calculated as (0.5 x O)/ $S_{C/O}$ (Farquhar et al., 1980).

6.3 Discussion

The results of this chapter affirm the versatility of the $^{cm}trL^{RNAi\text{-}S}$ line as a novel tobacco genotype for bioengineering Rubisco in leaf chloroplasts. Shown is the successful implementation of a dual L- and S-subunit transplastomic approach for producing tobacco genotypes capable of making adequate levels of Rubisco to support plant growth in air. The genetic precision and simultaneous modification of this *rbcL-rbcS* co-engineering approach provided a novel method for bioengineering Rubisco isoforms that comprised a homogenous population of L- and S-subunits – the key objective of this thesis (see Section 1.5). The novel method worked best for the Rubisco isoforms comprising tobacco L-subunits, suggesting the need to adhere to the specialised assembly requirements of this subunit. Limitations to S-subunit synthesis and possible structural complementarity issues with heterologous L-subunits also appear to impact the production of recombinant Rubisco in leaf chloroplasts. Overcoming these experimental hurdles pose significant challenges in fine tuning recombinant Rubisco bioengineering efforts.

6.3.1 The varying limitations to L- and S-subunit synthesis in chloroplasts

6.3.1.1 Meeting the chaperone requirements of the L –subunit is a core requirement

As summarised in Section 1.4.3, transplastomic studies on bioengineering Rubisco in tobacco chloroplasts have paid particular attention to replacing/modifying the plastome *rbcL* (Parry et al., 2013). Transformed genotypes producing wild-type or mutated tobacco *rbcL* that slow catalysis show little or no change in *rbcL* mRNA and L_8S_8 contents under conditions where autotrophic growth can be supported (e.g. high-CO_2) (Whitney et al., 1999; Whitney and Sharwood, 2008; Whitney et al., 2011b). In contrast, in genotypes where the tobacco *rbcL* is replaced with an alternative plant *rbcL*, highly varied amounts of hybrid Rubisco are produced (see Table 5.1 and Figure 6.1). In this thesis, the production of sunflower $^{S}L_8(^{S}S^{H6})_8$ and hybrid $^{S}L_8(^{t}S^{H6})_8$ Rubisco in the $LEV^{S}L^{T}S$ and $LEV^{S}L^{S}S$ genotypes (Figure 6.9) proved to be more impeded than prior ^{sun}*rbcL* mRNA transplastomic studies (Figure 6.1). The recurring impediment to sunflower L-subunit synthesis in tobacco chloroplasts is not likely to stem from problems with ^{Sun}*rbcL* mRNA translation initiation as its 5'UTR sequence and first 54 nt of coding sequence are identical to the ^{Tob}*rbcL* mRNA. As indicated in Sharwood et al. (2008), this level of homology also ensures the sunflower L-subunits undergo the same N-terminal post translational modifications (PTMs, *i.e.* Met-1, Ser-2 cleavage-

Pro-3 acetylation, Lys-14 trimethylation) that are thought to protect against proteolysis (Houtz et al., 1989; Nishimura et al., 2008; also see Section 4.3.1.2).

The highly comparable codon use of ^{Tob}*rbcL* and ^{Sun}*rbcL* provide little evidence for differences in translation elongation of both transcripts. Indeed a comparison of their 5'UTR sequences (Genbank accession number DQ383815.1 for *H. annuus* ^{Sun}*rbcL*) also shows high sequence identity (91%). In general, the multidimensional effects from synonymous site modification of genes for optimised chloroplast expression remain unclear (Ullrich et al., 2015). It is also important to remember that although mRNA acts as a direct source for protein translation, its levels are not always indicative of protein content (Bitton et al., 2008; Nagaraj et al., 2011). For example, the expression of protein antibiotics in tobacco plastids produced incoherent mRNA and protein expression levels that signified limitations in mRNA translational capacity (Oey et al., 2009). Testing for possible perturbations in translation initiation or elongation of ^{Sun}*rbcL* mRNA by sucrose gradient polysome analyses is yet to be examined in any sunflower L-subunit producing tobacco genotype and is clearly an important objective for future studies. Extending such analyses to compare the polysome association of the synthetic tobacco *rbcL-rbcS* mRNAs in the LEVLSSuH$^{♀}$ × ^{cm}trL$^{RNAi\text{-}S♂}$ and LEVL-TobS^{H6} genotypes (Chapter 5) relative to the LEV^{T}L^{T}S and LEV^{T}L^{S}S lines is also important as this would help decipher to what extent the "chloroplast optimised" codon use in the synthetic ^{Sun}*RbcS* and ^{Tob}*RbcS** (Table 6.1) improved chloroplast S-subunit synthesis.

Recent breakthroughs in deciphering the Rubisco biogenesis pathway in leaf chloroplasts indicate correct folding and assembly of the L-subunit is dependent on structural complementation with folding and assembly chaperones. Evolutionary divergence in the sequence of the sunflower and tobacco L-subunits appear to have perturbed this chaperone-complimentarity requirement to restrict sunflower L-subunit assembly in tobacco. One chaperone of particular impotance is the Rubisco specific chaperone RAF1. Characterisation of RAF1 form and function began through its discovery in a maize photosynthetic mutant library (PML) where it was postulated to facilitate assembly of the post-chaperonin folded L-subunits into L_8 core complexes for S-subunit assembly (Feiz et al., 2012). More recent work on another maize PML mutant suggests RAF1 may function with the aid of other Rubisco specialised chaperones called RAF2 and BSD2 (Brutnell et al., 1999; Feiz et al., 2014). To better understand the role of the RAF1 homo-dimer complex in leaf chloroplasts, recent work using a plastome transformation approach confirmed the dependency of complementarity between L-subunits and RAF1 for optimal L_8S_8 biogenesis (Whitney et al., 2015). That

is, in tobacco leaves producing *Arabidopsis* L-subunits the amount of hybrid $^{A}L_8{}^{t}S^{8}$ Rubisco (comprising *Arabidopsis* L- and tobacco S-subunits) was increased ~2-fold from ~3.5 μmol catalytic sites m^2 to ~7.5 μmol catalytic sites m^2 by co-expression of an *Arabidopsis* RAF1 isoform. Co-insertion of *raf1* in an operon with *rbcL* unfortunately compromised the *rbcL-raf1* mRNA levels by ~3-fold. When normalised relative to mRNA contents it was found RAF1 had increased $^{A}L_8{}^{t}S^{8}$ Rubisco biogenesis by more than 7-fold (Whitney et al., 2015).

The potential for improving the biogenesis of hybrid Rubisco comprising sunflower ^{S}L-subunits via co-expressing RAF1 from sunflower serves as a primary target for future testing. Current efforts have been stymied so far as sequences for *raf1* from sunflower remain to be determined. Facilitating further improvement to heterologous plant Rubisco production may extend further than RAF1 to include other L-subunit and S-subunit assembly chaperones (for potential examples see Table 4.1 and Figure 4.3). For example, recent success in producing cyanobacteria Rubisco in tobacco chloroplasts (*i.e.* the Se7942 tobacco genotypes, Table 5.1) found Rubisco assembly was augmented in those lines co-producing the complimentary CcmM35 protein (Lin et al., 2014). In cyanobacteria the CcmM forms the key shell protein of carboxysomes and has a C-terminus that shares sequence homology with the S-subunit which functions to co-ordinate Rubisco assembly inside the carboxysome (Long et al., 2007; Rae et al., 2012; Price and Howitt, 2014). Further discussion on potential Rubisco co-chaperone expression testing in the future is included in Section 7.6.

6.3.1.2 The contrasting restraints on L_8S_8 biogenesis in each tobacco genotype

The significant amount of recombinant Rubisco produced in $LEV^{T}L^{T}S$ and $LEV^{S}L^{T}S$ implies the alternative *rbcL-rbcS* operon structure utilised in this study (Figure 6.4A) was suitable for facilitating comparatively high levels of chloroplast S-subunit synthesis. This would suggest that severely limited levels of Rubisco produced in $LEV^{S}L^{T}S$ and $LEV^{S}L^{S}S$ lines was not limited by chloroplast S-subunit availability. This is consistent with that described in the section above where the primary restriction to Rubisco biogenesis is the capacity of sunflower ^{S}L-subunit to assemble into octameric cores (Sharwood and Whitney, 2010; see also Section 5.1.3). Impeded production of sunflower-L_8 cores in the $LEV^{S}L^{T}S$ and $LEV^{S}L^{S}S$ genotypes may therefore render the chloroplast made ^{T}S- and ^{S}S-subunits more prone to proteolysis. Prior Rubisco bioengineering work has shown the efficiency of protein proteolysis in the stroma. In ^{cm}trL that only makes L_2-Rubisco, rapid degradation of unassembled tobacco S-subunits

by stromal proteases prevents their detection (Whitney and Andrews, 2001b; Whitney and Andrews, 2003; Whitney and Sharwood, 2008).

As described in Section 6.2.3, an MSPQT substitution was made to the N-terminus of the ^{T}S- and ^{S}S-subunits in a bid to safeguard them against proteolysis (Houtz et al., 1989). Future experiments aim to investigate the level of protection afforded by these amino acid changes by *firstly* determining the S-subunit N-terminal sequence in the LEV^{T}L^{T}S, LEV^{T}L^{S}S, LEV^{S}L^{T}S and LEV^{S}L^{S}S genotypes using established mass spectrometry methods (Whitney et al., 2009). *Secondly*, rates of Rubisco translation and stability in the leaf chloroplasts of LEV^{T}L^{T}S and LEV^{T}L^{S}S (that make sufficient levels of Rubisco) will be undertaken via pulse-chase with [^{35}S]-Met/unlabelled-Met (Whitney et al., 2015; also outlined in Section 5.3.2.3). These experiments will determine if there are potential correlations between PTM-induced improvements in Rubisco subunit synthesis and stability. Such measurements may help decipher whether the acetyl-Pro modification of plant L-subunits might only provide proteolysis protection to subunits assembled within L_8S_8 complexes. This would support the hypothesis that the association of nascent and unfolded L- and S-subunit with one of their many complementary pre-assembly chaperones (Figures 4.1 and 4.3; Table 4.1) is required for their protection from proteolysis (Nakamura et al., 2001).

6.3.1.3 Rubisco mRNA limitations confine L_8S_8 biogenesis in LEV^{S}L^{T}S and LEV^{S}L^{S}S.

The amount of Rubisco made in the LEV^{S}L^{T}S and LEV^{S}L^{S}S genotypes (~0.1 to 0.4 μmol active sites m^2, Figure 6.7B) is ~10-fold lower relative to other tobacco genotypes producing hybrid Rubisco comprising sunflower ^{S}L-subunits and cytosol made tobacco S-subunits (Figure 6.1B). This suggests that additional factors other than ^{S}L-subunit chaperone complementarity limitations were affecting Rubisco biogenesis in these lines. They also shared the same reduced cellular viability and tissue culture dependency as the LEVL-S^{H6} genotypes. As discussed in Section 5.3.1, the reduced fitness of these plants likely contributed to the reduced mRNA levels. At the other end of the spectrum, the wild-type like growth phenotype of the LEV^{T}L^{T}S and LEV^{T}L^{S}S genotypes could be supported in soil under elevated CO_2 (Figure 6.6). Accordingly their pools of *rbcL-rbcS* mRNAs more closely matched the *rbcL* mRNA level produced in WT (Figure 6.9B).

6.3.2 L_8S_8 biogenesis is influenced by structural complementarity between the L-subunit and S-subunits

As mentioned above (see Section 6.3.1.2) the new *rbcL-S* transgene structure tested in this chapter appears capable of producing relatively high levels of Rubisco comprising a homogeneous population of chloroplast made Rubisco L- and S-subunits. While folding and assembly of heterologous L-subunits appears to interfere with recombinant Rubisco biogenesis in leaf chloroplasts (see Section 6.3.1), structural complementarity requirements between the subunits also appear important determinants of assembly capacity. As recently shown by Joshi et al. (2015) the assembly of *R. sphaeroides* "red" Rubisco L-subunits with S-subunits from cyanobacteria or algae was dependent on the inclusion of an extended C-terminal βE/βF loop (Figure 5.3A). Interestingly the chimeric L_8S_8 Rubiscos showed very little or no catalytic activity. The pioneering mutagenic studies on Rubisco performed in *E. coli* in the 80's and 90's showed similar impediments in the catalytic potential and holoenzyme assembly of cyanobacteria Rubisco L-subunits (that can fold and assemble as L_8 cores in *E. coli*) with S-subunits sources from either plants (e.g. tobacco, rice, wheat and spinach) (Andrews and Lorimer, 1985; Wang et al., 2001), algae (e.g. *Prochloron*, *P. tricornutum* and *Cylindrotheca*) (Andrews and Ballment, 1984; Read and Tabita, 1992) or proteobacteria (*Alcaligenes euthrophus*). According to the Rubisco contents shown in Figure 6.7B, these subunit complementation requirements appear to also extend to the tobacco lines described in this chapter. That is, the hybrid Rubisco levels made in LEV^TL^SS and LEV^SL^TS are, respectively, reduced 2 to 3-fold relative to the LEV^TL^TS and LEV^SL^SS genotypes where the S-subunits are cognate to the L-subunit.

An explanation for the reduced assembly capacity of the heterologous tobacco and sunflower L- and S- subunits may stem from disturbances in the L- and S-subunit ionic interactions that are important in correct quaternary structure assembly (van Lun et al., 2011). For example at least 10 of the 29 differences in residues between the tobacco and sunflower L-subunit (Figure 6.2A) are located in the L/S-subunit interface region. Potential limitations in the interactivity of tobacco chaperones and the sunflower S-subunit in the stroma may also limit the duration required for proper folding/assembly. For example the differences at L-subunit residues 25 (Glu to Gln) and 28 (Ser to Lys) are at positions shown to interact with residues in the S-subunit (Kanevski et al., 1999). An obvious next step is therefore to test the extent to which this compatibility requirement between subunits influences the biogenesis of other hybrid plant Rubisco in tobacco chloroplasts by applying the same *rbcL-rbcS* co-engineering strategy shown in

Figure 6.4. More rigorous testing in the longer term might target specific structural regions within the S-subunit to more clearly define those that impart assembly specificity with the L_8 core.

6.3.3 Modification to the S-subunit C-terminus can slow catalysis.

Prior mutagenic studies of plant S-subunits have produced contrasting results with regard to their influence on catalysis (summarised in Section 1.4.2 and Section 3.1.1). As most mutagenic studies on Rubisco have focused on the L-subunit and the S-subunit βA/βA and βE/βF loops (Kellogg and Juliano, 1997; Spreitzer, 2003; Joshi et al., 2015) the influence of modifications to the S-subunit C-terminus on Rubisco catalysis has not been investigated. An attempt by Whitney and Andrews (2001) to produce tobacco Rubisco with S^{H7}-subunits containing a hepta-histidine (H7) C-terminal extension was unable to measure any effect on catalysis as the Rubisco produced primarily comprised the endogenous cytosolic made ^{cyt}S-subunits instead of chloroplast made S^{H7}-subunits (detailed in Section 4.1.4). As shown in Chapter 4, pollination of these transplastomic genotypes (e.g. RVtpSSuH) with $^{cm}trL^{RNAi\text{-}S}$ pollen successfully silenced ^{cyt}S-subunit synthesis in their progeny to produce $L_8(S^{H7})_8$. The additional H7 sequence on the S-subunit slowed down the enzyme without effect on $S_{C/O}$ (Table 4.2) as seen here for the $^{T}L_8(^{T}S^{H6})_8$ and hybrid $^{T}L_8(^{S}S^{H6})_8$ enzymes produced in $LEV^{T}L^{T}S$ and $LEV^{T}L^{S}S$ respectively (Table 6.2). Measures of the K_m for CO_2 under ambient O_2 levels (*i.e.* $K_C^{21\%O2}$) of the three differing Rubisco forms did vary. For the $^{T}L_8(^{T}S^{H6})_8$ and hybrid $^{T}L_8(^{S}S^{H6})_8$ enzymes the modified S-subunits had no significant influence of Rubisco CO_2-affinity as their $K_C^{21\%O2}$ values matched those measured for wild-type tobacco and sunflower Rubisco (Table 6.2). The accuracy of these values are consistent with the rates of photosynthesis measured in the $LEV^{T}L^{T}S$ and $LEV^{T}L^{S}S$ leaves (Figure 6.10). The lower $K_C^{21\%O2}$ values measured for the $L_8(S^{H7})_8$ enzyme are therefore likely a consequence of experimental error associated with the $^{14}CO_2$-fixation assays used (see Section 2.5.3). This primary source of error appears associated with the low amounts of enzyme produced in the RVtpSSuH♀ × $^{cm}trL^{RNAi\text{-}S}$♂ genotype. This resulted in low measurable carboxylase activities, particularly in the assays measured under lower, sub-saturating CO_2 levels. The low carboxylase rates measured compromised accurate extrapolation of $K_C^{21\%O2}$ using the Michaelis-Menten equation. This finding highlights the importance of optimising the enzyme levels in these CO_2-fixing assays to ensure suitable rates of activity can be measured.

From the perspective of the Rubisco quaternary structure it is difficult to rationalise how the appended C-terminal polyhistidine sequences slowed catalysis. Nevertheless the location of the S-subunit C-terminus is distant from the catalytic sites that are found at the interface of adjoined L-subunits and located nearer to the central equatorial circumferences of the enzyme (Andersson and Backlund, 2008; van Lun et al., 2011). Interestingly comparable 6×His modifications to cyanobacteria and *Rhodobacter sphaeroides* S-subunits also lead to reductions in k_C^{cat} (Whitney et al., unpublished). This common compromise to Rubisco activity cautions against incorporating affinity tags on the S-subunit C-terminus in future structure-function experiments on Rubisco. In the context of bioengineering plant Rubisco in tobacco chloroplasts, the continued stability and efficiency of S-subunit silencing in the $^{cm}trL^{RNAi\text{-}S}$ genotype suggests that future use of such tags is unwarranted.

6.3.4 A new pathway for studying Rubisco structure-function.

The plastome transformation approach in $^{cm}trL^{RNAi\text{-}S}$ used to generate $LEV^{T}L^{T}S$ and $LEV^{T}L^{S}S$ genotypes affirms the potential for producing Rubisco complexes in tobacco chloroplasts comprising homogeneous populations of L- and S-subunits made exclusively in the chloroplast. As described above (and explored further in Chapter 7) there is room for improvement. These include adapting the advances made in recent years on polycistronic operon design to incorporate co-expression with other molecular partners involved in Rubisco biogenesis (e.g. RAF1, RAF2, BSD2, RbcX, Cpn60; see Figure 4.3), elements that optimise mRNA stability and translation (e.g. inclusion of IEE elements) (Zhou et al., 2007; Lin et al., 2014) as well as strategies to facilitate recycling of the *aadA* marker to allow for subsequent plastome transformation opportunities (Day and Goldschmidt-Clermont, 2011). Tailoring such improvements into the plastome transformation undertakings in $^{cm}trL^{RNAi\text{-}S}$ are key to future mutagenic studies of tobacco and foreign Rubisco L- and S-subunits to identify structural features in each subunit that define their assembly complementarity (see Section 6.3.2) and potential to impact on the enzymes catalytic properties. As detailed in Section 6.2.9, this transplastomic approach is benefited by being able to detect changes in Rubisco content and catalysis by both biochemical methods (using isolated enzyme) and in a translational context in how leaf photosynthesis and plant growth is influenced.

CHAPTER 7 – GENERAL DISCUSSION

The versatility of bioengineering Rubisco in leaf chloroplasts has advanced significantly over the last 15 years. These advances have been somewhat restricted to manipulation of the larger, catalytic L-subunit through targeted changes to *rbcL* in the plastome (Parry et al., 2013). Extending these recombinant enzyme applications to encompass the S-subunit has been limited by the alternative location of *RbcS* in the nucleus (Whitney et al., 2011; see also Section 1.4.2). The apparent preferential assembly of the endogenous cytosol made S-subunits over recombinant alternatives made in the chloroplast have also constrained their bioengineering in leaves. Eliminating this constraint by silencing *RbcS* mRNA synthesis using an RNAi targeted approach has obvious consequences to plant viability since Rubisco catalysis forms the cornerstone of photosynthetic CO_2 assimilation and thus is crucial for growth.

As described in Chapter 3 the research of this thesis took an alternative approach that proved highly successful. This approach targeted RNAi silencing of the multiple *RbcS* transcripts made in the ^{cm}trL tobacco genotype (Figure 3.6). As this genotype produces the bacterial *R. rurbum* L_2 Rubisco it does not require S-subunits (Figure 7.1). The resulting generation and analysis of the homozygous ^{cm}trL$^{RNAi\text{-}S}$ genotype showed it efficiently, and stably, silenced accumulation of *RbcS* mRNA without effect on plant phenotype (Figure 3.10). The stability of the RNAi-*RbcS* genotype through successive ^{cm}trL$^{RNAi\text{-}S}$ generations (Figure 3.9) was exploited using two complementation strategies that successfully produced varying genotypes making recombinant Rubisco isoforms that comprised homogenous populations of chloroplast made L- and S-subunits. As summarized in Figure 7.1 this included a cross-pollination approach to transfer the RNAi-*RbcS* allele into transplastomic lines already expressing recombinant chloroplast made S-subunits (Chapter 4). The alternative transgenic approach tested directly replaced *rbcM* in the plastome of ^{cm}trL$^{RNAi\text{-}S}$ (that codes *R. rubrum* L_2 Rubisco) with synthetic *rbcL-rbcS* operons coding alternative plant and algae L- and S-subunits (Chapters 5 and 6).

While successful in meeting the objective of developing an efficient bioengineering platform for targeted manipulation of tobacco and foreign L- and S-subunits in leaf chloroplasts, the findings highlighted a number of future challenges. As summarized in Figure 7.2 these challenges include understanding the combinatorial effects of transcript abundance/stability, subunit synthesis, folding, and compatibility requirements for heterologous subunit assembly. These factors were found to

differentially influence recombinant Rubisco biogenesis in tobacco chloroplasts. Described in this chapter are potential experimental approaches to address these challenges and the possible uses of the ^{cm}trL genotype in other bioengineering applications.

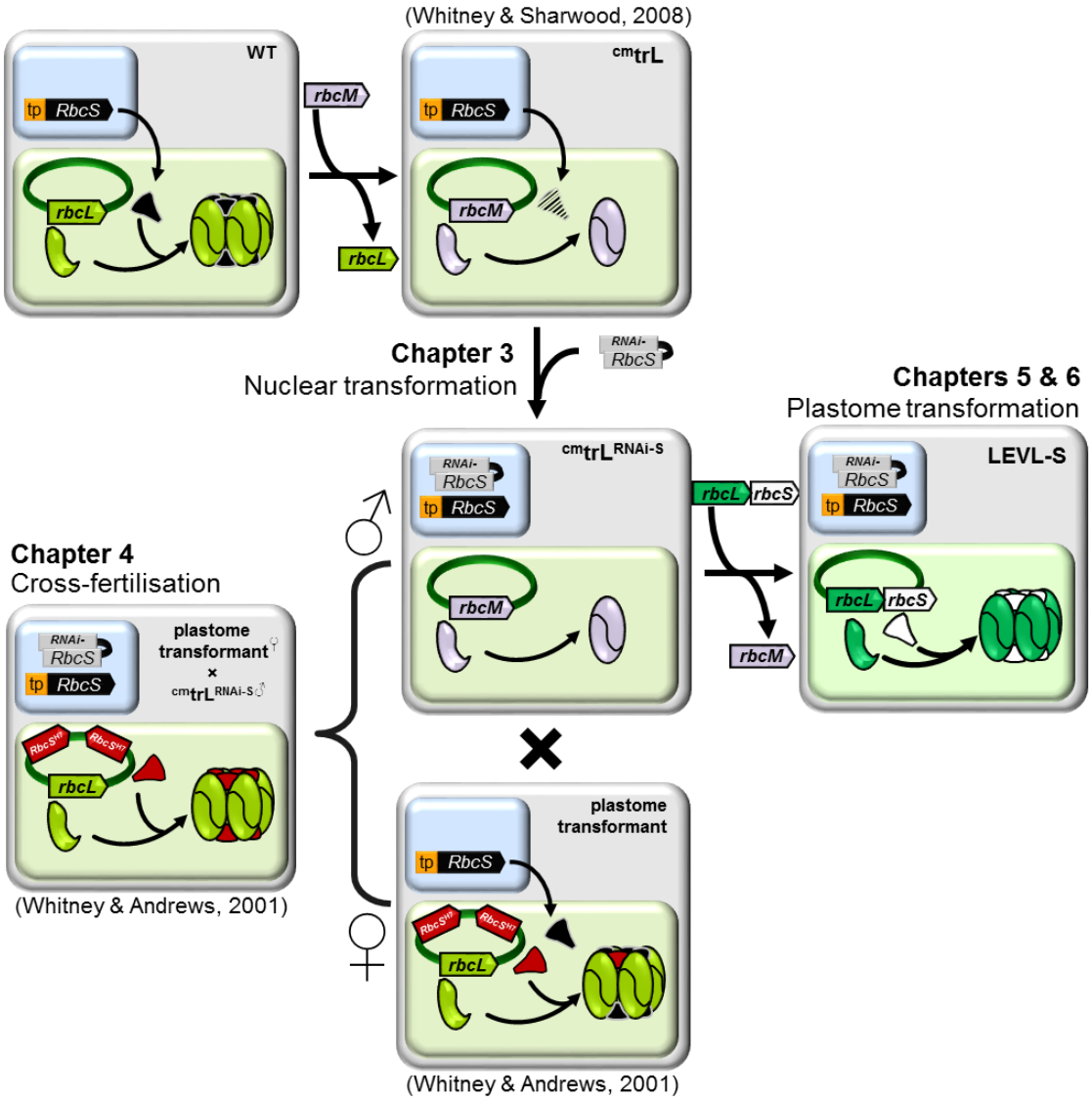

Figure 7.1 Transgenic approaches to enable S-subunit bioengineering in tobacco chloroplasts.

Flow diagram of the transgenic process undertaken to develop the photosynthetically viable RNAi-*RbcS* tobacco genotype ^{cm}trL$^{RNAi\text{-}S}$ that produces no Rubisco S-subunits (Chapter 3). Tobacco genotypes producing Rubisco comprising homogeneous populations of chloroplast made L- and S-subunits where generated by (i) cross-pollination transfer of the RNAi-*RbcS* allele from ^{cm}trL$^{RNAi\text{-}S}$ into transplastomic lines already expressing recombinant chloroplast made S-subunits (Chapter 4) or (ii) by directly replacing *rbcM* in the ^{cm}trL$^{RNAi\text{-}S}$ plastome with synthetic *rbcL-rbcS* operons coding alternative L- and S-subunits (Chapters 5 and 6).

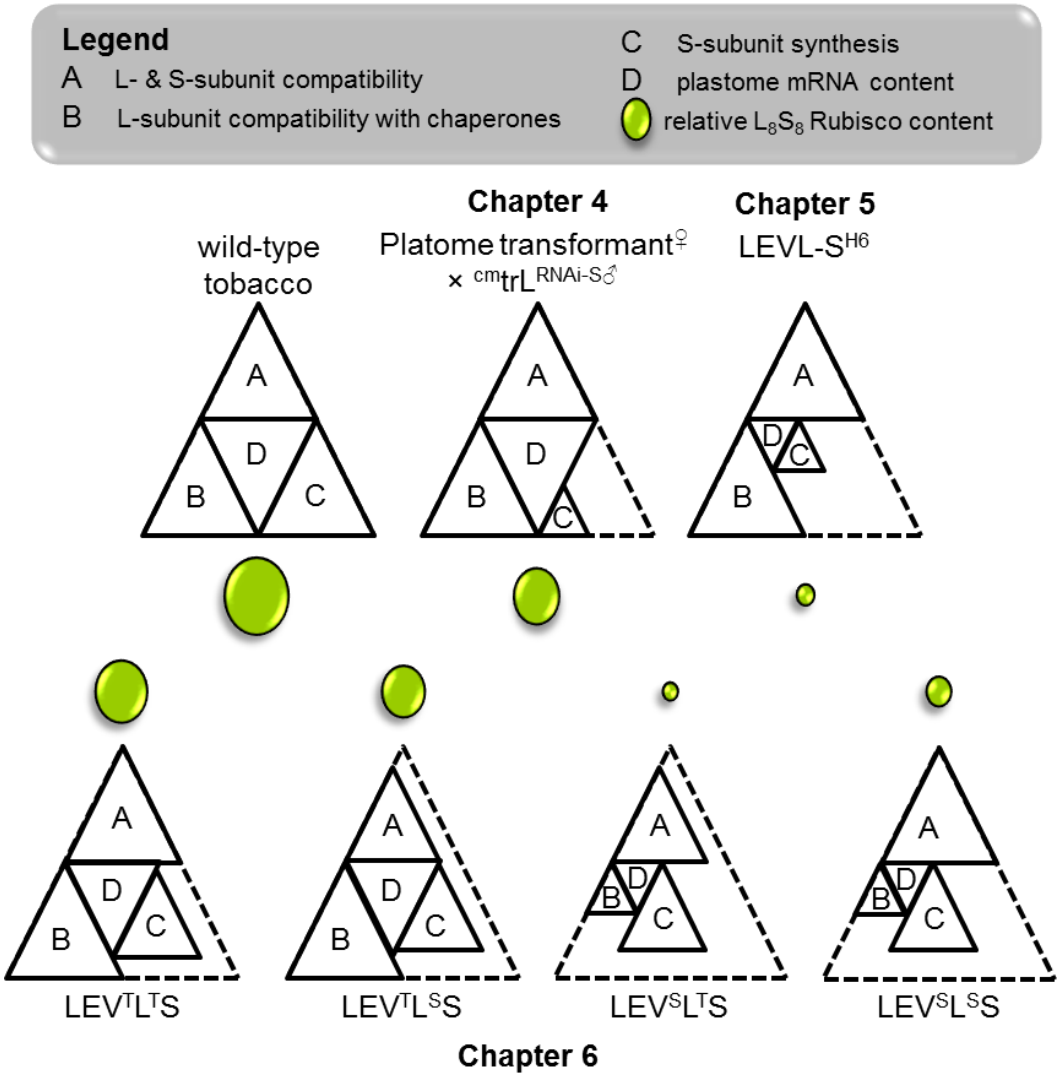

Figure 7.2 Schematic summary of the relative Rubisco content and factors influencing L_8S_8 biogenesis in the tobacco genotypes detailed in Chapters 4 to 6.

Graphic representation depicting the relative amount of recombinant Rubisco made (represented by different sized green oval shapes) in the different tobacco genotypes studied in this thesis and how this was impacted by four key parameters impacting Rubisco biogenesis in chloroplasts (listed A to D in legend; the more affected a property, the smaller the size of triangle). As Rubisco levels correlate with the rate of photosynthesis, the size of the triangles likely correlate with the metabolic capacity of the plant.

7.1 Using $^{cm}trL^{RNAi\text{-}S}$ to study chloroplast protein translation and Rubisco assembly requirements in leaf chloroplasts

As evident from the phenotypic variations in the tobacco genotypes generated in this thesis, the level of Rubisco biogenesis directly correlates with photosynthetic capacity and growth – a finding well-documented from anti-*RbcS* studies in different plant species (Rodermel et al., 1988; Hudson et al., 1992; see also Section 3.1.1) and in transplastomic genotypes with no or altered *rbcL* (Kanevski and Maliga 1994; Whitney et al., 2011; see also Table 5.1). The indispensable requirement of S-subunits for plant Rubisco biogenesis, coupled with the correlation between Rubisco content and plant

growth (*i.e.* photosynthetic potential) highlights the potential application of the L- and/or S-subunits as marker proteins for studying recombinant protein production in tobacco plastids. Application of this approach is somewhat dependent on the $^{cm}trL^{RNAi\text{-}S}$ genotype. By transforming into the $^{cm}trL^{RNAi\text{-}S}$ genotype the extent of recombinant L- and/or S-subunit synthesis can be simply assessed by ndPAGE analysis of relative L_8S_8 synthesis in the soluble protein from regenerating plant material (Whitney and Sharwood, 2008; see also Figures 4.9A, 5.6B and 6.5). Once fully homoplasmic and growing in tissue culture or in soil, a simpler indicative screen of Rubisco biogenesis capacity can be made by comparing plant growth and phenotype (Figures 3.10, 4.8, 5.7 and 6.6). Genotypes producing less than 10 µmol L-subunits m^2 of Rubisco characteristically grow increasingly slower and have thinner, paler green leaves. In genotypes where Rubisco levels are too low, their survival necessitates growth in tissue culture on medium containing sucrose. These differing phenotypes provide a useful initial screen for assessing the relative success of recombinant Rubisco bioengineering.

Prior studies examining the genetic requirements of transcription and translation in tobacco chloroplasts have typically utilized "customary" marker genes such as those coding the green fluorescent protein (GFP) and aminoglycoside 3'-phosphotransferase (NPTII) enzyme (Kuroda and Maliga, 2001b; Drechsel and Bock, 2011). Of disadvantage is that neither protein is of biological relevance and in the case of GFP can be detrimental to plant growth when expressed in high levels (Haseloff et al., 1997). The following paragraphs describe potential applications of synthetic *rbcL-rbcS* transformations into $^{cm}trL^{RNAi\text{-}S}$ aimed at unravelling the genetic requirements for more reliable recombinant protein expression in leaf chloroplasts. A potential advantage of using Rubisco subunit bioengineering as marker proteins is the capacity to test for changes in Rubisco content and catalysis by both biochemical methods using isolated enzyme as well as by changes in photosynthetic CO_2 assimilation capacity (Figure 6.10) and plant growth rate (Whitney et al., 1999; Whitney and Andrews, 2001a; Whitney and Andrews, 2003; Sharwood et al., 2008; Whitney et al., 2011a; Whitney et al., 2015).

7.2 What caused the differing rates of S-subunit synthesis between genotypes?

Determining the underpinning cause for the varying levels of Rubisco made in LEVLSSuH♀ × $^{cm}trL^{RNAi\text{-}S}$♂ (Chapter 4), LEVL-TobS^{H6} (Chapter 5) and LE$V^{T}L^{T}S$ (Chapter 6) is of immediate interest. All three genotypes share comparable operon structures, identical regulatory elements and each share the wild-type tobacco *rbcL* but produce vastly different amounts of the same tobacco L_8S_8 Rubisco (Figure 7.3). This

difference does not arise from intercistronic processing of their *rbcL-RbcS* and *rbcL-RbcS-aadA* polycistronic mRNA's. The difference in S-subunit synthesis must therefore arise from the differences in their *RbcS* sequences (*i.e.* codon use) or/and the 18 nucleotide differences in the intergenic sequence downstream of the SD of *RbcS*. In the LEV^{T}L^{T}S genotype this region replicated the *rbcL* TCR that extended into the first four codons of S-subunit coding sequence (Figure 6.4). Potentially these sequence differences may influence the stability of the *rbcL-RbcS* and *rbcL-RbcS-aadA* mRNAs. Indeed the abundance of these transcripts in the genotypes producing less Rubisco were reduced 3 to 10-fold. However, as these polycistronic mRNA's did not undergo intercistronic processing (*i.e.* RNA cutting) then they would possess identical 5′- and 3′UTR sequences. These are the regions most associated with forming stabilising secondary structures and interacting with stabilising accessory binding proteins to prevent exonuclease activity (Barkan et al., 1994). As discussed in Section 5.3.1, it is more likely the reduced mRNA levels may simply arise as a consequence of the impaired cellular viability in the genotypes producing little or no Rubisco.

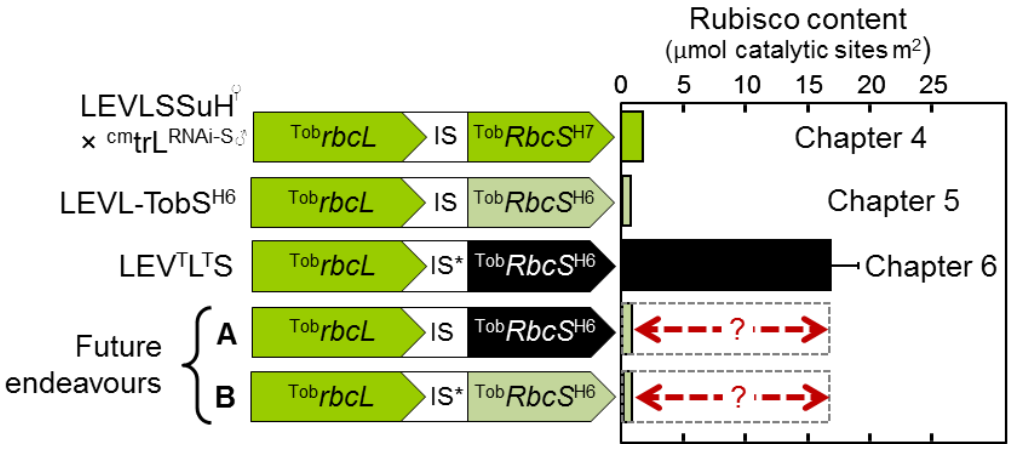

Figure 7.3 Identifying the elements that increase chloroplast S-subunit synthesis.

Summary of putative follow-up plastome transformation experiments to test how differences in the *RbcS* codon use and/or inclusion of the *rbcL* translational coding region (TCR: signified by an asterix, *) in the intergenic sequence (IS) led to the large difference in S-subunit synthesis (and hence L_8S_8 Rubisco content) in the LEV^{T}L^{T}S genotypes compared to the LEVLSSuH♀ × ^{cm}trL$^{RNAi\text{-}S}$♂ and LEVL-TobS^{H6} lines. See text for more details.

Differences in the translational potential of the varying *RbcS* mRNA sequences in the different tobacco genotypes shown in Figure 7.3 therefore seem more likely to be responsible for the difference in S-subunit synthesis (parameter C in Figure 7.2). The relatively high levels of S-subunits (and hence Rubisco) made in LEV^{T}L^{T}S indicates that (i) *RbcS* in this line was efficiently translated without need of intercistronic cleavage and (ii) its SD was efficiently recognized by the chloroplast translational

components. Potential starting points for testing the impact of the *rbcL* TCR and differing codon use on S-subunit synthesis could commence with the generation of two additional transplastomic lines (Figure 7.3). The importance of codon use would be supported if Rubisco levels could be enhanced in LEVL-TobS^{H6} by altering the codon use of its *RbcS* to match that used in LEV^{T}L^{T}S (option A in Figure 7.3). A reciprocal test would involve swapping the TCR domain in LEV^{T}L^{T}S with the corresponding sequence from LEVL-TobS^{H6} (option B in Figure 7.3). Increases in Rubisco production in this genotype would signify the importance of translation initiation in plastid S-subunit synthesis and that of other recombinant protein synthesis in general. The findings of these preliminary tests would set the scene for subsequent mutagenic testing. For example if inclusion of the TCR sequence was a key driver for increased S-subunit synthesis, then directed mutagenesis of nucleotides in this region might help pinpoint what nucleotide sequence(s) are essential for optimizing translation initiation. Examining computational predictions of RNA secondary structure to ascertain mutations that favour ribosome engagement have yet to be tested. Such tests could build on the SD mutagenic studies of Drechsel and Bock (2011) who identified SD expression elements useful for high-level recombinant expression.

7.3 Can chloroplast S-subunit synthesis be enhanced further?

7.3.1 Via a $^{cm}trL^{RNAi\text{-}S}$ cross pollination approach

Prior success in increasing the level of chloroplast made S-subunit synthesis was achieved by inserting tobacco *RbcS* into the *trnI-trnA* intergenic region within the 25 kb inverted repeat region of the plastome (Dhingra, 2004). The *trnI-trnA* is located between the small (*rrn16*) and large (*rrn23)* rRNA subunit genes that are co-transcribed by promoters upstream of *rrn16* as a polycistronic *rrn* operon (Daniell, 2005; Lutz, 2007). As the *rrn* operon mRNA is highly abundant and efficiently processed, transgenic mRNA inserted between *trnI* and *trnA* are produced in high abundance, especially when an additional promoter is included to drive transgene expression. Consequently, insertion of the *RbcS* transgene into this region produced more *RbcS* mRNA than in genotypes where *RbcS* was inserted into the *trnV*-3′*rps12* region of the plastid genome (Whitney and Andrews, 2001) using earlier generation pPRV transforming vectors (Zoubenko, 1994). This would suggest that pollinating the two *trnI-RbcS-trnA* tobacco genotypes produced by Dhingra et al. (2004) (called Nt-pLDAD*psb*A*Rbc*S and Nt-pLDADg10*Rbc*S) with pollen from $^{cm}trL^{RNAi\text{-}S}$ would produce progeny making more tobacco Rubisco (comprising chloroplast made S- and L-subunits) relative to that made

in the RVtpSSuH♀ × ^{cm}trL$^{RNAi\text{-}S}$♂ plants described in Chapter 4. This experiment remains to be undertaken.

A potential drawback of bioengineering into the *trnI-trnA* region is the desire and the likely need to develop a plastome transformation process for co-engineering changes to both *rbcL* and *rbcS*. While experimentally feasible for duplicating the copy number of a gene of interest (GOI), the process of generating an RNAi-*RbcS* genotype comparable to ^{cm}trL$^{RNAi\text{-}S}$ would require a number of transgenic steps. A first step would be to introduce an *R. rubrum rbcM* into the *trnI-trnA* region of the tobacco genome, preferentially a genotype where *rbcL* has already been excised; for example the Δ*rbcL* tobacco genotypes of Kode et al. (2006) or Kanevski and Maliga (1994). Recycling of *aadA* would likely need to be considered for which there are now a range of strategies available for marker gene recycling (Day and Goldschmidt-Clermont, 2011). Like the ^{cm}trL$^{RNAi\text{-}S}$ genotype made in this thesis (Chapter 3) the resulting L_2-Rubisco expressing genotype would be amenable to RNAi directed silencing of *RbcS* without detriment to its phenotype. The final product would be an RNAi-*RbcS* genotype amenable to plastome transformation directed replacement of the *rbcM* transgene in the *trnI-trnA* region with *rbcL-rbcS* transgenes. Whether such a protracted engineering process is of benefit will depend on whether future approaches can enhance tobacco and foreign Rubisco production in ^{cm}trL$^{RNAi\text{-}S}$ to levels comparable to wild-type. The approaches include increasing *RbcS* mRNA levels, improving S-subunit translation (see Section 7.3.2) and/or enhancing foreign L-subunit assembly (see Section 7.4).

7.3.2 Stimulating rbcL-rbcS mRNA cleavage to increase RbcS mRNA production and translation.

As discussed in see Section 5.3.2.1, possible limitations in the capacity of the chloroplast translational machinery to recognise SD sequences within polycistronic transcripts may explain why chloroplast polycistronic mRNA's often undergo intercistronic cleavage to produce monocistronic mRNAs that are more amenable to translation (Drechsel and Bock, 2011). In support of this hypothesis, a few transplastomic studies have found merit in using the small 50 nt RNA element coined the intercistronic expression element (IEE, Zhou et al., 2007; see also Figure 7.4A) to stably and correctly process di- and polycistronic transgene mRNAs (Figure 7.4B). Transplastomic uses of the IEE include the introduction of genes into the tocopherol pathway of tobacco and tomato chloroplasts (Lu et al., 2013) as well as helping to

produce cyanobacteria Rubisco and an associated CcmM35 carboxysome protein in tobacco (Lin et al., 2014; see also Figure 5.1).

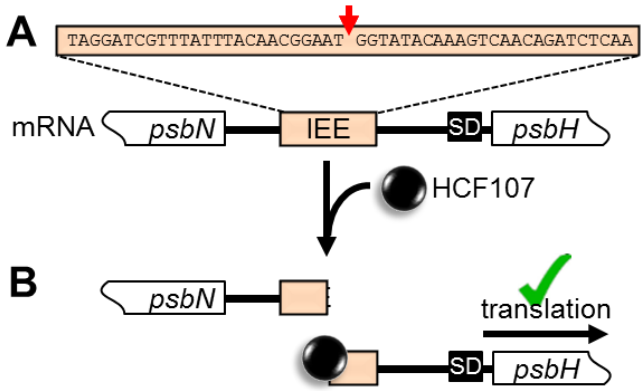

Figure 7.4 Sequence and function of the IEE in tobacco chloroplasts.

Shown is (A) the IEE sequence located between *psbN* and *psbH* in the LSC region of the tobacco plastome and its processing site (red arrow) by the protein HCF107 (black circle). (B) Schematic showing mRNA products following HCF107 scission with the protein remained bound to the 5' end to provide protection for exonucleases and to promote protein translation (green tick) through removal of inhibitory hairpin structures (Scharff and Bock, 2014).

The scission of synthetic polycistronic mRNAs by the IEE is highly efficient, independent of flanking sequence and produces stable monocistronic mRNAs with apparent enhanced translation potential (Lu et al., 2013; Scharff and Bock, 2014; Zhou et al., 2007). The IEE sequence is naturally located between *psbN* (coding a PSII P680 apoprotein) and *psbH* (coding a 10 kDa PSII phosphoprotein) in the large coding region of the tobacco plastome (77,037-77,086 nt; Genbank accession number Z00044.2) (Felder et al., 2001; see also Figure 7.4A). The IEE sequence is recognized by the tetratricopeptide repeat (TPR)-like protein HCF107. As a half-a-TPR (HAT) helical repeat protein, the HCF107 protein binds to the IEE sequence located –67 to –18 upstream (*i.e.* 5') of the AUG initiator codon in the *psbH* mRNA. The HCF107 cleaves the mRNA midway in the IEE stem-loop structure (Figure 7.4A). After this scission HCF107 continues to occupy the 5' end of the processed hairpin (Hammani et al., 2012). This binding is thought to have a dual effect. Firstly it forms a protective barrier to 5'-3' exonuclease activity on the mRNA (Figure 7.4B); second it is thought to activate *psbH* mRNA translation by removing inhibitory RNA folding structures that, in the unprocessed mRNA, would otherwise hinder ribosome engagement and translation initiation (Zhou et al., 2007; Stoppel and Meurer, 2013). This function is very similar to a number of pentatricopeptide repeat (PPR) proteins that function to stabilize and/or activate the translation of specific chloroplast RNAs (Barkan and Small, 2014).

As outlined in Figure 7.5A, exploiting the potential benefits of using the IEE sequence to enhance chloroplast S-subunit synthesis needs to be tested in ^{cm}trL$^{RNAi\text{-}S}$. Initial testing would focus on generating a transplastomic line where the intergenic sequence used in LEV^{T}L^{T}S is replaced with a terminator sequence and IEE sequence (Figure 7.5A). Tested example terminator sequences that could be introduced downstream of tobacco *rbcL* include the *rbcL* 3'UTR sequence from *Chlamydomonas reinhardtii* (Lu et al., 2013), the 3'UTR sequence from *Arabidopsis rps16* (Kuroda and Sugiura, 2014) or *psbA* (Coloapa-Soto et al., 2012). A comparison of the *RbcS* and *rbcL* mRNA levels and L_8S_8 Rubisco contents relative to those made in the LEV^{T}L^{T}S genotype would be used to gauge the relative merit of using the IEE transgenic approach to enhancing chloroplast S-subunit synthesis in ^{cm}trL$^{RNAi\text{-}S}$.

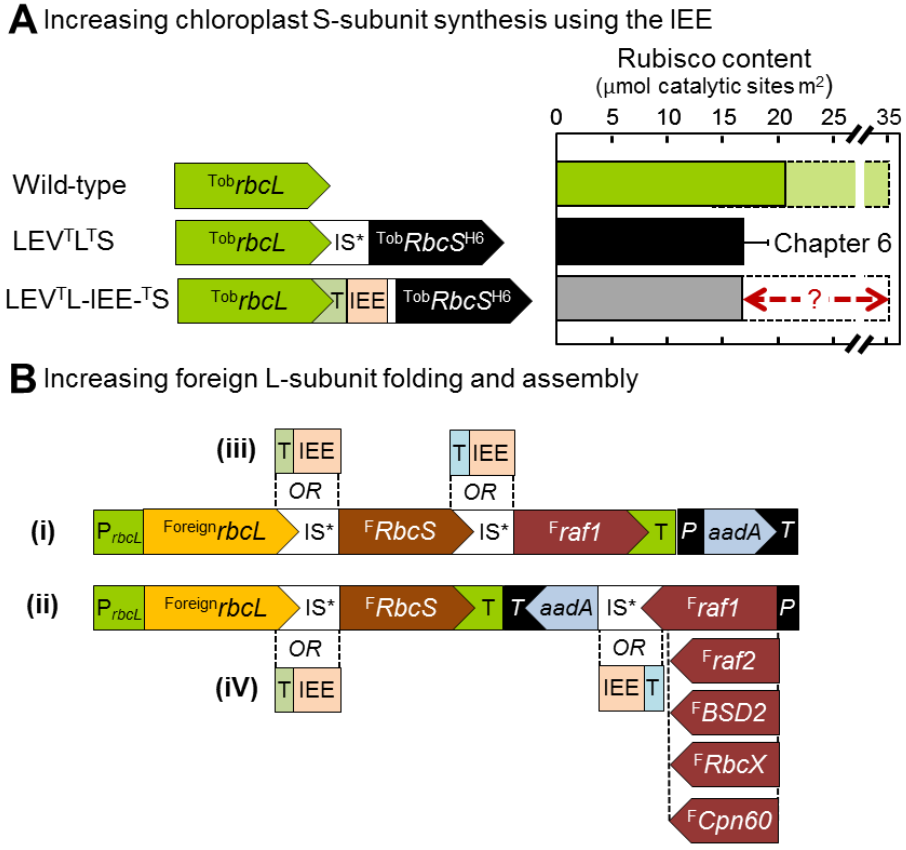

Figure 7.5 Increasing recombinant Rubisco biogenesis in ^{cm}trL$^{RNAi\text{-}S}$.

Possible future strategies to test how to improve L- and S-subunit synthesis in chloroplasts include (A) increasing S-subunit production by replacing the synthetic intergenic sequence (IS*) between *rbcL* and synthetic *RbcS* in LEV^{T}L^{T}S with a 'weak' terminator (T, light green) and IEE sequence (see text in Section 7.3.2 for more detail). (B) Strategies for increasing foreign L-subunit assembly include co-transforming in genes coding a cognate S-subunit (^{F}*RbcS*) and one or more complimentary assembly chaperones (e.g. RAF1, RAF2, BSD2, RbcX,) or chaperonin subunit (Cpn60α) (see Figure 4.3 and Sections 6.3.1 and 7.4 for more details). Testing the efficiency of transgene expression and Rubisco production might compare transplastomic lines producing a polycistronic ^{F}*rbcL*-^{F}*RbcS*-^{F}*raf1* mRNA (example [i]), separate and inverted genes coding ^{F}*rbcL*-^{F}*RbcS* and ^{F}*raf1-aadA* mRNAs (example [ii]) or monocistronic ^{F}*rbcL*, ^{F}*RbcS* and ^{F}*raf1* mRNA's by incorporating differing "weak" terminator (shaded light green and blue) and IEE sequences between the transgenes (examples [iii] and [iv]) to increase mRNA stability and enhance translation.

7.4 Enhancing L-subunit synthesis to increase recombinant L_8S_8 assembly

A key impediment to foreign L-subunit synthesis in tobacco chloroplasts appears associated with differences in their folding and assembly requirements. As indicated in Section 5.1.1, the folding and assembly requirements of Rubisco subunits from algae cannot be met in leaf chloroplasts (Whitney and Andrews, 2001b). Even L-subunits derived from plant species show differing levels of compatibility with assembling in tobacco chloroplasts (Parry et al., 2013) – in some cases due to single amino acid differences (Whitney et al., 2011b). One reason for these incompatibilities stem from differences in the chaperoning requirements between species. Bioinformatics sequence comparisons in a recent study showed strong complementarity in the evolution pathways of the L-subunit and its assembly chaperone RAF1 (Whitney et al., 2015). This was experimentally tested using a transplastomic approach to produce genotypes expressing *Arabidopsis* Rubisco L-subunits alone or in combination with a complementary RAF1. As detailed in Section 6.1.3, Rubisco biogenesis was enhanced in the genotypes co-producing the cognate *Arabidopsis* RAF1 despite the very low amounts of polycistronic *rbcL-raf1-aadA* mRNA produced (Whitney et al., 2015). This demonstrated the L-subunit assembly role of RAF1 and how foreign Rubisco biogenesis in tobacco leaves can be enhanced by its co-expression.

Increasing (or enabling) foreign Rubisco biogenesis in tobacco chloroplasts clearly needs to address the requirements for co-expression of complementary folding and assembly chaperone(s)/chaperonin proteins. In addition to RAF1, these might include other Rubisco specialized chaperones such as RAF2, BSD2, RbcX (Feiz et al., 2012; Parry et al., 2013; Feiz et al., 2014; see also Figure 4.3 and Section 6.3.1) and possibly the chloroplast targeted chaperonin 60 alpha subunit (Cpn60α) (Barkan, 1993; Kim et al., 2013; see also Figure 7.5B). Four possible plastome transformation approaches for co-introducing genes of foreign Rubisco subunits and their homologous chaperones into the $^{cm}trL^{RNAi\text{-}S}$ plastome are shown in Figure 7.5B. These include replacing *rbcM* in $^{cm}trL^{RNAi\text{-}S}$ with a genetic structure that produces either a single ^{F}*rbcL*-^{F}*RbcS*-^{F}*chaperone*1 polycistronic mRNA and independent *aadA* mRNA (option [i]) or separate ^{F}*rbcL*-^{F}*RbcS* and ^{F}*chaperone*1-*aadA* mRNAs (option [ii]). Alternative options might be to integrate "weak" terminator (shaded light green and blue) and IEE sequences (options [iii] and [iv]) to produce monocistronic ^{F}*rbcL*, ^{F}*RbcS* and ^{F}*chaperone* mRNA's. A comparison of mRNA levels and Rubisco content in all four genotypes would determine to what extent (1) incorporating the T-IEE sequences enhanced transgene mRNA content and their translation and (2) which chaperones can

augment foreign Rubisco biogenesis in tobacco leaf chloroplasts. This approach would identify the ancillary proteins considered vital for Rubisco biogenesis in plastids and provide potential genetic approaches for transforming the genes for one or more of these proteins with the *rbcL* and *RbcS* of their cognate Rubisco.

7.5 The effect of the S-subunit on catalysis

As discussed in Section 6.3.2, sequence differences between heterologous L- and S-subunits can impede L_8S_8 biogenesis, but not necessarily catalysis. As shown in Table 6.2, L_8S_8 Rubisco comprising tobacco L-subunits and either 6×His-tagged tobacco or sunflower S-subunits share the same catalytic properties. As summarized in Table 5.1, this finding is akin to finding that the assembly of tobacco S-subunits with L-subunits from sunflower, *Flaveria* and tomato Rubisco have little or no influence on catalysis (Kanevski et al., 1999; Whitney et al., 2001b; Zhang et al., 2011). More recently however the assembly of tobacco S-subunits with *Arabidopsis* L-subunits was found to slow catalysis by ~25% (Whitney et al., 2015). These contrasting influences of heterologous S-subunits on hybrid Rubisco catalysis highlight the need to better understand the structure-function interactions between L- and S-subunits.

Analyses of crystal structure information for varying L_8S_8 isoforms provide valuable insights into amino acid interactions at the L/L-, L/S- and S/S-subunit interfaces (van Lun et al., 2011). A deficiency of such structural analyses is being able to ascertain the functional significance of these interactions and any subunit sequence differences. This requires experimental testing. As presented in Section 1.2.2, the majority of mutagenic studies examining S- and L-subunit interactions have been undertaken using *Chlamydomonas reinhardtii* (Spreitzer, 2003; Karkehabadi et al., 2005; Genkov and Spreitzer, 2009) or forms that can be functionally expressed in *E. coli* (e.g. Rubisco from cyanobacteria and photosynthetic proteobacteria) (Read and Tabita, 1994; Kellogg and Juliano, 1997; Joshi et al., 2015). The $^{cm}trL^{RNAi\text{-}S}$ genotype developed in thesis however now provides a viable opportunity to start expanding these structure-function studies to the L- and S-subunits of higher plant Rubisco (although likely with some optimization as described above in Sections 7.3 and 7.4). The proven efficiency and stability of the RNAi-*RbcS* silencing of S-subunit synthesis through multiple generations of the $^{cm}trL^{RNAi\text{-}S}$ genotype (Figure 3.9) is of particular benefit as it negates the need to include an affinity tag on the recombinant S-subunit, which was shown to slow Rubisco catalysis by ~one-third (see Section 6.3.3).

While the $^{cm}trL^{RNAi\text{-}S}$ genotype poses new opportunities to surgically unravel L- and S-subunit structural interactions via targeted mutagenesis using chloroplast transformation, the challenge is to identify the starting point(s) for this mutagenic testing. The work of Spreitzer et al. (2005) highlights the potential benefit of altering *Chlamydomonas* Rubisco catalysis by directed changes to the S-subunit βA/βB loop and the adjoining L-subunit amino acids. Identifying changes to make in the comparable regions of higher plant Rubisco L- and S-subunits poses a potentially good starting point – if viable alternatives were apparent. Identifying beneficial amino acid modifications may however require a more strategic approach. For example a more detailed study of the natural variation in Rubisco catalysis and their L- and S-subunit sequences may provide better guidance on amino acid mutations to test (Parry et al., 2013). A more focused approach may simply concentrate on the significance of the natural S-subunit diversity within a species. For example, the four S-subunit isoforms produced in *Arabidopsis* (that are each 123 amino acids in length) vary by up to 8 amino acids (The *Arabidopsis* Initiative, 2000). Whether these S-subunit differences alter Rubisco catalysis remains unknown. A preliminary analysis of the Phytozome plant genome database (http://www.phytozome.net) for *RbcS* sequences in eucalyptus (*Eucalyptus grandis*), potato (*Solanum tuberosum*) and cassava (*Manihot esculenta*) (representative species whose L-subunits can fold and assemble in tobacco chloroplasts) (Kapralov and Whitney, unpublished) identified varying degrees of sequence diversity in their mature S-subunits (Figure 7.6). The number of *RbcS* alleles were identified: five in eucalyptus, four in potato and three in cassava. A comparison of the translated amino acid sequence for the mature coding region of each allele found they each coded different S-subunit sequences of varying diversity. The S-subunits in cassava show between 54 and 87% identity, in potato between 59 and 96% identity and in eucalyptus between 59 and 89% identity (Figure 7.6). This large sequence variation in S-subunit sequence within these three species contrasts with the modest amino acid diversity (*i.e.* only 7.3%) found among the 9 different S-subunit isoforms produced in tobacco (*N. tabacum*) (Figure 3.6B).

Compelling questions that remain untested include how the S-subunit sequence diversity in eucalyptus, potato and cassava (and to a lesser extent *Arabidopsis* and tobacco) influence the catalytic properties of plant Rubisco and can this help identify catalytic switches in S-subunits and/or L-subunits? Testing these questions is now experimentally feasible using the $^{cm}trL^{RNAi\text{-}S}$ genotype given its capacity to produce L_8S_8 Rubisco comprising a homogeneous population of L- and S-subunits – both made

in the chloroplast. A key outcome of preliminary experiments would be to identify the extent to which each S-subunit isoform differentially affects catalysis. Subsequent comparisons of the structure-function data would help identify candidate amino acid residues ("catalytic switches") responsible for any changes in catalysis, thus providing targets for further mutagenic testing using ^{cm}trL$^{RNAi\text{-}S}$. An experimental pathway such as this will be critical for reaching the ultimate objective of identifying solutions for engineering Rubisco L- and S-subunits to improve catalysis.

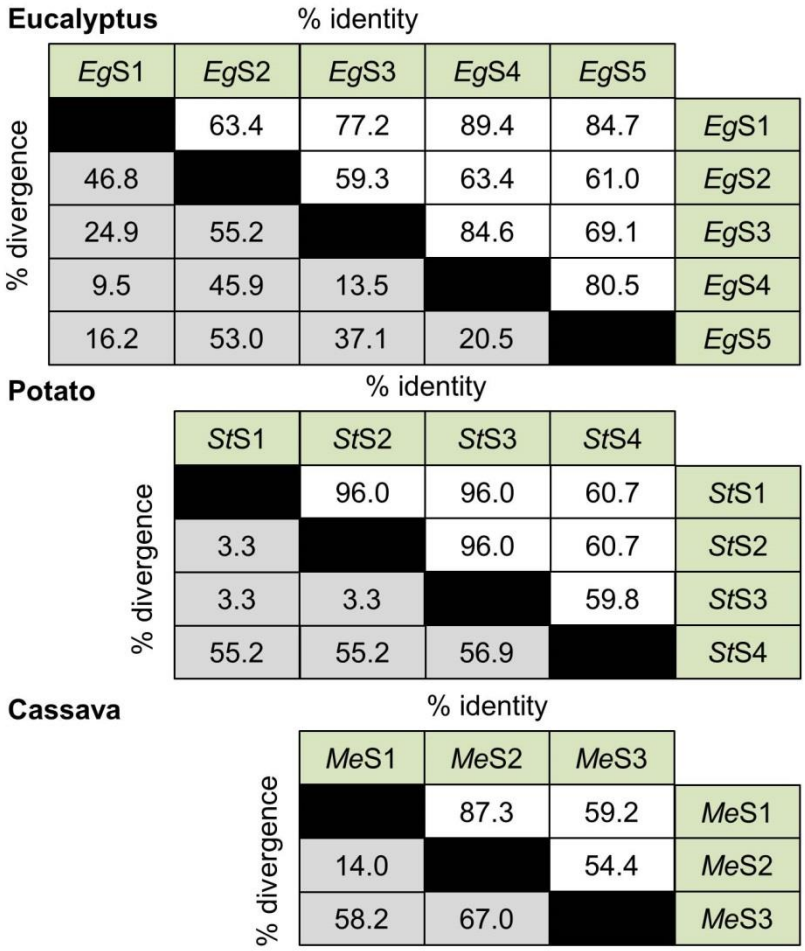

Figure 7.6 S-subunit sequence diversity amongst various plant species.

Matrix of sequence identities (white) and divergence (shaded grey) for the mature S-subunits produced in eucalyptus (*Eg*S; *Eucalyptus grandis*), potato (*St*S; *Solanum tuberosum*) and cassava (*Me*S: *Manihot esculenta*). Sequences were obtained from Phytozome (http://www.phytozome.net) and aligned using Clustal W algorithm in MEGALIGN (DNASTAR).

7.6 Exploiting the RNAi silencing efficiency of ^{cm}trL to study the ancillary protein requirements of Rubisco

Additional applications for the ^{cm}trL genotype to study the biogenesis and activity regulatory requirements of Rubisco in leaf chloroplasts using RNAi-silencing are shown in Figure 7.7. Using plastome transformation or cross-pollination approaches, the

proposed RNAi-silencing applications take advantage of the atypical assembly and regulatory requirements of the *R. rubrum* L_2 Rubisco produced in ^{cm}trL. Unlike plant L_8S_8 Rubisco, the L_2 Rubisco has little or no accessory protein requirements for assembly or need for Rubisco activase for regulating activity. Analogous to the approach used in this thesis to generate the four ^{cm}trL$^{RNAi\text{-}S}$ lines (Chapter 3), the various nucleus encoded ancillary proteins considered important for L_8S_8 Rubisco biogenesis could be systematically silenced by RNAi in ^{cm}trL (Figure 7.7). The practicality of such an endeavor has been simplified by the recent availability of the *N. tabacum* genome sequence (Sierro et al., 2014). Initial targets for testing would be the putative Rubisco specific chaperones RAF1, RAF2 and BSD2 identified through the screening of maize photosynthetic mutants (Feiz et al., 2014). Also of interest is the potential role of RbcX on Rubisco assembly in leaf chloroplasts. While shown to assist in the assembly of cyanobacteria Rubisco in *E. coli* (Saschenbrecker et al., 2007), a functional role for RbcX in Rubisco biogenesis in cyanobacteria is unclear (Emlyn-Jones et al., 2006) and also unproven in leaf chloroplasts (Parry et al., 2013; Whitney et al., 2015). The systematic silencing of the mRNAs coding each of these (and other) ancillary proteins in ^{cm}trL by RNAi should have no effect on plant growth and phenotype if specific to L_8S_8 Rubisco biogenesis. This specificity would be confirmed by the reduction, or elimination, of L_8S_8 biogenesis in the progeny of wild-type tobacco that incorporated the RNAi-alleles via pollination with pollen from a ^{cm}trL$^{RNAi\text{-}chaperone}$ genotype (Figure 7.7). The ^{cm}trL$^{RNAi\text{-}chaperone}$ genotypes would also serve as suitable transformation hosts for the chloroplast transformation tests proposed in Figure 7.5B to test chaperone complementarity requirements for heterologous Rubisco assembly in tobacco chloroplasts subunits.

In addition to studying the proteins required for Rubisco biogenesis, there is increasing interest in studying the role of Rubisco activase (Premkumar et al., 2001) on photosynthesis (Parry et al., 2013; Carmo-Silva et al., 2014). The importance of RCA in maintaining Rubisco catalysis has been studied in many plant species by antisense-*rca* approaches (Jiang et al., 1994; Hammond et al., 1998; Jin et al., 2006). The higher sensitivity of RCA to inhibition under elevated temperatures relative to other photosynthetic proteins has drawn attention to increasing its thermal tolerance as a means to sustaining photosynthetic capacity under elevated heat stress (Kurek et al., 2007). Eliminating tobacco RCA production in ^{cm}trL by RNAi should again have no effect on plant phenotype and growth if its function is specific to L_8S_8 Rubisco. Potential uses of a ^{cm}trL$^{RNAi\text{-}RCA}$ genotype might be to extend on those proposed in

Figure 7.5B to include co-introduction of *rbcL*, *rbcS* and *rca* by chloroplast transformation. This would allow for simultaneous mutagenic structure-function studies of Rubisco and RCA to identify which sequences determine the species-specific interactions between these enzymes (Larson et al., 1997; Ott et al., 2000; Li et al., 2005) as well as more effectively test how transplantation of mutated or foreign RCA isoforms with higher thermal tolerance can improve the response of photosynthesis to elevated temperatures.

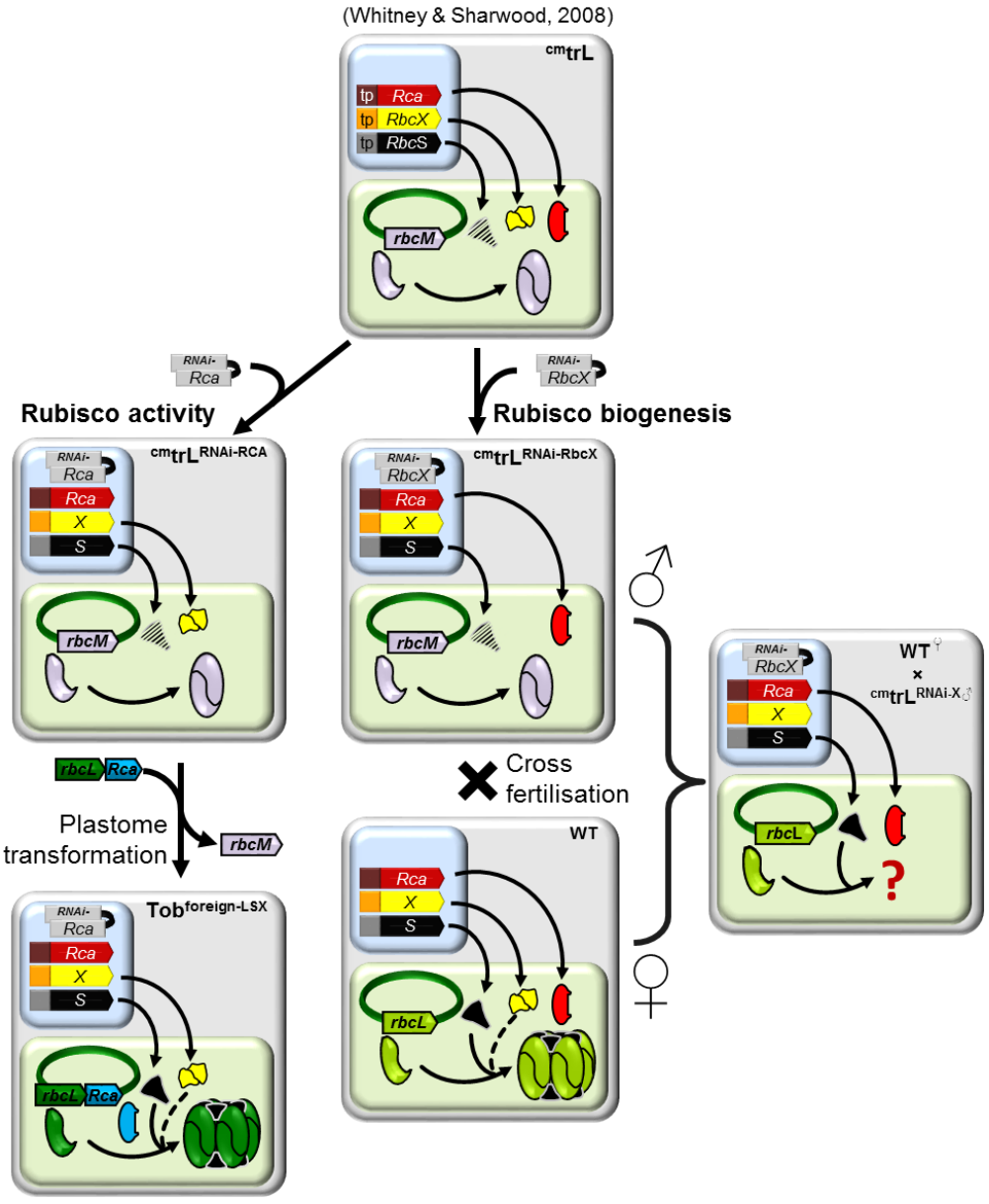

Figure 7.7 Strategies for studying other Rubisco-associated proteins in chloroplasts.

Using ^{cm}trL as a transformation host, the mRNA of other genes in the nucleus coding Rubisco ancillary proteins are silenced by RNAi. The examples shown demonstrate approaches for producing transgenic genotypes to study Rubisco-Rubisco activase interactions (Premkumar et al., 2001) and the putative role of the RbcX chaperone in L_8S_8 Rubisco biogenesis in leaf chloroplasts. Plastome transformation of the ^{cm}trL$^{RNAi\text{-}RCA}$ mutant is proposed to study Rubisco-RCA interactions compared with producing cross-pollinated wild-type♀ × ^{cm}trL$^{RNAi\text{-}RbcX}$♂ progeny to determine whether RbcX is needed for tobacco L_8S_8 biogenesis.

7.7 What is the minimal Rubisco amount needed to grow tobacco in soil?

A question among Rubisco bioengineers often raised is the lower limit of Rubisco needed for plants to be grown in soil under elevated CO_2. Obviously this will vary depending on the catalytic properties of the Rubisco in question (*i.e.* such that the slower the enzyme, the more that will be needed). Indeed one objective of putting a faster, more efficient Rubisco into plants is so less of the enzyme would be required to maintain current photosynthetic rates. This is seen as a strategy for potentially improving the nitrogen use of the plant (see Section 1.3.1) as seen in C_4 plants (Ghannoum et al., 2005). In the context of this thesis's findings and those of other transplastomic studies (Table 5.1 and Figure 6.1) the minimal amount of tobacco Rubisco (or catalytically comparable isoform) required for growth in soil at high-CO_2 is ~1 μmol Rubisco catalytic sites m^2. This value is derived from the observed success in being able to grow the RVSSuH♀ × ^{cm}trL$^{RNAi\text{-}S}$♂ genotype in soil under high-CO_2 (Figure 4.8C, ~1.2 μmol Rubisco catalytic sites m^2; see also Figure 4.9B) but not the LEVL-TobS^{H6} lines (Figure 5.7, <0.3 μmol Rubisco catalytic sites m^2; see also Figure 5.8B). Notably the growth rate of tobacco producing 1 μmol Rubisco catalytic sites m^2 would be very slow, even in air with 2% (v/v) CO_2 (Figure 4.8C).

7.8 Concluding remarks

Efforts to increase photosynthesis by modifying Rubisco catalysis have gained great momentum over recent years with the development of novel plastome transformation techniques and expansion of the technology to a range of crop plants (Whitney et al., 2011a; Parry et al., 2013). This thesis describes the development of new, innovative plastome transformation capabilities that will greatly aid these goals. The new ^{cm}trL$^{RNAi\text{-}S}$ genotype (or "2nd generation master-line") (Whitney and Sharwood, 2008) opens up new avenues for targeted studies of both the L- and S-subunits of plant Rubisco. With further experimental refinement of the transformation process (see Section 7.3), and better understanding of Rubisco biogenesis (see Sections 7.4 and 7.6), the ^{cm}trL$^{RNAi\text{-}S}$ genotype promises new frontiers in the bioengineering of Rubisco in higher plant chloroplasts.

REFERENCES

Abbaspour J, Ehsanpour AA, Amini F (2012) The role of Gibberellic acid on some physiological responses of transgenic tobacco (*Nicotiana tabacum L.)* plant carrying Ri T-DNA. Journal of Cell and Molecular Research **3:** 75-80

Adam Z, Frottin F, Espagne C, Meinnel T, Giglione C (2011) Interplay between N-terminal methionine excision and FtsH protease is essential for normal chloroplast development and function in *Arabidopsis*. The Plant Cell **23:** 3745-3760

Ahmadovich Bozorov T, Prakash Pandey S, Dinh ST, Kim S-G, Heinrich M, Gase K, Baldwin IT (2012) DICER-like proteins and their role in plant-herbivore interactions in *Nicotiana attenuata*. Journal of Integrative Plant Biology **54:** 189-206

Ainsworth EA, Ort DR (2010) How do we improve crop production in a warming world? Plant Physiology **154:** 526-530

Alban C, Tardif M, Mininno M, Brugière S, Gilgen A, Ma S, Mazzoleni M, Gigarel O, Martin-Laffon J, Ferro M, Ravanel S (2014) Uncovering the protein lysine and arginine methylation network in *Arabidopsis* chloroplasts. PLoS ONE **9:** e95512

Alkatib S, Fleischmann TT, Scharff LB, Bock R (2012) Evolutionary constraints on the plastid tRNA set decoding methionine and isoleucine. Nucleic Acids Research **40:** 6713-6724

Alonso H, Blayney MJ, Beck JL, Whitney SM (2009) Substrate-induced assembly of *Methanococcoides burtonii* d-Ribulose-1,5-bisphosphate Carboxylase/Oxygenase dimers into decamers. Journal of Biological Chemistry **284:** 33876-33882

Andersen K, Caton J (1987) Sequence analysis of the *Alcaligenes eutrophus* chromosomally encoded ribulose bisphosphate carboxylase large and small subunit genes and their gene products. Journal of Bacteriology **169:** 4547-4558

Andersson I (2008) Catalysis and regulation in Rubisco. Journal of Experimental Botany **59:** 1555-1568

Andersson I, Backlund A (2008) Structure and function of Rubisco. Plant Physiology and Biochemistry **46:** 275-291

Andersson I, Taylor TC (2003) Structural framework for catalysis and regulation in ribulose-1, 5-bisphosphate carboxylase/oxygenase. Archives of Biochemistry and Biophysics **414:** 130-140

Andrews TJ (1988) Catalysis by cyanobacterial ribulose-bisphosphate carboxylase large subunits in the complete absence of small subunits. Journal of Biological Chemistry **263:** 12213-12219

Andrews TJ, Ballment B (1983) The function of the small subunits of ribulose bisphosphate carboxylase/oxygenase. The Journal of Biological Chemistry **258:** 7514-7518

Andrews TJ, Ballment B (1984) A rapid, sensitive method for quantitating subunits in purified ribulose bisphosphate carboxylase preparations. Plant Physiology **75:** 508-510

Andrews TJ, Hudson GS, Mate CJ, von Caemmerer S, Evans JR, Arvidsson YBC (1995) Rubisco: The consequences of altering its expression and activation in transgenic plants. Journal of Experimental Botany **46:** 1293-1300

Andrews TJ, Lorimer GH (1985) Catalytic properties of a hybrid between cyanobacterial large subunits and higher plant small subunits of ribulose

bisphosphate carboxylase-oxygenase. Journal of Biological Chemistry **260:** 4632-4636

Andrews TJ, Lorimer GH & Tolbert NE (1971). Incorporation of molecular oxygen into glycine and serine during photorespiration in spinach leaves. Biochemistry **10:** 4777-4782

Andrews TJ, Whitney SM (2003) Manipulating ribulose bisphosphate carboxylase/oxygenase in the chloroplasts of higher plants. Archives of Biochemistry & Biophysics **414:** 159-169

Angov E (2011) Codon usage: Nature's roadmap to expression and folding of proteins. Biotechnology Journal **6:** 650-659

Ashida H, Danchin A, Yokota A (2005) Was photosynthetic RuBisCO recruited by acquisitive evolution from RuBisCO-like proteins involved in sulfur metabolism? Research in Microbiology **156:** 611-618

Assali N-E, Martin W, Sommerville C, Loiseaux-de Goër S (1991) Evolution of the Rubisco operon from prokaryotes to algae: Structure and analysis of the *rbcS* gene of the brown alga *Pylaiella littoralis*. Plant Molecular Biology **17:** 853-863

Badger MR, Andrews TJ, Whitney S, Ludwig M, Yellowlees DC, Leggat W, Price GD (1998) The diversity and coevolution of Rubisco, plastids, pyrenoids, and chloroplast-based CO_2-concentrating mechanisms in algae. Canadian Journal of Botany **76:** 1052-1071

Badger MR, Bek EJ (2008) Multiple Rubisco forms in proteobacteria: Their functional significance in relation to CO_2 acquisition by the CBB cycle. Journal of Experimental Botany **59:** 1525-1541

Bailey KJ, Battistelli A, Dever LV, Lea PJ, Leegood RC (2000) Control of C_4 photosynthesis: effects of reduced activities of phosphoenolpyruvate carboxylase on CO_2 assimilation in *Amaranthus edulis* L. Journal of Experimental Botany **51:** 339-346

Barkan A (1993) Nuclear mutants of maize with defects in chloroplast polysome assembly have altered chloroplast RNA metabolism. The Plant Cell **5:** 389-402

Barkan A, Small I (2014) Pentatricopeptide repeat proteins in plants. Annual Review of Plant Biology **65:** 415-442

Barkan A, Walker M, Nolasco M, Johnson D (1994) A nuclear mutation in maize blocks the processing and translation of several chloroplast mRNAs and provides evidence for the differential translation of alternative mRNA forms. The European Molecular Biology Organisation Journal **13:** 3170-3181

Basturea GN, Zundel MA, Deutscher MP (2011) Degradation of ribosomal RNA during starvation: Comparison to quality control during steady-state growth and a role for RNase PH. RNA **17:** 338-345

Bernacchi CJ, Bagley JE, Serbin SP, Ruiz-Vera UM, Rosenthal DM, Vanloocke A (2013) Modelling C_3 photosynthesis from the chloroplast to the ecosystem. Plant, Cell & Environment **36:** 1641-1657

Bernacchi CJ, Singsaas EL, Pimentel C, Portis AR, Long SP (2001) Improved temperature response functions for models of Rubisco-limited photosynthesis. Plant, Cell & Environment **24:** 253-259

Bitton DA, Okoniewski MJ, Connolly Y, Miller CJ (2008) Exon level integration of proteomics and microarray data. BMC Bioinformatics **9:** 118-118

Black MT, Meyer D, Widger WR, Cramer WA (1987) Light-regulated methylation of chloroplast proteins. Journal of Biological Chemistry **262:** 9803-9807

Black, RC, Binns, AN, Chang, CF, & Lynn, DG (1994) Cell-Autonomous Cytokinin-Independent Growth of Tobacco Cells Transformed by Agrobacterium tumefaciens Strains Lacking the Cytokinin Biosynthesis Gene. Plant Physiology **105:** 989-998

Blankenship RE (2002) Molecular mechanisms of photosynthesis. Blackwell Science, Cornwall, Great Britain.

Blayney MJ, Whitney SM, Beck JL (2011) NanoESI mass spectrometry of Rubisco and Rubisco activase structures and their interactions with nucleotides and sugar phosphates. Journal of the American Society for Mass Spectrometry **22:** 1588-1601

Blevins T, Rajeswaran R, Shivaprasad PV, Beknazariants D, Si-Ammour A, Park H-S, Vazquez F, Robertson D, Frederick Meins J, Hohn T, Pooggin MM (2006) Four plant Dicers mediate viral small RNA biogenesis and DNA virus induced silencing. Nucleic Acids Research **34:** 6233–6246

Block MD, Botterman J, Vandewiele M, Dockx J, Thoen C, Gosselé V, Movva NR, Thompson C, Montagu MV, Leemans J (1987) Engineering herbicide resistance in plants by expression of a detoxifying enzyme. The European Molecular Biology Organisation Journal **6:** 2513-2518

Bogorad L, Vasil IK (1991) The photosynthetic apparatus: Molecular biology and operation, Vool 7B. Elsevier Science, San Diego, California.

Bonham-Smith PC, Bourque DP (1989) Translation of chloroplast-encoded mRNA: Potential initiation and termination signals. Nucleic Acids Research **17:** 2057-2080

Bowes G, Ogren WL, Hageman RH (1971) Phosphoglycolate production catalyzed by ribulose diphosphate carboxylase. Biochemical and Biophysical Research Communications **45:** 716-722

Boynton JE, Gillham NW, Harris EH, Hosler JP, Johnson AM, Jones AR, Randolph. BL, Robertso. D, Klein TM, Shark KB (1988) Chloroplast transformation in Chlamydomonas with high-velocity microprojectiles. Science **240:** 1534-1538

Bracher A, Sharma A, Starling-Windhof A, Hartl FU, Hayer-Hartl M (2015) Degradation of potent Rubisco inhibitor by selective sugar phosphatase. Nature Plants **1**

Bracher A, Starling-Windhof A, Hartl FU, Hayer-Hartl M (2011) Crystal structure of a chaperone-bound assembly intermediate of form I Rubisco. Nature Structural & Molecular Biology **18:** 875-880

Bräsen C, Esser D, Rauch B, Siebers B (2014) Carbohydrate metabolism in archaea: Current insights into unusual enzymes and pathways and their regulation. Microbiology and Molecular Biology Reviews **78:** 89-175

Brutnell TP, Sawers RJH, Mant A, Langdale JA (1999) BUNDLE SHEATH DEFECTIVE2, a novel protein required for post-translational regulation of the *rbcL* gene of maize. Plant Cell **11:** 849-864

Buchan JR, Stansfield I (2007) Halting a cellular production line: Responses to ribosomal pausing during translation. Biology of the Cell **99:** 475-487

Carmo-Silva E, Scales JC, Madgwick PJ, Parry MAJ (2014) Optimizing Rubisco and its regulation for greater resource use efficiency. Plant, Cell & Environment

Chen C, Wang J, Zhao X (2016). Leaf senescence induced by EGY1 defection was partially restored by glucose in Arabidopsis thaliana. Botanical Studies, **57:** 1-9.

Chen K, Dorlhac de Borne F, Szegedi E, Otten L (2014) Deep sequencing of the ancestral tobacco species *Nicotiana tomentosiformis* reveals multiple T-DNA inserts and a complex evolutionary history of natural transformation in the genus *Nicotiana*. The Plant Journal **80:** 669-682

Chen Y-C, Aravin A (2015) Non-coding RNAs in transcriptional regulation. Current Molecular Biology Reports**:** 1-9

Choquet Y, Wollman F-A (2002) Translational regulations as specific traits of chloroplast gene expression. Federation of European Biochemical Societies Letters **529:** 39-42

Christie M, Croft LJ, Carroll BJ (2011) Intron splicing suppresses RNA silencing in *Arabidopsis*. The Plant Journal **68:** 159-167

Coate JE, Schlueter JA, Whaley AM, Doyle JJ (2011) Comparative evolution of photosynthetic genes in response to polyploid and nonpolyploid duplication. Plant Physiology **155:** 2081-2095

Coloapa-Soto D, Vargas-Suárez M, Loza-Tavera H (2012) Purification of an *Arabidopsis* chloroplast extract with *in vitro* RNA processing activity on *psbA* and *petD* 3′-untranslated regions. Journal of Plant Physiology **169:** 429-433

Daniell H, Kumar S, Dufourmantel N (2005) Breakthrough in chloroplast genetic engineering of agronomically important crops. Trends in Biotechnology **23:** 238-245

Day A, Goldschmidt-Clermont M (2011) The chloroplast transformation toolbox: Selectable markers and marker removal. Plant Biotechnology Journal **9:** 540-553

de Cosa B, Moar W, Lee S-B, Miller M, Daniell H (2001) Overexpression of the Bt cry2Aa2 operon in chloroplasts leads to formation of insecticidal crystals. Nature Biotechnology **19:** 71-74

Delwiche CF (1999) Tracing the thread of plastid diversity through the tapestry of life. The American Naturalist **154:** S164-S177

Dhingra A, Portis AR, Daniell H (2004) Enhanced translation of a chloroplast-expressed *RbcS* gene restores small subunit levels and photosynthesis in nuclear *RbcS* antisense plants. Proceedings of the National Academy of Sciences of the United States of America **101:** 6315-6320

Dobberstein B, Blobel G, Chua NH (1977) *In vitro* synthesis and processing of a putative precursor for the small subunit of ribulose-1,5-bisphosphate carboxylase of *Chlamydomonas reinhardtii*. Proceedings of the National Academy of Sciences of the United States of America **74:** 1082-1085

Drechsel O, Bock R (2011) Selection of Shine-Dalgarno sequences in plastids. Nucleic Acids Research **39:** 1427-1438

Duan C-G, Wang C-H, Guo H-S (2012) Application of RNA silencing to plant disease resistance. Silence **3:** 5

Durão P, Aigner H, Nagy P, Mueller-Cajar O, Hartl FU, Hayer-Hartl M (2015) Opposing effects of folding and assembly chaperones on evolvability of Rubisco. Nature Chemical Biollogy **11:** 148-155

Eberhard S, Finazzi G, Wollman FA (2008) The dynamics of photosynthesis. Annual Review of Genetics **42:** 463-515

Edwards GE, Franceschi VR, Voznesenskaya EV (2004) Single-cell C_4 photosynthesis versus the dual-cell (Kranz) paradigm. Annual Review of Plant Biology **55:** 173-196

Eichelmann H, Talts E, Oja V, Padu E, Laisk A (2009) Rubisco in planta k_{cat} is regulated in balance with photosynthetic electron transport. Journal of Experimental Botany **60:** 4077-4088

Ellis RJ (1979) The most abundant protein in the world. Trends in Biochemical Sciences **4:** 241-244

Emlyn-Jones D, Woodger FJ, Price GD, Whitney SM (2006) RbcX can function as a Rubisco chaperonin, but is non-essential in *Synechococcus* PCC7942. Plant and Cell Physiology **47:** 1630-1640

Ercolano MR, Ballvora A, Paal J, Steinbiss H-H, Salamini F, Gebhardt C (2004) Functional complementation analysis in potato via biolistic transformation with BAC large DNA fragments. Molecular Breeding **13:** 15-22

Esau B, Snyder G, Portis Jr A (1998) Activation of ribulose-1,5-bisphosphate carboxylase/oxygenase (Rubisco) with chimeric activase proteins. Photosynthesis Research **58:** 175-181

Evans JR (2013) Improving photosynthesis. Plant Physiology **162:** 1780-1793

Farquhar GD, von Caemmerer S, Berry JA (1980) A biochemical model of photosynthetic CO_2 assimilation in leaves of C_3 species. Planta **149:** 78-90

Feiz L, Williams-Carrier R, Belcher S, Montano M, Barkan A, Stern DB (2014) A protein with an inactive pterin-4a-carbinolamine dehydratase domain is required for Rubisco biogenesis in plants. The Plant Journal **80:** 862-869

Feiz L, Williams-Carrier R, Wostrikoff K, Belcher S, Barkan A, Stern DB (2012) Ribulose-1,5-bis-phosphate carboxylase/oxygenase Accumulation Factor1 is required for holoenzyme assembly in maize. The Plant Cell Online **24:** 3435-3446

Felder S, Meierhoff K, Sane AP, Meurer J, Driemel C, Plücken H, Klaff P, Stein B, Bechtold N, Westhoff P (2001) The nucleus-encoded HCF107 gene of *Arabidopsis* provides a link between intercistronic RNA processing and the accumulation of translation-competent *psbH* transcripts in chloroplasts. The Plant Cell **13:** 2127-2142

Feller U, Anders I, Mae T (2008) Rubiscolytics: Fate of Rubisco after its enzymatic function in a cell is terminated. Journal of Experimental Botany **59:** 1615-1624

Filipenko EA, Deineko EV, Shumnyi VK (2009) Specific features of T-DNA insertion regions in transgenic plants. Russian Journal of Genetics **45:** 1289-1301

Flores-Pérez Ú, Jarvis P (2013) Molecular chaperone involvement in chloroplast protein import. Biochimica et Biophysica Acta - Molecular Cell Research **1833:** 332-340

Fukayama H, Koga A, Hatanaka T, Misoo S (2015) Small subunit of a cold-resistant plant, timothy, does not significantly alter the catalytic properties of Rubisco in transgenic rice. Photosynthesis Research **124:** 57-65

Furbank RT, Chitty JA, von Caemmerer S, Jenkins CLD (1996) Antisense RNA inhibition of *RbcS* gene expression reduces rubisco level and photosynthesis in the C_4 plant *Flaveria bidentis*. Plant Physiology **111:** 725-734

Furbank RT, Hatch MD (1987) Mechanism of C_4 photosynthesis: The size and composition of the inorganic carbon pool in bundle sheath cells. Plant Physiology **85:** 958-964

Galmés J, Flexas J, Keys AJ, Cifre J, Mitchell RAC, Madgwick PJ, Haslam RP, Medrano H, Parry MAJ (2005) Rubisco specificity factor tends to be larger in plant species from drier habitats and in species with persistent leaves. Plant, Cell & Environment **28:** 571-579

Galmés J, Kapralov MV, Andralojc PJ, Conesa MÀ, Keys AJ, Parry MAJ, Flexas J (2014) Expanding knowledge of the Rubisco kinetics variability in plant species: Environmental and evolutionary trends. Plant, Cell & Environment **37:** 1989-2001

Genkov T, Meyer M, Griffiths H, Spreitzer RJ (2010) Functional hybrid Rubisco enzymes with plant small subunits and algal large subunits: Engineered *RbcS* cDNA for expression in *Chlamydomonas* Journal of Biological Chemistry **285:** 19833-19841

Genkov T, Spreitzer RJ (2009) Highly conserved small subunit residues influence Rubisco large subunit catalysis. Journal of Biological Chemistry **284:** 30105-30112

Getzoff TP, Zhu G, Bohnert HJ, Jensen RG (1998) Chimeric *Arabidopsis thaliana* ribulose-1,5-bisphosphate carboxylase/oxygenase containing a pea small subunit protein Is compromised in carbamylation. Plant Physiology **116:** 695-702

Ghannoum O, Evans JR, Chow WS, Andrews TJ, Conroy JP, von Caemmerer S (2005) Faster Rubisco is the key to superior nitrogen-use efficiency in NADP-Malic enzyme relative to NAD-Malic enzyme C_4 grasses. Plant Physiology **137:** 638-650

Ghannoum O, Evans JR, von Caemmerer S (2011) Nitrogen and water use efficiency of C_4 plants. *In* AS Raghavendra, RF Sage, eds, C_4 Photosynthesis and related CO_2 concentrating mechanisms, Vol 32. Springer Netherlands, pp 129-146

Gleason JE, Galaleldeen A, Peterson RL, Taylor AB, Holloway SP, Waninger-Saroni J, Cormack BP, Cabelli DE, Hart PJ, Culotta VC (2014) *Candida albicans* SOD5 represents the prototype of an unprecedented class of Cu-only superoxide dismutases required for pathogen defense. Proceedings of the National Academy of Sciences of the United States of America **111:** 5866-5871

Gong L, Olson M, Wendel JF (2014) Cytonuclear evolution of Rubisco in four allopolyploid lineages. Molecular Biology and Evolution **31:** 2624-2636

Goodin MM, Zaitlin D, Naidu RA, Lommel SA (2008) *Nicotiana benthamiana*: Its history and future as a model for plant-pathogen interactions. Molecular Plant-Microbe Interactions Journal **21:** 1015-1026

Gray JC, Kung SD, Wildman SG, Sheen SJ (1974) Origin of *Nicotiana tabacum* L. detected by polypeptide composition of Fraction I protein. Nature **252:** 226-227

Gunn L (2014) Exploring novel *in planta* and *in vitro* approaches for bioengineering Rubisco (Doctoral dissertation). Australian National University, Canberra

Gupta PK (2009) Cell and molecular biology. Rastogi, Meerut

Gustafsson C, Govindarajan S, Minshull J (2004) Codon bias and heterologous protein expression. Trends in Biotechnology **22:** 346-353

Haimovich-Dayan M, Lieman-Hurwitz J, Orf I, Hagemann M, Kaplan A (2014) Does 2-phosphoglycolate serve as an internal signal molecule of inorganic carbon deprivation in the cyanobacterium *Synechocystis* sp. PCC 6803? Environmental Microbiology **17:** 1794-1804

Hammani K, Cook WB, Barkan A (2012) RNA binding and RNA remodeling activities of the half-a-tetratricopeptide (HAT) protein HCF107 underlie its effects on gene expression. Proceedings of the National Academy of Sciences of the United States of America **109:** 5651-5656

Hammond ET, Andrews TJ, Woodrow IE (1998) Regulation of ribulose-1,5-bisphosphate carboxylase/oxygenase by carbamylation and 2-Carboxyarabinitol 1-Phosphate in tobacco: Insights from studies of antisense plants containing reduced amounts of Rubisco activase. Plant Physiology **118:** 1463-1471

Han M-H, Goud S, Song L, Fedoroff N (2004) The *Arabidopsis* double-stranded RNA-binding protein HYL1 plays a role in microRNA-mediated gene regulation. Proceedings of the National Academy of Sciences of the United States of America **101:** 1093-1098

Hanson TE, Tabita FR (2001) A ribulose-1,5-bisphosphate carboxylase/oxygenase (RubisCO)-like protein from *Chlorobium tepidum* that is involved with sulfur metabolism and the response to oxidative stress. Proceedings of the National Academy of Sciences of the United States of America **98:** 4397-4402

Hartl FU, Bracher A, Hayer-Hartl M (2011) Molecular chaperones in protein folding and proteostasis. Nature **475:** 324-332

Haseloff J, Siemering KR, Prasher DC, Hodge S (1997) Removal of a cryptic intron and subcellular localization of green fluorescent protein are required to mark transgenic *Arabidopsis* plants brightly. Proceedings of the National Academy of Sciences of the United States of America **94:** 2122-2127

Haußühl K, Andersson B, Adamska I (2001) A chloroplast DegP2 protease performs the primary cleavage of the photodamaged D1 protein in plant photosystem II. The European Molecular Biology Organisation Journal **20:** 713-722

Havaux M, Tardy F (1999) Loss of chlorophyll with limited reduction of photosynthesis as an adaptive response of Syrian barley landraces to high-light and heat stress. Functional Plant Biology **26:** 569-578

Heitzer M, Eckert A, Fuhrmann M, Griesbeck C (2007) Influence of codon bias on the expression of foreign genes in microalgae. *In* R León, A Galván, E Fernández, eds, Transgenic Microalgae as Green Cell Factories, Vol 616. Springer New York, pp 46-53

Herrmann M, Rusznyák A, Akob DM, Schulze I, Opitz S, Totsche KU, Küsel K (2015) Large fractions of CO_2-fixing microorganisms in pristine limestone aquifers appear to be involved in the oxidation of reduced sulfur and nitrogen compounds. Applied and Environmental Microbiology **81:** 2384-2394

Hibberd JM, Sheehy JE, Langdale JA (2008) Using C_4 photosynthesis to increase the yield of rice—rationale and feasibility. Current Opinion in Plant Biology **11:** 228-231

Hily J-M, Ravelonandro M, DAmsteegt V, Bassett C, Petri C, Liu Z, Scorza R (2007) Plum pox virus coat protein gene intron-hairpin-RNA (ihpRNA) constructs provide resistance to plum pox virus in *Nicotiana benthamiana* and *Prunus domestica*. The Journal of the American Society for Horticultural Science **132:** 850-858

Hoekema A, Hirsch PR, Hooykass PJJ, Schilperoort RA (1983) A binary plant vector strategy based on separation of *vir*- and T-region of the *Agrobacterium tumefaciens* Ti-plasmid. Nature **303:** 179-180

Houtz RL, Magnani R, Nayak NR, Dirk LMA (2008) Co- and post-translational modifications in Rubisco: Unanswered questions. Journal of Experimental Botany **59:** 1635-1645

Houtz RL, Mulligan RM (1991) Protection of tryptic-sensitive sites in the large subunit of ribulosebisphosphate carboxylase/oxygenase by catalysis. Plant Physiology **96:** 335-339

Houtz RL, Stults JT, Mulligan RM, Tolbert NE (1989) Post-translational modifications in the large subunit of ribulose bisphosphate carboxylase/oxygenase. **86:** 1855-1859

Huang S, Cerny RE, Qi Y, Bhat D, Aydt CM, Hanson DD, Ness LA (2003) Transgenic studies on the involvement of Cytokinin and Gibberellin in male development. Plant Physiology, **131:** 1270-1282

Hudson GS, Evans JR, von Caemmerer S, Arvidsson YBC, Andrews TJ (1992) Reduction of ribulose-1,5-bisphosphate carboxylase/oxygenase content by antisense RNA reduces photosynthesis in transgenic tobacco plants. Plant Physiology **98:** 294-302

Intrieri MC, Buiatti M (2001) The horizontal transfer of *Agrobacterium rhizogenes* genes and the evolution of the genus *Nicotiana*. Molecular Phylogenetics and evolution **20:** 100-110

Ishikawa C, Hatanaka T, Misoo S, Miyake C, Fukayama H (2011) Functional incorporation of sorghum small subunit increases the catalytic turnover rate of Rubisco in transgenic rice. Plant Physiology **156:** 1603-1611

Izumi M, Tsunoda H, Suzuki Y, Makino A, Ishida H (2012) R*BCS*1A and R*BCS*3B, two major members within the *Arabidopsis RBCS* multigene family, function to yield sufficient Rubisco content for leaf photosynthetic capacity. Journal of Experimental Botany **63:** 2159-2170

Jiang C-Z, Quick WP, Alred R, Kliebenstein D, Rodermel SR (1994) Antisense RNA inhibition of Rubisco activase expression. The Plant Journal **5:** 787-798

Jin S-H, Hong J, Li X-Q, Jiang D-A (2006) Antisense inhibition of Rubisco activase increases Rubisco content and alters the proportion of Rubisco activase in stroma and thylakoids in chloroplasts of rice leaves. Annals of Botany **97:** 739-744

Johnson X, Wostrikoff K, Finazzi G, Kuras R, Schwarz C, Bujaldon S, Nickelsen J, Stern DB, Wollman F-A, Vallon O (2010) MRL1, a conserved pentatricopeptide repeat protein, is required for stabilization of *rbcL* mRNA in *Chlamydomonas* and *Arabidopsis*. The Plant Cell **22:** 234-248

Joshi J, Mueller-Cajar O, Tsai Y-CC, Hartl FU, Hayer-Hartl M (2015) Role of small subunit in mediating assembly of red-type form I Rubisco. Journal of Biological Chemistry **290:** 1066-1074

Justice NB, Norman A, Brown CT, Singh A, Thomas BC, Banfield JF (2014) Comparison of environmental and isolate Sulfobacillus genomes reveals diverse carbon, sulfur, nitrogen, and hydrogen metabolisms. BMC Genomics **15:** 1107

Juszczak I, Rudnik R, Pietzenuk B, Baier M (2012) Natural genetic variation in the expression regulation of the chloroplast antioxidant system among *Arabidopsis thaliana* accessions. Physiologia Plantarum **146:** 53-70

Kabeya Y, Miyagishima S-y (2013) Chloroplast DNA replication is regulated by the redox state independently of chloroplast division in *Chlamydomonas reinhardtii*. Plant Physiology **161:** 2102-2112

Kanai R, Edwards GE (1999) The biochemistry of C_4 photosynthesis. Academic Press, UK

Kane H, Viil J, Entsch B, Paul K, Morell M, Andrews T (1994) An improved method for measuring the CO_2/O_2 specificity of ribulosebisphosphate carboxylase-oxygenase. Functional Plant Biology **21:** 449-461

Kanevski I, Maliga P (1994) Relocation of the plastid *rbcL* gene to the nucleus yields functional ribulose-1,5-bisphosphate carboxylase in tobacco chloroplasts. Proceedings of the National Academy of Sciences of the United States of America **91:** 1969-1973

Kanevski I, Maliga P, Rhoades DF, Gutteridge S (1999) Plastome engineering of ribulose-1,5-bisphosphate carboxylase/oxygenase in tobacco to form a sunflower large subunit and tobacco small subunit hybrid. Plant Physiology **119:** 133-142

Kannappan B, Gready JE (2008) Redefinition of Rubisco carboxylase reaction reveals origin of water for hydration and new roles for active-site residues. Journal of the American Chemical Society **130:** 15063-15080

Kapralov MV, Kubien DS, Andersson I, Filatov DA (2011) Changes in Rubisco kinetics during the evolution of C_4 photosynthesis in *Flaveria* (Asteraceae) are associated with positive selection on genes encoding the enzyme. Molecular Biology and Evolution **28:** 1491-1503

Karkehabadi S, Peddi SR, Anwaruzzaman M, Taylor TC, Cederlund A, Genkov T, Andersson I, Spreitzer RJ (2005) Chimeric small subunits influence catalysis without causing global conformational changes in the crystal structure of ribulose-1,5-bisphosphate carboxylase/oxygenase. Biochemistry **44:** 9851-9861

Karki S, Rizal G, Quick W (2013) Improvement of photosynthesis in rice (*Oryza sativa* L.) by inserting the C_4 pathway. Rice **6:** 28

Kaufman AJ (2014) Early earth: Cyanobacteria at work. Nature Geoscience **7:** 253-254
Kellogg E, Juliano N (1997) The structure and function of RuBisCO and their implications for systematic studies. American Journal of Botany **84:** 413
Kerschen A, Napoli CA, Jorgensen RA, Müller AE (2004) Effectiveness of RNA interference in transgenic plants. Federation of European Biochemical Societies Letters **566:** 223-228
Khrebtukova I, Spreitzer RJ (1996) Elimination of the *Chlamydomonas* gene family that encodes the small subunit of ribulose-1,5-bisphosphate carboxylase/oxygenase. Proceedings of the National Academy of Sciences of the United States of America **93:** 13689-13693
Khvorova A, Reynolds A, Jayasena SD (2003) Functional siRNAs and miRNAs exhibit strand bias. Cell **115:** 209-216
Kim J, Mullet J (1994) Ribosome-binding sites on chloroplast *rbcL* and *psbA* mRNAs and light-induced initiation of D1 translation. Plant Molecular Biology **25:** 437-448
Kim S-R, Yang J-I, An G (2013) OsCpn60α1, encoding the plastid chaperonin 60α subunit, is essential for folding of *rbcL*. Molecules and Cells **35:** 402-409
Kisaki T, Tolbert N (1969) Glycolate and glyoxylate metabolism by isolated peroxisomes or chloroplasts. Plant Physiology **44:** 242-250
Kitano K, Maeda N, Fukui T, Atomi H, Imanaka T, Miki K (2001) Crystal structure of a novel-type archaeal Rubisco with pentagonal symmetry. Structure **9:** 473-481
Kriechbaumer V, Nabok A, Mustafa MK, Al-Ammar R, Tsargorodskaya A, Smith DP, Abell BM (2012) Analysis of protein interactions at native chloroplast membranes by ellipsometry. PLoS ONE **7:** e34455
Kubien DS, Sage RF (2008) The temperature response of photosynthesis and metabolites in anti-*RbcS* tobacco. *In* J Allen, E Gantt, J Golbeck, B Osmond, eds, Photosynthesis. Energy from the Sun. Springer Netherlands, pp 857-861
Kubien DS, von Caemmerer S, Furbank RT, Sage RF (2003) C_4 photosynthesis at low temperature. A study using transgenic plants with reduced amounts of Rubisco. Plant Physiology **132:** 1577-1585
Kumar A, Li C, Portis A, Jr. (2009) *Arabidopsis thaliana* expressing a thermostable chimeric Rubisco activase exhibits enhanced growth and higher rates of photosynthesis at moderately high temperatures. Photosynthesis Research **100:** 143-153
Kurek I, Chang TK, Bertain SM, Madrigal A, Liu L, Lassner MW, Zhu G (2007) Enhanced thermostability of *Arabidopsis* Rubisco activase improves photosynthesis and growth rates under moderate heat stress. The Plant Cell **19:** 3230-3241
Kurihara Y, Takashi Y, Watanabe Y (2006) The interaction between DCL1 and HYL1 is important for efficient and precise processing of pri-miRNA in plant microRNA biogenesis. RNA **12:** 206-212
Kuroda H, Maliga P (2001a) Complementarity of the 16S rRNA penultimate stem with sequences downstream of the AUG destabilizes the plastid mRNAs. Nucleic Acids Research **29:** 970-975
Kuroda H, Maliga P (2001b) Sequences downstream of the translation initiation codon are important determinants of translation efficiency in chloroplasts. Plant Physiology **125:** 430-436
Kuroda H, Maliga P (2003) The plastid clpP1 protease gene is essential for plant development. Nature **425:** 86-89

Kuroda H, Sugiura M (2014) Processing of the 5′-UTR and existence of protein factors that regulate translation of tobacco chloroplast psbN mRNA. Plant Molecular Biology **86:** 585-593

Larson EM, O'Brien CM, Zhu G, Spreitzer RJ, Portis AR (1997) Specificity for activase is changed by a Pro-89 to Arg substitution in the large subunit of ribulose-1,5-bisphosphate carboxylase/oxygenase. Journal of Biological Chemistry **272:** 17033-17037

Leister D (2012) Retrograde signaling in plants: From simple to complex scenarios. Frontiers in Plant Science **3:** 135

Li C, Salvucci ME, Portis AR (2005) Two residues of Rubisco activase involved in recognition of the Rubisco substrate. Journal of Biological Chemistry **280:** 24864-24869

Li H-M, Chiu C-C (2010) Protein transport into chloroplasts. Annual Review of Plant Biology **61:** 157-180

Lin MT, Occhialini A, Andralojc PJ, Parry MAJ, Hanson MR (2014) A faster Rubisco with potential to increase photosynthesis in crops. Nature **513:** 547-550

Liu C, Young AL, Starling-Windhof A, Bracher A, Saschenbrecker S, Rao BV, Rao KV, Berninghausen O, Mielke T, Hartl FU, Beckmann R, Hayer-Hartl M (2010) Coupled chaperone action in folding and assembly of hexadecameric Rubisco. Nature **463:** 197-202

Long BM, Badger MR, Whitney SM, Price GD (2007) Analysis of carboxysomes from *Synechococcus* PCC7942 reveals multiple Rubisco complexes with carboxysomal proteins CcmM and CcaA. Journal of Biological Chemistry **282:** 29323-29335

Long BM, Price GD, Badger MR (2005) Proteomic assessment of an established technique for carboxysome enrichment from *Synechococcus* PCC7942. Canadian Journal of Botany **83:** 746-757

Long SP, Marshall-Colon A, Zhu X-G (2015) Meeting the global food demand of the future by engineering crop photosynthesis and yield potential. Cell **161:** 56-66

Lu Y, Rijzaani H, Karcher D, Ruf S, Bock R (2013) Efficient metabolic pathway engineering in transgenic tobacco and tomato plastids with synthetic multigene operons. Proceedings of the National Academy of Sciences of the United States of America **110:** E623–E632

Ludwig M (2013) Evolution of the C_4 photosynthetic pathway: Events at the cellular and molecular levels. Photosynthesis Research **117:** 147-161

Lutz KA, Azhagiri AK, Tungsuchat-Huang T, Maliga P (2007) A guide to choosing vectors for transformation of the plastid genome of higher plants. Plant Physiology **145:** 1201-1210

Lutz KA, Knapp JE, Maliga P (2001) Expression of *bar* in the plastid genome confers herbicide resistance. Plant Physiology **125:** 1585-1590

Mäenpää P, Gonzalez EB, Chen L, Khan MS, Gray JC, Aro EM (2000) The *ycf 9* (*orf 62*) gene in the plant chloroplast genome encodes a hydrophobic protein of stromal thylakoid membranes. Journal of Experimental Botany **51:** 375-382

Makino A, Shimada T, Takumi S, Kaneko K, Matsuoka M, Shimamoto K, Nakano H, Miyao-Tokutomi M, Mae T, Yamamoto N (1997) Does decrease in ribulose-1,5-bisphosphate carboxylase by antisense *RbcS* lead to a higher N-use efficiency of photosynthesis under conditions of saturating CO_2 and light in rice plants? Plant Physiology **114:** 483-491

Maliga P (2002) Engineering the plastid genome of higher plants. Current Opinion in Plant Biology **5:** 164-172

Maliga P (2003) Progress towards commercialization of plastid transformation technology. Trends in Biotechnology **21:** 20-28

Maliga P (2004) Plastid transformation in higher plants. Annual Review of Plant Biology **55:** 289-313

Maliga P, Bock R (2011) Plastid biotechnology: Food, fuel, and medicine for the 21st century. Plant Physiology **155:** 1501-1510

Mallmann J, Heckmann D, Bräutigam A, Lercher MJ, Weber AP, Westhoff P, Gowik U (2014) The role of photorespiration during the evolution of C_4 photosynthesis in the genus *Flaveria*. Elife **3:** e02478

Manzara T, Gruissem W (1988) Organization and expression of the genes encoding ribulose-1,5-bisphosphate carboxylase in higher plants. Photosynthesis Research **16:** 117-139

Martin W, Kowallik K (1999) Annotated English translation of Mereschkowsky's 1905 paper 'Über natur und ursprung der chromatophoren imPflanzenreiche'. European Journal of Phycology **34:** 287-295

Martinez J, Tuschl T (2004) RISC is a 5′ phosphomonoester-producing RNA endonuclease. Genes & Development **18:** 975-980

Mašek T, Valášek L, Pospíšek M (2011) Polysome analysis and RNA purification from sucrose gradients. *In* H Nielsen, ed, RNA, Vol 703. Humana Press, pp 293-309

Maurino VG, Peterhansel C (2010) Photorespiration: Current status and approaches for metabolic engineering. Current Opinion in Plant Biology **13:** 248-255

Mayfield SP, Yohn CB, Cohen A, Danon A (1995) Regulation of chloroplast gene expression. Annual Review of Plant Physiology and Plant Molecular Biology **46:** 147-166

Michelet L, Zaffagnini M, Morisse S, Sparla F, Pérez-Pérez ME, Francia F, Danon A, Marchand CH, Fermani S, Trost P, Lemaire SD (2013) Redox regulation of the Calvin–Benson cycle: Something old, something new. Frontiers in Plant Science **4:** 470

Mohajjel-Shoja H, Clément B, Perot J, Alioua M, Otten L (2011) Biological activity of the *Agrobacterium rhizogenes*-derived *trolC* gene of *Nicotiana tabacum* and its functional relation to other plast genes. Molecular Plant-Microbe Interactions **24:** 44-53

Morell MK, Kane HJ, Andrews TJ (1990) Carboxylterminal deletion mutants of ribulosebisphosphate carboxylase from *Rhodospirillum rubrum*. Federation of European Biochemical Societies Letters **265:** 41-45

Morita K, Hatanaka T, Misoo S, Fukayama H (2014) Unusual small subunit that is not expressed in photosynthetic cells alters the catalytic properties of Rubisco in rice. Plant Physiology **164:** 69-79

Mueller-Cajar O, Badger MR (2007) New roads lead to Rubisco in archaebacteria. BioEssays **29:** 722-724

Mueller-Cajar O, Stotz M, Wendler P, Hartl FU, Bracher A, Hayer-Hartl M (2011) Structure and function of the AAA+ protein CbbX, a red-type Rubisco activase. Nature **479:** 194-199

Mueller-Cajar O, Whitney S (2008) Directing the evolution of Rubisco and Rubisco activase: First impressions of a new tool for photosynthesis research. Photosynthesis Research **98:** 667-675

Nagaraj N, Wisniewski JR, Geiger T, Cox J, Kircher M, Kelso J, Pääbo S, Mann M (2011) Deep proteome and transcriptome mapping of a human cancer cell line. Molecular Systems Biology **7:** 548-548

Nakamura M, Sugiura M (2007) Translation efficiencies of synonymous codons are not always correlated with codon usage in tobacco chloroplasts. The Plant Journal **49:** 128-134

Nakamura M, Sugiura M (2009) Selection of synonymous codons for better expression of recombinant proteins in tobacco chloroplasts. Plant Biotechnology **26:** 53-56

Nakamura T, Ohta M, Sugiura M, Sugita M (2001) Chloroplast ribonucleoproteins function as a stabilizing factor of ribosome-free mRNAs in the stroma. Journal of Biological Chemistry **276:** 147-152

Nakashita H, Arai Y, Shikanai T, Doi Y, Yamaguchi I (2001) Introduction of bacterial metabolism into higher plants by polycistronic transgene expression. Bioscience, Biotechnology, and Biochemistry **65:** 1688-1691

Napoli C, Lemieux C, Jorgensen R (1990) Introduction of a chimeric chalcone synthase gene into petunia results in reversible co-suppression of homologous genes in trans. The Plant Cell Online **2:** 279-289

Nishimura K, Ogawa T, Ashida H, Yokota A (2008) Molecular mechanisms of RuBisCO biosynthesis in higher plants. Plant Biotechnology **25:** 285-290

O'Connor PBF, Li G-W, Weissman JS, Atkins JF, Baranov PV (2013) rRNA: mRNA pairing alters the length and the symmetry of mRNA-protected fragments in ribosome profiling experiments. Bioinformatics **29:** 1488-1491

Oaks A (1994) Efficiency of nitrogen utilization in C_3 and C_4 cereals. Plant Physiol. **106:** 407-414

Oey M, Lohse M, Kreikemeyer B, Bock R (2009) Exhaustion of the chloroplast protein synthesis capacity by massive expression of a highly stable protein antibiotic. The Plant Journal **57:** 436-445

Ogawa S, Suzuki Y, Yoshizawa R, Kanno K, Makino A (2011) Effect of individual suppression of *RBCS* multigene family on Rubisco contents in rice leaves. Plant, Cell & Environment **35:** 546-553

Ohtani T, Galili G, Wallace J, Thompson G, Larkins B (1991) Normal and lysine-containing zeins are unstable in transgenic tobacco seeds. Plant Molecular Biology **16:** 117-128

Olinares PDB, Kim J, Davis JI, van Wijk KJ (2011) Subunit stoichiometry, evolution, and functional implications of an asymmetric plant plastid ClpP/R protease complex in *Arabidopsis*. The Plant Cell **23:** 2348-2361

Orr DJ (2013) Plant Rubiso biogenesis: A study of the requirements and processing steps during co- and post-translational modification of the large subunit (Doctoral dissertation). Australian National University, Canberra

Ott CM, Smith BD, Portis AR, Spreitzer RJ (2000) Activase region on chloroplast ribulose-1,5-bisphosphate carboxylase/oxygenase: Nonconservative substitution in the large subunit alters species specificity of protein interaction. Journal of Biological Chemistry **275:** 26241-26244

Outchkourov NS, Rogelj B, Strukelj B, Jongsma MA (2003) Expression of sea anemone equistatin in potato. Effects of plant proteases on heterologous protein production. Plant Physiology **133:** 379-390

Paila YD, Richardson LGL, Schnell DJ (2015) New insights into the mechanism of chloroplast protein import and its integration with protein quality control, organelle biogenesis and development. Journal of Molecular Biology **427:** 1038-1060

Park W, Li J, Song R, Messing J, Chen X (2002) CARPEL FACTORY, a Dicer homolog, and HEN1, a novel protein, act in microRNA metabolism in *Arabidopsis thaliana*. Current Biology **12:** 1484-1495

Parry MAJ, Andralojc PJ, Mitchell RAC, Madgwick PJ, Keys AJ (2003) Manipulation of Rubisco: The amount, activity, function and regulation. Journal of Experimental Botany **54:** 1321-1333

Parry MAJ, Andralojc PJ, Scales JC, Salvucci ME, Carmo-Silva AE, Alonso H, Whitney SM (2013) Rubisco activity and regulation as targets for crop improvement. Journal of Experimental Botany **64:** 717-730

Parry MAJ, Keys AJ, Madgwick PJ, Carmo-Silva AE, Andralojc PJ (2008) Rubisco regulation: A role for inhibitors. Journal of Experimental Botany **59:** 1569-1580

Pearce F (2006) Catalytic by-product formation and ligand binding by ribulose bisphosphate carboxylases from different phylogenies. Biochemical Journal **399:** 525-534

Peeters NM, Hanson MR (2002) Transcript abundance supercedes editing efficiency as a factor in developmental variation of chloroplast gene expression. RNA **8:** 497-511

Pengelly JJL, Förster B, von Caemmerer S, Badger MR, Price GD, Whitney SM (2014) Transplastomic integration of a cyanobacterial bicarbonate transporter into tobacco chloroplasts. Journal of Experimental Botany **65:** 3071-3080

Perdomo J, Cavanagh A, Kubien D, Galmés J (2015) Temperature dependence of in vitro Rubisco kinetics in species of *Flaveria* with different photosynthetic mechanisms. Photosynthesis Research **124:** 67-75

Perlak FJ, Fuchs RL, Dean DA, McPherson SL, Fischhoff DA (1991) Modification of the coding sequence enhances plant expression of insect control protein genes. Proceedings of the National Academy of Sciences of the United States of America **88:** 3324-3328

Pierce J, Carlson TJ, Williams JG (1989) A cyanobacterial mutant requiring the expression of ribulose bisphosphate carboxylase from a photosynthetic anaerobe. Proceedings of the National Academy of Sciences of the United States of America **86:** 5753-5757

Pinto H, Sharwood RE, Tissue DT, Ghannoum O (2014) Photosynthesis of C_3, C_3–C_4, and C_4 grasses at glacial CO_2. Journal of Experimental Botany **65:** 3669-3681

Pohl S, Hasilik A (2015) Chapter 4 - Biosynthesis, targeting, and processing of lysosomal proteins: Pulse–chase labeling and immune precipitation. *In* P Frances, P Nick, eds, Methods in Cell Biology, Vol Volume 126. Academic Press, pp 63-83

Portis AR, Li C, Wang D, Salvucci ME (2008) Regulation of Rubisco activase and its interaction with Rubisco. Journal of Experimental Botany **59:** 1597-1604

Premkumar A, Mercado JA, Quesada MA (2001) Effects of in vitro tissue culture conditions and acclimatization on the contents of Rubisco, leaf soluble proteins, photosynthetic pigments, and C/N ratio. Journal of Plant Physiology **158:** 835-840

Price GD, Howitt SM (2014) Plant science: Towards turbocharged photosynthesis. Nature **513:** 497-498

Price GD, Sültemeyer D, Klughammer B, Ludwig M, Badger MR (1998) The functioning of the CO2 concentrating mechanism in several cyanobacterial strains: A review of general physiological characteristics, genes, proteins, and recent advances. Canadian Journal of Botany **76:** 973-1002

Proshkin S, Rahmouni AR, Mironov A, Nudler E (2010) Cooperation between translating ribosomes and RNA polymerase in transcription elongation. Science **328:** 504-508

Pumplin N, Voinnet O (2013) RNA silencing suppression by plant pathogens: Defence, counter-defence and counter-counter-defence. Nature Reviews Microbiology **11:** 745-760

Rae BD, Long BM, Badger MR, Price GD (2012) Structural determinants of the outer shell of β-carboxysomes in *Synechococcus elongatus* PCC 7942: Roles for CcmK2, K3-K4, CcmO, and CcmL. PLoS ONE **7:** e43871

Raines CA (2003) The Calvin cycle revisited. Photosynthesis Research **75:** 1-10

Raines CA (2011) Increasing photosynthetic carbon assimilation in C_3 plants to improve crop yield: Current and future strategies. Plant Physiology **155:** 36-42

Raven JA (2013) Rubisco: Still the most abundant protein of Earth? New Phytologist **198:** 1-3

Read BA, Tabita FR (1992) A hybrid ribulose bisphosphate carboxylase/oxygenase enzyme exhibiting a substantial increase in substrate specificity factor. Biochemistry **31:** 5553-5560

Read BA, Tabita FR (1994) High substrate specificity factor ribulose bisphosphate carboxylase/oxygenase from eukaryotic marine algae and properties of recombinant cyanobacterial Rubisco containing "algal" residue modifications. Archives of Biochemistry and Biophysics **312:** 210-218

Reed ML, Wilson SK, Sutton CA, Hanson MR (2001) High-level expression of a synthetic red-shifted GFP coding region incorporated into transgenic chloroplasts. The Plant Journal **27:** 257-265

Reutter K, Atzorn R, Hadeler B, Schmülling T, Reski R (1998) Expression of the bacterial ipt gene in Physcomitrella rescues mutations in budding and in plastid division. Planta **206:**196-203

Richter LJ, Thanavala Y, Arntzen CJ, Mason HS (2000) Production of hepatitis B surface antigen in transgenic plants for oral immunization. Nature Biotechnology **18:** 1167-1171

Richter S, Lamppa GK (2003) Structural properties of the chloroplast stromal processing peptidase required for its function in transit peptide removal. Journal of Biological Chemistry **278:** 39497-39502

Richter S, Zhong R, Lamppa G (2005) Function of the stromal processing peptidase in the chloroplast import pathway. Physiologia Plantarum **123:** 362-368

Robinson SP, Portis Jr AR (1988) Release of the nocturnal inhibitor, carboyarabinitol-1 -phosphate, from ribulose bisphosphate carboylase/oxygenase by rubisco activase. Federation of European Biochemical Societies Letters **233:** 413-416

Robinson SP, Portis Jr AR (1989) Adenosine triphosphate hydrolysis by purified Rubisco activase. Archives of Biochemistry and Biophysics **268:** 93-99

Rodermel SR, Abbott MS, Bogorad L (1988) Nuclear-organelle interactions: Nuclear antisense gene inhibits ribulose bisphosphate carboxylase enzyme levels in transformed tobacco plants. Cell **55:** 673-681

Rose AB, Emami S, Bradnam K, Korf I (2011) Evidence for a DNA-based mechanism of intron-mediated enhancement. Frontiers in Plant Science **2:** 98

Saghai-Maroof MA, Soliman KM, Jorgensen RA, Allard RW (1984) Ribosomal DNA spacer-length polymorphisms in barley: Mendelian inheritance, chromosomal location, and population dynamics. Proceedings of the National Academy of Sciences of the United States of America **81:** 8014-8018

Sakamoto W (2006) Protein degradation machineries in plastids. Annual Review in Plant Biology **57:** 599-621

Sambrook J, Fritsch EF, Maniatis T, eds (1989) Molecular cloning: A laboratory manual, Ed 2. Cold Spring Harbor Laboratory Press, New York

Sasanuma T (2001) Characterization of the *rbcS* multigene family in wheat: Subfamily classification, determination of chromosomal location and evolutionary analysis. Molecular Genetics and Genomics **265:** 161-171

Saschenbrecker S, Bracher A, Rao KV, Rao BV, Hartl FU, Hayer-Hartl M (2007) Structure and function of RbcX, an assembly chaperone for hexadecameric Rubisco. Cell **129:** 1189-1200

Scharff LB, Bock R (2014) Synthetic biology in plastids. The Plant Journal **78:** 783-798

Scharff LB, Koop H-U (2007) Targeted inactivation of the tobacco plastome origins of replication A and B. The Plant Journal **50:** 782-794

Schulze S, Mallmann J, Burscheidt J, Koczor M, Streubel M, Bauwe H, Gowik U, Westhoff P (2013) Evolution of C_4 photosynthesis in the genus *Flaveria*: Establishment of a photorespiratory CO_2 pump. The Plant Cell **25:** 2522-2535

Seemann JR, Berry JA, Freas SM, Krump MA (1985) Regulation of Rubisco activity *in vivo* by a light-modulated inhibitor of catalysis. Proceedings of the National Academy of Sciences of the United States of America **82:** 8024-8028

Senthil-Kumar M, Mysore KS (2010) RNAi in plants: Recent developments and applications in agriculture. *In* Catalano AJ eds, Gene Silencing: Theory, techniques and applications Chapter VII, pp 183-199

Servaites JC (1990) Inhibition of ribulose 1,5-bisphosphate carboxylase/oxygenase by 2-carboxyarabinitol-1-phosphate. Plant Physiology **92:** 867-870

Sharwood RE, von Caemmerer S, Maliga P, Whitney SM (2008) The catalytic properties of hybrid rubisco comprising tobacco small and sunflower large subunits mirror the kinetically equivalent source Rubiscos and can support tobacco growth. Plant Physiology **146:** 83-96

Sharwood RE, Whitney SM (2010) Engineering the sunflower Rubisco subunits into tobacco chloroplasts: New considerations. *In* CA Rebeiz, C Benning, HJ Bohnert, H Daniell, JK Hoober, HK Lichtenthaler, AR Portis, BC Tripathy, eds, The Chloroplast, Ed Basics and applications Vol 31, pp 285-306

Sharwood RE, Whitney SM (2014) Correlating Rubisco catalytic and sequence diversity within C_3 plants with changes in atmospheric CO_2 concentrations. Plant, Cell & Environment **37:** 1981-1984

Shi L-X, Theg SM (2013) The chloroplast protein import system: From algae to trees. Biochimica et Biophysica Acta (BBA) - Molecular Cell Research **1833:** 314-331

Shinozake K, Ohme M, Tanaka M, Wakasugi T, Hayashida N, Matsubayashi T, Zaita N, Chunwonse J, Obokata J, Yamaguchi-Shinozaki K, Ohto C, Torazawa K, Meng BY, Sugita m, Deno H, Kamogashira T, Yamada K, Kusuda J, Takaiwa F, Kato A, Tohdoh N, Shimada H, Suguira M (1986) The complete nucleotide sequence of the tobacco chloroplast genome: Its gene organization and expression. The European Molecular Biology Organisation Journal **5:** 2043-2049

Sierro N, Battey JND, Ouadi S, Bakaher N, Bovet L, Willig A, Goepfert S, Peitsch MC, Ivanov NV (2014) The tobacco genome sequence and its comparison with those of tomato and potato. Nature Communications **5**

Silva EN, Silveira JAG, Ribeiro RV, Vieira SA (2015) Photoprotective function of energy dissipation by thermal processes and photorespiratory mechanisms in *Jatropha curcas* plants during different intensities of drought and after recovery. Environmental and Experimental Botany **110:** 36-45

Smith HH (1968) Recent cytogenetic studies in the genus *Nicotiana*. *In* EW Caspari, M Demerec, eds, Advances in genetics, Vol 14. Academic Press, London, pp 1-43

Somanchi A, Mayfield SP (1999) Nuclear–chloroplast signaling. Current Opinion in Plant Biology **2:** 404-409

Spreitzer RJ (2003) Role of the small subunit in ribulose-1,5-bisphosphate carboxylase/oxygenase. Archives of Biochemistry & Biophysics **414:** 141-149

Spreitzer RJ, Esquivel MG, Du Y-C, McLaughlin PD (2001) Alanine-scanning mutagenesis of the small-subunit βA−βB loop of chloroplast ribulose-1,5-bisphosphate carboxylase/oxygenase: Substitution at Arg-71 affects thermal stability and CO_2/O_2 specificity. Biochemistry **40:** 5615-5621

Spreitzer RJ, Peddi SR, Satagopan S (2005) Phylogenetic engineering at an interface between large and small subunits imparts land-plant kinetic properties to algal Rubisco. Proceedings of the National Academy of Sciences of the United States of America **102:** 17225-17230

Spreitzer RJ, Salvucci ME (2002) Rubisco: Structure, regulatory interactions, and possibilities for a better enzyme. Annual Review of Plant Biology **53:** 449-475

Staub JM, Maliga P (1993) Accumulation of D1 polypeptide in tobacco plastids is regulated via the untranslated region of the *psbA* mRNA. The European Molecular Biology Organisation Journal **12:** 601-606

Staub JM, Maliga P (1994) Translation of *psbA* mRNA is regulated by light via the 5′-untranslated region in tobacco plastids. The Plant Journal **6:** 547-553

Stec B (2012) Structural mechanism of RuBisCO activation by carbamylation of the active site lysine. Proceedings of the National Academy of Sciences of the United States of America **109:** 18785-18790

Stitt M, Schaewen A, Willmitzer L (1991) "Sink" regulation of photosynthetic metabolism in transgenic tobacco plants expressing yeast invertase in their cell wall involves a decrease of the Calvin-cycle enzymes and an increase of glycolytic enzymes. Planta **183:** 40-50

Stoppel R, Meurer J (2013) Complex RNA metabolism in the chloroplast: An update on the *psbB* operon. Planta **237:** 441-449

Storz G, Vogel J, Wassarman KM (2011) Regulation by small RNAs in bacteria: Expanding frontiers. Molecular Cell **43:** 880-891

Stotz M, Mueller-Cajar O, Ciniawsky S, Wendler P, Hartl FU, Bracher A, Hayer-Hartl M (2011) Structure of green-type Rubisco activase from tobacco. Nature Structural & Molecular Biology **18:** 1366-1370

Sugiura M (1992) The chloroplast genome. Plant Molecular Biology **19:** 149-168

Sunkar R, Zhu J-K (2007) Micro RNAs and short-interfering RNAs in plants. Journal of Integrative Plant Biology **49:** 817-826

Suzuki Y, Makino A (2012) Availability of Rubisco small subunit up-regulates the transcript levels of large subunit for stoichiometric assembly of its holoenzyme in rice. Plant Physiology **160:** 533-540

Suzuki Y, Miyamoto T, Yoshizawa R, Mae T, Makino A (2009) Rubisco content and photosynthesis of leaves at different positions in transgenic rice with an overexpression of *RBCS*. Plant, Cell & Environment **32:** 417-427

Suzuki Y, Ohkubo M, Hatakeyama H, Ohashi K, Yoshizawa R, Kojima S, Hayakawa T, Yamaya T, Mae T, Makino A (2007) Increased Rubisco content in transgenic rice transformed with the 'sense' *rbcS* gene. Plant and Cell Physiology **48:** 626-637

Svab Z, Hajdukiewicz P, Maliga P (1990) Stable transformation of plastids in higher plants. Proceedings of the National Academy of Sciences of the United States of America **87:** 8526-8530

Tabita FR, Hanson TE, Li H, Satagopan S, Singh J, Chan S (2007) Function, structure, and evolution of the RubisCO-like proteins and their RubisCO homologs. Microbiology and Molecular Biology Reviews **71:** 576-599

Tabita FR, McFadden BA (1974) D-Ribulose 1, 5-diphosphate carboxylase from Rhodospirillum rubrum II. Quaternary structure, composition, catalytic, and immunological properties. Journal of Biological Chemistry **249:** 3459-3464

Tabita FR, Satagopan S, Hanson TE, Kreel NE, Scott SS (2008) Distinct form I, II, III, and IV Rubisco proteins from the three kingdoms of life provide clues about Rubisco evolution and structure/function relationships. Journal of Experimental Botany **59:** 1515-1524

Tcherkez G (2013) Modelling the reaction mechanism of ribulose-1,5-bisphosphate carboxylase/oxygenase and consequences for kinetic parameters. Plant, Cell & Environment **36:** 1586-1596

Tcherkez GGB, Farquhar GD, Andrews TJ (2006) Despite slow catalysis and confused substrate specificity, all ribulose bisphosphate carboxylases may be nearly perfectly optimized. Proceedings of the National Academy of Sciences of the United States of America **103:** 7246-7251

The *Arabidopsis* Initiative (2000) Analysis of the genome sequence of the flowering plant *Arabidopsis thaliana*. Nature **408:** 796-815

Timmis JN, Ayliffe MA, Huang CY, Martin W (2004) Endosymbiotic gene transfer: Organelle genomes forge eukaryotic chromosomes. Nature Reviews Genetics **5:** 123-135

Travella S, Klimm TE, Keller B (2006) RNA interference-based gene silencing as an efficient tool for functional genomics in hexaploid bread wheat. Plant Physiology **142:** 6-20

Tregoning JS, Nixon P, Kuroda H, Svab Z, Clare S, Bowe F, Fairweather N, Ytterberg J, Wijk KJv, Dougan G, Maliga P (2003) Expression of tetanus toxin Fragment C in tobacco chloroplasts. Nucleic Acids Research **31:** 1174-1179

Tsai Y-CC, Mueller-Cajar O, Saschenbrecker S, Hartl FU, Hayer-Hartl M (2012) Chaperonin Cofactors, Cpn10 and Cpn20, of green algae and plants function as hetero-oligomeric ring complexes. Journal of Biological Chemistry **287:** 20471-20481

Ullrich KK, Hiss M, Rensing SA (2015) Means to optimize protein expression in transgenic plants. Current Opinion in Biotechnology **32:** 61-67

van Lun M, van der Spoel D, Andersson I (2011) Subunit interface dynamics in hexadecameric rubisco. Journal of Molecular Biology **411:** 1083-1098

van Wijk KJ (2015) Protein maturation and proteolysis in plant plastids, mitochondria, and peroxisomes. Annual Review of Plant Biology **66:** 75-111

Vitlin Gruber A, Nisemblat S, Azem A, Weiss C (2013) The complexity of chloroplast chaperonins. Trends in Plant Science **18:** 688-694

Voinnet O (2002) RNA silencing: Small RNAs as ubiquitous regulators of gene expression. Current Opinion in Plant Biology **5:** 444-451

von Caemmerer S, Evans JR (2010) Enhancing C_3 Photosynthesis. Plant Physiology **154:** 589-592

von Caemmerer S, Evans JR, Hudson GS, Andrews TJ (1994) The kinetics of ribulose-1,5-bisphosphate carboxylase/oxygenase in vivo inferred from measurements of photosynthesis in leaves of transgenic tobacco. Planta **195:** 88-97

Vriet C, Edwards A, Smith A, Wang T (2014) Sucrose and starch metabolism. *In* S Tabata, J Stougaard, eds, The Lotus japonicus Genome. Springer Berlin Heidelberg, pp 97-115

Wachter R, Salvucci M, Carmo-Silva AE, Barta C, Genkov T, Spreitzer R (2013) Activation of interspecies-hybrid Rubisco enzymes to assess different models

for the Rubisco–Rubisco activase interaction. Photosynthesis Research **117:** 557-566

Waegemann K, Soll J (1996) Phosphorylation of the transit sequence of chloroplast precursor proteins. Journal of Biological Chemistry **271:** 6545-6554

Walter NG (2006) Michaelis-Menten is dead, long live Michaelis-Menten! Nature Chemical Biology **2:** 66-67

Wang Y-L, Zhou J-H, Wang Y-F, Bao J-S, Chen H-B (2001) Properties of hybrid enzymes between *Synechococcus* large subunits and higher plant small subunits of ribulose-1,5-bisphosphate carboxylase/oxygenase in *Escherichia coli*. Archives of Biochemistry and Biophysics **396:** 35-42

Wang Z-Y, Snyder GW, Esau BD, Archie R. Portis J, Ogren WL (1992) Species-dependent variation in the interaction of substrate-bound ribulose-1,5-bisphosphate carboxylase/oxygenase (Rubisco) and Rubisco activase. Plant Physiol. **100:** 1858-1862

Waterhouse PM, Graham MW, Wang M-B (1998) Virus resistance and gene silencing in plants can be induced by simultaneous expression of sense and antisense RNA. Proceedings of the National Academy of Sciences of the United States of America **95:** 13959-13964

Whitney SM, Andrews TJ (2001a) The gene for the ribulose-1,5-bisphosphate carboxylase/oxygenase (Rubisco) small subunit relocated to the plastid gnome of tobacco directs the synthesis of small subunits that assemble into Rubisco. The Plant Cell Online **13:** 193-205

Whitney SM, Andrews TJ (2001b) Plastome-encoded bacterial ribulose-1,5-bisphosphate carboxylase/oxygenase (RubisCO) supports photosynthesis and growth in tobacco. Proceedings of the National Academy of Sciences of the United States of America **98:** 14738-14743

Whitney SM, Andrews TJ (2003) Photosynthesis and growth of tobacco with a substituted bacterial rubisco mirror the properties of the introduced enzyme. Plant Physiology **133:** 287-294

Whitney SM, Baldet P, Hudson GS, Andrews TJ (2001) Form I Rubiscos from non-green algae are expressed abundantly but not assembled in tobacco chloroplasts. The Plant Journal **26:** 535-547

Whitney SM, Birch R, Kelso C, Beck JL, Kapralov MV (2015) Improving recombinant Rubisco biogenesis, plant photosynthesis and growth by coexpressing its ancillary RAF1 chaperone. Proceedings of the National Academy of Sciences **112:** 3564-3569

Whitney SM, Houtz RL, Alonso H (2011a) Advancing our understanding and capacity to engineer nature's CO_2-sequestering enzyme, Rubisco. Plant Physiology **155:** 27-35

Whitney SM, Kane HJ, Houtz RL, Sharwood RE (2009) Rubisco oligomers composed of linked small and large subunits assemble in tobacco plastids and have higher affinities for CO_2 and O_2. Plant Physiology **149:** 1887-1895

Whitney SM, Sharwood RE (2008) Construction of a tobacco master line to improve Rubisco engineering in chloroplasts. Journal of Experimental Botany **59:** 1909-1921

Whitney SM, Sharwood RE, Orr D, White SJ, Alonso H, Galmés J (2011b) Isoleucine 309 acts as a C_4 catalytic switch that increases ribulose-1,5-bisphosphate carboxylase/oxygenase (rubisco) carboxylation rate in *Flaveria*. Proceedings of the National Academy of Sciences of the United States of America **108:** 14688-14693

Whitney SM, von Caemmerer S, Hudson GS, Andrews TJ (1999) Directed mutation of the Rubisco large subunit of tobacco influences photorespiration and growth. Plant Physiology **121:** 579-588

Whitney SM, Yellowlees D (1995) Preliminary investigations into the structure and activity of Ribulose bisphosphate carboxylase from two photosynthetic dinoflagellates. Journal of Phycology **31:** 138-146

Wolter FP, Fritz CC, Willmitzer L, Schell J, Schreier PH (1988) *rbcS* genes in *Solanum tuberosum*: Conservation of transit peptide and exon shuffling during evolution. Proceedings of the National Academy of Sciences of the United States of America **85:** 846-850

Woodson JD, Chory J (2008) Coordination of gene expression between organellar and nuclear genomes. Nature Reviews Genetics **9:** 383-395

Wostrikoff K, Stern D (2007) Rubisco large-subunit translation is autoregulated in response to its assembly state in tobacco chloroplasts. Proceedings of the National Academy of Sciences of the United States of America **104:** 6466-6471

Xie Q, Michaeli S, Peled-Zehavi H, Galili G (2015) Chloroplast degradation: One organelle, multiple degradation pathways. Trends in Plant Science **20:** 264-265

Yamaguchi K, von Knoblauch K, Subramanian AR (2000) The plastid ribosomal proteins: Identification of all the proteins in the 30 S subunit of an organelle ribosome (chloroplast). Journal of Biological Chemistry **275:** 28455-28465

Yang L, Liu Z, Lu F, Dong A, Huang H (2006) SERRATE is a novel nuclear regulator in primary microRNA processing in *Arabidopsis*. The Plant Journal **47:** 841-850

Yukawa M, Tsudzuki T, Sugiura M (2005) The 2005 version of the chloroplast DNA sequence from tobacco (*Nicotiana tabacum*). Plant Molecular Biology Reporter **23:** 359-365

Zerges W (2000) Translation in chloroplasts. Biochimie **82:** 583-601

Zhang J, Khan SA, Hasse C, Ruf S, Heckel DG, Bock R (2015) Full crop protection from an insect pest by expression of long double-stranded RNAs in plastids. Science **347:** 991-994

Zhang X-H, Ewy RG, Widholm JM, Portis AR (2002) Complementation of the nuclear antisense *rbcS*-induced photosynthesis deficiency by introducing an *rbcS* gene into the tobacco plastid genome. Plant and Cell Physiology **43:** 1302-1313

Zhang X-H, Webb J, Huang Y-H, Lin L, Tang R-S, Liu A (2011) Hybrid Rubisco of tomato large subunits and tobacco small subunits is functional in tobacco plants. Plant Science **180:** 480-488

Zhou F, Karcher D, Bock R (2007) Identification of a plastid intercistronic expression element (IEE) facilitating the expression of stable translatable monocistronic mRNAs from operons. The Plant Journal **52:** 961-972

Zoubenko OV, Allison LA, Svab Z, Maliga P (1994) Efficient targeting of foreign genes into the tobacco plastid genome. Nucleic Acids Research **22:** 3819-3824

APPENDIX A

Genoypes used in this thesis and localisation of genes introduced/alterations to their plastome.

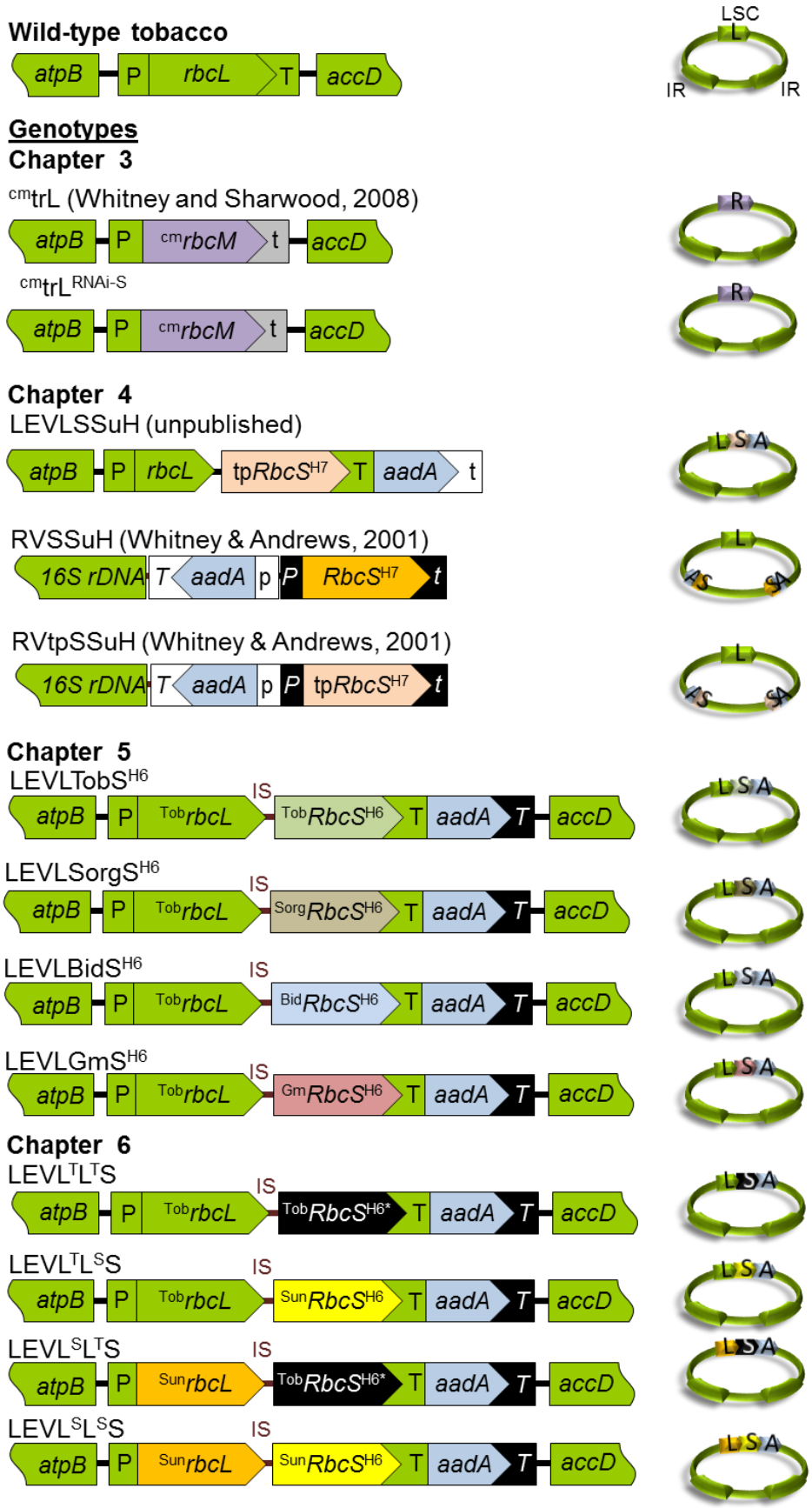

APPENDIX B

Genbank accession numbers of *N. tabacum RbcS* genes.

N. tabacum RbcS gene	Genbank accession numbers
*Nt*S1a	KM025316 AYMY 01063898 AWOK 01325204
*Nt*S1b	KM025317 AWOJ 01341371 AYMY 01150982
*Nt*T1	KM025327 AWOK 01216412 AYMY 01074636 AWOJ 01591438
*Nt*S2	KM025318 AWOK 01128788 AYMY 01119856 AWOJ 01130916
*Nt*T2	KM025329 AYMY 01062145
*Nt*S3	KM025320 AWOK 01296120 AYMY 01008402 AWOJ 01273024
*Nt*T3a	KM025331 AWOJ 01199719
*Nt*T3b	KM025332 AYMY 01119856
*Nt*S4	KM025322 AYMY 0110318 AWOJ 01086791
*Nt*T4a	KM025334 AWOK 01197301 AYMY 01208782 AWOJ 01199719
*Nt*T4b	KM025335 AWOK 01310353 AYMY 01103181 AWOJ 01086791
*Nt*S5	KM025325 AWOJ 01024298 AYMY 01008401 AWOK 01019267
*Nt*T5	KM025337 AYMY 01062145